STUDIES IN PHOTOELECTRIC INTERFERENCE SPECTROSCOPY IN THE ULTRAVIOLET

by

Brian Bates M.Sc.

A Thesis submitted for the

Degree of Doctor of Philosophy

Department of Physics

Imperial College of Science and Technology

London.

August 1966.

ABSTRACT.

The superior angular dispersion of the Fabry-Perot interferometer and its large gain in luminosity over grating dispersers is now widely exploited in laboratory spectroscopy. These advantages of the interferometer are of considerable importance for astronomical spectroscopy from space vehicles.

Factors affecting the performance of the interferometer and Fabry-Perot type interference filters in the far and vacuum ultraviolet are considered. An improvement in performance of the interferometer and filters in the far ultraviolet and an extension of their useful spectral range into the vacuum ultraviolet is reported arising from the development of new semi-transparent reflecting coatings. Methods of preparation and optical properties of aluminium and aluminium-magnesium fluoride coatings for multiple-beam interferometry in the ultraviolet ($\geq$1800 Å) are discussed. Effects of evaporation conditions on optical properties are considered and a comparison made with computed data. The coating performance for interferometry is summarised and illustrated with interferograms of λ 1849 Å of Hg I.

Transmission characteristics of filters for wavelengths 1700 - 2400 Å are described. Peak transmissions of 25% with bandwidths $<$ 300 Å are obtained for first order filters. Second order filters give a narrower bandwidth. Effects of optical properties of the reflecting layers on filter performance are discussed.

The application of the interferometer combined with an electron -

optical image detector for simultaneous time, spatial and spectral resolution of rapidly changing sources is discussed and comparison is made with oscillating interferometers. Merits of this combination for ultraviolet interference spectroscopy are considered.

Finally, consideration is given to a new use of the interferometer for space research. The approach to an experiment using the interferometer to obtain ultraviolet solar line profiles and their variation across the solar disc is briefly considered. This experiment requires a stable, high finesse etalon. The development of an optically contacted interferometer for rocket spectroscopy is described.

LIST OF CONTENTS.

CHAPTER 1.

A BACKGROUND TO THE PRESENT INVESTIGATION.

1.1. Introduction.

The definition of the term 'interference spectroscopy' given by Jacquinot (1960) is one of degree rather than kind since in reality, all the techniques of spectroscopy involve the phenomena of interference. The term interference spectroscopy has now become generally applied to techniques in which high orders of interference are used by employing instruments such as the Lummer plate, the Michelson echelon or the Fabry-Perot interferometer. For these instruments, the interference order is usually in excess of 10^4. This definition thus excludes grating instruments where the order of interference is only a few units or exceptionally several hundreds of units as in the case of the echelon grating. The subject matter covered in the present investigation is largely concerned with the development and the application of one instrument which has been widely used for interference spectroscopy - namely, the Fabry-Perot interferometer.

The interferometer first described by Fabry and Perot in 1897 was one of several high resolution instruments developed in the latter part of the last century. However it was not widely used for the examination of spectral lines until 1927 when the discovery of the relation between nuclear spin and hyperfine structure resulted in a considerable interest in high resolution spectroscopy. Even so, in spite of the many well known uses of the interferometer in astronomical spectroscopy, high resolution

spectrocopy, wavelength standard determinations etc, the apparatus was very little developed until Jacquinot and Dufour described the first scanning interferometer (the F.P. spectrometer) in 1948. Since this time there has been a great revival of interest in the use of the interferometer.

With the development of laser sources the F.P. interferometer has now become a commonplace instrument in many laboratories since the high resolving power required for the spectral examination of such sources can be acheived by interferometric means only. However for some recent applications, the interferometer has not necessarily been used for its ability to provide a high spectral resolving power, for which it is most commonly known, but for its superior angular dispersion and light gathering power compared with grating instruments of the same area and resolving power. (Jacquinot 1954). These superior qualities have been exploited for the increasing number of problems in which time resolution and repetition rate are of major importance in particular for laboratory plasma physics where few instruments have the versatility and simplicity of the scanning F.P. interferometer for measuring time-resolved spectral profiles. Yet for high spectral resolution and time-resolved interference spectroscopy in the nanosecond region, and this is now required with the development of Q spoiled laser systems, the F.P. spectrometer has several limitations which at present make such a time resolution impracticable. The reasons for this short coming will be discussed in later sections where consideration is given to the interferometer-image intensifier combination which overcomes many of the limitations of the scanning interferometer.

Dunham (1956) has shown how the high luminosity and the large angular dispersion of the interferometer can be exploited for astronomical spectroscopy from ground based telescopes when a high spectral resolving power is required and the 'seeing' conditions are not necessarily very good. A similar consideration can be made for space research applications where the guidance limitations of the space vehicle now replace the seeing restrictions introduced by the earth's atmosphere. With the added advantage of speed of recording and compactness it is likely that in the near future the interferometer will become exploited for the first time in the field of space spectroscopy from rockets and satellites (Bradley 1966). Much of the subject matter of this present investigation has been concerned with the development of the interferometer and with techniques of interference spectroscopy with this end in view.

The interferometer as first described consisted of two transparent optical flats each coated with a semi-transparent reflecting film. The flats were aligned so that the reflecting layers, separated by an air gap, were mounted parallel to each other. In the original form of the instrument one of the plates was mounted on a moveable carriage enabling the plate separation to be easily changed. However, this form of the instrument soon became obsolete because of the difficulty in working the moveable carriage to maintain the high degree of accuracy required in the plate parallelism. (Some 60 years later this problem, and the additional difficulty of rapidly vibrating one plate about a mean position, was overcome leading to the development of oscillating interferometers for time resolved spectroscopy). In a later instrument described by Fabry and Perot the plates were separated by fixed spacers of quartz and parallelism was obtained by a small mechanical compression of the plates against the spacers. This form of the instrument became known as the Fabry-Perot etalon.

For many years the F.P. etalon employed with the photographic method of detection played an important role in high resolution spectroscopy and the majority of investigations of hyperfine structure of spectral lines have been made by this method(Tolansky 1947). So too has the interferometer employed in the spectrographic method of use played a significant role in astronomical spectroscopy (Ring 1956). Fabry and Perot themselves measured wavelengths of Fraunhofer lines in the solar spectrum as early as 1902 and in 1911 Fabry and Buisson investigated the spectrum of the great nebula of Orion. Many of the earlier applications of the interferometer, including its very important use for establishing absolute wavelength standards, have been reviewed by Kuhn (1951).

For a long time the apparatus was very little developed and its use was limited to the above types of investigation. In 1948 it was shown that the interferometer could be sucessfully used outside the photographic region and the first really major development of the instrument came with the description of the F.P. spectrometer by Jacquinot and Dufour (1948). In this method of employment, the wavelength transmitted by the etalon was varied (scanned) by variation of the pressure (and therefore refractive index) of the gaseous medium between the elaton plates. Line profiles were recorded from the light flux received by a photoelectric detector after passing through a small diaphragm placed at the centre of the Haidinger ring pattern. Subsequently various scanning systems, other than that of pressure variation, have been devised (see later).

Recent advances in the practical development of the interferometer

have made it necessary to examine in greater detail the theoretical aspects of the instrument. In particular, the main theoretical progress has been due to Chabbal (1953), (1958) who has investigated the parameters which influence the properties of resolution and luminosity of the F.P. spectrometer. Chabbal has shown that these properties are very much dependent on the quality of the etalon flats and on the optical quality of the reflecting coatings. The results of Chabbal's analysis which are relevant to the present investigation are discussed in Chapter 2.

A further major theoretical development has been due to Jacquinot (1954) who compared the luminosities of grating, prism and F.P. spectrometers under the conditions of equal areas of dispersing element and equal resolving powers. This analysis showed that the interferometer could have a gain of some two orders of magnitude in luminosity over that of grating dispersers which themselves are more favourable in this respect than prisms. The realisation of this has lead to the increasing use of the interferometer as already stated.

Much of the emphasis of the present work has been largely concerned with a further phase in the development of the interferometer, namely the extension of its spectral range into the far and vacuum ultraviolet. For space research applications, for diagnosis of high temperature plasma sources and for spectroscopic examination of laser light higher harmonics the superior qualities of the interferometer will be increasingly required for this spectral region. In the past, attempts at using the interferometer in the far ultraviolet have been restricted by certain technological limitations. These limitations are considered in the

following sections where also, the aims and the approach to the present investigation will be discussed.

1.2. The Extension of the Spectral Range of the Interferometer into the Far Ultraviolet.

Applications of the F.P. interferometer have been largely confined to wavelengths greater than 2400 Å and apart from absolute wavelength determinations to about 2200 Å, it has been seldom used in the far ultraviolet. There have been no reported applications of the interferometer at wavelengths shorter than 2000 Å. The two factors which, in the past, have limited the spectral range of the interferometer in the ultraviolet have been the transmission and optical finish of the interferometer flats and the availability of suitable reflecting coatings. Of these limitations, the latter has been the major obstacle and this will be considered first.

At wavelengths greater than 2400 Å there has been an improved performance in terms of resolution and luminosity of the interferometer resulting from improved semi-transparent coatings. In particular, this has been realised by the development of dielectric multilayer films capable of giving a high reflectivity together with a very low absorption loss. (The significance of coating reflectivity and absorption is discussed in Chapter 2.). The worst situation occurs at wavelengths shorter than 2400 Å since in this spectral region there is no high index material at present available of sufficiently low absorption for dielectric multilayer films.

In the 1950's the accelerated interest in vacuum ultraviolet spectroscopy resulted in a great deal of effort being devoted to easing experimental limitations which had existed for such a long time. One of the significant advances in this direction has been the development of high reflectance films for the vacuum ultraviolet. It had been known for some years that opaque, evaporated aluminium films possessed a higher normal incidence reflectance than any other single material studied for the wavelength region 1100 to 3000 Å (Sabine 1939). However, the practical use of such films was severely restricted in the far and vacuum ultraviolet because of the decrease in reflectance caused by oxidation of the film, the effect of oxidation becoming more serious with decreasing wavelength.

A detailed study by Hass, Tousey and co-workers of the factors influencing the optical properties of evaporated aluminium films led to the production of coatings having a much improved reflectance in the vacuum ultraviolet. However, it was more the technique of overcoating a high quality aluminium film with MgF_2 or LiF to prevent oxidation and enhance reflectance, which has enabled the real advance to be made. Such coatings are now widely exploited for mirrors and gratings to be used in the vacuum ultraviolet.

In 1961, Hass and Waylonis produced semi-transparent aluminium films having considerably improved optical properties over previously reported measurements and they extended experimental data to λ 2200 Å. The methods of preparation and the optical properties of these aluminium and the above aluminium-dielectric films are discussed in Chapter 3 since

they provide a considerable part of the background to the present investigation.

The improved techniques for producing aluminium films and the principle of overcoating an opaque aluminium film with a transmitting dielectric layer suggested that an improvement could be made to the optical performance of semi-transparent films similarly overcoated. The main emphasis of the present work has been the preparation and an investigation of the optical properties of semi-transparent aluminium and aluminium - MgF_2 coatings with which the aim was to extend the spectral range of F.P. interference spectroscopy as far as possible into the ultraviolet. Special techniques devised for the preparation of these coatings are described in Chapter 5 and their optical properties and application to multiple beam interferometry are discussed in Chapter 6. During this investigation, the first reported F.P. interferograms obtained for $\lambda < 2000$ Å were obtained employing the coatings developed in this work.

1.3. The Extension of the Spectral Range of Interference Filters.

Closely allied to the problem of producing low absorption interferometer coatings for the far ultraviolet is that of manufacturing F.P. type interference filters for the same spectral region. In the F.P. etalon two independently worked flats are employed and the parallel reflecting surfaces are separated by a distance generally in excess of 1 m.m. The simplest form of interference filters are prepared by vacuum deposition onto a plane substrate of two semi-transparent reflecting films separated by a thin spacer layer. The transmission characteristics of such filters

consist of a series of bands which become more widely separated in wavelength as the thickness of the spacer layer is reduced. Usually, this layer is made only one or a few half-wavelengths in optical thickness. Both the peak transmission and the spectral width at half peak transmission i.e. the filter bandwidth, are very much dependent on the optical properties of the reflecting films (See Chapter 2).

In the first type of F.P. interference filters, which appear to have been developed by Geffken in Germany during World War II, silver reflecting films were employed separated by a magnesium fluoride or cryolite spacer layer (see e.g. Kuhn 1951). Later, the metal reflecting films were replaced by highly reflecting, low absorption multilayer stacks giving much improved performance in terms of peak transmission and filter bandwidth. (Ring and Wilcock (1953) Lissberger and Ring(1955))

Again, the main obstacle in extending the spectralrange of interference filters into the far and vacuum ultraviolet, as in the case of interferometer coatings, has been the lack of a suitable high index material for dielectric multilayer reflectance stacks.

For broad-band photometry and for auxiliary filtering of spectrometers and spectrographs flown in rockets and satellites, the isolation of a few hundreds of angstroms is now required for wavelengths shorter than 3000 Å. With their high luminosity, compactness and simplicity of mounting F.P. type interference filters are particularly suitable for space spectroscopy. In addition, the transmission characteristics of this type of filter can, within limits, be optimised during manufacture to suit particular experimental requirements.

The first major discussion regarding the feasibility of producing interference filters for the far & vacuum ultraviolet was given by Schroeder (1962) on the basis of an extropolation of the optical constants derived by Hass and Waylonis (1961) from measurements of the properties of semi-transparent aluminium films. Schroeder computed transmission characteristics of filters of the type aluminium - MgF_2 - aluminium concluding that filters having a peak transmission of 25% and bandwidths less than 250 Å could be produced for wavelengths down to λ 1500 Å. Such filters are of extreme importance for both space research and laboratory applications and they possess a particularly attractive feature in that they become 'self-blocking' at longer wavelengths because of the attenuation of the aluminium films.

Because of difficulties in experimental technique (Chapter 3) Schroeder gives only one experimental transmission curve for a filter having a wavelength peak $<\lambda$2000 Å and this filter had a peak transmission of $\pm$1% (at λ 1950 Å). Also, all Schroeder's filters show characteristics which are inferior to theoretical expectations. This was in part due to experimental technique (Chapter 3) but also due to an error in calculating filter bandwidths since a phase change term on reflection at the aluminium - MgF_2 boundaries was omitted (Chapter 2).

A second aspect of the present investigation, and one which is closely related to the development of the interferometer coatings, has been the production and an investigation of the properties of interference filters for wavelengths shorter than 2400 Å. During this work, interference filters having transmission peaks at wavelengths $\leq$1900 Å were reported.

(Bates and Bradley 1966). Methods of filter preparation are described in Chapter 5 and characterstics of first and second order filters and the effect of the optical properties of the aluminium reflecting films on filter performance are discussed in Chapter 6. The relevant formulae used for calculating spacer layer thickness etc. are given in Chapter 2.

1.4. The Wavelength Region Covered by the Present Investigation.

The optical properties of the semi-transparent aluminium and aluminium - MgF_2 coatings have been determined only to a wavelength of 1800 Å. Restriction to wavelengths above this value enables measurements of reflection and transmission coefficients to be made using relatively simple techniques by employing a reflectometer attatched to a nitrogen purged grating monochromator (see Chapter 6). For measurements at shorter wavelengths a vacuum monochromator is essential and experimental techniques become considerably more difficult (e.g. Madden 1963). However, the emphasis in the present work has been on the type of coatings which might be successfully employed for F.P. spectroscopy at wavelengths below 2400 Å and this investigation is merely a first step towards this end. This restriction in wavelength to 1800 Å is not terribly serious since at present it is not forseeable that the spectral range of the interferometer can be extended to wavelengths much shorter than 1650 Å. The reason for this is two fold. On the one hand it will be seen in Chapters 4 and 6 that the properties of the aluminium - MgF_2 coatings for multiple beam interferometry are deteriorating with decreasing wavelength. This illustrates the need to extend measurements of coating properties to

shorter wavelengths than has been done in the present work. But perhaps the more serious limitation is that of obtaining suitable materials for optical flats having an adequate transmission and which can also be polished to the high degree of flatness and smoothness required. It must be remembered that the demands on plate polishing become more stringent at shorter wavelengths (Chapter 2).

Fused silica etalon flats (Thermal Syndicate 'Spectrosil A') have been used in the present work and for a 5 mm. plate thickness required, an optical transmission of >50% can be obtained down to about 1670 Å. If polished with care a surface finish of r.m.s. roughness of approximately 3 Å can be achieved (Bennett and Porteus 1961) whilst the plates can now be worked to match better than $\lambda/150$ in the green over a 6 cm diameter. If the plates are also adjusted parallel to $\lambda/150$ then a defects finesse (Chapter 2) in the range 16-24 is attainable with flats transmitting a useful fraction of the light in the spectral region 1600 to 2400 Å. For smaller plate apertures a correspondingly higher defects finesse should be obtained and if spherical mirrors are employed then the aperture required is greatly reduced. (Jackson 1961).

To shorter wavelengths sapphire and LiF have an adequate transmission but for these materials, the difficulties of polishing to the optical quality required for etalon flats have not yet been overcome. (Yates 1966). However, during the past few years such enormous advances have been made in producing extremely high quality flats that it is quite possible that as demands arise, corresponding improvements will be made in the techniques for polishing materials such as LiF.

For interference filters the demands on the optical finish of the substrate are not so critical since the evaporated reflecting and spacer layers contour the substrate surface (Tolansky 1960). In this application, LiF and sapphire may be used as substrate material to extend the spectral range of interference filters below the absorption limit of 'Spectrosil'. Techniques for measuring the transmission characteristics of filters are easier than those involved in the measurement of optical properties of coatings and the author has been fortunate to obtain the use of vacuum monochromators (at Imperial College and the U.K.A.E.A. Culham Laboratory) to determine filter characteristics to λ 1500 Å (Chapter 6).

The extension of the spectral range of the interferometer by the few hundreds of Angstroms covered in this investigation is an important advance in its development since this range of wavelength is equivalent to an energy range in excess of that covered by the whole of the visible spectrum. However before other aspects of the present investigation are discussed it is convenient at this point to briefly consider the elementary theory of the etalon.

1.5. The Elementary Theory of the Etalon.

The interferometer consists of two transparent plates of which the faces are, in principle, perfectly flat, smooth and parallel and are coated with reflecting layers of reflection coefficient (R), transmission coefficient (T) and absorption coefficient (A) (Fig.1.1.).

An incident ray at an angle of incidence θ suffers multiple reflections at the two surfaces and the transmitted rays which emerge

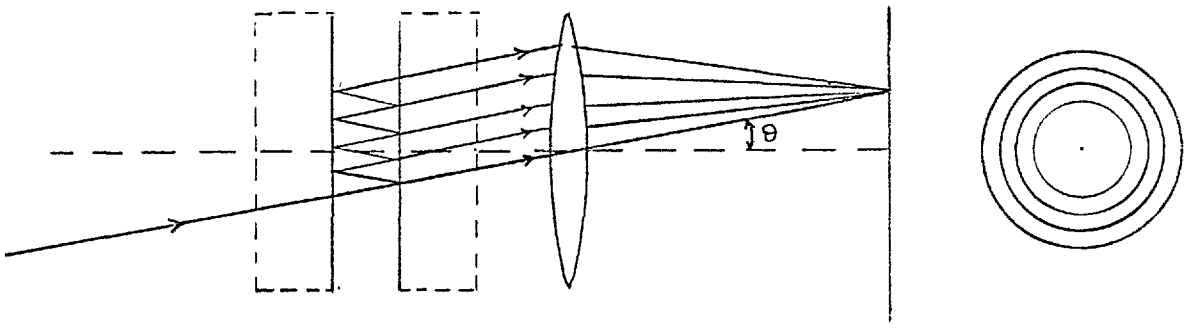

FIG. 1.1. THE F-P INTERFEROMETER

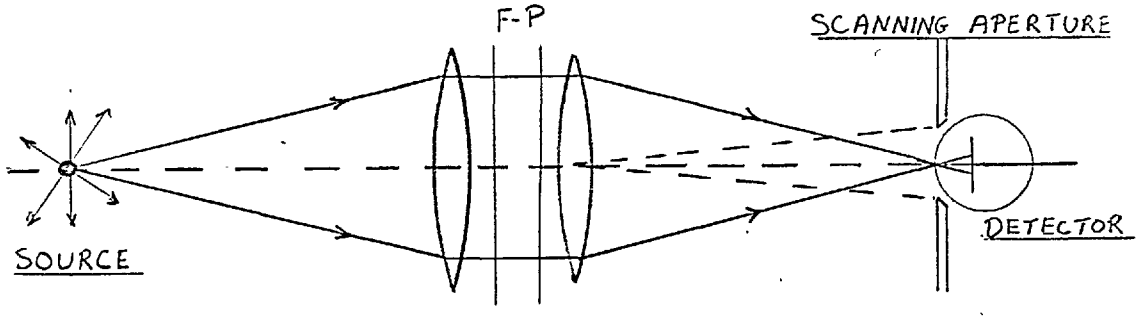

FIG. 1.2. SCHEMATIC DIAGRAM OF THE F-P. SPECTROMETER

parallel to each other are brought to focus by a converging lens. The optical path difference between successive transmitted rays is $2\,nt\,\cos\theta$ where t is the separation of the reflecting surfaces and n the refractive index of the medium between them.

The condition for constructive interference is

$$2\,nt\,\mathrm{Cos}\,\theta = m\lambda = m/\sigma \qquad 1.1.$$

where m is an integer (the order of interference) and λ the wavelength of the incident light (σ = wave number). The etalon therefore acts as a wavelength filter and monochromatic light from an extended source gives rise to circular fringes of equal inclination; all light incident along the surfaces of cones of semi-angle θ contributing to form a circular fringe when

$$2\,nt\,\mathrm{Cos}\,\theta = m\lambda$$

The intensity distribution at the focal plane of the lens is given by the Airy formula (e.g. Born and Wolf 1964)

$$\frac{I}{Io} = \frac{T^2}{(1-R)^2} \quad \frac{1}{1+\frac{4R}{(1-R)^2}\,\mathrm{Sin}^2\frac{\delta}{2}} \qquad 1.2.$$

where $\delta = \frac{2\pi}{\lambda}\,2nt\,\mathrm{Cos}\,\theta = 2\pi\sigma 2nt\,\mathrm{Cos}\,\theta.$

and Io is the intensity of the incident light.

As $\mathrm{Sin}\,\delta/2$ varies between 0 and 1, then the intensity varies continuously between its maximum value $T^2/(1-R)^2$ and its minimum value $T^2/(1+R)^2$. If A is zero then R + T = 1 and I/Io is unity for $\mathrm{Sin}\,\frac{\delta}{2} = 0$; but otherwise

$$\frac{I}{Io} = \frac{1}{(1+A/T)^2}.$$

This effect of coating absorption is considered further in Chapter 2.

The relationship between fringe radius and order of interference is readily obtained from

$$m = m_o \cos\theta$$
$$= m_o (1 - \theta^2/2) \quad \text{since } \theta \text{ is small} \qquad 1.3.$$

If the order of interference of the p^{th} ring from the centre of the fringe pattern is

$$m = m_o - p$$

then the angular radius of the p^{th} ring is

$$\theta = \left(\frac{2p}{m_o}\right)^{\frac{1}{2}} \qquad 1.4.$$

and the radius of this ring is

$$R = f \left(\frac{2p}{m_o} \right)^{\frac{1}{2}} \qquad 1.5$$

where f is the focal length of the lens used to bring the parallel rays to a focus.

It is seen from equation 1.1. that the wavelength interval between successive maxima is given by

$$\Delta\lambda = \frac{\lambda^2}{2\,nt\cos\theta}$$

and this wavelength interval is called the 'free spectral range'. (expressed in wave numbers $\Delta\sigma = 1/2\,nt\cos\theta$). Also from equation 1.1. it can be shown that the angular dispersion $d\theta/d\lambda = 1/\lambda\tan\theta$ and is therefore infinite at the centre of the fringe pattern ($\theta = 0$). The significance of this high dispersion for small θ will become apparent in later sections of this thesis.

The elementary theory of the etalon is somewhat insufficient to explain completely the intensity distribution in the fringe pattern. This will be considered in more detail in Chapter 2.

1.6. The Photographic Use of the F.P. Interferometer.

In the spectrographic method of using the etalon the optical path difference $2nt\,\mathrm{Cos}\,\theta$ depends on the inclinations θ. Different radiations of the spectrum are transmitted in different directions and a photographic emulsion placed at the focal plane of the camera lens records a series of circular fringes for each radiation, according to $\mathrm{Cos}\,\theta = m\lambda/2nt$. For two close lines separated by a wavenumber difference $d\sigma$, the corresponding fringes will be separated by a fraction of an order dm such that

$$d\sigma = dm/2nt\,\mathrm{Cos}\,\theta$$

Various methods for evaluating the quantity dm from measurements made upon the fringes have been discussed in some detail (e.g. Tolansky 1947).

1.7. Photoelectric Spectrometry Employing the F.P. Interferometer.

In this application of the interferometer the photographic emulsion is replaced by a photoelectric detector placed behind a suitable diaphragm. This diaphragm isolates a region of the focal plane which receives rays of the same wavelength. Since the etalon behaves as a wavelength filter, the wavelength transmitted can be altered by variation of $2\,nt\,\mathrm{Cos}\,\theta$. This may be acheived by varying θ (i.e. translation of the ring pattern in front of the diaphragm) or by varying the optical thickness

nt (expansion and contraction of the ring pattern in front of the fixed diaphragm).

1.8. Exploration of the Spectrum.

Many different methods have been suggested for exploring i.e. scanning the spectrum employing the interferometer. One method, namely that of the pressure scanning system of Jacquinot and Dufour (1948) has already been briefly mentioned. The subject matter of this thesis is not intimately connected with a scanning interferometer but in a later chapter a comparison will be made between the use of the etalon with an electron-optical image detector and a fast scanning F.P. spectrometer for time-resolved spectroscopy.

The most satisfactory method for scanning, where time resolution and repetition rate of scan are of importance, is that in which the separation of etalon plates (t) is varied. A displacement of one of the plates by an amount $\lambda/2$ is sufficient to explore the free spectral range at all wavelength resolutions. The major difficulty in developing 'oscillating' F.P. interferometers has been that of maintaining plate parallelism during scanning. An electromechanically driven scanning interferometer discussed by Tolansky and Bradley 1959, Bradley (1961), (1962) enabled the free spectral range to be explored in a time of 10^{-4} secs whilst the finesse was maintained better than 25. More recently, a system has been devised in which scanning is acheived by the rapid extension and contraction of a piezo-electric tube to which one of the interferometer plates is attatched. (Cooper and Greig 1963). This instru-

ment is reported to have an ultimate time resolution $\sim 10^{-7}$ secs. Further developments in this field include a piezo-electric scanning interferometer with automatic control to maintain parallelsim during scan (Ramsey and Mugridge 1962.). Details of scanning interferometers and the relative merits of these instruments have been given by Bradley (1961) and Greig (1965).

1.9. Further Aspects of the Present Investigation.

The oscillating F.P. interferometer has proved to be a very powerful tool in time-resolved spectroscopy particularly for the diagnostics of plasma discharges. In a plasma source the physical conditions are changing considerably during the discharge and the recording of radiation without time scan is not in general very enlightening. Studies of the shape of emission lines can yield information on the ion temperature (Doppler broadening), electron number density(Stark broadening) or the magnetic field (Zeeman effect). The application of the piezo-electric driven interferometer to electron density determinations has been discussed by Peacock, Cooper and Grieg (1964). Profiles of hydrogen and helium lines in a critically damped Z pinch were recorded in times of 10^{-6} secs with an etalon finesse of about 10.

A disadvantage of the oscillating F.P. is that time and wavelength dispersions are superposed. It is therefore necessary to scan at a rate N times greater than the rate of change of the phenomena studied (N being the etalon finesse, Chapter 2) which leads to a decrease in the signal-noise ratio obtainable with a given source and in addition does not permit

continuous monitoring. Moreover, since a point source is utilised simultaneous time and spatial resolution of the source cannot be obtained.

With the development of Q - spoiled laser systems (McClung and Hellwarth 1963) with outputs lasting $\lesssim$20 nsec and spectral widths <0.01 cm^{-1} (Bradley et.al. 1964), time resolved interference spectroscopy in the nanosecond region is now required. For such time resolutions the moveable interferometer plate would have to be oscillated at very high speeds. For example, to scan one free spectral range in a time of 1 n.sec requires a velocity of the plate $\sim 10^4$ cm sec^{-1}. At these speeds, time sequential spectral scanning results in a distorted recorded profile because of Doppler shifts at the moving mirror. Other limitations of the scanning interferometer applied to time resolved spectroscopy are considered in Chapter 7.

The development of image intensifiers (McGee 1961) combining the high quantum efficiency of photocathodes with the information capacity of the photographic plate have opened up new possibilities for time resolved interference spectroscopy.(Malyshev, Razdobarin and Sokolova, 1963). In chapter 7, the F.P. interferometer and image intensifier combination is discussed which overcomes many of the limitations of the oscillating instrument and the results of preliminary investigations of the potential performance of this combination are given. Also in Chapter 7, a general account is given of the employment of the interferometer with electron-optical image detection for interference spectroscopy in the far ultraviolet.

Finally, in Chapter 8 some consideration is given to a new application of the interferometer, namely that of its use for solar and stellar spectroscopy from space vehicles. Because of its very high angular dispersion the interferometer should permit, for a given resolving power, greater tolerance in the guidance requirements of the space vehicle. In addition, there is the added profit of physical compactness arising from the use of the etalon spectrometer or spectrograph. The superior luminosity and illumination of the interferometer can be exploited to give shorter exposure times and greater time resolution. This would allow for example, a greater spatial coverage of the solar disc to be made in the limited observation time during a rocket flight.

With the type of coatings developed in the present investigation it should now be possible to undertake high resolution studies of the solar Fraunhofer spectrum down to λ 1800 Å. Also of course, the interferometer will permit absolute wavelength determinations to be made. Used Photographically, it will be possible to determine the shape of particular line profiles and simultaneously, their variation across the solar disc. This is a problem of particular importance. In addition, a scanning interferometer could be employed to determine time-resolved line profiles at particular points on the solar disc.

Two experiments are already in progress in which the interferometer will be used in both the spectrographic and spectrometer methods to study profiles of the resonance lines of Mg II (2795, 2802 Å). These experiments are briefly discussed in Chapter 8. The first of these experiments requires a very stable fixed gap interferometer and in Chapter 8, the

development of an optically contacted etalon is described which remains stable in adjustment over very long periods of time.

1.10. The Aims and the Development of the Present Investigation.

It is apparent from the previous sections that the work covered in this thesis embraces several different fields of study. It will perhaps assist the reader if the relationship between these different topics and the development of the present project is traced out.

The work was begun in February 1962 in the Applied Physics Dept. (Prof.J.D. McGee) at Imperial College under the supervision of Dr. D.J. Bradley. Very broadly, the initial aims of the project were two fold:-

(1) To investigate the image intensifier - F.P. interferometer combination for time-resolved spectroscopy and for far ultraviolet spectroscopy.

(2) To extend the spectral range of the interferometer and the techniques of multiple-beam interferometry as far as possible into the ultraviolet (for space research applications and for plasma and laser source diagnostics) by developing suitable reflecting coatings. This aspect of the work was a natural development to the investigations of Hass and co-workers on opaque aluminium - MgF_2 films and on improved semi-transparent aluminium films.

In the early stages of this programme it was not foreseen that the techniques of preparation and the optical properties of the interferometer coatings would have quite such an impact on the production of interference filters for the far and vacuum ultraviolet. This was fully realised early

in 1963 following the publication in December 1962 by Schroeder who discussed the feasibility of producing aluminium - MgF_2 filters for this spectral region. With the first promising results of coating and filter properties the author's investigation swung more in this direction. It was decided in mid-1963 to design and construct a new coating plant giving much improved vacuum conditions over that used for the initial investigations, in an attempt to improve on the optical properties of the filters and coatings. Results of investigations obtained using the two different conditions for preparation are compared and contrasted in Chapter 6. In addition, the optical properties of coatings of the type developed in this investigation have been computed from extrapolated optical constants to give a comparison with experimental data (Chapter 4).

In late 1962 and early 1963 investigations were carried out concurrent with the work on coatings on the use of the interferometer with different types of image intensifier for time-resolved spectroscopy. The technique used was a simple one employed merely to illustrate the potential of the method and to enable a rapid assessment of performance to be made. This work was started by the author and continued by C.O.L. Juulman who undertook most of this investigation. Some results of this investigation, which are given in Chapter 7, show that the technique is indeed a powerful one ideally suited to time-resolved examination of plasma and laser sources. This aspect of the work has been further developed with much success by using the image tube as an optically active element. (Bradley and Majumdar 1966)

The construction of an image intensifier with ultraviolet transmitting

window (S.Majumdar) and the development of the ultraviolet coatings enabled the author to obtain F.P. interferograms of λ1849 Å of Hg I (Feb 1964). These were the first interferograms reported for $\lambda < 2000$ Å. An additional project, although one which has not yet seen fulfillment, was concerned with the development of an image intensifier with a 'solar blind' CsI photocathode. The CsI cathode responds only to radiation shorter than ~2000 Å and would therefore eliminate the effects of stray light of longer wavelengths which so often are an undesirable feature of vacuum ultraviolet spectroscopy. The usefulness of such an image tube is made apparent from the interferograms of λ1849 (Hg I) obtained by direct photography using interference filters to isolate this line. For in this case the more intense λ2537 radiation causes a background to the 1849 Å fringe pattern which could be eliminated by using a tube with a Cs I cathode. In view of the promise of such a device for ultraviolet interference spectroscopy it is hoped that difficulties encountered (Majumdar 1966) will be overcome and that it will be possible to continue this work. More generally, the image intensifier applied to ultraviolet interference spectroscopy permits conversion of the incident radiation to a visible output. The advantages of this process are illustrated and discussed in Chapter 7. In addition for a given spectral resolving power the large angular dispersion of the interferometer reduces the demands made on the linear resolution of the detector. This is important for space research applications if image tubes including T.V. camera tubes are to be employed and the potential of the interferometer combined with a simple image tube is illustrated in Chapter 7.

The emphasis of the author's work in the latter part of this investigation shifted more towards space research applications of the interferometer. This followed the proposals by Dr. D.J. Bradley for two experiments to study solar Mg II resonance lines employing Skylark rocket flights utilising the servo-guidance system developed by U.K.A.E.A. (Culham Laboratory). Some considerations of the design of the first of these experiments and the use of the interferometer for space research applications are given in Chapter 8.

Published Reports.

Some of the contents of this thesis has already been published or submitted for publication in a condensed form.

Bradley, Bates and Juulman (1963)

Bradley, Bates, Juulman and Majumdar (1964 a); (1964 b); (1964 c).

Bradley, Bates, Juulman and Kohno (1966).

Bates, Bradley, Kohno and Yates (1966).

Bates and Bradley (1966 a); (1966 b).

CHAPTER 2.

THE RELEVANT THEORETICAL BACKGROUND OF THE F.P. ETALON AND F.P. INTERFERENCE FILTERS.

2.1. Introduction.

The purpose of the F.P. spectrometer and spectrograph is to produce a recorded spectral profile which gives a representation of the variation of luminous intensity with wavelength of a source under examination. However, because of distortions introduced by both the dispersing element and the detecting system employed, this representation is not perfect. It is found that when the recorded profile is made a progessively closer copy of the true spectral profile, that is when the resolution of the instrument is increased, then the amount of light flux falling on the detector becomes progressively smaller. There is therefore, a compromise to be made between the properties of resolution and luminosity and this is also true of spectroscopic instruments employing prism and grating dispersers. Jacquinot (1954) has compared the properties of different types of spectrometer and has shown that for equal areas of dispersing element and for the same resolving power the luminosity of the F.P. spectrometer can greatly exceed that of a grating instrument which in turn is much superior to spectrometers employing prism dispersers.

The departure of the F.P. interferometer from ideal performance, that is the performance represented by the Airy function (Chapter 1), has been the subject of several investigations in particular by Chabbal (1953),(1958). Chabbal has discussed in great detail the dependence of the properties of

resolution and luminosity of the F.P. spectrometer on the quality of the reflecting surfaces and the optical flats of the etalon. Such detail is not required here. In this chapter the main emphasis is simply to illustrate how the performance of the interferometer and the transmission characteristics of F.P. type interference filters are dependent on the properties of the reflecting surfaces, since in a later chapter the optical properties of coatings for the far ultraviolet are given and their application to multiple-beam interferometry in this wavelength region is discussed.

2.2. Spectral Resolution.

The property of resolution of a spectroscopic device is completely determined by the representation it gives of a perfectly monochromatic spectral line. If the total luminance of the source

$$\int_0^\infty B(\sigma)\, d\sigma$$

is located in a wave number interval of zero width (i.e. $B(\sigma) = \delta(\sigma - \sigma_o)$; δ being the Dirac function) then the spectral profile of this line yielded by the instrument is spread out over a small wave number interval described by the function

$$Y = W(\sigma - \sigma_o)$$

where $W(\sigma - \sigma_o)$ is defined as the 'Instrument function' and σ_o is the wavenumber corresponding to the centre of the spectral line.

Thus, if the instrument is illuminated by radiation of spectral density $B(\sigma)$ (the source function) then the spectral profile produced by the instrument differs from the source function according to

$$Y(\sigma) = \int_{0}^{\infty} W(\sigma - \sigma_o) \; B(\sigma_o) \; d\sigma_o$$

The function Y is obtained from the convolution of the instrument function with the source function and may be written symbolically as

$$Y(\sigma) = W(\sigma) \ast B(\sigma).$$

The area of $Y(\sigma)$ is equal to the product of the areas of $W(\sigma)$ and $B(\sigma)$ and the halfwidth (y) of the function Y is dependent on the halfwidth and the form of the functions B and W.

As the width w of the instrument function becomes smaller in comparison with the variations in the source function then the spectral profile yielded by the instrument resembles the source function more and more closely.

Two monochromatic lines may be considered to be resolved when their wavenumber separation $(\sigma_2 - \sigma_1)$ exceeds a certain valve $\delta\sigma$, the effective limit of resolution. The relationship between $\delta\sigma$ and w depends on the criterion adopted for resolution, on the form of the instrument function and also on the definition of the width of the instrument function. Jacquinot (1960) has used the relation $\delta\sigma = w$ as a criterion of resolution and defines w to be the width at half height of a Gaussian curve or the separation between maximum and first zero of a diffraction curve.

2.3. A More Detailed Theory of the Etalon.

The representation of a spectral profile yielded by the F.P. spectrometer would be perfect if the detector received only radiation according to the equation

$$2\,nt\,\mathrm{Cos}\,\theta = m/\sigma$$

t being the separation of the reflecting surfaces, n the refractive index of the medium between these surfaces and θ the angle of incidence of the radiation falling on the etalon.

For this to be realised the following conditions would have to be fulfilled:-

a) The plate separation t at all points over the utilised area of the etalon is constant.

b) The Airy function is zero for all wavenumbers except those given by the above equation.

c) All rays arriving at the detector after passing through the etalon come from the same angle of incidence. θ.

In an actual instrument each of these conditions is unfulfilled and they all contribute to a certain degree, to the instrument function (W) thus setting a limit to the spectral resolution. The degree of the contributions (a) and (b) is now considered following Chabbal. The contribution (c) arising from the finite width of the scanning diaphragm when a photo-electric detector is employed or from the finite grain size of the photographic plate in photographic detection need not be considered here. This contribution is discussed fully by Chabbal.

2.3.1. The Airy Function.

For perfect interferometer flats which are also in perfect adjustment for parallelism, the optical path difference between succesive interfering beams is

$$\Delta = 2\,nt\,\cos\theta \quad .$$

If the reflection coefficient of the coatings was unity and if the plates were sufficiently large so that no beams were lost then there would be an infinite number of interfering beams each having an amplitude of unity. In such a case, interference would be destructive for all wavenumbers except those satisfying the relationship

$$\sigma m = \frac{m}{\Delta}$$

Under these conditions, the instrument function would be represented by a series of infinitely sharp peaks of the form

$$W = \sum_{0}^{\infty} \delta(\sigma - \sigma m)$$

and the peaks would be separated by a wavenumber inerval given by

$$\Delta\sigma = \frac{1}{\Delta} = \frac{1}{2\,nt\,\cos\theta}.$$

This wavenumber interval is the 'free spectral range'.

Since of course the coating reflectivity must be less than unity, the instrument function is given by the Airy function (e.g. Born and Wolf 1964).

$$\frac{I}{Io} = A(\sigma) = \left(\frac{T}{1-R}\right)^2 \frac{1}{1 + \left(\frac{4R}{(1-R)}\right)^2 \sin^2 \pi\sigma\Delta} \qquad 2.1.$$

where R and T are the reflection and transmission coefficients of the

coatings.

The half intensity width (a) of any particular fringe in the transmitted intensity distribution (expressed in wavenumbers) is the half intensity width of the Airy function and is given by

$$a = \Delta\sigma \frac{(1-R)}{\pi R^{\frac{1}{2}}} = d\sigma.$$

Thus 'a' is dependent only on the free spectral range (hence plate separation) and the coating reflectivity. A value N_R can be defined such that

$$d\sigma = \frac{\Delta\sigma}{N_R}$$

where $N_R = \pi R^{\frac{1}{2}}/(1-R)$.

is termed the 'reflection finesse' of the etalon coatings and is clearly a measure of the optical resolution attainable with the etalon. The dependence of N_R on R is shown in figure 2.1.

The transmission of the fringe maximum has the value from equation 2.1.

$$\mathcal{T}_A = \frac{I_{MAX}}{Io} = \frac{T^2}{(1-R)^2}$$

$$= \frac{1}{(1 + \frac{A}{T})^2} \qquad 2.2.$$

This value differs from unity simply because of absorption (A) in the reflecting coatings. There are two effects of this absorption in the reflecting layers:-

1) It reduces the maximum value of R and hence N_R since $R + T + A = 1$.

2) It reduces the value of $\mathcal{T}_A$. For a given reflectivity and hence N_R, film absorption reduces the value of $\mathcal{T}_A$ in the manner shown in figure 2.2.

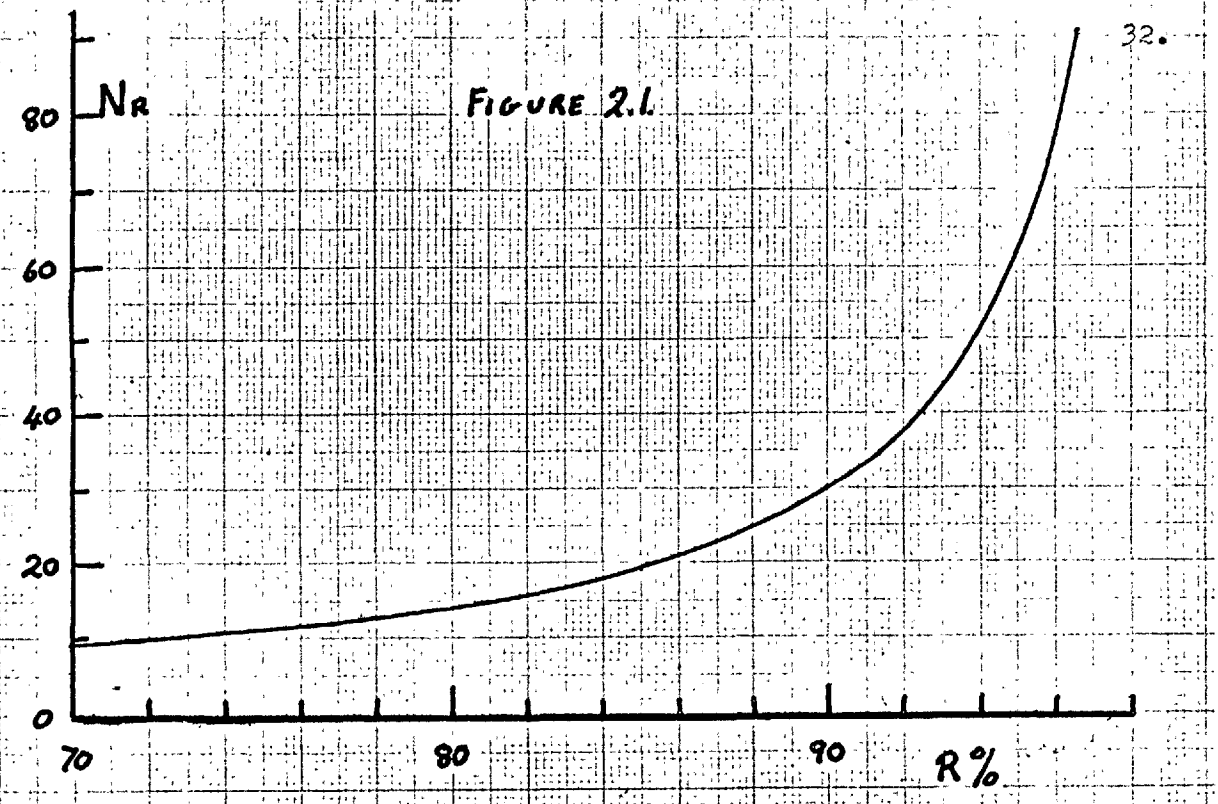

FIGURE 2.1

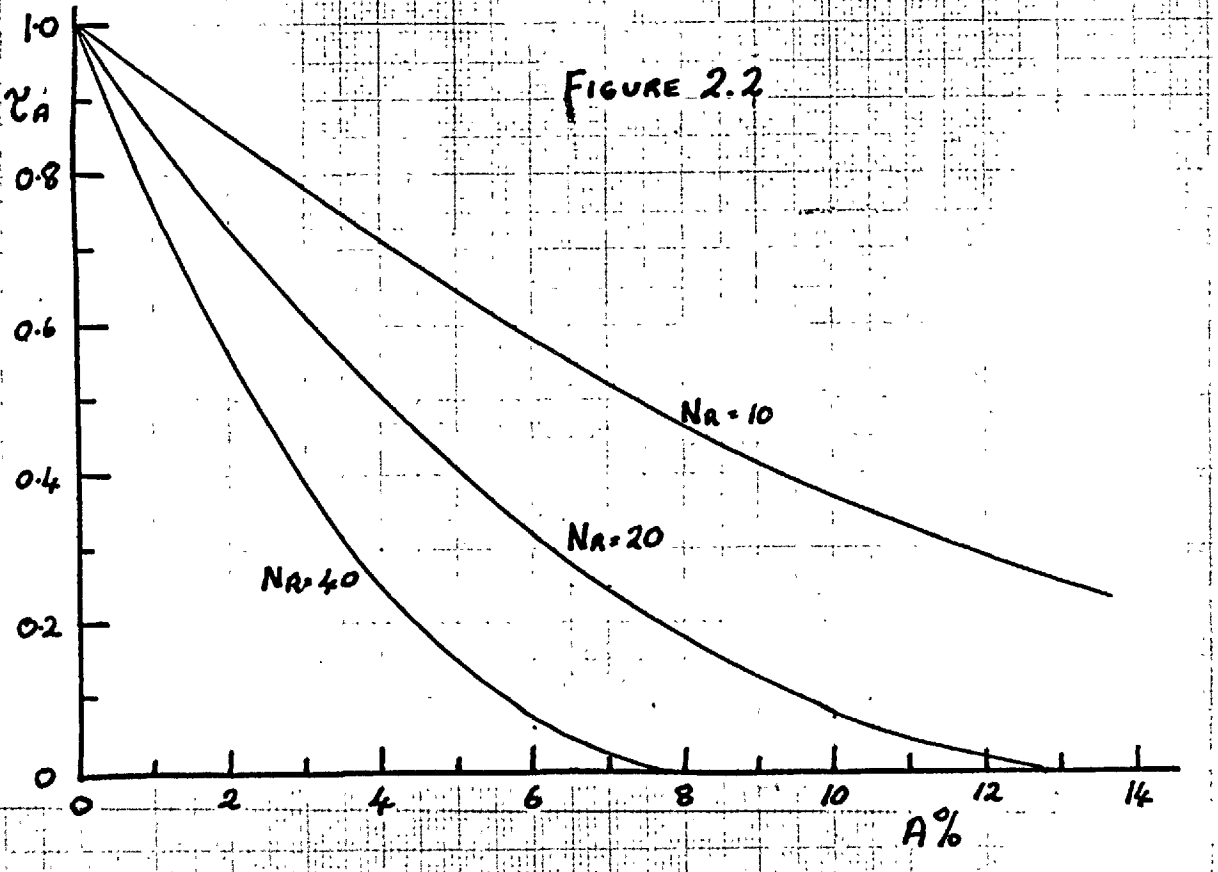

FIGURE 2.2

It is the problem of absorption in the reflecting coatings which has been the major obstacle in extending the spectral range of the F.P. interferometer and of F.P. type interference filters into the far ultraviolet. In later chapters the method of preparation and the properties of improved coatings for extending this spectral range down to wavelengths of 1800 Å are described.

2.3.2. Imperfections of the Etalon Plates.

In practice the interferometer plates are not perfectly flat, perfectly smooth and in perfect adjustment and as a consequence there is a contribution to fringe broadening arising from each of these defects. When such defects occur the optical path length over the aperture of the etalon is not constant. Therefore the equation 2.1. does not coincide for all surface elements within the utilised aperture of the etalon and the fringes are broadened. Since the energy is now distributed over wider fringes then the peak fringe intensity is necessarily reduced.

The effect of plate imperfections can be calculated by assuming that all the irregularities occur in one etalon plate and the second plate may be considered to be perfect. The area of the etalon S may be divided into a number of small elements in which the plate separations (t) vary from one element to another. Then the assembly of elementary etalons with separations in the range $(t + x)$ to $(t + x + dx)$ which are associated with wavenumbers in the range $(\sigma - \sigma')$ to $(\sigma - \sigma' - d\sigma')$ has an area dS which can be characterised by a distribution function

$$dS = D(\sigma')\, d\sigma'$$

where D (σ') is the 'surface defects' function. Chabbal has derived formulae for D (σ') for each of the three major plate defects; spherical curvature, surface irregularities and lack of parallelism. The results of Chabbal's analysis are as follows:-

Spherical Curvature.

The plate curvatures met in practice are small and can be approximated to spherical curvature, If the departure from flatness is by an amount X_1 (fig. 2.3.(a)) then the defects function for this imperfection is a rectangular function. The width of this function expressed in wavenumbers ($d\sigma_1$) can be given in terms of a 'defects finesse' characteristic of this defect and the free spectral range. Thus,

$$d\sigma_1 = \frac{\Delta\sigma}{N_{D_1}}$$

The value of N_{D_1} is dependent on the value of the sagitta X_1 and is $N_{D_1} = \lambda/2\ X_1$. It is usual to express the plate flatness to a fraction of a wave such that the sagitta $X_1 = \lambda/n_1$ in which case the value of N_{D_1} becomes

$$N_{D_1} = n_1/2.$$

Surface Irregularities.

Etalon flats suffer from surface micro-defects which may be assumed to be random and to follow a Gaussian distribution.

If the r.m.s. deviation from smoothness is $\sqrt{X_2^2}$ and if this is expressed as a fraction of a wave λ/n_2 then the width (in wavenumbers) of the function characterising this type of defect is

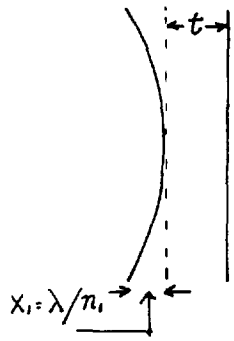

FIG 2.3 a

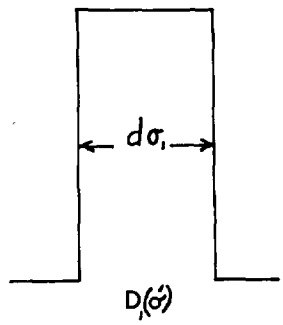

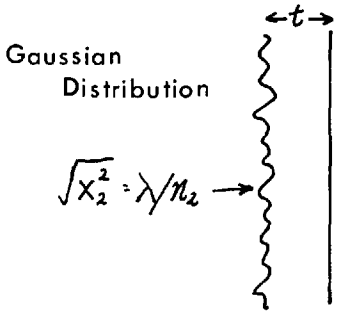

FIG 2 3 b

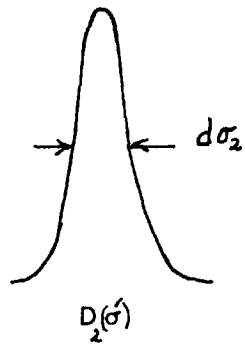

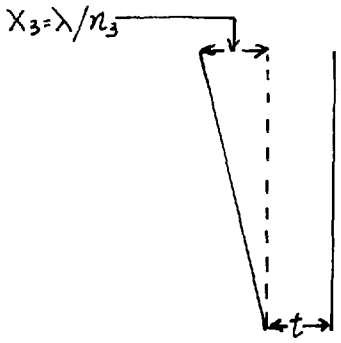

FIG 2.3 c

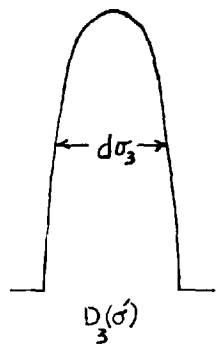

$$d\sigma_2 = \frac{\Delta\sigma\sqrt{32 \ln 2}}{n_2} \simeq \frac{\Delta\sigma\ 4.7}{n_2}$$

Again expressing this width in terms of a defect finesse then

$$d\sigma_2 = \frac{\Delta\sigma}{N_{D_2}}$$

where $N_{D_2} = n_2/4.7.$

Departure from Parallelism.

The defect function characterising a departure from parallelism is a parabalic function of halfwidth

$$d\sigma_3 = \frac{\sqrt{3}\,\Delta\sigma}{n_3}$$

where the departure from parallelism X_3 is expressed as a fraction of a wave λ/n_3 (fig.2.3.(c)). Again the halfwidth of this function can be expressed in terms of a defects finesse such that

$$d\sigma_3 = \frac{\Delta\sigma}{N_{D_3}}$$

where $$N_{D_3} = \frac{n_3}{\sqrt{3}}$$

In practice the three types of defect will exist simultaneously and although the individual defects functions take different forms they can all be approximated to rectangular functions. To a reasonable approximation the overall defects finesse N_D is given by

$$\frac{1}{N_D^2} = \frac{1}{N_{D_1}^2} + \frac{1}{N_{D_2}^2} + \frac{1}{N_{D_3}^2}$$

Since the width of the resulting defects function is

$$d\sigma = \frac{\Delta\sigma}{N_D}$$

it is apparent that as the coating reflectivity is increased the fringe sharpness approaches a limit dependent on the magnitude of the imperfections of the etalon plates.

The existance of plate defects presents a further difficulty in extending the spectral range of the interferometer into the far ultraviolet. If for example, the major plate defect was plate curvature and if the plates were figured to $\lambda/100$ (λ 5500 Å) then the limiting finesse at the wavelength λ would be 50. However, at a wavelength 1850 Å then the limiting finesse is now in the order of 17. Therefore, the demands on plate flatness, smoothness and their adjustment for parallelism became more stringent when used at shorter wavelengths.

2.4. Resolving Power and Resolution Limit.

It has already been stated that the limit of resolution of the F.P. spectrometer is determined by the width (w) of the instrument function (W) and it is seen that w is dependent on the Airy function (A) and the plate defects function (D). The etalon is then followed by a detecting system from which the final record of the intensity distribution of the fringe pattern is obtained. Again there is introduced a contribution to fringe broadening which can be characterised by a scanning function (F) and which arises in the manner briefly mentioned in section 2.3. For the present work however we are concerned only with the etalon

itself and the scanning function need not be discussed in detail here.

When the etalon is illuminated by a perfectly monochromatic source the resulting intensity distribution will be a series of peaks separated by a wavenumber interval

$$\Delta\sigma = \frac{1}{2\,nt\,\cos\theta}$$

each peak having a half width $d\sigma = W = \Delta\sigma/N$, where N is the overall finesse taking account of both N_R and N_D.

$$R = \frac{\sigma}{d\sigma} = \frac{\sigma}{\Delta\sigma} \times \frac{\Delta\sigma}{d\sigma}$$

$$= 2\,nt\,\cos\theta\,N\sigma$$

$$\simeq 2\,t\,N\,\sigma$$

Thus for a given value of σ the resolving power can be increased by an increase in t or N. Increasing t will reduce the free spectral range. Obviously t must be chosen such that the free spectral range is sufficiently large to avoid overlapping of orders and the value of t is in general set by the particular type of problem under consideration. It is preferable to increase the finesse N but this factor cannot be increased indefinitely because of the inherent limitation N_D.

If the width (f) of the scanning function (F) was zero then the instrument function would be the convolution of the functions A (σ) and D (σ)

$$\text{Thus, } Y(\sigma) = B(\sigma) * A(\sigma) * D(\sigma)$$

$$= B(\sigma) * E(\sigma)$$

where E (σ) is termed the 'etalon function'. For f other than zero

then.

$$Y(\sigma) = B(\sigma) * E(\sigma) * F(0)$$

The following conclusions regarding the halfwidth (e) of the function E can be made in terms of the half widths (a) and (d) of the functions A and D.

a) e is greater than the individual values a and d.

b) e is smaller than a + d

c) $e = \sqrt{2}\, d$ if $a = d$

The width (e) expressed in wavenumbers is simply $e = \Delta\sigma/N_E$ where the etalon finesse N_E depends on N_R and N_D. For a given pair of etalon plates the maximum value of N_D is fixed. The value of N_E/N_D is dependent on the coating reflectivity and the variation of N_E/N_D with N_R/N_D is shown in figure 2.4. for a rectangular and a Gaussian defects function. For very large values of coating reflectivity N_E/N_D approaches the maximum value of unity. Figure 2.4. also shows that for reflectivities beyond the value such that $N_R = N_D$, the variation of N_E/N_D with increasing N_R/N_D is comparatively small. This is considered further in section 2.6.

2.5. Luminosity.

The property of luminosity (L) is defined by the light flux collected by the detector (in the case of the spectrometer) or the flux falling on a spatial resolution element (in the case of the spectrograph) for a source of luminance equal to unity. This luminosity is proportional to the normal area of the output beam (S), the solid angle (Ω) subtended by the output aperture or spatial resolution element) and the transmission

FIG 2.4

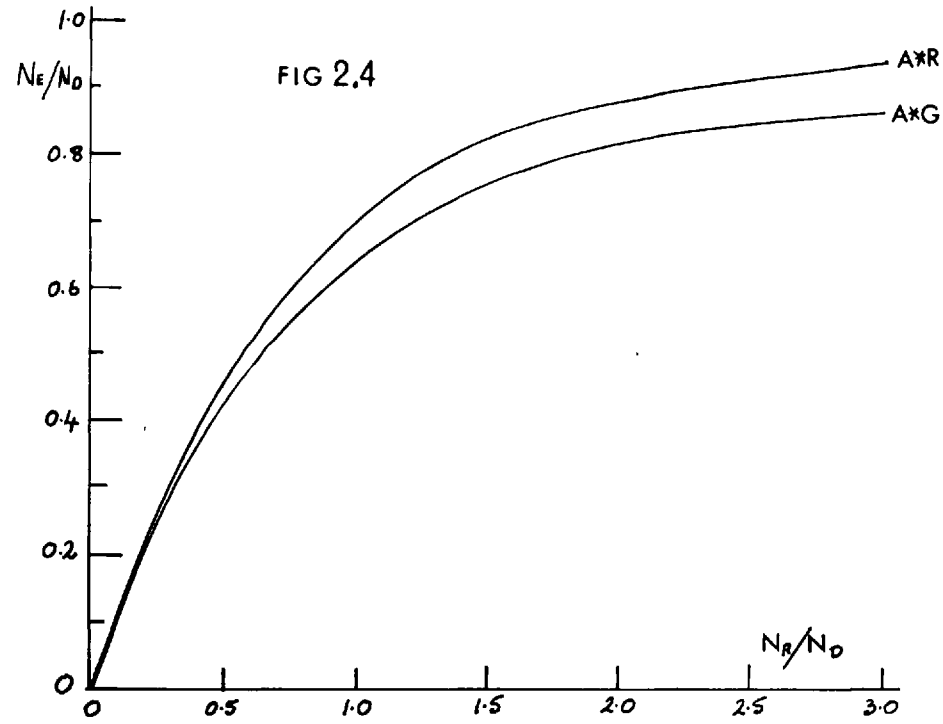

FIG 2.5

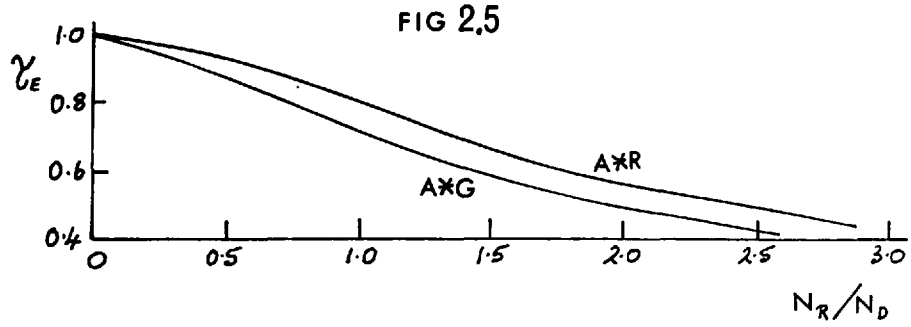

FIG 2.6

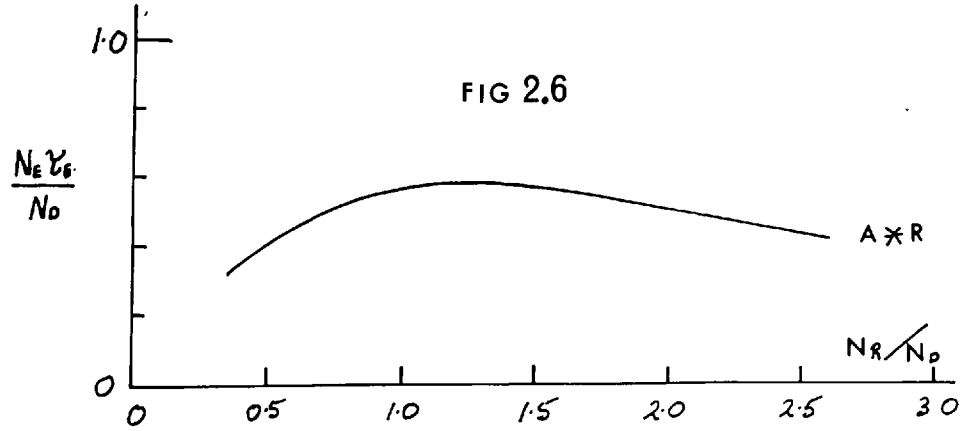

coefficient of the whole system (τ). Thus, the maximum flux passing through the output aperture for a source of luminance B at the wavelength concerned is

$$\dot{Q} = B \tau \Omega S \quad .$$

The transmission coefficient (τ), is itself the product of several factors, and in the case of the F.P. spectrometer is

$$\tau = \tau_A \ \tau_B \ \tau_E \ \tau_F.$$

The factor τ_B arises because the source is not monochromatic and τ_F is the transmission coefficient associated with the scanning aperture. Again Chabbal has treated these transmission coefficients in great detail deriving curves showing the variation of τ_B, τ_E and τ_F with the width of the functions B, E and F. For the present work we are concerned only with the properties of the etalon itself and thus in the factors τ_E and τ_A.

The factor τ_A, which has already been discussed in section 2.3.1, is the maximum fringe transmission given by the Airy function and is

$$\tau_A = \frac{I_{MAX}}{Io} = \frac{1}{(1 + \frac{A}{T})^2}.$$

This would be the maximum fringe transmission if the etalon plates were perfect in all respects. In such a case the flux per unit solid angle which would pass through an etalon (area S) having perfect flats would be

$$\dot{Q} = B_M \ A_M \ S.$$

where A_M is the peak of the Airy function. (τ_A). Because of plate

imperfections the actual flux is

$$\overset{\rightarrow}{\Phi}_1 = B_M \; E_M \quad S.$$

where E_M is the maximum value of the etalon function. The transmission coefficient τ_E is defined as the ratio of these fluxes and is therefore

$$\tau_E = \frac{E_M}{A_M}$$

$$= \frac{1}{A_M} \int A(\sigma - \sigma_o) \, D(\sigma) \, d\sigma.$$

The value of τ_E is dependent on the form of the functions D (σ) and on the ratio of the widths of the functions D (σ) and A (σ). For perfect etalon plates the width of the function D (σ) is zero and τ_E is unity but otherwise, τ_E is less than unity and its variation with N_R/N_D is shown in figure 2.5. (Chabbal).

2.6. The Choice of Coating Reflectivity.

The properties of resolution and luminosity of instruments employing the etalon are dependent on the ratio of N_R/N_D. Chabbal has made several conclusions regarding the optimum condition for the use of the F.P. etalon. The optimum choice of coating reflectivity for a particular pair of flats having a finesse N_D can be derived from Figures 2.4. and 2.5. It is seen that increasing the reflectivity increases the value of N_E but also causes a reduction in τ_E. Figure 2.6. shows the product $N_E \tau_E$ as a function of N_R/N_D and $N_E \tau_E$ is a maximum for reflectivities such that $N_R \simeq N_D$. Provided N_R/N_D lies between the values 0.75 and 1.75

then associated values of $N_E \tau_E$ are within 90% of the maximum value of this product.

This conclusion is of great importance because as we have already seen, the defects finesse N_D decreases with decreasing wavelength and it is therefore apparent that the demands on the value of the coating reflectivity for optimum use become less critical in the far ultraviolet.

2.7. F.P. Type Interference Filters.

When a F.P. etalon is placed in a parallel beam of 'white' light there is a maximum in transmission for wavelengths (λ) satisfying the relationship.

$$\delta = \frac{2\pi}{\lambda} \; 2 \text{ nt Cos}\theta \; + \; 2(\pi - \beta) \; = 2 \text{ m } \pi . \qquad 2.3.$$

where nt is the optical thickness of the spacer layer separating the reflecting surfaces and β is the absolute phase change on reflection at the spacer—reflecting layer boundary. This phase change is discussed in Chapter 4. In the previous discussion of the etalon the term β has been neglected from the expression for the optical path between the reflecting surfaces since in general t is greater than 1 m.m. If however the optical thickness of the spacer layer is made only one or a few half-wavelengths in thickness then the transmission bands are of low order (m) and become more widely separated in wavelength. For such small optical thicknesses the phase charge term becomes very important.

F.P. interference filters are prepared by evaporating onto a plane substrate the reflecting and spacer layers. In the present work interference filters have been produced for the far ultraviolet which are of

the type aluminium - MgF_2- aluminium and are illustrated schematically in figure 2.7.

If for normal incidence a filter of this type is to have a so called m^{th} order peak at a wavelength λ_o then the optical thickness of the spacer layer (nt) is (from equation 2.3.).

$$nt = \frac{\lambda_o}{2\pi} \left((m-1)\pi + \beta \right). \qquad 2.4.$$

which for an Al-MgF_2-Al filters having a 1st order peak centered on λ 2000 Å ($m = 1$; $\beta = 112^\circ$) gives nt = 622 Å. The equation 2.4. gives the thickness of the spacer layer without ambiguity since it involves the absolute phase change (β) on reflection at the MgF_2 - aluminium boundary strictly defined in Chapter 4 (equation 4.3.).

As in the case of the F.P. etalon there is an upper limit to the useful reflectivity for the reflecting layers which is set by the defects finesse (N_D) arising from variations in the optical separation of the reflecting surfaces over the aperture of the filter. For interference filters however, departures from planeness of the substrate surface on which the filter is prepared are not so critical since the evaporated films contour the substrate surface (Tolansky (1960)). Thus, the variation in optical separation of the reflecting layers can be made much smaller than is possible for the two independently worked flats of the etalon and consequently higher reflectivities may be employed since N_D is correspondingly greater.

If the optical separation of the reflecting surfaces is constant over the utilised area of the filter then the peak transmission (τ)

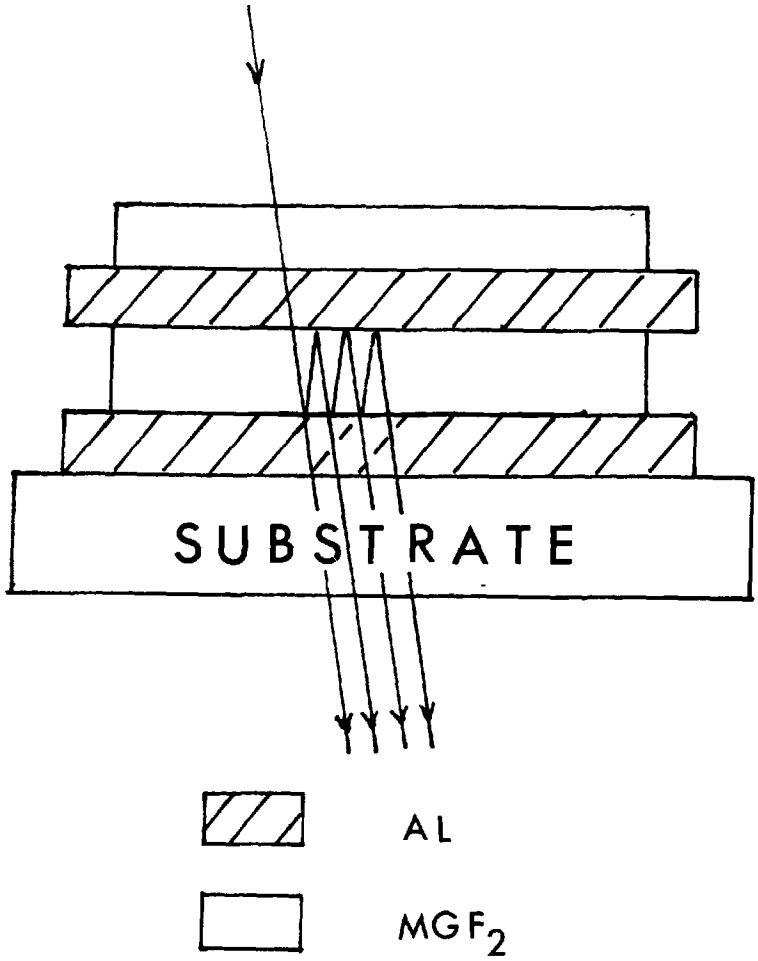

FIGURE 2.7

is given by the maximum value of the Airy function i.e.

$$\tau = \frac{1}{(1 + \frac{A}{T})^2} \qquad 2.5.$$

where as before A and T are the absorption and transmission coefficients of the reflecting layers.

Filter Bandwidth.

The bandwidth of an interference filter is the wavelength interval of the transmission characteristic corresponding to transmissions of half the peak transmission (τ). The phase difference between successive transmitted beams is, in the case of the aluminium - MgF_2 filters

$$\delta = \frac{2\pi}{\lambda_o} 2nt + 2(\pi - \beta) \qquad \text{(normal incidence).}$$

and therefore a change $\Delta\delta$ in δ corresponds to a change $\Delta\lambda_o$ in λ_o given by

$$\Delta\delta = \left[-\frac{4\pi nt}{\lambda_o^2} - 2\frac{d\beta}{d\lambda} \right] \Delta\lambda_o.$$

provided that the dispersion in the spacer layer material can be neglected over this wavelength interval. Substituting for nt from equation 2.4. gives

$$\Delta\delta = \frac{2\pi}{\lambda_o} \left\{ -(m-1)\frac{-1}{\pi} \left(\frac{d}{d\lambda} (\beta\lambda_o) \right) \right\} \Delta\lambda_o$$

The value of $\Delta\lambda_o$ corresponding to the halfwidth value of the Airy function is say $(\Delta\lambda_o)_{H.W.}$ and is given by a change in $\Delta\delta = 4/\sqrt{F}$ where $F = 4R/(1-R)^2$. (see e.g. Born and Wolf 1964).

Then, $$(\Delta\lambda_o)_{H.W.} = \frac{2\lambda_o}{\pi\sqrt{F}\left| (m-1) + \frac{1}{\pi}\frac{d}{d\lambda}(\beta\lambda_o) \right|}.$$

$$= \frac{\lambda_o}{N_R \left[(m-1) + \frac{1}{\pi} \frac{d}{d\lambda} (\beta_{\lambda_o})\right]} \qquad 2.6.$$

In the derivation of this expression for the filter halfwidth it is assumed that the optical thickness of the spacer layer is constant over the utilised aperture of the filter and that the 'defects' finesse can be neglected. Furthermore this expression does not take into account the variation of the reflection and transmission coefficients of the reflecting coatings with wavelength over the range $(\Delta\lambda_o)_{H.W.}$ An assessment of the effect of variation in the optical thickness of the spacer layer can be readily made using equation 2.4. For a first order filter

$$\Delta(nt) \simeq \frac{\beta}{2\pi} \Delta\lambda_o. \qquad 2.7.$$

where $\Delta\lambda_o$ is the shift in wavelength of the transmission peak caused by a variation of optical thickness $\Delta(nt)$. An examination of experimental filters over an area 6 x 5 mm in sections of 6 x 1 mm (the area of sample normally used for determination of filter transmission characteristics), reveals a shift $\Delta\lambda_o$ of 15 Å or less. This implies from equation 2.7. that for $\lambda_o \sim 2000$ Å; $\beta \sim 112^\circ$ the variation in optical thickness (nt) over this area is in the order of 5 Å. For such a small variation in optical thickness, the corresponding defects finesse can be neglected and equation 2.6. may be used to derive the value N_R for the reflecting surfaces.

The second factor to be considered regarding the use of equation 2.6. namely that of the variation with wavelength of the optical properties (R, T and A) of the reflecting coatings, is one which is more difficult

to assess. The transmission of the filter is

$$\tau = \tau_A \frac{1}{1 + F \sin^2 \delta/2}.$$

and equation 2.6. has been derived on the assumption that F is not wavelength dependent. This is not always the case and it will be seen in later chapters that there is a decrease in R and an increase in A and T for aluminium films in the far ultraviolet as the wavelength is decreased. Because of the dependence of the factor F on wavelength the transmission profile for aluminium - $M_g F_2$ - aluminium filters will not be symmetrical about the wavelength (λo) of the transmission peak but will be narrower at wavelengths greater than λo. However, the expressions for the filter bandwidth and peak transmission may be used to permit a useful comparison between optical properties of the reflecting coatings derived from measured filter characteristics and this has been done in Chapter 6.

Schroeder (1962) has used the expression for a 1st order filter

$$(\Delta\lambda o)_{H.W.} = \frac{\lambda o}{N_R}$$

and omits the phase term given in equation 2.6. Thus calculated values of bandwidth given by Schroeder are low on account of the omission of this phase term.

In order to produce a narrow band filter then the reflectivity of the reflecting coatings should be as high as possible. The limitation in increasing the reflectivity is that the coating transmission becomes comparable with and eventually less than the coating absorption and there is a corresponding decrease in the peak transmission of the filter.

In chapter 6 the properties of 1st and 2nd order filters for the far ultraviolet region will be discussed.

CHAPTER 3

REFLECTING COATINGS AND FILTERS FOR THE FAR AND VACUUM ULTRAVIOLET.

3.1. Introduction.

It was shown in Chapter 2 that the properties of resolution and luminosity of the F.P. interferometer and the transmission characteristics of F.P. type interference filters are very much dependent on the optical quality of the reflecting coatings. In recent years, improvements to the quality of reflecting coatings have been an important factor to the general improvement of F.P. spectroscopy, particularly in the visible and near ultraviolet regions of the spectrum.

The optimum conditions for using the etalon require that the reflectivity of the coatings be chosen such that the reflection finesse is approximately matched to the plate defects finesse. In the visible and near ultraviolet this condition can be fulfilled by the use of multilayer dielectric films. In many cases, evaporated silver films may be adequate for the visible region (Bradley 1963) with the added advantage that when necessary these coatings can be more easily removed and fresh coatings applied.

In the ultraviolet, multilayer dielectric coatings are now commercially available down to wavelengths of about 2500 Å. It is below this wavelength that the real difficulties of producing suitable interferometer coatings arise since no high index transmitting material suitable for multilayer dielectric coatings has been discovered so far.

(Apfel (1966) has reported on the use of MgO as a high index material for multilayer films for the ultraviolet to λ 2000 Å. Used with MgF_2 as low index material the ratio of refractive indices is 5:4. In view of this low ratio many $\lambda/4$ layers are required to give a high reflectance stack. For a 27 layer film combination a reflectance of 96.8% was obtained for λ 2200 Å which is higher than any known metal or metal-dielectric combination at this wavelength. Extension of this high performance to wavelengths $<$ 2000 Å is prevented by the rapidly increasing absorption in the oxide film.)

Evaporated aluminium films possess a higher normal incidence reflectance than any other single material in the far and vacuum ultraviolet to wavelengths of approximately 1100 Å and during the past few years there has been much effort devoted to the improvement of the optical properties of such films for this wavelength region. The reflectance of opaque aluminium films has been found to be strongly dependent on many of the factors involved in their preparation. However, even if produced under 'optimum' conditions exposed aluminium films show a deterioration of reflectance with time due to oxidation. Whilst for wavelengths above 2200 Å the effects of a thin oxide layer on reflectance are relatively small (for highest quality films) this is not the case at shorter wavelengths where the oxide layer has an increasingly detrimental effect on reflectance as the wavelength is reduced. Because of this oxidation the practical use of unprotected aluminium films is severly restricted in the vacuum ultraviolet.

The oxidation of an evaporated aluminium film can be considerably

reduced if it is immediately overcoated with a transparent dielectric film. Moreover, if this overcoated layer is of correct thickness then a reflectance enhancement can be obtained arising from multiple interference between waves reflected from the vacuum-dielectric and dielectric-aluminium boundaries. To date, the aluminium-dielectric combination is the most efficient reflector in the vacuum ultraviolet (to about λ 1000 Å) and is now widely exploited.

By comparison with the recent work on opaque films there has been comparatively little study of the properties of partially transmitting aluminium layers in the far and vacuum ultraviolet. A detailed investigation of the optical properties of semi-transparent aluminium films, from which the optical constants of aluminium have been derived, has been made down to a wavelength of 2200 Å. (Hass and Waylonis 1961) These optical constants are used in Chapter 4 for the purpose of computing the properties of an aluminium - MgF_2 film combination. However no such systematic investigation has been made for wavelengths shorter than 2200 Å although the optical constants for aluminium films have been determined at a few isolated wavelengths between 1000 and 2000 Å . (Berning, Hass and Madden 1960).

In this chapter, the parameters involved in the preparation of evaporated aluminium films which have been found to influence the reflectance in the far ultraviolet are discussed, since the results of these investigations have been applied to the present work. The inadequacy of unprotected aluminium films due to oxidation is illustrated and results are given for the aluminium-dielectric film combination showing the much

improved performance over that of single aluminium films. Finally, a brief review is made of both absorption and interference filters for the far ultraviolet.

The emphasis in this chapter is on the type of reflecting films which might provide a basis for coatings for multiple-beam interferometry in the far ultraviolet. This is at present limited in practice to aluminium and aluminium-dielectric film combinations. A considerable number of investigations have been made on single materials and combinations of different materials for reflectors at wavelengths shorter than about 1400 Å. Such materials are outside the scope of the present work but have been discussed in a comprehensive review made by Madden (1963). Also, the present work is concerned largely with wavelengths shorter than 2400Å where multilayer dielectric films are at present impracticable.

In view of this emphasis on wavelengths shorter than 2400 Å, the properties of multilayer dielectric coatings and all dielectric interference filters which are currently employed in the ultraviolet will not be discussed. Much of the earlier work in this field has been reviewed by Jacquinot (1960) but this review is now somewhat dated and no subsequent one appears to have been made. This in part is due to the fact that information regarding the choice of materials, the number of layers and the techniques of preparation of many commercial multilayer films and filters is not readily available.(Bifford 1966).

3.2. The Optical Properties of Semi-Transparent Aluminium Films Prior to the Investigations of Hass and Co-workers.

It is appropriate at this point to briefly consider some of the earlier investigations of the properties of transmitting, evaporated aluminium films in the ultraviolet. This will at least fulfil the purpose of illustrating the progress which has been made during recent years.

Crawford et.al. (1949) noted that the optical properties were dependent on the rate of deposition but this factor was not examined in very great detail. Values of film reflectivity (R) and transmission (T) were measured in the wavelength region 4000 to 2500 Å for films prepared at 'fast' deposition rates (deposition time of 20 secs) and 'slow' deposition rates (deposition time 20 mins to 2 hours). The values of (R + T) obtained for the fast deposition rates were in the range 88% (4000 Å) to 83% (2500 Å). For films prepared at slower rates the (R + T) values were much lower and need not be considered here.

The deposition rate corresponding to the fast evaporation was in the order of 10 to 15 Å sec^{-1}. Compared with the work of Hass and that of the present investigation this would be considered to be a slow deposition.

Burridge et.al. (1953) made a more detailed study of the dependence of optical properties on the deposition time. It was found as above, that the higher optical quality films were associated with the shortest deposition times but again, the deposition rate was comparatively low. The shortest deposition times used were 30 secs corresponding to a

a deposition rate of the order 5 to 10 Å sec^{-1}. The evaporation pressure in these experiments was about 10^{-5} Torr .

However, the optical quality of these films was superior to those of Crawford et.al. whilst the values of (R + T) were found to decrease almost linearly with increasing film transmission. At λ2600 Å, the shortest wavelength of measurement, (R + T) varied between 88% and 91% for films transmitting 10% and 1% respectively. It is not very clear why the optical quality of these films was superior to those of Crawford since the deposition rates and evaporation pressure were closely comparable.

However, this improvement may have been due to improved aluminium purity, substrate cleaning etc which are known to have a considerable influence on optical performance. Full experimental details are not given by the former authors.

It was concluded by Burridge et.al. that the quality of the evaporated film is dependent on the relative rates of arrival at the substrate of the vapour atoms and impurity gas molecules present in the coating chamber. On this basis, it would be expected that improved vacuum conditions and the use of faster deposition rates would lead to an improvement in optical performance. This was indeed found to be the case by Hass and co-workers whose results are discussed in following sections. From the point of view of application to multiple beam interferometry, an analysis of the results of Burridge et.al. shows that at 2600 Å values of $N_R = 20$ with $\mathcal{A} = 10\%$ could be obtained with their aluminium coatings.

Lés and Lés (1962) have also given properties of semi-transparent aluminium to wavelengths of 2900 Å; films were prepared at a pressure of 5×10^{-5}, Torr. Values of (R + T) were found to decrease with increasing film transmission but insufficient data is given to form any conclusions on the dependence of (R + T) with T.

The Optical quality of their films were slightly inferior to those of Burridge et.al. but because of lack of experimental details, in particular that of deposition rate, an explanation for this cannot be readily given. However, a more intersting aspect of this work is that of overcoating an aluminium film (R = 60 to 70%) with alternate layers of MgF2 and PbF2 (see also Lés, Lés and Gabla 1963). In the wavelength region 2600 to 2800 Å the absorption for an aluminium film overcoated with 6 layers of effective optical thickness equal to $\lambda/4$ is only 2.5%. This is roughly one third that obtainable with best quality single aluminium films and is also closely comparable with high quality multilayer films in this wavelength region. (Perkin-Elmer Inc. 1965). The advantages of the metal-dielectric combination over that of all dielectric multilayers for F.P. coatings is that they readily permit visual adjustment of the etalon. Moreover, this type of coating reduces transmission of visible radiation because of the attenuation of aluminium layers at longer wavelengths. This second aspeot might well be of importance for application to ultraviolet spectroscopy from rockets or satellites for additional filtering of visible radiation.

The most detailed investigation so far reported on semi-transparent aluminium films has been that of Hass and Waylonis (1961) in which the

detailed influence of evaporation conditions on optical performance have been considered and measurements of film properties extended to λ 2200 Å. These results are considered in section 3.4. In the following section, the conditions for producing high reflectance opaque aluminium films for the far ultraviolet will be outlined since these conditions form a considerable part of the basis for the development of the coatings produced in the present investigation.

3.3. The Necessary Conditions for Producing High Ultraviolet Reflectance, Aluminium Films.

Since the mid 1950's an extensive programme in far and vacuum ultraviolet reflectance problems has been undertaken by the Engineer Research and Development Laboratory (Fort Belvoir) and the Naval Research Laboratory (Washington). Much of the effort has been centred on the effects of the conditions of preparation on the reflectance of aluminium films. As a result of these investigations there has been a much improved efficiency in the quality of mirror and grating coatings for the vacuum ultraviolet. This of course is of tremendous benefit to spectroscopy in general and it has been a considerable factor in the improvement of speed of recording of ultraviolet spectra obtained from rocket investigations

3.3.1. Aluminium Purity.

The effect of aluminium purity on the reflectance of opaque aluminium films in the wavelength region 900 to 2200 Å has been studied

by Hass, Hunter and Tousey (1957). For wavelengths between 1400 and 2000 Å, films prepared from 99.99% pure material posses a reflectance some 10% greater than films prepared from 99.5% pure aluminium. In the visible region of the spectrum this corresponding difference in reflectance in only some 0.5%.

The main impurities in the deposited film (99.99% purity) were found to be Cu, Fe and Si in the same proportion as in the original material Tungsten wire filaments were used to evaporate the aluminium charge but no trace of tungsten was found in the deposited film.

3.3.2. The Evaporation Pressure and Speed of Evaporation.

These two parameters have a considerable influence on the reflectance of opaque aluminium layers in the vacuum ultraviolet. Figure 3.1. shows the effect of these factors on the reflectance of an opaque film (800 Å thick) deposited in the times indicated (Hass and Tousey 1959).

Again it is seen that the shortest evaporation times yield the highest quality films as found by the authors cited in section 3.2. In this case however, much faster rates of deposition were used up to 400 Å sec^{-1}. For the fastest deposition rates there appears to be little difference in reflectance for films deposited at pressures of 10^{-4} or 10^{-5} torr. However, it should be noted that these films were exposed to the atmosphere for 24 hours prior to measurement and later work shows that below ~ 2000 Å there is a decrease in reflectance occurring only seconds after deposition arising from oxidation. (Madden and Cranfield 1961; Madden et.al. 1963).

FIG. 3.1.

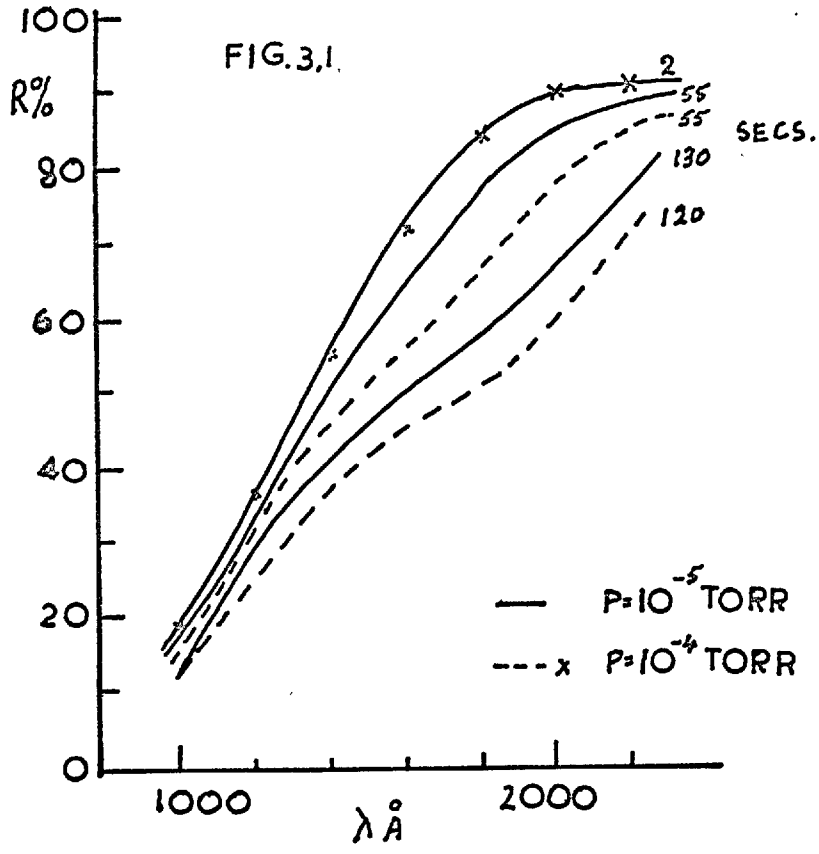
100
R%
80
60
40
20
0
1000
λ Å
2000
2
55
55
SECS.
130
120
P=10^-5 TORR
P=10^-4 TORR

FIG. 3.2.

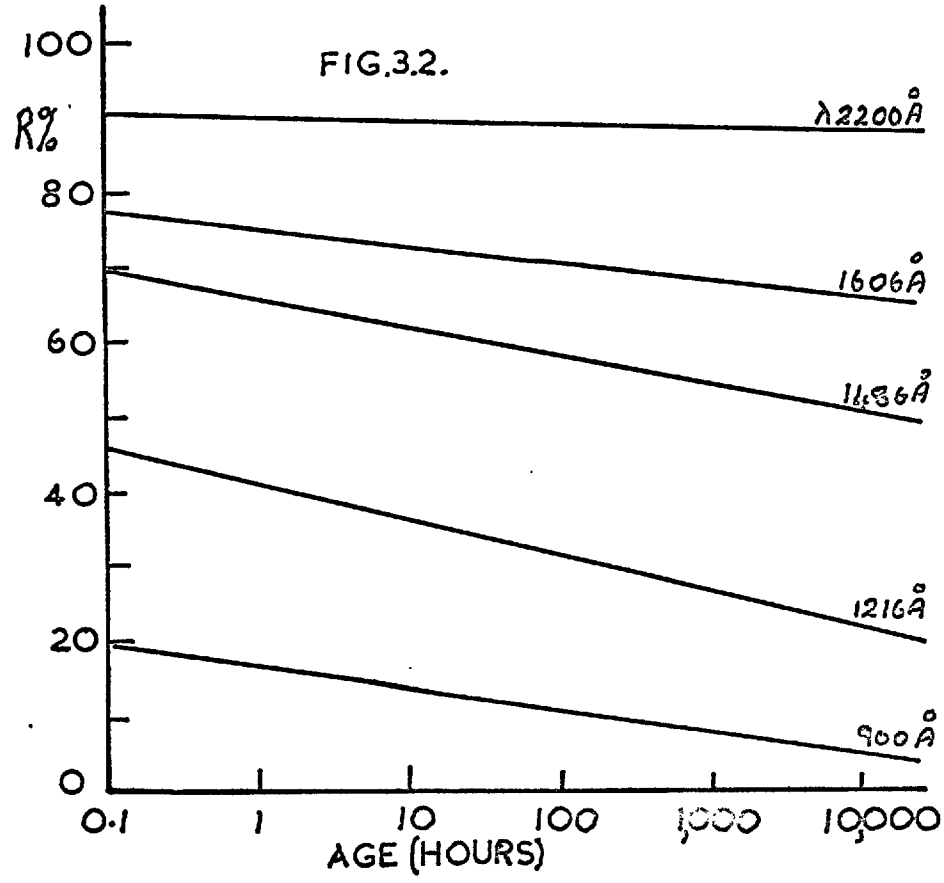
100
R%
80
60
40
20
0
λ2200Å
1606Å
1136Å
1216Å
900Å
0·1
1
10
100
1,000
10,000
AGE (HOURS)

The improved quality of aluminium films deposited at low pressures and high deposition rates is due to the fact that under these conditions fewer oxygen and other residual gas molecules of the coating chamber are trapped in the film; the film is therefore more compact and grows a thinner, tighter oxide layer than those prepared under poorer conditions and lower deposition rates. (Hass and Tousey 1959). Under normal evaporation conditions for film preparation there is ample opportunity for residual gas molecules to be trapped in the growing film. Since the concentration of impurity molecules trapped in the film during deposition depends directly on the evaporation pressure and inversly proportional to deposition rate (Dushman - 1949) it is not surprising that an improved optical efficiency should result from an improvement to these two factors.

A further aspect arises from the effect of deposition rate on the structure of the deposited film. This has not been discussed by Hass and co-workers but it is a factor which is briefly considered in Chapter 6.

3.3.3. Substrate Temperature.

Aluminium like many other materials has an improved adherence if it is deposited onto a heated substrate. With increasing substrate temperature however, crystal size and surface roughness will increase and this can cause a significant drop in the specular reflectance in the far and vacuum ultraviolet. This parameter has been studied by Hass, Hunter and Tousey (1957) who found that if the substrate temperature is raised above about 60°C during deposition then there is an associated decrease in specular reflectance. The reflectance of an opaque film (at λ 2200 Å)

deposited onto a substrate at a temperature of 50°C is 91% whilst the corresponding reflectance for a film deposited onto a substrate at 200°C is only 81%. The effect of substrate temperature on reflectance becomes far more pronounced at shorter wavelengths.

Besides the effect of substrate temperature on the surface roughness and crystallite size of the deposited film it must also be remembered that the oxidation of the aluminium layer will be enhanced as the substrate temperature is raised.(see e.g. Eley and Wilkinson 1959).

During the present investigation the aluminium films and aluminium - MgF_2 double layers have in general been deposited onto a substrate at room temperature. No attempt has been made to make a systematic examination of the effect of substrate temperature on the properties of the transmitting films. It has been observed however that several films deposited onto substrates at a temperature of about 90°C possessed lower values of R and (R + T) by some 2-3% (at λ2200) compared with films deposited onto a non-heated substrate. This difference in optical properties is somewhat greater than corresponding values obtained by Hass and Tousey for opaque films at λ 2200 Å.

3.3.4. The Vapour Angle of Incidence.

The angle of incidence of the vapour stream onto the target substrate can greatly influence the reflectance of aluminium films. This effect has been studied by Hass and Waylonis (1961) who measured for wavelengths down to 2200 Å, the properties of films approximately 600 and 2000 Å thick prepared at vapour angles of incidence of 0°, 30° and 60°. Two sets of

evaporation conditions were chosen

'Optimum' - deposition rate 300 Å Sec^{-1}; pressure 10^{-5} Torr.

'Poor' - deposition rate 10 Å Sec^{-1}; pressure 10^{-4} Torr.

Films of thickness ~ 600 Å prepared under optimum conditions show little variation of reflectance with vapour angle of incidence. This variation increases for thicker films and depends on evaporation conditions in the following manner. (Values of reflectance (%) are given for 2200 Å, the shortest wavelength of measurement).

Vapour Angle of Incidence	0°	30°	60°
t = 600 Å; optimum conditions	91.5	91.4	90.4
t = 2000 Å; optimum conditions	91.2	90.7	75.0
t = 600 Å poor conditions	83.5	82.6	81.4
t = 2000 Å poor conditions	65.9	60.5	31.8

An explanation for the dependence of reflectivity of an aluminium film on the vapour angle of incidence has been proposed by Holland (1956). For a smooth substrate surface the vapour atoms are fairly uniformly condensed over the surface and the nuclei are evenly dispersed. As deposition proceeds and the film thickens then for vapour atoms arriving at high angles of incidence the nuclei tend to grow preferentially in the direction of the incident vapour beam. Condensation is then restricted to the upper surfaces of the grains which further prevent vapour atoms reaching the inter-spaces between grains. The resulting film therefore possesses an irregular surface, the magnitude of the irregularities increasing with the film thickness. Expressions relating the roughness

of a plane reflecting surface to its reflectance have been given by Bennett and Porteus (1961). This analysis shows that the surface roughness has an increasingly detrimental effect on specular reflectance with decreasing wavelength.

For the present work, films of thickness in the order of 200 to 300 Å have been required and vapour angles of incidence have been kept below 8°. For such film thicknesses this vapour angle of incidence should not greatly influence the film properties.

3.4. The Improved Performance of Semi-Transparent Aluminium Films.

Following the improvements in deposition technique Hass and Waylonis (1961) have investigated the properties of semi-transparent aluminium films in the visible and ultraviolet down to wavelengths of 2200 Å. From measurements of film reflectance (R) transmittance (T) and film thickness, the optical constants for aluminium films have been derived from equations developed by Hadley and Dennison (1947).

Films were prepared at an evaporation pressure of 10^{-5} Torr using deposition rates in the order of 100 A Sec^{-1}. The values of (R + T) are the highest reported for semi-transparent aluminium films in the ultraviolet (91.8% at λ 2200 Å).

An analysis of the Hass and Waylonis results shows that for multiple-beam interferometry a reflecting finesse of 20 with a value of $\mathcal{A} \simeq 20\%$ can be obtained at a wavelength of 2200 Å. For the same reflection finesse this is a factor of two in improvement of performance over the results given by Burridge et.al. for a wavelength of 2600 Å.

There are two features of these results which are quite different from previously reported data (section 3.2.). Firstly, the values of (R + T) show only a small variation with wavelength and secondly, the (R + T) values in the far ultraviolet are independent of film thickness. In Chapter 6, the results of Hass and Waylonis will be compared with the results of the present investigation.

3.5. The Ageing Properties of Exposed Aluminium Films.

The change in optical properties of exposed aluminium films is of obvious practical importance. Figure 3.2. shows the decrease in reflectance for films 800 Å thick which were produced under 'optimum' conditions and stored over long periods of time (Hass and Tousey 1959). The reflectance decreases with time in an approximately exponential manner, with a larger rate of decrease in reflectance at shorter wavelengths. This decay was attributed to the growth of an oxide layer on the surface of the aluminium film.

To support this conclusion, calculations of the effect of an oxide layer on the reflectance of aluminium films have been made for a number of wavelengths and the oxidation rate of pure aluminium films in air has been measured (Berning, Hass and Madden 1960). It was found that for films deposited under optimum conditions an oxide layer some 10 - 12Å in thickness was formed in the first hour of exposure. This layer increased in thickness to 15 Å after 1 day and 22 Å after one month. There is little increase in oxide thickness after this period of exposure.

From these results and using the optical constants of aluminium (at λ1216 Å) derived from measurements of reflectance as a function of angle of incidence, a reasonable close agreement was found between measured and calculated values for the decrease in reflectance with time. For wavelengths above 2200 Å the change in reflectance with time was found to be very small but as the wavelength is decreased then a given thickness of oxide has an increasingly detrimental effect on the reflectance.

There are two reasons for this. Firstly, the absorption of the oxide increases at the shorter wavelengths and secondly, the changes in the optical constants of aluminium and its oxide at the shorter wavelengths cause the phase change at the aluminium - aluminium oxide interface to be more conducive to absorption.

The mechanisms suggested for the kinetics of the oxidation of aluminium films have been summarised by Eley and Wilkinson 1959, and the rate of uptake of oxygen by an aluminium film studied as a function of pressure, temperature and film thickness. The experiments showed that at a constant pressure and temperature the oxide layer increased in thickness as a logarithmic function of time in the early stages of growth.

3.6. The Reflectance of Unexposed Aluminium Films.

In the previous section the decrease in reflectance of opaque aluminium films exposed to the atmosphere was considered. Madden et.al. (1963) have made investigations to determine the 'true' reflectance of unexposed aluminium films. The films were prepared at an evaporation

pressure of $\sim 10^{-7}$ Torr at high deposition rates. A reflectometer was constructed such that measurements could be made in vacuum starting some 10 secs after the completion of the evaporation. Results of reflectance as a function of time and wavelength are shown in figure 3.3.

From these curves it is seen that even under these conditions the decay in reflectance is quite rapid at the shorter wavelengths. The effect of admission of oxygen and nitrogen to a pressure of 10^{-3} torr on the reflectance decay curve was also studied at a wavelength of 1216 Å. The admission of nitrogen caused no significant decrease in reflectance but in the case of oxygen, there was a sudden decrease of about 12%. It was concluded from this evidence that the partial pressure of oxygen in the coating chamber was the controlling factor in the rate of decrease in reflectance of aluminium films.

An indication of the true reflectance of unexposed aluminium films can be obtained by extrapolating the curves of figure 3.3. to zero time. It is then found that aluminium possesses a reflectance of 90% or greater from the infra red down to wavelengths of about 1500 Å, if prepared under these stringent conditions previously outlined.

The work of Madden et.al. allows a comparison to be made between measured values of reflectance and calculated values obtained by extrapolating the optical constants determined by Hass and Waylonis to shorter wavelengths (Schroeder 1962, see also Chapter 4). It is found that computed values of reflectance for the wavelength region 2000 to 1200 Å agree quite closely with the directly measured values given for

times of measurement within 200 to 250 seconds after deposition.

3.7. The Aluminium-Dielectric Double Layer Combination.

The potentially high reflectance in the vacuum ultraviolet of single aluminium films cannot be preserved upon exposure to the atmosphere because of the growth of a thin oxide layer. Hass and Tousey (1959) were the first to show that in the vacuum ultraviolet there was a great increase in reflectance over that of single aluminium films if the aluminium layer was quickly overcoated with an evaporated MgF2 film. The MgF2 coating prevents the formation of an oxide film and moreover, if the MgF2 layer is of correct thickness, there is a reflectance enhancement over that of the single film which arises from multiple interference between waves reflected from the vacuum-dielectric and dielectric-aluminium boundaries. Figure 3.4. shows a comparison between aluminium and aluminium - MgF2 double layers. In this case the MgF2 deposition was commenced some 30 secs after the completion of the aluminium evaporation. It is probably because of this delay time that the reflectance of the double layer film is lower than that of 'unexposed' aluminium films (section 3.6.) indicating that the aluminium film was partially oxidised before the MgF2 coating was applied. The deposition rate for the MgF2 film was 20 Å sec^{-1}.

For wavelengths shorter than about 1200 Å, MgF2 becomes inefficient as a reflectance increasing coating because of the high absorption in the MgF2 layer. The spectral range of the double layer film may be extended to about 1000 Å by using LiF rather than MgF2. At 1000 Å

FIG. 3.3

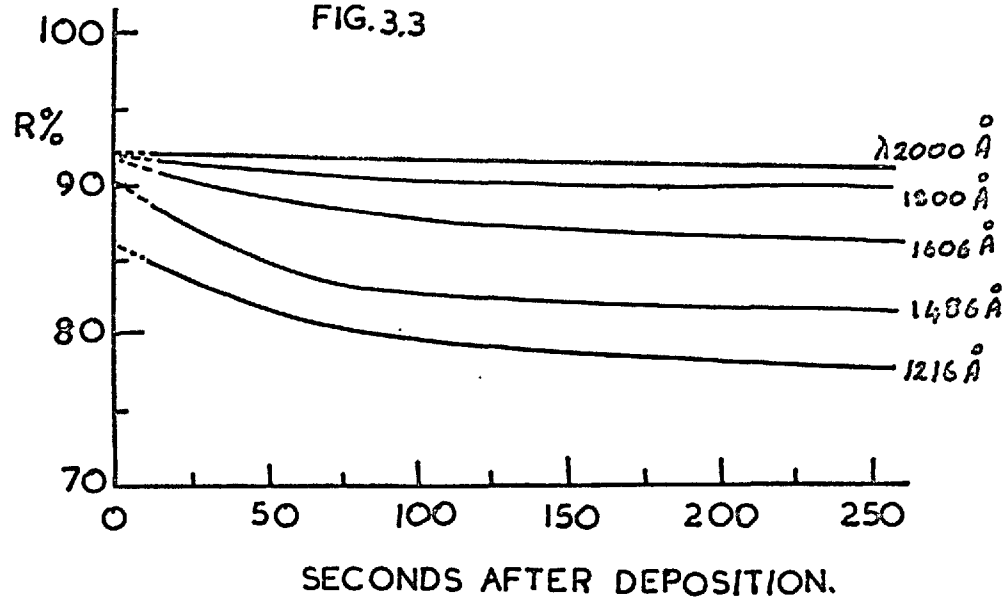
100
R%
90
80
70
0
50
100
150
200
250
λ2000 Å
1800 Å
1606 Å
1406 Å
1216 Å
SECONDS AFTER DEPOSITION.

FIG. 3.4

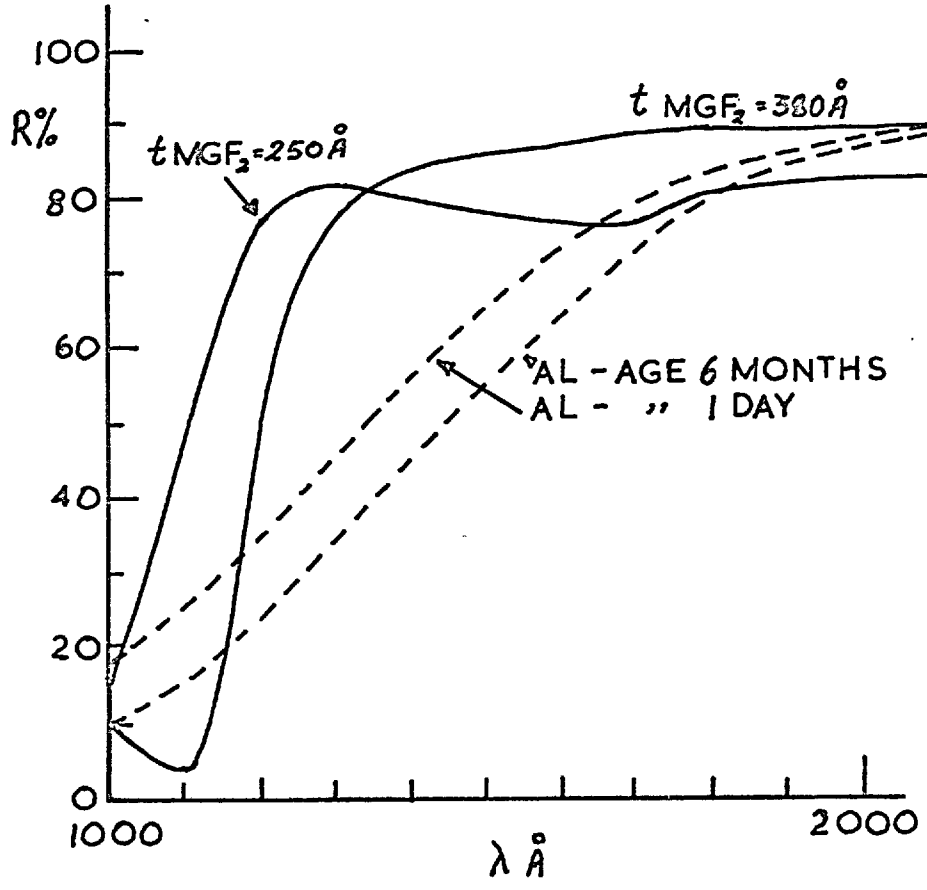
100
R%
80
60
40
20
0
1000
2000
λ Å
t MGF₂ = 250 Å
t MGF₂ = 380 Å
AL - AGE 6 MONTHS
AL - " 1 DAY

an aluminium - LiF mirror (LiF thickness 170 Å) has a reflectance of 55%. (Angel, Hunter and Tousey 1961). The reflectance for an aluminium mirror exposed to air for 24 hours is only about 18%.

The change in reflectance with time for dielectric coated mirrors is very small. Aluminium - MgF2 films stored under normal laboratory conditions (humidity 30 to 50%) for up to two years were found to decrease in reflectance by only 1 to 2% in the vacuum ultraviolet. With LiF protected mirrors again the deterioration with time is small provided the humidity is controlled to less than 40%. For humidities exceeding this value the reflectance decreases rapidly. This might be expected since the solubility of LiF in water is 0.27 gm cm^{-3} whilst that of MgF2 is only 0.0076 gm cm^{-3}.

The aluminium -MgF2 combination is now widely exploited for mirror and grating coatings in the vacuum ultraviolet. In the present investigation the techniques for producing high quality opaque aluminium - MgF2 reflectors have been applied to the case of semi-transparent aluminium films. The optical properties of such films to a wavelength of 1800 Å are described in Chapter 6 and their performance for multiple-beam interferometry in the far and vacuum ultraviolet is discussed.

3.8. Filters for the Ultraviolet.

3.8.1. Absorption Filters.

Aqueous solutions of nickel sulphate and cobalt sulphate have a fairly high transmission in the ultraviolet between 2300-3300Å & 2300-4000 Å respectively. The former solution also has transmission peaks at 5000 Å and 9000 Å whilst the latter solution absorbs strongly at these wavelengths. An aqueous solution containing both nickel and cobalt sulphates can yield a filter having a transmission of 50% for the wavelength region 2450-3200 Å with low transmission at other wavelengths. The transmission characteristic of such a filter is dependent on solution concentrations details of which have been given by Kasha (1948), (Braga and Lamb 1966).

Chemical solutions in conjunction with Corning glasses can be used to construct a set of band-pass filters for the region 2400 - 3800 Å. These filters have a maximum transmission of 30% and a typical bandwidth of about 200 Å. Details of solution concentrations and type of Corning glass required are given in the literature (see e.g. Kasha (1948) Bass (1948) Mohler and Loofbourow (1952)).

More recently organic compounds dissolved in polyvinyl alcohol or polystyrene substrates have provided a range of cut off filters from which absorption type filters can be produced. The properties of a series of short wavelength cut off filters are shown in figure 3.5. (McBride 1963).

A chemical filter particularly suitable for studying the λ1849 line of HgI since it has a low transmission to the considerably more intense λ2537 radiation has been described by Wolff and Pertel (1964). This filter consists of a solution of 9,10- dimethyl anthracene (DMA) in

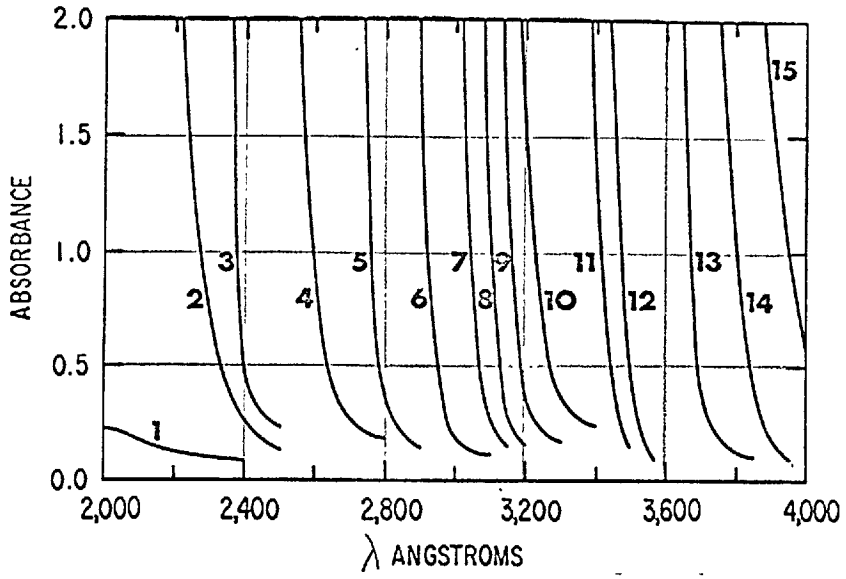

FIG. 3.5. Series of short-wavelength cutoff filters: (1) polytetrafluoroethylene (0.001 in., Teflon, du Pont); (2) filter glass No. 9863 (0.0369 in., Corning Glass Works); (3) potassium iodide crystal (0.1698 in.); (4) thiourea in polyvinyl alcohol (0.0015 in.); (5) polystyrene (0.002 in.); (6) cellulose triacetate (0.003 in.); (7) potassium biphthalate in polyvinyl alcohol (0.002 in.); (8) ethylene terephthalate (0.0005 in., Mylar, du Pont); (9) ethylene terephthalate (0.003 in., Mylar, du Pont); (10) 2-amino-4-methylpyridine in polyvinyl alcohol (0.002 in.); (11) methyl methacrylate (0.025 in., Plexiglas, Rohm and Haas); (12) potassium biphthalate and 2,7-dimethyl-3,6-diazocyclohepta-1,6-diene perchlorate in polyvinyl alcohol (0.004 in.); (13) 1,4-diphenyl butadiene in polystyrene (0.002 in.) (14) 2(2'-hydroxy-5'=methyl-phenyl)benzotriazole in polystyrene (0.002 in.); (15) 2,2'-dihydroxy-4-methoxy-benzophenone in polystyrene (0.003 in.).

cyclohexane. Absorption properties of the filter for the wavelengths 1849 and 2537 Å are given as a function of the solution concentration and cell length. By appropriate choice of these parameters it is possible to obtain a filter having a transmission of 20% at λ1849 Å and only 0.1% at λ 2537 Å. However increasing the filter transmission at λ1849 causes a reduction in contrast.

The properties of alkali metal films were studied by R.W.Wood in the late 1930's. Thin sodium films (0.5 to 1 μ thickness) transmit below λ2100 and absorb strongly at higher wavelengths. For potassium films of similar thickness the cut off is about λ3400. More recently the methods of producing Na - K alloy filmsof thickness 0.3 - 1μ in a quartz cell and the properties of such films have been described by Shaw and Foreman (1959). For an alloy of composition 25% Na; 75% K and thickness 0.5 μ a transmission of 20% is obtained at 2000 Å whilst at 4000 Å the transmission is reduced by a factor of approximately 10^5.

3.8.2. Interference Filters for the Far and Vacuum Ultraviolet.

The difficulties which have been discussed concerning the production of high reflectivity coatings for the far and vacuum ultraviolet apply also to the problem of producing F.P. type interference filters for this wavelength region. Thus, all dielectric interference filters have been produced for wavelengths to about 2400 Å but the extension of the spectral range of filters of this type is limited by the lack of a suitable high index, low absorption material. However, Baumeister and Costich (1965) have designed an interference filter for the 1849 line of HgI which is

aimed to have a high rejection for λ 2537 Å. This is acheived by using the system:-

Vacuum $(HL)^{10}$ H L' M L" M Substrate.

where M = Aluminium film 175 Å thickness

H = layer of Th F_4, optical thickness $\lambda/4$ for λ 2537 Å

L = layer of Na_3 AlF6, " " "

L' = 0.65 L.

L" = 0.89 L.

The transmission values of the filter at 1849 Å and 2537 Å are 15% and 0.2% respectively although the transmission increases again at longer wavelengths. This design of filter is considerably complex and appears to have little advantage over the more simple Al-MgF2-Al filters to be described, apart from the fact that the ratio of transmissions T1849/T2537 is 75 compared with about 45 obtainable with 1st order Al-MgF2 filters. However, two simple Al-MgF2 in series will give a much improved performance over the above complex filter.

According to Baumeister (1965) the optical properties of ThF_4 have not been studied at wavelengths shorter than 2000 Å.

The most suitable type of interference filters for wavelengths shorter than 2400 Å appear at present to be those which employ aluminium reflecting films. From extrapolated optical constants of aluminium films Schroeder (1962) has computed the transmission characteristics of filters of the type (L) M D M where M and D represent the aluminium and MgF2 films and L the total number of layers. For 3 M D M 1st order filters having a peak transmission of 25%, a bandwidth of less than 200 Å

is to be expected from Schroeder's analysis for filters having transmission peaks for wavelengths down to about 1700 Å. At wavelengths shorter than this there is an increase in bandwidth which arises from the deterioration in the properties of the aluminium reflecting layers.

The computed contrast of this type of filter, which Schroeder arbitarily defines as the ratio of peak transmission to transmission at λ 4000 Å, lies between 80 and 120. (This definition is given for filters peaked for the wavelengths near 2000 Å). Contrast can be increased by using multiple stacks of 3 M D M filters. For example, a 5 M D M filter (M - D - M' - D - M where M' has twice the thickness of M) gives a contrast of approximately 20 times that of a 3 M D M filter. A further gain of about 20 in contrast can be obtained from a 7 M D M filter.

Schroeder's experimental results for filters peaked near 2000 Å are disappointing and this was largely the result of difficulties in controlling the thickness of the aluminium films at the high deposition rates required. For a 3 M D M 1st order filter centred on 2050 Å a bandwidth of 400 Å with a peak transmission of 35% and a contrast of 100 was obtained. The transmission characteristics of two 5 M D M filters are given having transmission peaks in the region 1900 - 2000 Å. For a filter having two 1st order spacer layers the bandwidth is 325 Å and for a combined 1st and 2nd order filter the bandwidth is 200 Å. In both cases however, the peak transmission is only some 0.8%.

The bandwidths of the experimental filters are larger than calculated values. This was partly due to the fact that the aluminium films were deposited at less than the optimium rates. Also, Schroeder omits the

phase change term on reflection at the aluminium - MgF_2 boundary in computing filter bandwidths.(See Chapter 4).

In Chapter 6 improved 1st and 2nd order filters for the far and vacuum ultraviolet are discussed and transmission profiles given. From these experimental transmission curves the properties of the aluminium reflecting layers are derived.

CHAPTER 4.

RELEVENT THIN FILM THEORY AND COMPUTED OPTICAL PROPERTIES FOR TRANSMITTING ALUMINIUM AND ALUMINIUM - MgF2 FILMS.

4.1. Introduction.

Methods for calculating the optical properties of single and multilayer thin films from a knowledge of the optical constants of the individual materials, have received much attention in past years. Indeed, such theoretical approaches will also receive considerable attention in future years as the search for combinations of different materials for specific optical design problems is aided by modern methods of computation.

By present day standards, the calculation of the optical properties of a transmitting aluminium film overcoated with a thin dielectric layer may be considered to be a trivial problem. Yet, in the background to this present work the author has found that there is a considerable confusion of terms in the literature largely because the assumptions regarding sign conventions, the method for writing Fresnel's equations and the definition of phase change onreflection are not clearly stated.

In the present investigation semi-transparent aluminium - MgF2 double layers and aluminium - MgF2 - aluminium interference filters have been produced for the far ultraviolet. The thickness of the MgF2 layer determines the wavelength for optimum reflectance of the double layer film and also the wavelength of the principal pass-band of an interference filter. However, the actual thickness of the MgF2 film which is required for both of these problems is dependent on the phase change on reflection

at the MgF2 - aluminium boundary.

The absolute phase change on reflection at a metal-dielectric boundary has been strictly defined by Bennett (1964).

The equation derived by Bennett for an intensity maximum in the transmitted light for a F.P. interferometer consisting of two parallel metal surfaces separated by a medium of refractive index (n) is

$$N\lambda = 2\,nt - \frac{\lambda}{\pi}\beta$$

where t is the geometrical separation of the reflecting surfaces and β is the absolute phase change on reflection at each dielectric - metal boundary. This equation can be used to calculate the thickness of spacer layer for an interference filter which is required to have a transmission peak at a particular wavelength (λo). The minium value of t is obtained from the above equation by putting N = 0 which is the condition for a so called 1st order filter at wavelength λo. For a so called 2nd order filter N = 1 etc.

On the other hand Schroeder (1962) gives the optical thickness of spacer layer as

$$m\lambda = 2nt + \frac{\lambda}{\pi}\alpha$$

where m = 1 for 1st order filter but the phase change term (α) is not the absolute phase change on reflection. In this chapter the appropriate formulae are given for the dielectric layer thickness of the double layer films which without ambiguity satisfy the experimental conditions and which involve only the absolute phase change on reflection. This phase change term has already been met in connection with interference filters

in Chapter 2.

Also in this chapter results are given for computed optical properties of aluminium and aluminium - dielectric double layers in the far ultraviolet. The optical constants for aluminium films determined by Hass and Waylonis (1961) at wavelengths above 2200 Å have been extropolated to shorter wavelengths in the same manner as discussed by Schroeder (1962) who was concerned with the feasibility of using aluminium films for interference filters in the far ultraviolet. Calculations of the optical properties of single aluminium films have been made. In addition, the optical properties of the more important semi-transparent aluminium films overcoated with MgF2 have been computed. This investigation was considered to be important for several reasons:-

1) To obtain an indication of accuracy required for the control of the MgF2 layer thickness in order to obtain close to optimum performance.

2) To determine for a particular film combination the wavelength region over which there is a reflectance enhancement compared with single aluminium films.

3) To serve as a comparison with experimental data which will be discussed in Chapter 6.

The calculation of the optical properties of the double layer films is not a particularly difficult problem but one which is extremely lengthy. For the present work suitable programmes were devised for the Elliot 803 computor which was used for all the following calculations.

4.2. The Absolute Phase Change on Reflection.

4.2.1 The boundary Between Two Non-Absorbing Media.

Fresnel's equations form the basis for relating values of reflectance, transmittance and phase change to optical constants of a material.

For a plane wave incident normally on an interface between two dielectric media having refractive indices of n_o and n_1, then the Fresnel amplitude reflection coefficient (r) for the electric vector (E) is (for the wave incident from the medium n_o)

$$r = \frac{Er}{Ei} = \frac{n_o - n_1}{n_o + n_1} \qquad 4.1.$$

For $n_1 > n_o$, r is negative and the reflected electric vector Er will be 180^o out of phase with the incident vector Ei.

4.2.2. The Boundary Between Absorbing and Non-Absorbing Media.

Equation 4.1. holds for the boundary between a dielectric medium (index n_o) and an absorbing medium $\hat{n}_1$ if the index of the absorbing medium is allowed to be complex. If the refractive index $\hat{n}_1$ of the absorbing material is written as

$$\hat{n}_1 = n_1 - ik_1$$

where k_1 represents the attentuation of the wave per vacuum wavelength ($\hat{n}_1$ may be written in other forms, see e.g. Heavens 1955), equation 4.1. then becomes.

$$r = \frac{Er}{Ei} = \frac{n_o - \hat{n}_1}{n_o + \hat{n}_1}$$

which on rationalisation is

$$r = \frac{n_o^2 - n_1^2 - k_1^2 + 2i\, n_o k_1}{(n_o + n_1)^2 + k_1^2} \qquad 4.2.$$

$$= \frac{\rho_e i\beta}{}$$

where ρ and β are real.

The tangent of the phase angle between Er and Ei is the ratio of the imaginary to the real part of equation 4.2. and is given by

$$\tan \beta = \frac{2\, n_o\ k_1}{n_o^2 - n_1^2 - k_1^2} \qquad 4.3.$$

The angle β is defined as the absolute phase change on reflection.

A test for whether or not β is the absolute phase change is to consider the limiting case of $k \to o$. In this limit

$$\tan \beta \to o$$

for $n_o > n_1$; $\tan \beta$ is positive ie. $\beta \to o$

$n_o < n_1$; $\tan \beta$ is negative i.e. $\beta \to \pi$

The above equation for β is for an optically 'thick' absorbing (e.g. metallic) film. In the case of an optically 'thin'metallic film, the effects of multiple reflections must be considered and a new value for β is obtained which is extremely lengthy in form (see e.g. Bennett 1964). For the present work aluminium films of thickness 200 to 300 Å have been used. For films of this thickness and in the wavelength region considered the variation of the phase change with film thickness is small

(Schroeder 1962) and the value of β given by equation 4.3. is satisfactory for determining the MgF2 layer thickness required for the interferometer coatings and interference filters.

4.3. The Aluminium - MgF2 Film Combination - Conditions for Maximum and Minimum Reflectivity.

The type of coating considered is an aluminium film (index $\hat{n}_2 = n_2 - ik_2$) of thickness t deposited onto a thick non-absorbing substrate of index n_3, the aluminium film being overcoated with a MgF2 layer (assumed non-absorbing) of index n_1 and thickness d. However, in order to simplify the problem of obtaining an expression for the thickness of MgF2 layer required to give a maximum reflectivity, the aluminium film will be firstly considered as opaque. Later in this chapter computed values will be given for the practical problem under consideration which is defined by the parameters given above.

If the light is normally incident on the aluminium - MgF2 combination from a medium of index n_o (considered throughout as vacuum), then the Fresnel amplitude reflection coefficient for the vacuum-dielectric boundary is simply

$$r_1 = \frac{n_o - n_1}{n_o + n_1} = \frac{Er1}{Ei}$$

Thus, at this boundary, the electric vector of the reflected wave suffers a phase change of π relative to that of the incident wave.

Similarly, the Fresnel coefficient for the MgF2 - aluminium boundary is given by

$$r_2 = \frac{n_1 - \hat{n}_2}{n_1 + \hat{n}_2} = \frac{Er_2}{Ei}$$

$$= \frac{n_1^2 - n_2^2 - k_2^2 + 2i\, n_1\, k_2}{(n_1 + n_2)^2 + k_2^2} \qquad 4.4.$$

This expression may be written in the two forms

$$r_2 = \rho\, e^{i\beta}$$

and $$r_2 = \rho\, e^{-i\theta}$$

where β is defined as in equation 4.3. with substitution for the appropriate refractive indices.

$$\text{i.e. } \tan\beta = \frac{2\, n_1\, k_2}{n_1^2 - n_2^2 - k_2^2} = -\tan\theta \qquad 4.5.$$

The angle β is the absolute phase change on reflection at the MgF2 - aluminium boundary.

Besides this change of phase on reflection the wave reflected from this boundary suffers a phase retardation arising from two traversals of the MgF2 layer. Thus the reflected wave from the vacuum - MgF2 boundary may be written as, omitting the time dependent factor,

$$Er_1 = r_1\, Ei = \left[(n_o - n_1) / (n_o + n_1)\right] Ei$$

and for the MgF2 - aluminium boundary

$$Er_2 = r_2\, e^{-ix}\, Ei$$

$$= \rho\, e^{i(\beta - x)}\, Ei \text{ or } \rho\, e^{-i(\theta + x)}\, Ei$$

where $x = \frac{2\pi}{\lambda} 2n_1 d$, and λ is the wavelength of the light considered to be normally incident on the double layer film.

An expression for the complex Fresnel amplitude coefficient for the film combination can be derived by considering multiple reflections at the two above boundaries. Such an expression is given in the literature (see e.g.Heavens (1955); Vasicek (1960) Born and Wolf (1964)) and is

$$r\, e^{i\alpha} = \frac{r_1 + r_2\, e^{-ix}}{1 + r_1 r_2 e^{-ix}} \qquad 4.7.$$

The equation 4.7. can be used for the present application if we write r_2 in its complex form either as $r_2 = \rho e^{i\beta}$ or $r_2 = \rho e^{-i\theta}$. It is sometimes more convenient to consider r_2 in the second form since the phase change (θ) on reflection acts in the same manner as an increase in the thickness of the MgF2 layer. Substituting for r_2 then gives

$$r e^{i\alpha} = \frac{r_1 + \rho e^{-i(x+\theta)}}{1 + \rho e^{-i(x+\theta)}} \qquad 4.8.$$

The reflectivity of the combination is obtained by multiplying equation 4.8. by the conjugate complex expression $r\, e^{-i\alpha}$ and is

$$R = \frac{r_1^2 + \rho^2 + 2 r_1 \rho \cos(x+\theta)}{1 + r_1^2 \rho^2 + 2 r_1 \rho \cos(x+\theta)}. \qquad 4.9.$$

However, the use of the more convenient expression $r_2 = \rho e^{-i\theta}$ has introduced an ambiguity arising from the fact that θ is not the absolute phase change on reflection. This can be seen from equation 4.5. since:-

when $k_2 \to 0$: $\tan\theta \to 0$

but for $n_2 > n_1$, $\tan\theta$ is positive and $\theta \to 0$.

Under these conditions the absolute phase change should be 180° and not zero. In order to satisfy the boundary conditions and still use the more convenient expression $r_2 = \rho e^{-i\theta}$ then we must replace θ by $(\pi - \beta)$. Equation 4.9. for the reflectivity becomes

$$R = \frac{r_1^2 + \rho^2 + 2 r_1 \rho \cos (x + \pi - \beta)}{1 + r_1^2 \rho^2 + 2 r_1 \rho \cos (x + \pi - \beta)} \qquad 4.10.$$

For $x = o, 2\pi, 4\pi$ etc i.e. for a MgF2 layer of optical thickness $(n_1 d) = o; \lambda/2; \lambda$ etc, then the reflectivity of the combination is identical to that of an uncoated aluminium film.

The greatest reflectivity is obtained if

$(x + \pi - \beta) = 2\pi, 4\pi$ etc.

and the first maximum is obtained for a MgF2 thickness given by

$$x = \pi + \beta$$

$$\text{i.e. } n_1 d = \frac{\lambda}{4\pi} (\pi + \beta) \qquad 4.11$$

A minium in the reflectivity occurs when

$$(x + \pi - \beta) = \pi, 3\pi, 5\pi \text{ etc}$$

and the first minimum occurs for a MgF2 thickness

$$x = \beta$$

$$\text{i.e. } n_1 d = \frac{\lambda}{4\pi} \beta \qquad 4.12.$$

As an example, taking the optical constants for aluminium at λ 2000 Å as given by Schroeder

$$n_2 = 0.12; \quad k_2 = 2.12 \qquad \beta \sim 112^{\circ}$$

then $n_1 d \simeq 810$ Å for the first maximum

$n_1 d \simeq 310$ Å for the first minimum.

The values of maximum and minimum reflectivity for the film combinations are obtained from equation 4.10 and are simply

$$R_{max} = \left[\frac{r_1 + \rho}{1 + \rho r_1}\right]^2$$

and

$$R_{min} = \left[\frac{r_1 - \rho}{1 - \rho r_1}\right]^2$$

The equation 4.10. for the reflectance of an absorbing film overcoated with a dielectric layer of any optical thickness is unambiguous since it involves only the absolute phase change on reflection strictly defined in equations 4.3. and 4.5. and the Fresnel amplitude coefficients defined in equations 4.1. and 4.4.

4.4. The Method used for Computing Optical Properties.

Two main problems have been considered.

1) The properties of a thin absorbing film deposited onto a thick non-absorbing substrate e.g. an aluminium film on a 'Spectrosil' substrate. Values of R and T have been calculated for different thicknesses of aluminium at various wavelengths.

2) The properties of a thin absorbing film overcoated with a non-absorbing layer again deposited onto a thick non-absorbing substrate.

In both cases calculations have been limited to radiation at normal incidence.

The method adopted for calculating R and T is the matrix method which uses the fact that there is a linear relationship between the Fresnel amplitude reflection and transmission coefficients for the electric vectors

in successive layers of a multilayer film combination. Heavens (1955) has discussed in detail this method for calculating the optical properties of multilayer films and its application to specific problems similar to the type considered in the present work.

Film properties have been calculated from values of optical constants and film thicknesses by devising suitable programmes for an Elliot 803 computor. Programmes have been kept as simple as possible by introducing the appropriate optical constants for a given wavelength in the data input. Film properties are then calculated for a range of film thickness appropriate to the present investigation. The actual programmes used need not be described.

4.5. The Optical Constants used for Computation of Film Properties.

The calculation of the optical properties of single films and of different film combinations is dependent on a knowledge of the optical constants of the individual materials. In the case of evaporated aluminium films, the optical constants have not been experimentally determined in any detail for the wavelength region 1000 to 2200 Å. The optical constants (n,k) for aluminium films deposited under 'optimum' conditions (see Chapter 3) have been determined by Hass and Waylonis (1961) for wavelengths down to 2200 Å. Optical constants were derived from measurements of reflectance, transmittance and film thickness using equations relating those parameters given by Hadley and Dennison (1947). No allowance was made for the thin oxide layer formed on the aluminium films in deriving these optical constants.

An extrapolation of the optical constants of aluminium to wavelengths shorter than 2200 Å has been carried out in the same manner as described by Schroeder (1962). Extrapolations were made using the Cauchy Equations

$$n = B_1 + B_2 \lambda^{-2} + B_3 \lambda^{-4}$$

$$k = C_1 + C_2 \lambda^{-2} + C_3 \lambda^{-4}$$

where the complex refractive index for an aluminium film is expressed as $\hat{n} = n - ik$. The coefficients in these equations were determined by applying a least - squares fitting to the experimental data of Hass and Waylonis.

The optical constants for MgF2 have been taken from experimental data given by Hall (1957), Fabre (1964) and Fabre, Romand and Vodar (1964). For these calculations the k value in the complex refractive index has been taken as zero, since from the above experimental data $k \simeq 0.02$ for λ1600 Å and decreases at longer wavelengths. For calculations of the effect of a MgF2 layer on an opaque aluminium film at λ1216 Å, Cranfield, Hass and Waylonis (1966) have taken a value of k for MgF2 = 0.03. This value of k is lower than the value reported by Fabre et.al. The calculated effect of a surface film of n = 1.6 and values of k ranging from 0 to 0.1 on the reflectance of aluminium at 1216 Å have also been given by Cranfield et.al.

For the purpose of computing the effect of an oxide layer on the optical properties of an aluminium film, the oxide has been taken as non-absorbing of index 1.85. This of course is only an approximate representation of an oxide layer in the wavelength region considered

(1800 to 2800 Å). The optical constants for Al_2O_3 and sapphire are similar (Hass and Tousey 1959) and values of n for sapphire range from 1.81 (λ3000 Å) to 1.83 (λ2537 Å) (Malitson, Murphy and Rodney 1958). Optical properties of Al_2O_3 given by Bauple et.al. (1950) for the wavelength region 1400 to 2000 Å indicate that at 1900 Å n = 1.86 but the absorption begins to rapidly increase at shorter wavelengths. Hass, Hunter and Tousey (1957) for calculation purposes have taken the oxide to be non-absorbing of index 1.85 at 2200 Å.

The main reason for this particular calculation in the present case was to determine whether or not a surface oxide layer might account for the differences in optical properties of aluminium films prepared under two different evaporation conditions (Chapters 5 and 6).

4.6. Results of Computed Film Properties.

4.6.1. Single Aluminium Films.

The dependence of reflectance (R) and transmittance (T) on the thickness of an aluminium film deposited onto a substrate of refractive index=1.55, is shown in figure 4.1. for the wavelengths 1600, 1800 and 2200 Å. The wavelength 2200 Å corresponds to the lower wavelength limit of the experimental data given by Hass and Waylonis. According to these authors there is excellent agreement between computed and directly measured film properties for film thicknesses greater than 100 Å.

At 2200 Å, the dependence of (R + T) on film thickness is small. For example, (R + T) = 91.7% for a film 350 Å thick and 92.0% for a film 125 Å thick. With decreasing wavelength however, the dependence of (R + T)

on film thickness becomes greater and at 1600 Å calculated values of (R + T) for the two thicknesses 350 and 125 Å are 84.4% and 89.8% respectively.

The variation of optical properties with wavelength is shown in figure 4.2. for films of thickness 175 and 275 Å. This figure shows the decreasing values of R and (R + T) with shorter wavelengths. These results shown in figures 4.1. and 4.2. will be compared with experimental results obtained for wavelengths down to 1800 Å and will be discussed more fully in Chapter 6.

Values of optical constants used for these calculations are given in Table 4.1.

4.6.2. The Aluminium - MgF2 Combination.

The design of a suitable programme for calculating the optical properties of the aluminium - MgF2 film combination involved two main considerations.

1) The variation of optical properties with the thickness of both the aluminium and the MgF2 layers.

2) The wavelength dependence of the optical properties of a particular film combination.

The data used in this computation is given in table 4.1, the refractive index of the substrate being taken as 1.55.

Figure 4.3. shows for the wavelengths 1800 and 2500 Å the values of R and (R + T) for an aluminium film 275 Å thick overcoated with different thicknesses of MgF2. The difference between maximum and minimum

Figure 4.1

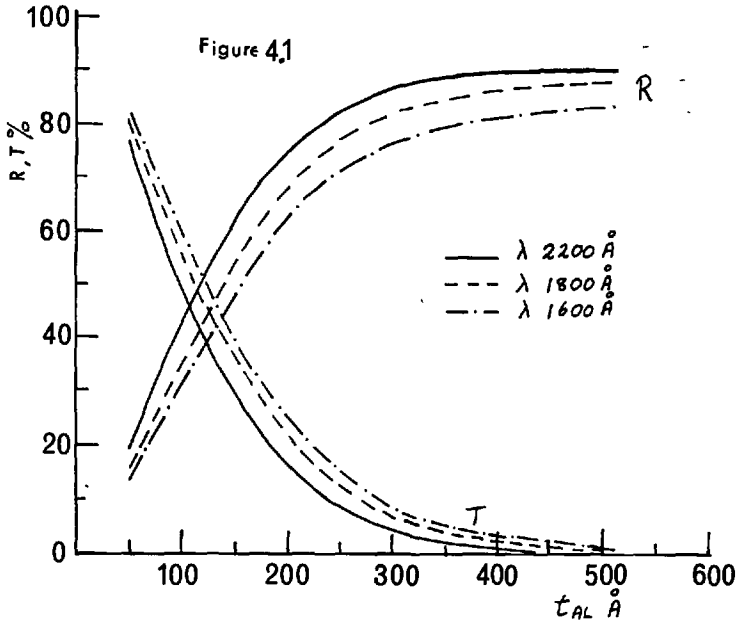

Figure 4.2

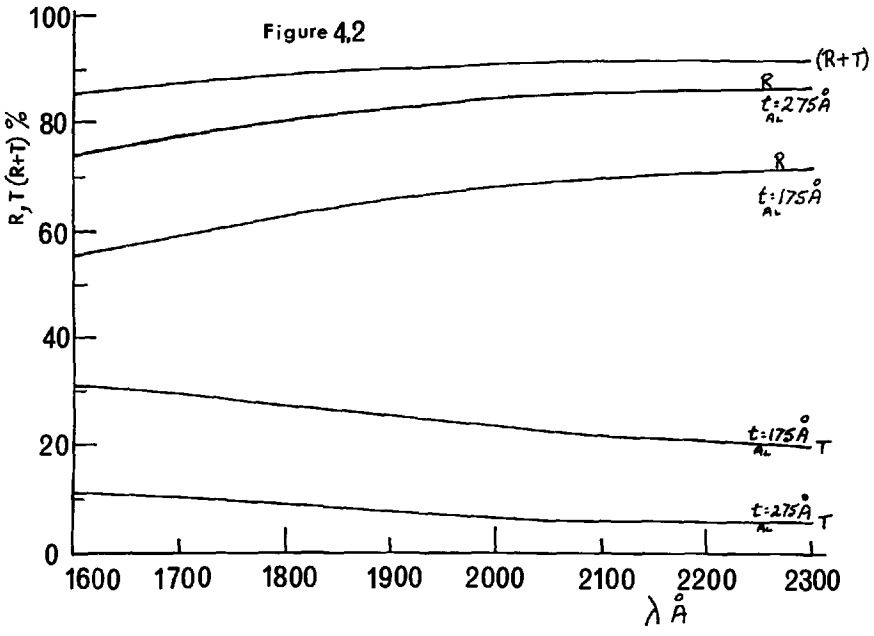

Table 4.1.

Optical Constants Used for Computing Film Properties.

	Aluminium		MgF2
	n	k	n
2800	0.21	3.04	1.40
2700	0.20	2.94	1.41
2600	0.19	2.85	1.41
2500	0.16	2.74	1.42
2400	0.15	2.58	1.42
2300	0.14	2.35	1.43
2200	0.14	2.35	1.43
2100	0.13	2.26	1.44
2000	0.12	2.12	1.44
1900	0.12	1.94	1.45
1800	0.13	1.80	1.46
1700	0.14	1.65	1.48
1600	0.15	1.53	1.50

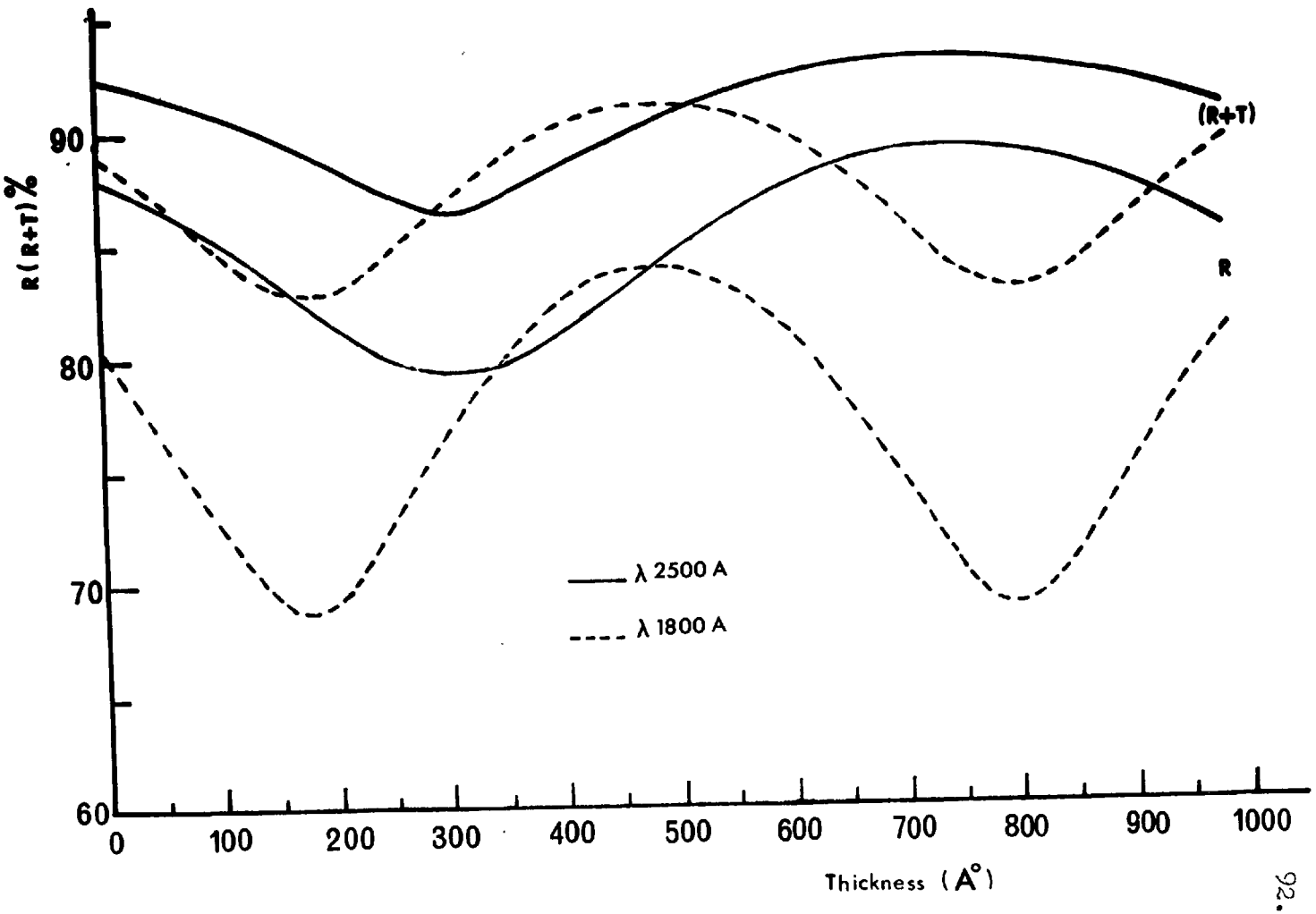
R(R+T)%
90
80
70
60
0
100
200
300
400
500
600
700
800
900
1000
Thickness (A°)
(R+T)
R
λ 2500 A
λ 1800 A

Figure 4.3.

reflectivity becomes greater as the wavelength decreases as also does the reflectance enhancement of the double layer film combination compared with the single aluminium film.

For a MgF2 film thickness corresponding to a maximum reflectivity there is also an increase in the value of (R + T) compared with that of the single aluminium film. Computed values showing the advantage of the double layer film over single aluminium films are summarised in Table 4.2. in which:-

a) t max and t min are the MgF2 thicknesses which give maximum and minimum reflectivity at the given wavelength; t_{AL} = 275 Å.

b) R_{AL}, $(R + T)_{AL}$ are appropriate values for a single aluminium film of the same thickness.

c) R max and R min are values of reflectivity for the double layer film corresponding to MgF2 thicknesses of t max and t min.

d) (R + T) max and (R + T) min are values of (R + T) for the double layer film corresponding to t max and t min.

The superiority of double layer films over single films increases with decreasing wavelength. Computed film properties show little variation in (R + T) as the aluminium film thickness is varied in the range 200 to 350 Å.

Of particular interest is the wavelength variation of the optical properties of a film which has been designed to give a reflectance maximum at a particular wavelength. This variation is shown in figure 4.4. for an aluminium film 275 Å thick coated with MgF2 whose thickness has been chosen to give a maximum reflectivity at the three wavelengths

TABLE 4.2.

Å	t max Å	t min Å	RAL%	$(R+T)A_L$%	R max%	R min%	(R+T)max%	(R+T)min%
2800	860	360	87.6	91.6	88.6	78.9	92.3	85.8
2700	820	340	87.4	91.6	88.5	78.6	92.3	85.7
2600	780	320	87.4	91.6	88.5	78.5	92.4	85.7
2500	740	300	87.9	92.4	89.1	79.3	93.2	87.0
2400	700	280	87.0	92.2	88.4	78.1	93.0	86.9
2300	660	260	86.4	91.7	88.0	77.0	92.7	86.0
2200	620	240	85.8	91.6	87.6	76.4	92.7	86.1
2100	600	220	85.8	91.7	87.8	76.4	92.9	86.3
2000	560	200	85.0	91.1	87.3	75.6	92.9	86.4
1900	520	190	82.6	90.6	85.6	72.1	92.2	84.9
1800	480	160	80.2	89.1	83.9	69.0	91.1	82.9
1700	440	150	77.1	87.1	82.0	64.6	89.9	80.0
1600	400	120	74.7	85.3	80.7	62.0	88.8	77.9

1600, 1800 and 1900 Å. The different wavelength variation of the properties of the Al-MgF2 double layers compared with the single aluminium film is clearly evident.

From the practical stand-point, the computed results show that the demands on the control of the MgF2 thickness are not too critical (Figure 4.3.). For example, at a wavelength of 1800 Å an error in MgF2 thickness of $\pm$ 40 Å from the optimum thickness of 480 Å will reduce R by 0.3% and (R + T) by 0.2%. However, this same error in thickness has a greater influence on the optical properties at longer wavelengths as seen from figure 4.3.

A comparison between these computed results and directly measured film properties is made in Chapter 6.

4.6.3. The Calculated Effect of a Surface Oxide Layer on the Properties of an Aluminium Film.

It is well known that freshly evaporated aluminium films become rapidly oxidised even when maintained at ambient pressures $< 10^{-6}$ Torr (Eley and Wilkinson, 1960 Madden, Cranfield and Hass 1963). Hass and Tousey (1959) have shown that the deterioration in reflectance of exposed, opaque films of aluminium in the vacuum ultraviolet and their change in reflectance with time can be largely attributed to the growth of a thin surface oxide layer. The thickness of oxide and its rate of growth are much reduced if films are prepared at high deposition rates and at low evaporation pressures (see Chapter 3.).

In the present investigation it has been found that the optical

Figure 4.4

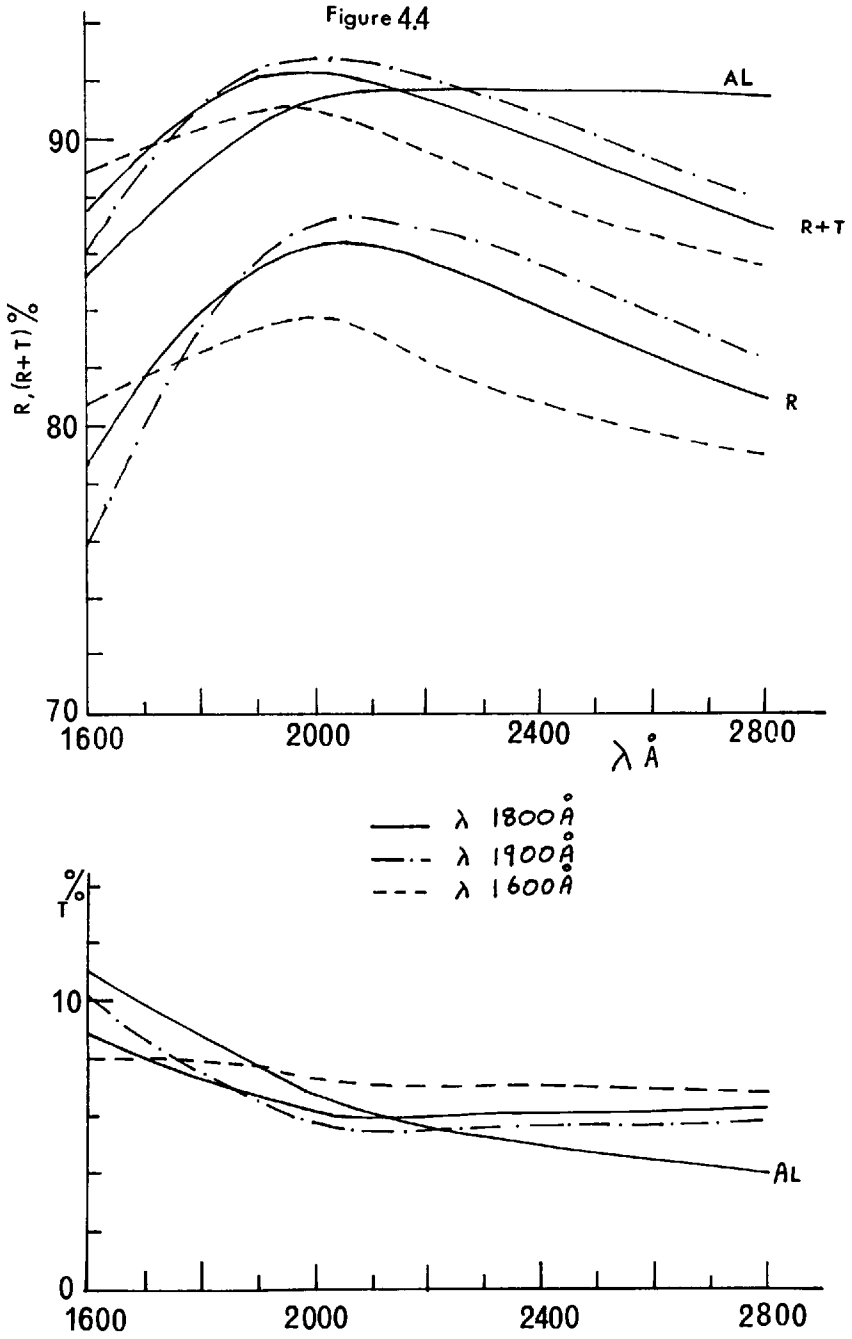
AL
R+T
R
R, (R+T)%
90
80
70
1600
2000
2400
2800
λ Å
λ 1800Å
λ 1900Å
λ 1600Å
T%
10
0
AL
1600
2000
2400
2800

properties of the exposed films were very much dependent on the vacuum conditions of preparation even when prepared at deposition rates of 100 to 150 Å sec^{-1} (Chapter 6). Also, the change in optical properties with time has been found to be greater for films prepared under 'poorer' evaporation conditions. On the other hand, the properties of the aluminium - MgF_2 double layers do not appear to be so critically dependent on the two different evaporation conditions which have been used.

At first sight these observations appear consistent with the fact that the single aluminium films produced under the poorer evaporation conditions grow a thicker oxide layer upon exposure to the atmosphere. Whilst this is undoubtedly true it is important to establish whether or not an increased growth of oxide can account completely for the difference in film properties. For this reason, calculations have been made of the effect of different thicknesses of surface layer of index 1.85 (see Section 4.5.) on the properties of an aluminium film having optical constants as given in table 4.1. Such a calculation is complicated by the fact that when there is a growth of surface oxide film, the thickness of the aluminium film is reduced.

In order to obtain an indication of the effect of this oxide layer, values of R and T have been calculated for different aluminium and 'oxide' film thicknesses. Calculated values of R and T for an aluminium film 275 Å thickness are shown in Figure 4.5. These results clearly show the effect of an increase in thickness of a non-absorbing layer on the properties of a semi-transparent film, even if the aluminium film thickness remained unchanged. In fact, the changes in R and T will be greater than

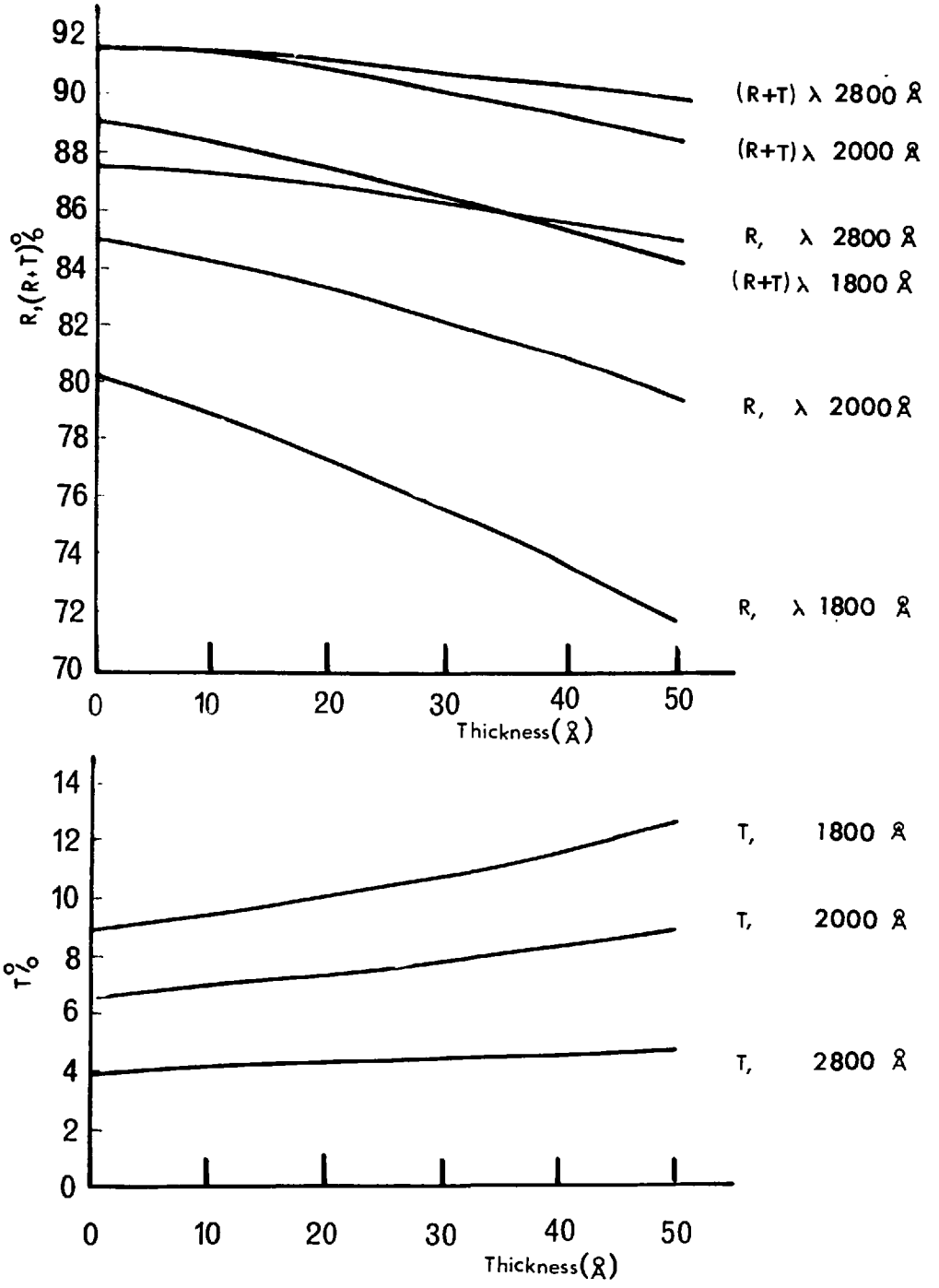
92
90
88
86
84
82
80
78
76
74
72
70
R,(R+T)%
0
10
20
30
40
50
Thickness(Å)
(R+T) λ 2800 Å
(R+T) λ 2000 Å
R, λ 2800 Å
(R+T) λ 1800 Å
R, λ 2000 Å
R, λ 1800 Å
14
12
10
8
6
4
2
0
T%
T, 1800 Å
T, 2000 Å
T, 2800 Å

Figure 4.5.

those shown in figure 4.5. because of the reduction in the thickness of aluminium during oxidation. This is discussed in greater detail in Chapter 6 where a comparison is made between computed and experimental data for exposed aluminium films.

CHAPTER 5.

THE APPARATUS AND METHOD FOR PRODUCING INTERFEROMETER COATINGS AND INTERFERENCE FILTERS FOR THE FAR ULTRAVIOLET.

5.1. Introduction.

In Chapter 3 the evaporation conditions necessary for producing high reflectivity aluminium films for the far and vacuum ultraviolet were discussed and it was shown that high optical quality films could only be produced if fast evaporation rates and low evaporation pressures were used. This led to the difficulty in the present work of depositing aluminium films at the fast rates required and yet controlling the film thickness to give a generally required transmission of a few per cent in the far ultraviolet. The requirements of high deposition rate and reproducibility in film thickness are too demanding for manual operation and as a consequence, it was found necessary to design a system whereby the thickness of the aluminium films could be automatically controlled during deposition.

A further requirement was for the control of the thickness of the dielectric layer used to overcoat the aluminium in the case of reflectance increasing coatings and for the control of the spacer layer thickness of the F.P. type interference filters. In this case however, the rate of evaporation need not be very great and the film thickness can be readily controlled by manual operation. The overall requirements for a film thickness monitoring and control system for the present work may be summarised as follows:-

1) Deposition of Aluminium films to thicknesses generally in the region 200 - 400 Å controlled to an accuracy within ± 30 Å at a deposition rate of about 100 Å/sec.

2) Deposition of dielectric films (MgF_2) to a chosen thickness in the range 400 - 1000 Å generally within an accuracy ± 20 Å. Rate of deposition not necessarily high.

3) Delay time between completion of the aluminium evaporation and commencement of dielectric evaporation to be kept as short as possible.

4) Monitoring system should be insensitive to the light produced by the heater vapour source filaments.

The design and construction of a control unit which has been developed to meet as simply as possible the requirements itemised above is described in section 5.3.

The importance of low evaporation pressure on the optical properties of aluminium films in the far and vacuum ultraviolet was also shown in Chapter 3. The development of ultra-high vacuum apparatus has made it possible to construct evaporation plants using getter ion pumps or high speed diffusion pumps with which pressures below 10^{-9} Torr can be obtained (Holland 1960). In order to attain these low pressures the apparatus must be baked to about 400 °C in order to lower the desorption rate and consequently, the cost of such a plant can be extremely high for a system of any reasonable size and complexity.

At the other end of the scale it is relatively simple to construct an unbakeable, demountable coating plant at low cost which uses elastomer gaskets for sealing and with which pressures in the order 10^{-5} Torr can

be obtained. It is the pressure region between 10^{-5} to 10^{-9}Torr which is inadequately covered by present coating plant design. This, however, is an important pressure region since it permits an improvement in the purity of deposited films with out involving the high cost and numerous difficulties associated with producing a coating plant capable of operating at pressures below 10^{-9} Torr.

Much of the present coating work has been carried out using a glass demountable system giving an evaporation pressure of about 10^{-5} Torr. This plant is not particularly novel in its construction and is only described briefly. During the course of the present work it was considered necessary to improve the evaporation conditions in an attempt to improve the quality of the transmitting aluminium films, upon which the performance of the F.P. interferometer and F.P. filters are so critically dependent. In section 5.2.2. a relatively simple and comparatively low cost evaporation plant is described which is designed to operate in the pressure region 10^{-6} to 10^{-8} Torr. With mild baking, evaporation pressures towards the lower end of this range can be obtained.

5.2. The Evaporation Plants.

5.2.1. Unbakeable Glass Demountable System.

The general outline of the vacuum system is shown schematically in figure 5.1. The coating vessel was evacuated by a mercury diffusion pump (Leybold Quick 100) and an air ballasted rotary pump (Edwards 2SC 50 B). A mecury rather than an oil diffusion pump was used since vapour emerging from the nozzels of an oil pump condenses in the water

cooled wall of the pump body where it forms a film. In time, oil may creep along the inside metal surfaces of the system into the vacuum chamber and oil molecules evaporating from this film will form part of the residual gas atmosphere. 'Teflon' creep barriers which do not become wetted by oil can now reduce considerably the effect of oil creepage. However, for the present work it was decided that possible hydrocarbon contamination should be avoided wherever possible.

The diffusion pump having a $2\frac{3}{4}$" throat and a nominal pumping speed of 100 litres/sec at 10^{-4} Torr, was connected to the chamber base plate through a 'butterfly valve' and a short pumping stem, neoprene 'O' rings providing the appropriate vacuum seals.

A Pirani gauge head (Edwards type M5B) was mounted both in the backing line and immediately below the coating chamber. The latter gauge enabled pressure measurements to be made during the discharge cleaning process whilst low pressure measurements were made with an ionisation gauge also mounted in the pumping stem immediately below the coating chamber.

The toughened glass base plate 14" diam, $\frac{1}{2}$" thick had provision for three copper electrodes ($\frac{5}{16}$ " diam) which were connected to the base plate as shown in figure 5.2.(a). The chamber consisted of a toughened glass cylinder seated into 'Duralium' rings at either end using 'Araldite' both for mechanical and vacuum seal. Each ring was grooved to take a $\frac{3}{16}$" 'O' ring (fig.5.2.b.). A toughened glass lid completed the chamber.

With this system an evaporation pressure of between 5×10^{-6} and 10^{-5}

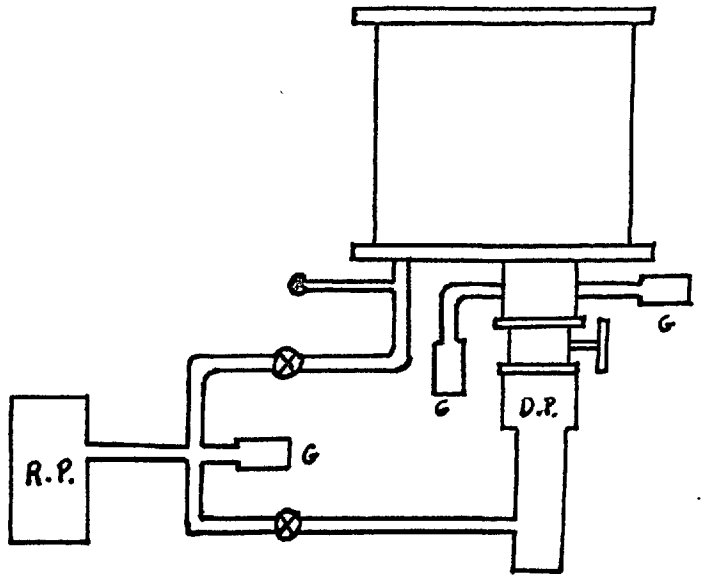

fig.5.1.

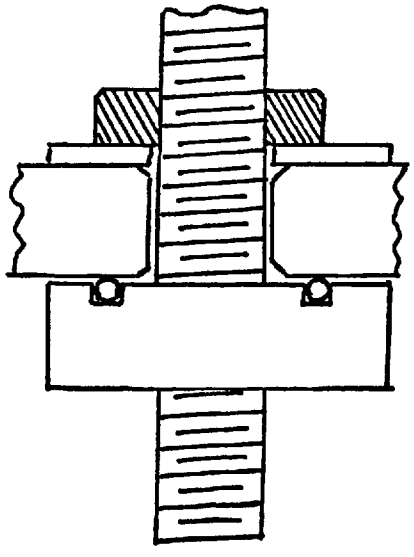

fig. 5.2 (a)

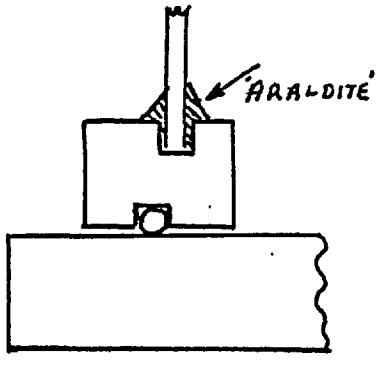

fig 5.2.(b)

Torr could be obtained. In the absence of metal parts in the vacuum chamber the ultimate pressure recorded was 10^{-6} Torr.

5.2.2. Bakeable Metal Demountable System.

A lower working pressure can be attained either by reducing the desorption rate from the vessel walls, gaskets etc. or by tolerating this outgassing and using faster pumping speeds. If however, too much reliance is placed on pumping speed then the film substrate can be exposed to molecular beams issuing from the gaskets and vessel walls, since the pressure inside the vessel is unlikely to be uniform. Thus, to reduce substrate contamination and the absorption of gases by a growing film it is necessary to keep the desorption rate to low values and not to rely exclusively on fast pumping (Holland and Bateman 1962).

For a vacuum system of large size and of fairly high complexity, for example where several power inputs are required into the coating chamber then metal rather than glass is to be preferred because of its greater robustness. Stainless steel has a low outgasing rate and is ideally suited to general vacuum use (Flecken and Nöller 1962). On the basis of the above considerations an evaporation plant has been constructed in which the components and materials have been chosen for their low outgassing properties whilst bearing in mind ease of assembly and general versatility of use. The plant to be described was constructed by Edwards High Vacuum Ltd. according to the design of Mr.N.Angel(Edwards) and the author.

Coating Chamber.

The stainless steel chamber, shown in figure 5.3, has an internal diameter of 12" and an internal height of 15". It is basically constructed from three parts, a cylinder $\frac{1}{10}$" thick, a top plate 1" thick and a lower ring $1\frac{1}{4}$" thick. These components are sealed together by argon arc welds. Viewing ports are mounted on both the top and the side of the chamber, the windows being either of fused silica (Spectrosil B) or toughened glass ($\frac{1}{4}$" thick). A vacuum seal is made by forming an overlapping loop of indium wire (0.5 mm diam), which is placed between the window and the stainless steel component. A flange with eight fixing screws for even compression holds the window in place and allows the indium wire to be compressed sufficiently to obtain a vacuum seal.

The seal between base plate and chamber is the only one which is required to be broken in order to gain access to the chamber. This seal is a Viton 'O' ring (bakeable to 200°C) which seats in a groove in the lower ring of the chamber as in figure 5.2.(b). Although a metal seal is to be preferred because of its lower outgassing rate the advantage of the greater versatility of the Viton seal for gaining access to the chamber outweighs the disadvantage of slightly greater outgassing rate. Moreover, provided care is taken to ensure that only small areas of Viton are exposed then the problem need not be serious. Also, the effect of outgassing from this seal can be reduced still further by the use of a liquid nitrogen cooled trap inside the vacuum chamber as discussed in the following section.

In order to allow a controlled leak into the chamber for control of

the discharge cleaning pressure a needle valve (Edwards type L B-1) is connected to the chamber through a 6" long, $\frac{1}{8}$" diam tube. The purpose of this tube is to reduce the outgassing rate from the valve which cannot be baked much above 60°C.

The Base Plate and Accessories.

The arrangement of the stainless steel baseplate ($13\frac{1}{2}$" diam, $\frac{7}{8}$" thick) is shown in figure 5.4. Seven electrodes of the type shown in figure 5.5. are fixed to the base plate. Also mounted on the underside of the baseplate is a window to enable light entry for film thickness monitoring and an ionisation gauge head (Mullard I OG 12) for low pressure measurements. All of these components are held in clamping flanges and each vacuum seal between component and baseplate is of indium.

The Meissner liquid nitrogen trap made of $\frac{1}{4}$" diam. copper tubing is mounted to the upper side of the baseplate using a Viton gasket for vacuum seal. This trap is roughly circular in form and is arranged to be in close proximity to the Viton 'o' ring seal between chamber and baseplate. (fig.5.4.) The purpose of this trap (Meissner 1960) is to condense vapours, particularly those of water and hydrocarbon, which then have a negligible vapour pressure at the trap temperature. A further function in the present case is to trap mercury atoms which may back stream beyond the cold trap of the diffusion pump into the chamber. This is acheived by the copper disc brazed to the Meissner coil (fig.5.4.) which is arranged to be just above the pumping part in the base plate. Typically, a lowering of the chamber pressure by almost an order of magnitude (in the pressure region 10^{-5} to 10^{-7} Torr) is obtained when

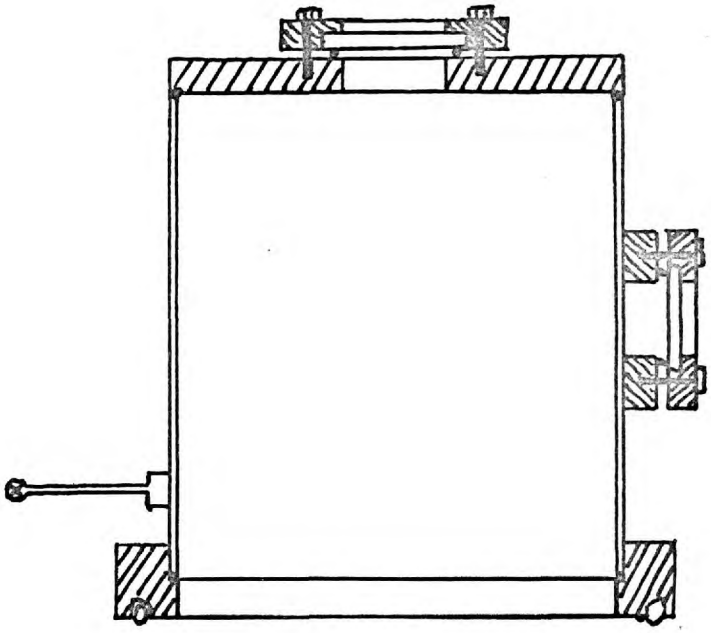

fig. 5.3

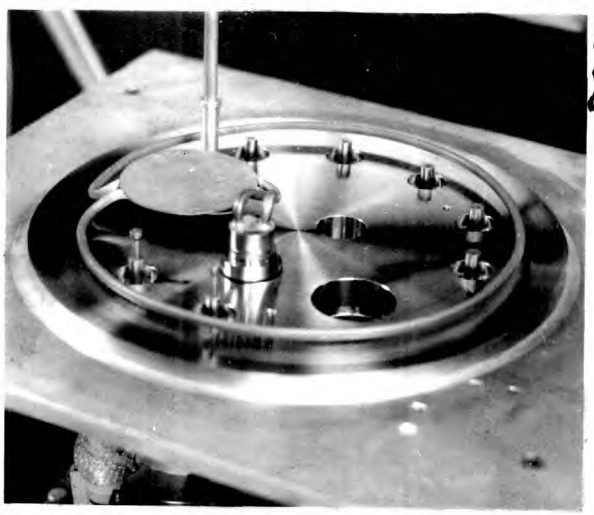

fig 5.4.

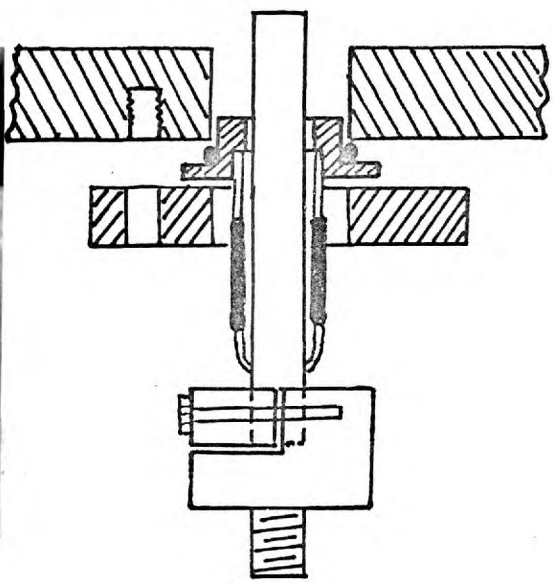

fig 5.5.

the trap is cooled to liquid nitrogen temperature.

Connecting the diffusion pump to the baseplate is a stainless steel pumping stem 7" long, $2\frac{3}{4}$" internal diameter which is welded to the baseplate, the seal between the pump and the stem being a Viton 'O' ring. The stem has provision for mounting a Pirani gauge head in order that pressure measurements can be made for the discharge cleaning process.

In the present system the 'butterfly' valve between diffusion pump and coating chamber (as in fig.5.1.) has been dispensed with since this valve cannot be baked. Consequently, the chamber is initially evacuated by pumping directly through the diffusion pump and the by-pass(roughing out) system shown in figure 5.1. is not incorporated in the present design.

A further addition, not shown in figure 5.1, is the inclusion of a liquid nitrogen trap mounted in the pumping line between the rotary and diffusion pumps. This acts as a trap for water vapour and also prevents back streaming of oil molecules from the rotary pump into the high vacuum line. An isolation valve is placed between this cold trap and the diffusion pump. This is closed at the end of the pumping cycle so that, as the cold trap is raised to ambient temperature the released vapours do not pass into the high vacuum line and the coating chamber.

5.2.3. The Pumping Performance.

In the absence of any metal parts inside the chamber the chamber pressure falls to approximately 2×10^{-6} Torr in 45 mins. Continued pumping for several hours reduces the pressure by only a small degree

and the ultimate pressure reached is about 10^{-6} Torr. A mild bake of the entire system above the liquid nitrogen trap of the diffusion pump (up to a temperature of about 110°C) causes the pressure to inorease by an order of magnitude and then to fall slowly. On cooling, the pressure continues to fall reaching about 7×10^{-8} Torr at room temperature. Liquid nitrogen circulation through the Meissner coil gives a further lowering of pressure and when the trap temperature reaches liquid nitrogen temperature, the final steady pressure obtained is about 10^{-8} Torr.

The work holder discharge cleaning unit, electrodes etc. introduce a considerable volume of outgassing parts to the coating chamber and there is a corresponding deterioration in pumping performance. Typically, a pressure of 8×10^{-6} Torr is reached prior to baking. After the baking cycle (110 °C) the chamber pressure reaches about 8×10^{-7} Torr. and falls to the evaporation pressure of $8 - 10 \times 10^{-8}$ Torr when the Meissner coil is cooled to liquid nitrogen temperature. There is an increase in pressure during the aluminium evaporation but the chamber pressure falls within seconds to a pressure $< 5 \times 10^{-7}$ Torr.

5.2.4. <u>The Substrate Holder and Shutter Mechanism.</u>

A tripod system consisting of $\frac{3}{8}$" diam. 'Duralium' rods screwed into the base plate supports the H.T. discharge cleaning assembly and the substrate holder and shutter (fig.5.6). The discharge cleaning unit consists basically of two aluminium ring electrodes, shielded from the vapour source, which are connected to a 4 K.V. A.C. supply. This is a standard technique described in detail by Holland (1956).

The 11" diam. aluminium substrate holder (fig.5.7.) has provision for two 6 cm diam. and two 4.5. cm diam. substrates, although in general only one sample is coated at a time. Figure 5.7. also shows the monitor plate holder with provision for eight separate open positions, The monitor plate itself is a glass disc (6 cm. diam.) which seats in the rotary holder. Prior to evacuation of the chamber the monitor plate holder is wound against a circular spring and is held in an open position by locating pins mounted on the underside of the holder. These pins engage with the solenoid arm shown in figure 5.7. When the solenoid is energised the monitor plate rotates through $22\frac{1}{2}^{\circ}$ and on de-energising through a further $22\frac{1}{2}$" i.e. into position for the next evaporation. This system was found to be a fast and reliable method for moving the monitor plate from one evaporation position to the next. Speed is important since as previously discussed the time interval between the completion of the aluminium evaporation and the commencement of the MgF2 evaporation must be kept as short as possible to minimise the oxidation of the aluminium flim. This method for moving the monitor plate was developed for the bakeable metal plant. For the previous glass vacuum system a slower method had been used in which the monitor plate was moved from one position to the next by means of an external magnet.

The choice of the reliable electro-mechanical method for operating the monitor plate and shutter mechanism (described below) introduces the problem of overcoming outgassing from the solenoid coils which are mounted inside the vacuum chamber. Enamelled covered copper wire whose electrical insulation can withstand baking up to 180°C was wound round

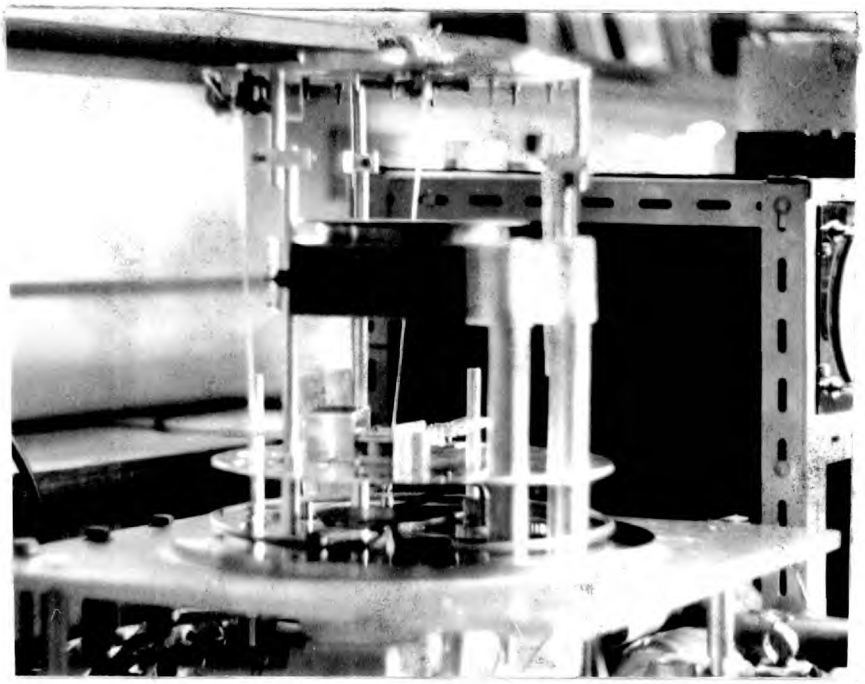

Fig.5.6.

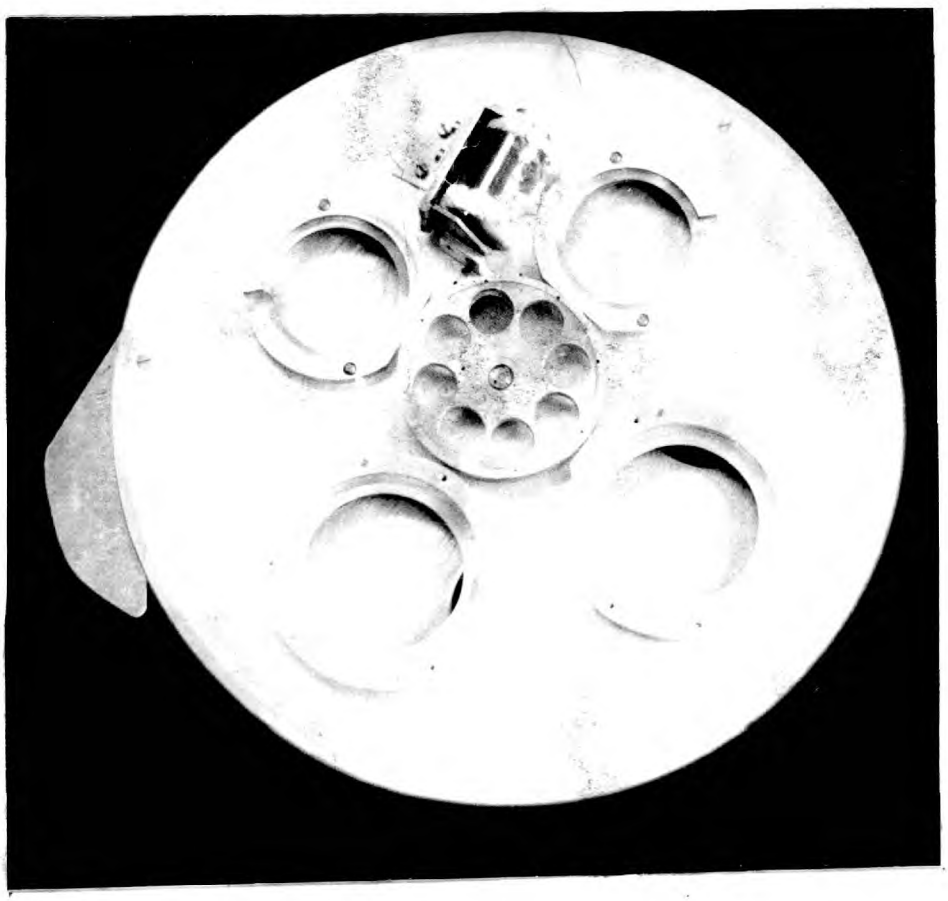

Fig.5.7.

a Duralium former. The coil was inserted into a close fitting glass cylinder having a short pumping stem, and a mechanical seal made between the coil former and glass cylinder using 'Araldite'. (Fig.5.8.). A vacuum seal was established by overcoating the sealing compound with 'Torr Seal' resin (Varian Associates Inc.) which has a very low vapour pressure and which can withstand about 120°C baking. One end of the coil is earthed to the coil former and the other end is brought out through the side of the glass cylinder, a vacuum seal being made as above. Finally, the complete assembly was evacuated and baked to 100°C before sealing off at a pressure of about 10^{-5} Torr. This method produced a reliable solenoid coil of good electrical insulation and having low outgassing properties.

Figure 5.9. shows the underside of the substrate holder and the shutter used to interrupt the vapour stream from both the target substrates and the monitor plate. The aluminium shutter is mounted $\frac{3}{8}$" below the substrate holder and is able to revolve freely on a 'ball-race' bearing shielded from the evaporation sources. The shutter is wound up against a 4" long coiled steel spring and can be held in an 'open' or 'closed' position, in a similar manner to that described above, when the coil is energised or de-energised respectively. Since the aluminium deposition is fast (2-3 secs) then the shutter must also be fast acting. The present design gives nine open and closed positions and with the spring under full tension the shutter closes in $\frac{1}{20}^{TH}$ sec. The shutter speed decreases with decreasing spring tension and is about

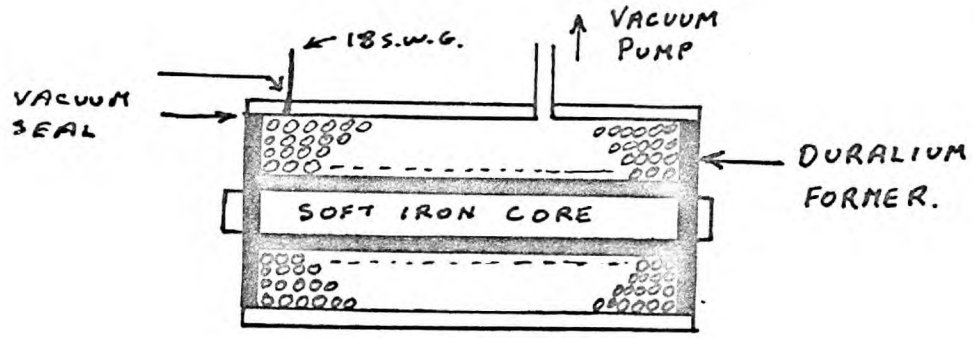

FIG 5.8. ENCAPSULATED SOLENOID FOR COATING CHAMBER.

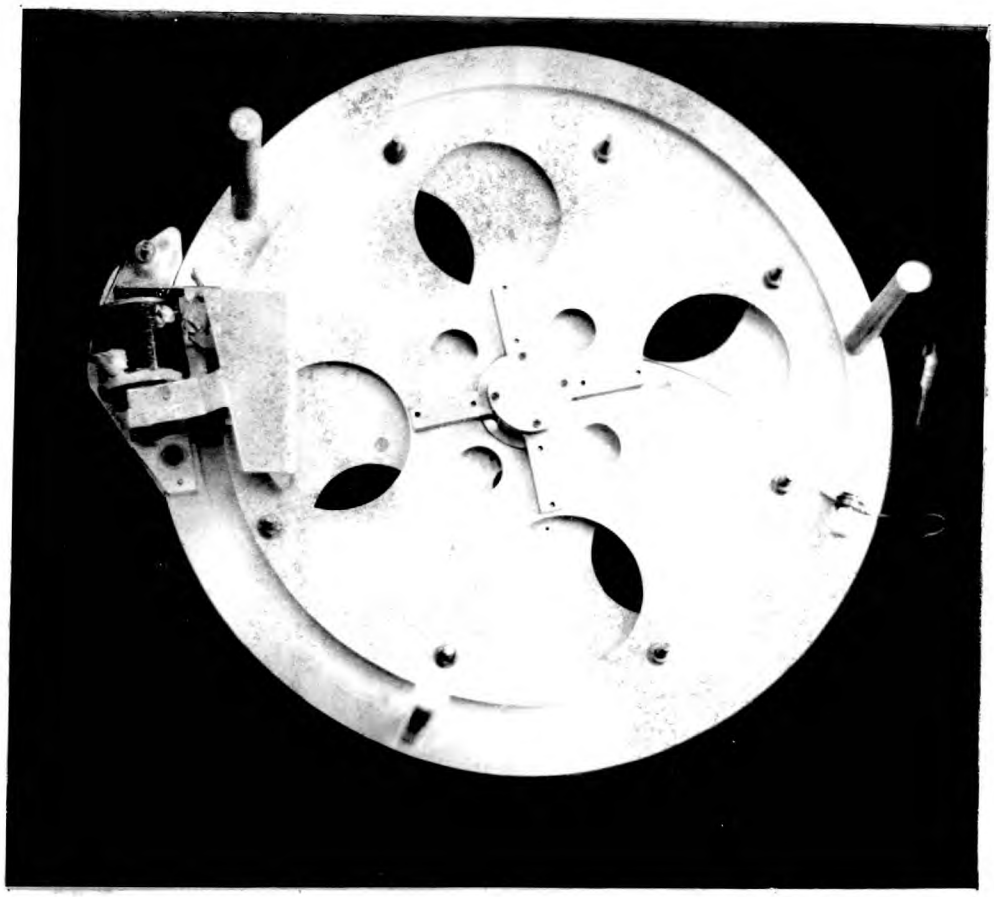

FIG 5.9.

$\frac{1}{10}^{TH}$ sec after the seventh shutter position.

Duralium lead-in electrodes are used to connect the glass-metal electrodes sealed in the chamber base plate to the vapour source filaments. Because of the danger of stressing these electrodes and breaking the glass-metal joint the 'lead-in' electrodes are made in two sections and joined by $\frac{1}{2}$" lengths of copper braiding which relieve any stress developed. The copper braid is shielded from the glow discharge to prevent sputtering of the copper and possible substrate contamination.

The vapour source filaments were connected to a common earth. For the present work, tungsten coils made from three strand 0.5 mm diam. wire have been used for the aluminium evaporation and a molybdenum boat (Made from 0.002" thick sheet) for the MgF2 evaporation. The merits of different materials for vapour source filaments have been discussed in detail by Holland (1956).

The power supply for each filament is a 10V 250A transformer whose input is controlled by a 'Variac'. Each filament has a separate power supply so that the MgF2 boat can be heated whilst the aluminium film is deposited. This reduces the delay time between evaporations.

5.3. Apparatus for Controlling Film Thickness during Deposition.

5.3.1. The Choice of Monitoring System.

Various types of apparatus have been developed for monitoring the thickness of both metallic and dielectric films during depositon. Where optical properties are of importance the ideal arrangement is to monitor

the reflectivity or the transmission of the sample at the wavelength region where the film is to be used. Such methods for monitoring in the visible and near ultraviolet regions have been described in the literature (see e.g. Holland 1956, Heavens 1955). However, the monitoring of film thickness in the far and vacuum ultraviolet presents many technological difficulties although for the present work it is not essential that this method is used. In the present case, film thickness has been monitored in the visible and related to the properties of the films in the far ultraviolet.

Also, it is not readily possible in the present work to monitor directly from the actual specimen required, particularly in the case of the F.P. interference filters. With this type of filter the principal wavelength of the pass-band can only be readily be determined once the final metallic layer has been deposited, since this wavelength depends not only on the thickness of the spacer layer but also on the phase change at the metal-spacer boundary. Thus, a system was chosen in which a fresh monitor plate was used for each deposition.

The choice between monitoring reflectivity or transmission depends largely on the problem under consideration, although transmission monitoring is technically easier. In the present work however, reflectivity was monitored since for multiple-beam interferometry this is the parameter which is usually required to be controlled and which determines very largely the finesse of the F.P. etalon or the bandwidth of a F.P. interference filter.

The choice of monitoring system finally decided on requires that a

relationship be determined between the optical properties of the coated substrate and a parameter dependent on the monitor plate reflectivity. For the aluminium deposition the optical properties of the coated substrate were measured in the far ultraviolet and related to a particular setting of the input load resistance of the control unit (section 5.3.4.) For the MgF_2 layers the film thickness on the substrate is related to a change in reflectance of the monitor plate, which is measured during deposition. Film thickness was measured by the Fizeau fringe technique described by Tolansky,(1948) and was also obtained from the pass band of interference filters.

5.3.2. The Light Source and Detectors.

Light from a tungsten filament lamp is chopped at a frequency of 1000 c/s and is partially reflected by a plain glass plate onto the 'Comparator' photomultiplier. The transmitted beam is reflected through the base plate window to strike the monitor plate where it returned through the same window onto the 'Monitor' photomultiplier. The angle of incidence of the beam striking the monitor plate is approximately 2°.

The light source is a 12V 36 watt bulb which is operated from a 12V transformer. A constant voltage transformer provides adequate stability in the source intensity, which is also variable by 'Variac' control of the 12V transformer input. Light from the lamp filament passes through a $1/32$ " aperture and is then chopped by a rotating disc having twenty equispaced circular holes. The disc is rotated at a speed of 3000 r.p.m. to give an approximate square wave light output of 1000 c/s.

The small aparture is focussed onto the cathode of the 'Monitor' photomultiplier where the image size is about $\frac{1}{2}$" diam.

Both photomultipliers are of the type EMI 6097 C and are operated from a stabalised high voltage supply (Philips PW 4024/01) giving a deviation of $<0.05\%$ in output voltage for a 10% fluctuation in mains voltage. Under operating conditions the overall voltage is IKV representing a bleeder chain current of 120μA whilst the photocurrent is 10μA.

The monitoring wavelength is selected by placing Kodak Wratten filters Nos 35 and 45 immediately before each photomultiplier photo cathode. In series, these filters isolate a wavelength region centred on 4400 Å having a bandwidth of approximately 250 Å.

5.3.3. Preliminary Considerations of the Control Circuit.

Basically the control circuit consists of a valve voltmeter which compares the input signals from the Comparator and Monitor photo-multipliers. For a given source intensity the signal from the Monitor depends on its variable load resistance and on the reflectance of the monitor plate whilst the signal from the Comparator, having a fixed load resistance, depends only on the source intensity. These signals are compared and their difference is amplified and applied to the grid of a triode which has a relay in its anode. For large differences between these signals the relay is energised. During the aluminium deposition, the monitor plate reflectance increases and the signal difference decreases until a pre-determined point is reached where the relay becomes de-energised.

This then causes the shutter inside the coating chamber to close and interrupt the deposition. The shutter actuating circuit which performs this operation is described in section 5.3.5.

The signal input from the Monitor has the two variables input load resistance and monitor plate reflectivity. It is therefore necessary to standardise in some manner before the control unit can be calibrated to a required reflectivity. The following procedure for standardisation has been adopted.

1) The source intensity is adjusted to give a certain signal output from the comparator which can be measured in terms of a meter reading. Thus, the source intensity can be set to the same value for each evaporation although this is not essential.

2) The monitor plate is used as a standard of reflectance. Although it is not necessary that this reflectance be known it is necessary that this is the same for each evaporation. In the present work Kodak cover slides have been used and one surface finely ground to elimate back surface reflection. Then, of these plates only those have been used whose reflectance falls within certain allowable limits.

3) The input load resistance of the Monitor is set to a certain value for standardisation purposes. The load resistance is a precision wire wound potentimeter (100 KΩ) to which a 6" diam.dial has been added for setting accuracy.

Thus, for the chosen monitor plate reflectance the relay should de-energise for the chosen standardisation dial setting. In practice, because the beam falling on the Monitor photomultiplier may not strike

the same area of cathode each time or because of dust on the mirrors used to reflect the beam along its path , the relay may not de-energise at the chosen dial setting (input resistance). This has been overcome by passing the monitor signal through a stage with variable gain before feeding it into the valve voltmeter. The gain control is then altered so that the relay de-energises at the chosen input resistance.

The standardisation therefore sets the conditions for the relay to de-energise for a constant factor Ro r_o, Ro being the reflectance of the uncoated monitor plate and r_o the input resistance (dial setting). During the aluminium deposition the monitor plate reflectance R will increase and it is only necessary that the input resistance r is set so that, for a required reflectivity R, then Rr = Ro r_o. When this condition is reached the relay will de-energise and the deposition will be interrupted. The required value of r (in terms of dial setting) is determined from a calibration experiment in which the optical properties of the coated substrate are ~~in~~ measured.

In the case of the MgF2 deposition the method of monitoring is simpler largely because the evaporation rate is much slower and can be controlled manually. The reflectance of the uncoated monitor plate is set in terms of a meter reading to full scale deflection by adjusting the Monitor input resistance (dial setting). As deposition occurs then the reflectance, which is a function of film thickness, firstly decreases reaching a minimum when the optical thickness of the film is $\lambda/4$ and then increases to the uncoated value when the optical thickness is $\lambda/2$, λ being the monitoring wavelength. Thus, the thickness of the MgF2 film

on the substrate can be measured and a relationship between film thickness and meter reading obtained. Then it is only necessary to interrupt the deposition when a required thickness (meter reading) is reached by manually closing the shutter.

5.3.4. Description of the Control Circuit.

The circuit diagram is shown in fig.5.10. The output from the Monitor photomultiplier, which consists of a D.C. component and negative pulses, appears across the variable 100 K potentiometer (V R1). The A.C. component of this output is fed through C_1 and appears across R_1, ~~and~~ R_2 and R_3. In switch positions 1 and 2 corresponding to the MgF2 deposition and standardisation positions the full output is applied to V1A whilst in switch position 3, for the aluminium deposition, then the signal is attenuated by a factor of approximately 20. Switch S_2 is simply a range switch for high or low reflectivity.

The valve V1A is used as a low gain pentode (gain $\simeq$ 24) and the output from V1A is applied to the grid of V1B, which is used in this case as a phase shift. This is necessary to restore the amplified signal from the Monitor input to the same phase as the signal from the Comparator input. The output from V1B, which is variable by VR_2, is applied to the grid of $V2_A$, D.C. restoration being acheived by either diode D_1 or D_2. In the former case positive signals appear on the grid of V_2A (for MgF2 monitoring) and in the latter case negative signals (for standardisation and aluminium deposition).

The double triode V_2 is a bridge voltmeter having a 200 μ A meter across the anodes of V_{2A} and V_{2B}. The bridge can be balanced for zero

input by V_{R3}. The output from the Comparator appears across R_{19} and is applied to the grid of V_{2B}, D.C. restoration being obtained by D_3. In switch position 1, a small positive voltage is applied to the grid of V_{2B} to balance the contact potential of D_1.

Differences between the output of V_{2A} and V_{2B} will be indicated by the 200μA meter and will also result in a signal across the primary of T_1. This difference in signals is amplified by T_1 which is peaked at 1000 c/s (gain $\simeq$ 9) and applied to the grid of V_{3A}, a triode amplifier having a gain $\simeq$ 11. The output from V_{3A} is rectified and smoothed (C9, R24,D4) to provide a positive voltage on the grid of V_{3B}. The diode D5 in the primary of T_1 prevents reappearence of the signal once the balance point has been passed.

A high positive voltage applied to the grid of V_{3B} causes the anode current to rise and energise the relay in the anode of V_{3B}. As the aluminium deposition occurs and the monitor plate reflectance increases, then the voltage difference across the bridge and hence the voltage on the grid of V_{3B} will decrease. Eventually, a point is reached where for a given signal difference the relay will de-energise. The grid voltage at which this occurs can be varied by V_{R5} and is normaly set to 12V.

5.3.5. The Shutter Actuating Circuit.

The shutter which interrupts deposition when the required reflectance is reached is operated by a solenoid mounted inside the vacuum chamber. This solenoid in turn is controlled by the relay in the anode of V_{3B}.

Fig.5.10.

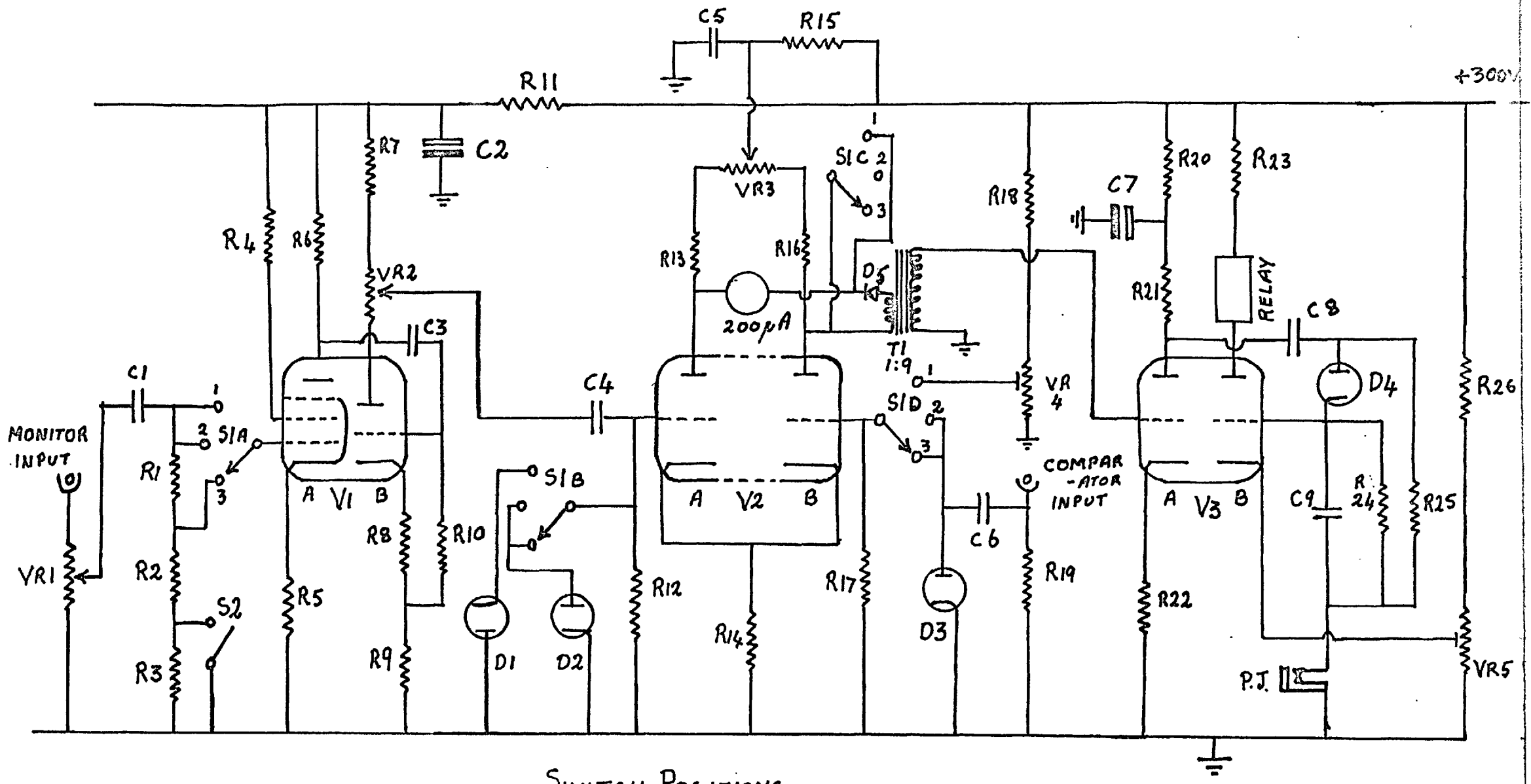

SWITCH POSITIONS

S_1

1 MgF_2

2 STANDARDISATION

3 ALUMINIUM

S_2 CLOSED FOR HIGH REFLECTIVITY

FIG 5.10

Values of Components shown in Figure 5.10.

Resistances (ohms.)

R_1	940K	R_2	47K	R_3	47K	R_4	270	R_5	370
R_6	22K	R_7	5K	R_8	1K	R_9	10K	R_{10}	1M
R_{11}	10K	R_{12}	1M	R_{13}	47K	R_{14}	1K	R_{15}	47K
R_{16}	47K	R_{17}	1M	R_{18}	100K	R_{19}	100K	R_{20}	22K
R_{21}	47K	R_{22}	2.2K	R_{23}	6.8K	R_{24}	1M	R_{25}	470K
R_{26}	100K								

Variable Resistances (ohms.)

V_{R_1}	100K	V_{R_2}	5K	V_{R_3}	25K	V_{R_4}	200	V_{R_5}	10K

Capacitors (μF).

C_1	0.001	C_2	16	C_3	0.1.	C_4	0.001
C_5	0.002	C_6	0.1	C_7	16	C_8	0.1
C_9	0.05						

V_1 - ECF80; $V_{2,3}$ - 12 AU7.

$D_{1,2,3,4}$ - M8212 D_5 - OA5.

for the aluminium (automatic) deposition or it can be operated manually. The circuit for actuating the solenoid shutter is shown in figure.5.11.

Automatic Operation.

Switch S_2 is set to automatic which opens both S_{2A} and S_{2B}. Prior to deposition relay 1 in the anode of V_{3B} is energised through a 22 KΩ resistance connected to the H.T. supply (+300V). The shutter is opened manually by switch S_1 and deposition occurs. When the required reflectivity is reached relay 1 de-energises and its contacts short the coil of relay 2 which then also becomes de-energised. In this condition, the solenoid circuit is broken and the shutter closes. However, with the shutter closed there will be a large voltage on the grid of V_{3B} and relay 1 will again energise. The purpose of introducing relay 2 is to prevent the shutter from automatically re-opening as would otherwise occur. In fact, the shutter cannot be opened again until switch S_{1A} has been manually opened since the contacts of relay 2 short its own coil and prevent it from energising.

Manual Operation.

Switch S_2 is set to manual which closes both S_{2A} and S_{2B} thus shorting the coils of relays 1 and 2. The shutter is now controlled by switch 1 only. On manual operation the shutter is open for fairly lengthy periods and to prevent undue heating of the solenoid a 10 ohm resistance is switched in series with the solenoid approximately $\frac{1}{4}$ sec after it has been actuated. Thus, although it requires a current of about 1.2 A to actuate the solenoid it requires only 0.4 A to maintain the solenoid energised. The contacts of relay 3 open and unshort the

Fig.5.11.

FIG 5.11. SHUTTER ACTUATING CIRCUIT.

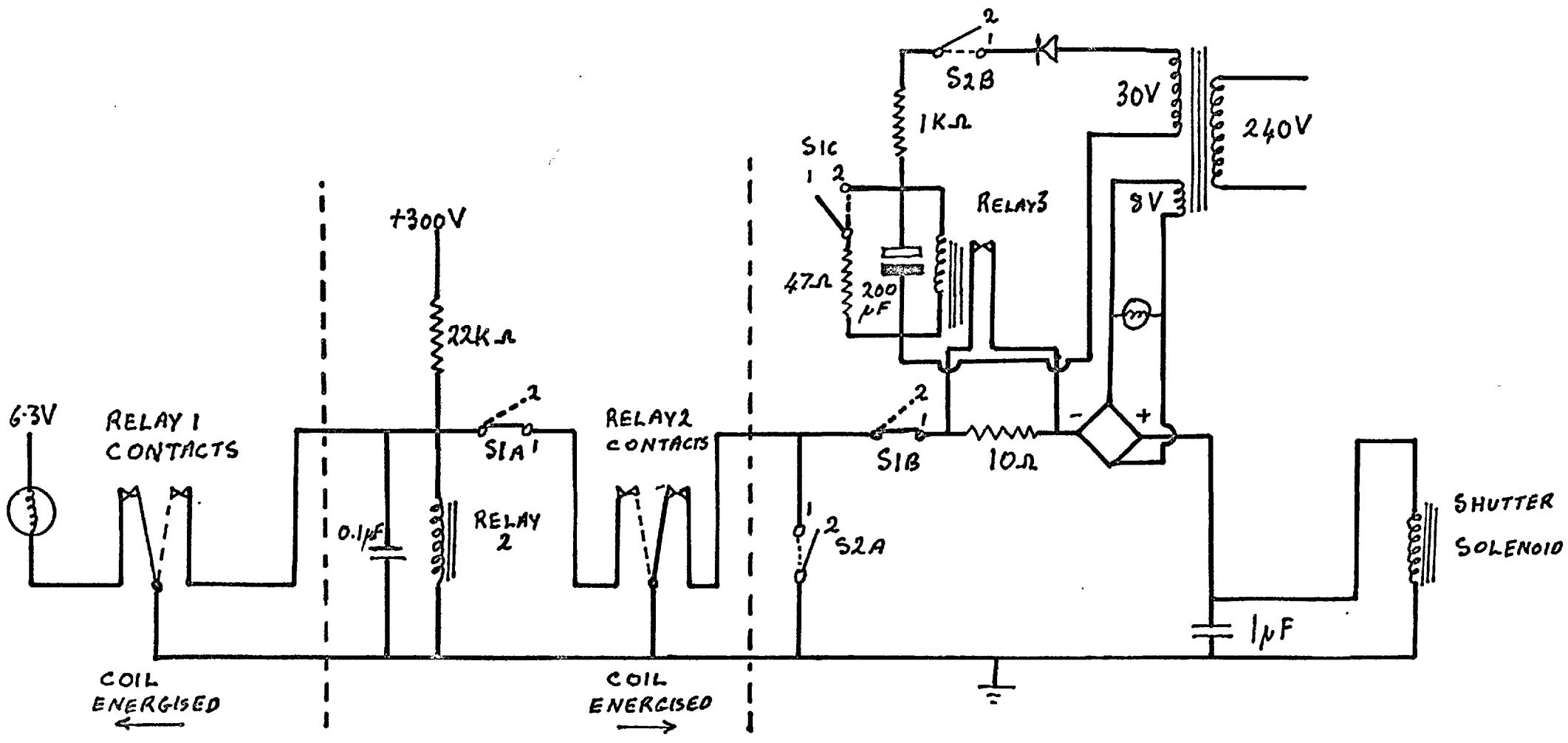

SWITCH POSITIONS SHOWN FOR AUTOMATIC SHUTTER OPERATION.

S1 IN POSITION 1 - SHUTTER OPEN
" " " 2 - " CLOSED
S2 " " 1 - MANUAL OPERATION
" " " 2 - AUTOMATIC "

10 ohm resistance $\frac{1}{4}$ sec after opening S_{1C}, the time delay being provided by the 200μF condenser and the 1 K ohm resistance. When the shutter is closed (i.e. S_{1C} closed) the 200μF condenser is discharged through the 47Ω resistance ready for the next cycle.

The 1μF condenser across the shutter solenoid and the 0.1μF across relay 2 absorb back e.m.f's produced on de-energising these coils which could otherwise pass back to the bridge.

A similar circuit (not shown) is used to actuate the monitor plate movement between evaporations.

5.4. Substrate Preparation.

A number of techniques have been advocated for preparing highly clean glass surfaces before depositing films by vacuum evaporation since, in order to obtain adherent, low absorption coatings free from 'pin holes', a substrate must be free from contaminant films such as grease, absorbed water, dust particles etc.

Putner (1959) has found that vapour degreasing in isopropyl alcohol produces a high standard of cleanliness although if the surface is grossly contaminated ultrasonic cleaning is necessary prior to the vapour degreasing. A cleaned surface rapidly becomes 'dirty' when exposed to the atmosphere even for short periods of time, but such surface contaminants condensed from the atmosphere can be removed from the substrate by subjecting it to bombardment from high velocity ions in the vacuum chamber prior to deposition.(Holland 1956). Surfaces can be cleaned by rubbing with cotton wool impregnated with detergent and subsequently

dried by rubbing with several changes of cotton wool. The author, in the present work, has found that this is not a satisfactory method for producing high quality films since the surface develops an electrostatic charge which attracts minute particles firmly to the cleaned surface. The following procedure for cleaning fused silica substrates was found to be very satisfactory for the present work producing surfaces free from streaks and water marks.

The substrates were soaked in dilute (50 - 50) HCl for about 30 mins, washed and ultrasonically cleaned in a 'Teepol' detergent solution for 2 mins. After further washing the substrates were mounted and held by their edges in spring loaded racks and were then rinsed in de-ionised water followed by A.R. isopropyl alcohol. The rack was then immersed in an isopropyl alcohol degreasing chamber and was withdrawn and transferred to a dessicator when the substrates had reached the temperature of the vapour. After cooling in the dessicator, the substrates were loaded onto the coating jig and the chamber was immediately evacuated. In general, substrates were exposed to the atmosphere after removal from the degreasing bath, for a period of less than 20 sec.

The aluminium charge was cleaned before loading onto the tungsten filaments by immersion in 50-50 Hcl, washing in water and acetone and ultrasonically cleaning in acetone.

5.5. The Evaporation Procedure.

The vacuum chamber is initially flushed with dry, oxygen free nitrogen during the early stages of evacuation with the rotary pump

(This technique was not used for films produced in the glass demountable vacuum system). When the chamber pressure falls to $<10^{-5}$ Torr nitrogen is again admitted to raise the chamber pressure to 0.03 - 0.06 Torr, at which pressure the glow discharge cleaning is carried out by applying a voltage of about 1.5 KV (current $\sim$ 150mA) for about 3 mins to the aluminium ring electrodes (section 5.2.4.).

With the substrate shielded from the vapour source filaments and at a chamber pressure of $<10^{-5}$ Torr both the aluminium and MgF2 charges are heated. In the case of the MgF2, evaporated from a molybdenum boat, the boat temperature is raised to the evaporation temperature of MgF2 over a period of about 20 mins in order to slowly outgass the charge. For the aluminium, the tungsten filaments are heated to melt the aluminium and the filaments are held at a temperature just below the melting point of aluminium for a period of about 10 mins.

Approximately 15 mins before evaporation, liquid nitrogen is pumped through the Meissner coil to reduce the chamber pressure to 10^{-7} Torr. At this stage the film thickness control unit is standardised and set to the required reflectivity as described in section 5.3.3. With the shutter between source and substrate closed the MgF2 charge is raised to dull red heat to reduce the delay time between completing the aluminium evaporation and commencing the MgF2 evaporation. The aluminium charge is then heated and when evaporation proceeds at a fast rate the shutter is opened and deposition occurs. It is important that the aluminium is allowed to evaporate at a fast rate before commencing the deposition since the initial aluminium stream acts as a getter for oxygen and also

reacts with water vapour to form Al_2O_3 and H_2. (Holland 1956).

When the required reflectivity is reached the shutter automatically closes interrupting deposition and the tungsten filaments are switched off. The MgF2 charge is then raised quickly to evaporation temperature, the monitor plate moved to the next evaporation position, the shutter re-opened and the control unit set for monitoring the MgF2 film thickness. These processes can be carried out quickly and the deposition of the MgF2 layer generally begins some 20 secs after completing the aluminium evaporation. The MgF2 evaporation rate is about 15 Å/sec and when the required thickness is reached the shutter is closed manually.

For the case of the F.P. type interference filters the process is repeated as additional layers of aluminium and MgF2 are required.

CHAPTER 6.

OPTICAL PROPERTIES OF EVAPORATED ALUMINIUM AND ALUMINIUM-MgF2 FILMS AND TRANSMISSION CHARACTERISTICS OF F.P. TYPE INTERFERENCE FILTERS IN THE FAR ULTRAVIOLET.

In this chapter the optical properties of semi-transparent aluminium and aluminium-MgF2 coatings are given down to a wavelength of 1800 Å. Two different vacuum conditions of preparation have been used for preparing the coatings and the effect of these different conditions on the optical properties is discussed. The superior optical properties of the aluminium-dielectric combination over single aluminium films are clearly evident and the performance of this combination for multiple-beam interferometry in the far ultraviolet is discussed and illustrated by F.P. interferograms obtained for the λ1849 line of HgI.

In the final part of this chapter the transmission characteristics of F.P. type aluminium -MgF2-aluminium filters for the wavelength region 1700 to 2400 Å are described. From these characteristics the optical properties of the aluminium reflecting layers have been derived. The effects of these properties on filter performance are considered and a comparison is made between calculated and measured values of filter bandwidth for a given filter peak transmission.

The methods which have been employed for measuring the optical properties of the coatings and the transmission characteristics of filters are described in the following section.

6.2. Method of Measurement.

6.2.1. Method for Measuring the Reflection and Transmission Coefficients of the Interferometer Coatings.

The principle of the method employed for measuring the reflection(R) and transmission (T) coefficients of the coatings is illustrated in figure 6.1. A substrate (30 .m.m dia; 1 m.m. thick) carrying the deposited film is mounted above a movable table upon which the detector (D) is mounted. The position of the sample is arranged so that the axis of rotation of the table passes approximately through the reflecting surface. The substrate holder can be rotated about an axis 'O' to allow the incident light beam to fall directly onto the detector.

The reflectometer is attached to a nitrogen purged optica CF4 grating spectrometer and is enclosed in a light tight box which can also be purged. Measurements of film properties at wavelengths shorter than 3800 Å are made using a deuterium lamp as source and in the visible region a tungsten filament lamp is employed. The wavelength interval isolated for measurement can be altered by simultaneous adjustment of the exit and entrance slits of the monochromator. The dispersion is 20 Å m.m.$^{-1}$ in the plane of the exit slit. For measurement of coating properties a wavelength interval of 10 to 20 Å is normally employed. The spectrometer output slit is imaged onto the detector by a concave mirror of focal length = 15 cm. With this optical system the maximum area of sample inspected at a time is approximately 2 m.m. x 6 m.m. for a sampling bandwidth of 20 Å.

In position I the detector receives light from the source either

FIG 6.1 THE OPTICAL SYSTEM FOR MEASUREMENT OF FILM PROPERTIES.

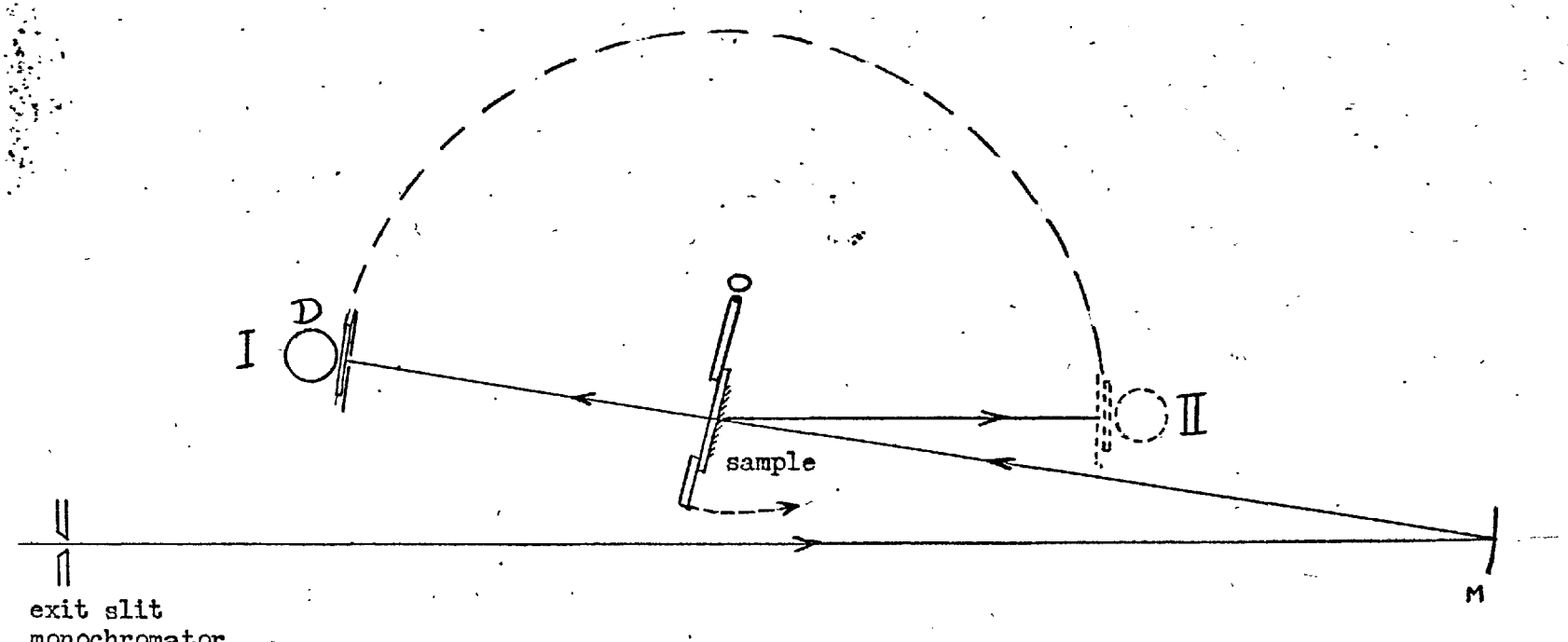

direotly or after passing through the sample. In position II it receives light reflected from the sample at an angle of incidence of about 10^{o}. Thus, the intensities observed in those two positions will be in the ratio of I:T:R.

The procedure adopted for setting up the reflectometer is as follows. Using visible light, an image of the exit slit is focussed onto a ground glass screen mounted approximately 1 m.m. in front of the photomultiplier (deteotor) window. Mounted in front of this screen is a slit aperture of dimensions slightly larger than the image of the monochromator exit slit. The concave mirror is arranged such that the incident light beam passes through the centre of the specimen and the aperture position is adjusted so that the whole of this beam falls onto the glass screen. The detector is turned to the position for reflectivity measurement and the substrate holder is adjusted by a 3 screw, spring loaded mount so that the angle of incidence of the beam onto the sample is about 10^{o} and also to ensure that the reflected beam passes through the slit aperture. After these adjustments the incident and reflected beams are approximately normal to the axis of rotation of the detector platform.

The photomultiplier (Type E.M.I. 9662 A) is enclosed in a metal container to shield the cathode from stray light. Also, since the aperture of the photomultiplier used is small then diffuse reflection from the sample does not greatly contribute to the photomultiplier signal. Stray and diffuse reflected light was found to have a negligible effect on measurements,

In the method of measurement adopted the detector is rotated until

a maximum signal response is obtained for all three measuring positions; direct, transmitted and reflected intensities. The photomultiplier has a thin 'Spectrosil' envelope and can be employed for radiation intensity measurement to a least 1800 Å. However, it was found that if the photomultiplier was used directly then the signal response as a function of photomultiplier position was very critical and did not enable the maximum response to be located both precisely and rapidly. A more convenient arrangement was found to be one in which a sodium salicylate screen was mounted just in front of the photomultiplier. Very uniform phosphor screens were produced by a method similar to that described by Knapp (1963) in which the salicylate is dissolved in alcohol and sprayed onto a cleaned glass substrate which, in this case, was heated to a temperature of about 60°C. The efficiency of such screens as a function of salicylate thickness has been discussed by Seya and Masuda (1963). In the present work a surface density of about 1.5. m.gm. cm^{-2} was employed by spraying onto the substrate a given volume of solution of known concentration. A solution concentration of 20 m.gm cm^{-3} was found to be very satisfactory for this purpose. Using this phosphor screen method the photomultiplier response was still sufficiently sharp for the maximum to be easily located. The reduction in sensitivity which resulted from the employment of the phosphor screen was not at all serious. No differences in values of R and T (within limits of experimental error) were obtained from the two methods of use but because of the ease of rapidly locating the maximum response, the phosphor screen method was preferred.

The photomultiplier was connected directly to a galvanometer whose linearity to current was checked. Signal currents of up to 5 μ A were used and the bleeder chain current was normally about 300μ A. supplied by a Philips stabilised high voltage supply (section 5.3.2.) Each value of R and T for a particular wavelength was determined from at least 6 readings and disagreements in individual values of R greater than 0.5% were seldom found. The most difficult spectral range for measurement was between 1800 and 1900 Å where instabilities in the rate of flow of the purging gas could cause some fluctuations in the readings. For this spectral region the number of observations for each value of R and T was increased. It was found that it was possible to remove and replace the sample such that the value of R was reproduced to within $\pm$ 0.3%. The experimental error in the determination of R was estimated to be within 0.3% whilst the accuracy in T was a little greater. Thus, the error in the value of (R + T) should seldom exceed 0.5%.

As a check on the accuracy of optical properties of coatings determined from the reflectometer measurements the values of R and T were derived for a number of samples by employing the normal incidence method of Giacomo (1952). In this method only the comparatively more simple transmission measurements are required. Two samples are used and the transmission of each (T_1 and T_2) is determined. The samples are set up as in the F.P. etalon with the two reflecting surfaces parallel to each other. The transmission (T_3) of the assembly is then determined using a source of spectral width $\Delta\lambda \geq \lambda^2/2t$ (t being the separation of the reflecting surfaces) such that the spectral width of

the source covers several successive orders of interference. The optical properties are obtained using the relationship

$$T_3 = T_1T_2 \left(1 + R^2 + R^4 + \text{- - - -} \right.$$

$$= \frac{T_1T_2}{1 - R^2}$$

where R^2 is the product R_1R_2. Corrections must be made for reflections from the uncoated substrate surfaces and the magnitude of these corrections can be easily determined. It was found that the results obtained for single aluminium films were in good agreement with reflectometer values within the error of (R + T) of $\pm$ 0.5%

6.2.2. Measurement of Filter Transmission Characteristics.

The transmission characteristics of filters have been determined to a wavelength of 1800 Å using a similar experimental arrangement as described in the previous section. In this case a narrower bandwidth of about 4Å was generally employed. A vacuum Seya monochromator (Spectroscopy Group, Imperial College) was used to check measurements to 2400 Å and to extend the transmission characteristics to 1500 Å. The properties of a number of filters were also checked in the wavelength region 1500 to 1900 Å using a normal incidence vacuum monochromator (Dr.C.B.Lucas, U.K.A.E.A. Culham Laboratory).

Filter transmissions were measured at normal incidence over an area of sample approximately 1 m.m. x 6 m.m. The accuracy of measure-

ment in transmission is $\pm$ 0.2% for wavelengths greater than 1900 Å and $\pm$ 0.4% at shorter wavelengths.

6.2.3. Corrections for Substrate Losses.

The values of R and T for the coatings which are given in the following sections have been corrected for substrate reflection and absorption losses. The method for correction is as follows.

Front Surface Reflection.(see Fig. 6.2.(a)).

Rm = measured value of reflection coefficient.

Tm = measured value of transmission coefficient.

t = transmission coefficient of the substrate/air boundary.

r = reflection coefficient of the substrate/air boundary.

a = the absorption loss when the beam passes once through the substrate.

R = reflection coefficient of the coating

T = transmission coefficient of the coating.

Then $Rm = R + r\,T^2\,(1-a)^2 + r^2\,(1-a)^4\,T^2\,R + \cdots$ 6.1.

and $Tm/T = t\,(1-a) + t\,r\,(1-a)^3\,R + \ldots$ 6.2.

The coefficients r, t and a were determined from measurements of reflection and transmission characteristics for a number of spectrosil samples. The reflection coefficient for a single surface was also determined. Then, if Rm and Tm are the measured reflection and transmission coefficients for the Spectrosil sample (Fig.6.2.(b)).

$$Tm = t^2\,(1-a)\,(1 + r^2(1-a)^2 + r^4(1-a)^4 + \cdots \quad 6.3.$$

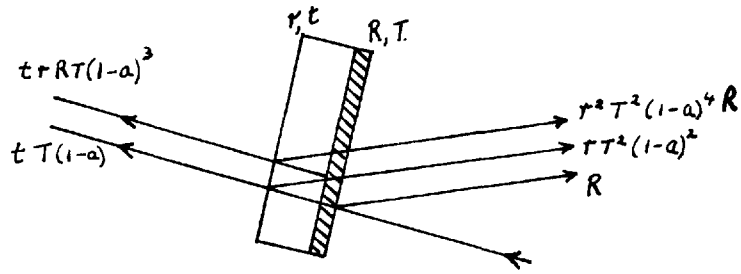

Fig 6.2 a

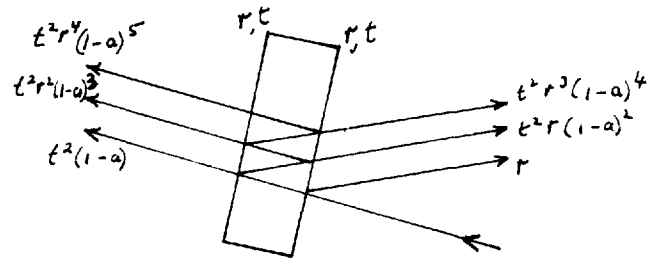

Fig 6.2 b

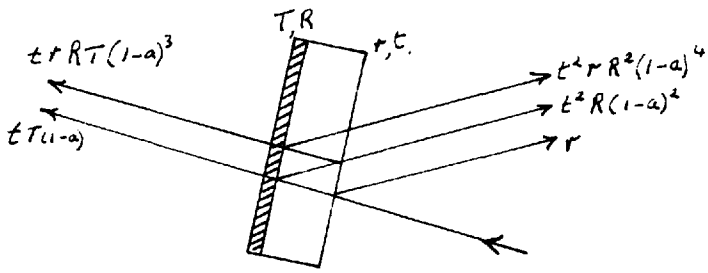

Fig 6.2 c

and $Rm = r + t^2 r (1-a)^2 + t^2 r^3 (1-a)^4 + ----$ 6.4.

The value of r determined from the single surface reflection was found to be in reasonable agreement with r derived from refractive index data given for spectrosil to λ 2000 Å by Gerrard and Turpin (1965). (see r^1 in Table 6.1.).

Table 6.1. gives measured data obtained for several 1.m.m thick Spectrosil samples.

The magnitude of the corrections for substrate absorption and reflection losses can be obtained from table.6.1. For example, if $R > 70\%$ then the second term of equation 6.1. is only $\simeq 0.05\%$ whilst higher terms can be neglected. In equation 6.2, the first term is $\simeq 0.95$, the second term $\simeq 0.04$ and remaining terms of r^2 and higher can be neglected. The errors in r, t and a used for corrections cause an insignificant increase in the errors of R ant T derived from measurements of Rm and Tm. These experimental errors are within $\pm$ 0.3% and $\pm$ 0.2% of the incident light.

Back Surface Reflection (Fig.6.2.(c)).

The optical properties of a number of samples have also been derived from measurements of back surface reflectance i.e. measurements made with the substrate facing the incident beam. The purpose of these measurements was to determine whether or not a deposited film showed a different reflectance between the initial layers in contact with the substrate and the final exposed layers (after allowing for substrate refractive index).

The correction for Rm is given by (see fig.6.2.c.)

$$Rm = r + t^2 R(1-a)^2 + t^2 r R^2 (1-a)^4 + ----$$ 6.5.

Table 6.1.

	Tm% ± 0.2%	t	r	a%	r'
2800	92.0	0.96 ± 0.002	0.043 ± 0.003	0	0.039
2600	91.8	0.958	0.044	0	0.040
2400	91.5	0.956	0.045	0	0.041
2200	91.5	0.956	0.046	0	0.043
2000	91.0	0.955	0.048 ± 0.004	0	0.046
1900	89.5	0.945	0.051	~ 1	
1800	88.5	0.940	0.054 ± 0.005	~ 1	

Values of a were calculated from eqns. 6.3. and 6.4.

where in this case R is now the reflection coefficient for the film-substrate boundary.

The relationship between T and Tm is identical with that given in equation 6.2. It is now seen that the error in the derived value of R will be increased since it involves the term (Rm-r). The value of R was corrected from a film-substrate boundary to a film-air boundary using optical constants for aluminium given by Hass and Waylonis (1961) and refractive index data for spectrosil given by Gerrard and Turpin.(1965)

6.3. The Optical Properties of Semi-Transparent Aluminium Films in the Far Ultraviolet.

In this section the optical properties for single aluminium films are given which were prepared under the two different vacuum conditions described in Chapter 5. These results will be put into the two categories according to the vacuum conditions of preparation:-

1) 'Poorer conditons' - in which coatings were deposited in the glass demountable coating system.(initial evaporation pressure = 10^{-5} Torr)

2) 'Improved conditions' - films prepared in the stainless steel coating plant in which special attention was paid to reducing the water vapour content of the residual gas atmosphere. (Initial evaporation pressure of 10^{-7} Torr.)

6.3.1. Films Prepared under the Poorer Vacuum Conditions.

The variation of the reflection coefficient (R) and the transmission

coefficient (T) with wavelength for a number of aluminium films deposited on to 'Spectrosil B' substrates is shown in figure 6.3. These films were deposited in a time of 2 to 3 secs (deposition rate of about 100 to 150 Å sec^{-1}). Film properties shown in figure 6.3. were measured after 2 to 24 hours exposure to air. Values of R and T have been corrected for substrate reflection and absorption losses as described in section 6.2.

The optical properties of these films were very disappointing. Values of (R + T) are some 2.5 to 3% lower than corresponding values reported by Hass and Waylonis (1961) for the wavelength region 2200 to 2800 Å. At shorter wavelengths (R + T) values are also about 3% lower than the reflectance of opaque aluminium films reported by Hass, Hunter and Tousey (1957). These results were somewhat surprising in view of the fact that there was not a great difference between the deposition rate and evaporation pressure used during this investigation and that of Hass and Waylonis. In addition, the (R + T) values at 2600 Å are little different from those of Burridge et.al.(1953) where the deposition rate was approximately an order of magnitude lower.

Opaque films prepared in this plant also possess values of R closely following the curves 1,2, shown in figure. 6.3.

Back Surface Measurements.

Values of R and T have also been measured for several of the thicker films and for opaque films from the substrate side of the coating. Values of (R + T) obtained after correction for substrate losses and refractive index are shown in figure 6.3. (curve $(R + T)'_B$). Considering the greater errors in the back surface measurements (section 6.2.3.) the

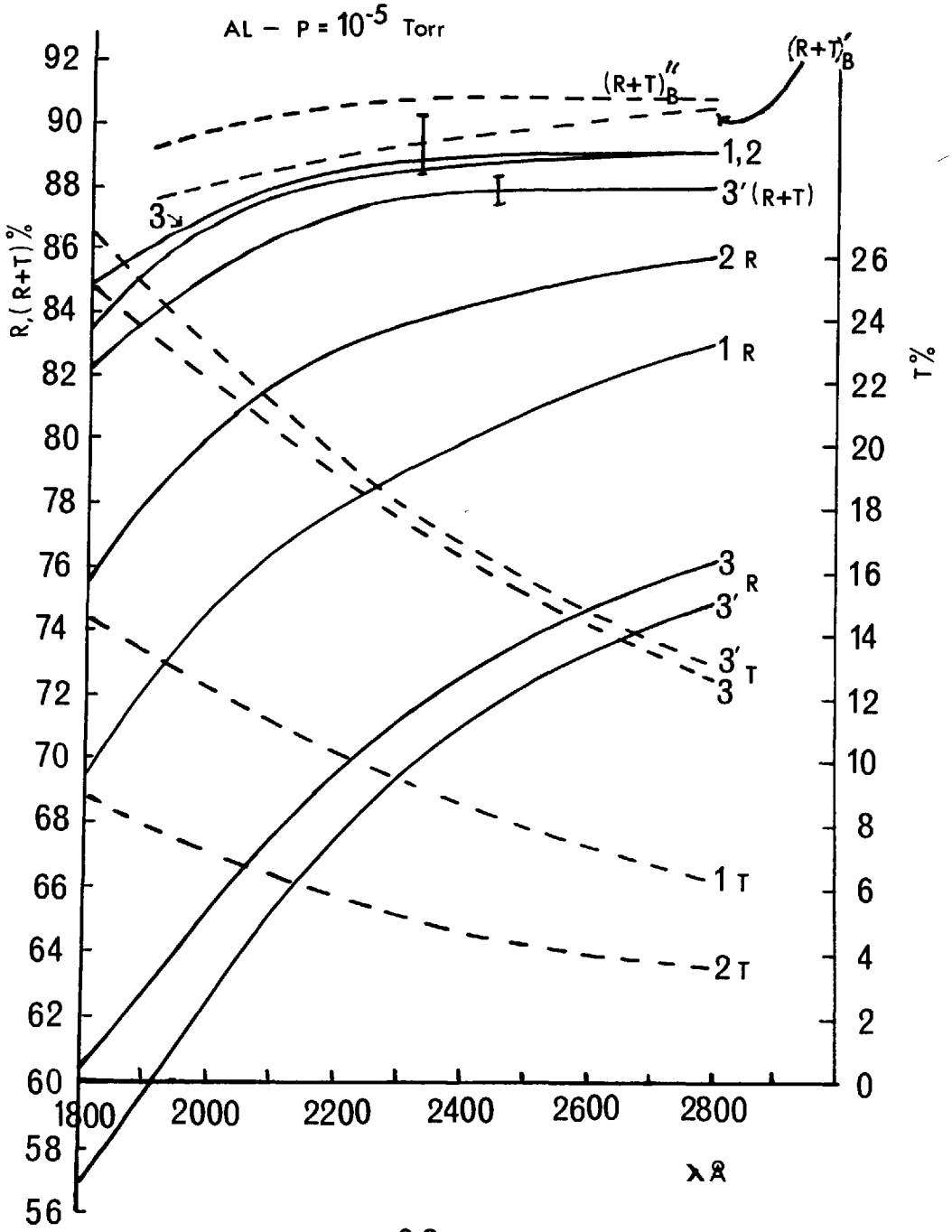
AL – P = 10⁻⁵ Torr
(R+T)″B
(R+T)′B
1,2
3′ (R+T)
2 R
1 R
3 R
3′
3′ T
3
1 T
2 T
R,(R+T)%
T%
λ Å
92
90
88
86
84
82
80
78
76
74
72
70
68
66
64
62
60
58
56
26
24
22
20
18
16
14
12
10
8
6
4
2
0
1800
2000
2200
2400
2600
2800

Figure 6.3.

difference in (R + T) values is not greatly significant. These optical properties derived from back surface measurements are still very much inferior to those of Hass and Waylonis.

Change in Film Properties with Time.

Figure 6.3. also shows the change in R and T with time for optical properties measured after 15 mins and 24 hours exposure to the atmosphere (curves 3 and 3' respectively). The magnitude of the changes in both R and T increases at the shorter wavelengths. Changes in the optical properties of aluminium films with time are discussed further in section 6.4.2.

Variation of Film Absorption with Film Thickness.

No significant variation of film absorption with film thickness was observed for samples transmitting up to about 12% (at λ 2000 Å). However, films having a transmission greater than this value are characterised by an increased film absorption. The absorption increases as the thickness of the aluminium film is reduced.

6.3.2. Films Prepared under the 'Improved' Vacuum Conditions.

An investigation of the optical properties of single, semi-transparent aluminium films has been made in which the coatings were prepared under the improved vacuum conditions described in Chapter 5. The rate of deposition was the same as that used for preparing films under the poorer vacuum conditions.

The variation of R, T and (R + T) with wavelength for a number of samples is shown in figure 6.4. Optical properties were measured

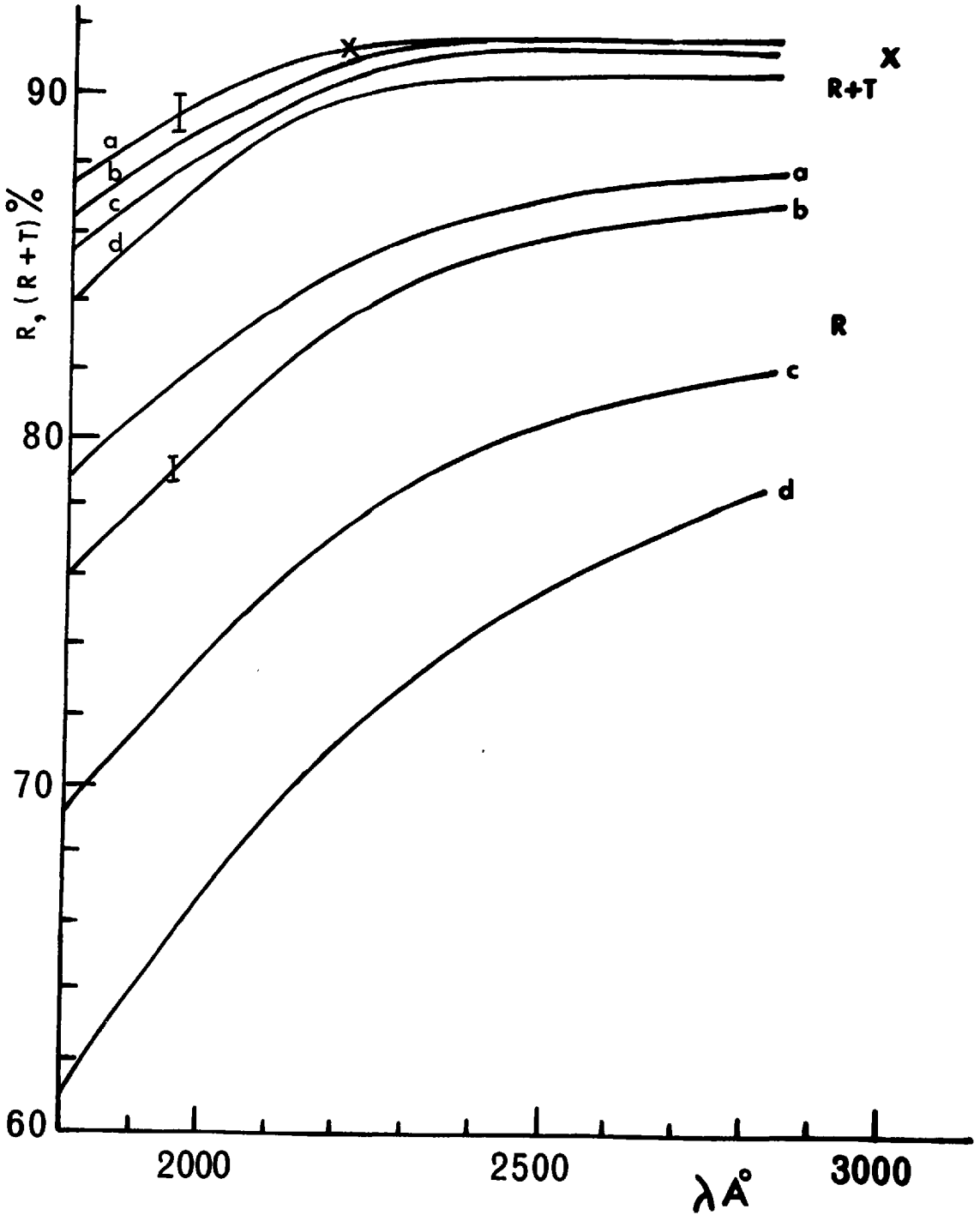

Figure 4.4.

after 24 hours exposure to the atmosphere. It can be seen that the improved vacuum conditions have resulted in an overall improvement in optical performance. For wavelengths above 2200 Å the values of (R + T) are in close agreement with corresponding values given by Hass and Waylonis whose results are indicated at the wavelengths 2200 and 3000 Å. In the wavelength region 1800 to 2200 Å, these (R + T) values also agree closely with values of reflectance reported for opaque aluminium coatings, (Hass, Hunter and Tousey 1957).

Back Surface Measurements.

Optical properties were again determined, for several thicker and opaque films from back surface measurements. Results for (R + T)(corrected for substrate refractive index) are shown in figure 6.3.(curve $(R+T)"_B$).

These values of (R + T) so derived are greater than for films produced under the poorer vacuum conditions (fig.6.3.). The back surface measurements reveal little difference in reflectance between the aluminium-substrate boundary (corrected for substrate refractive index) and the reflectance at the exposed aluminium surface.

The Effect of Deposition Rate.

Whilst the effect of deposition rate on film properties has not been studied in great detail figure 6.5. compares the values of R and (R + T) for films deposited in times of 2 and 20 secs under the improved vacuum conditions. Also shown is the effect of interrupting deposition. In this case the total evaporation time was 20 secs but the substrate was shielded from the vapour stream for a period of 4 secs after deposition has proceeded for 12 seconds. The influence of the deposition

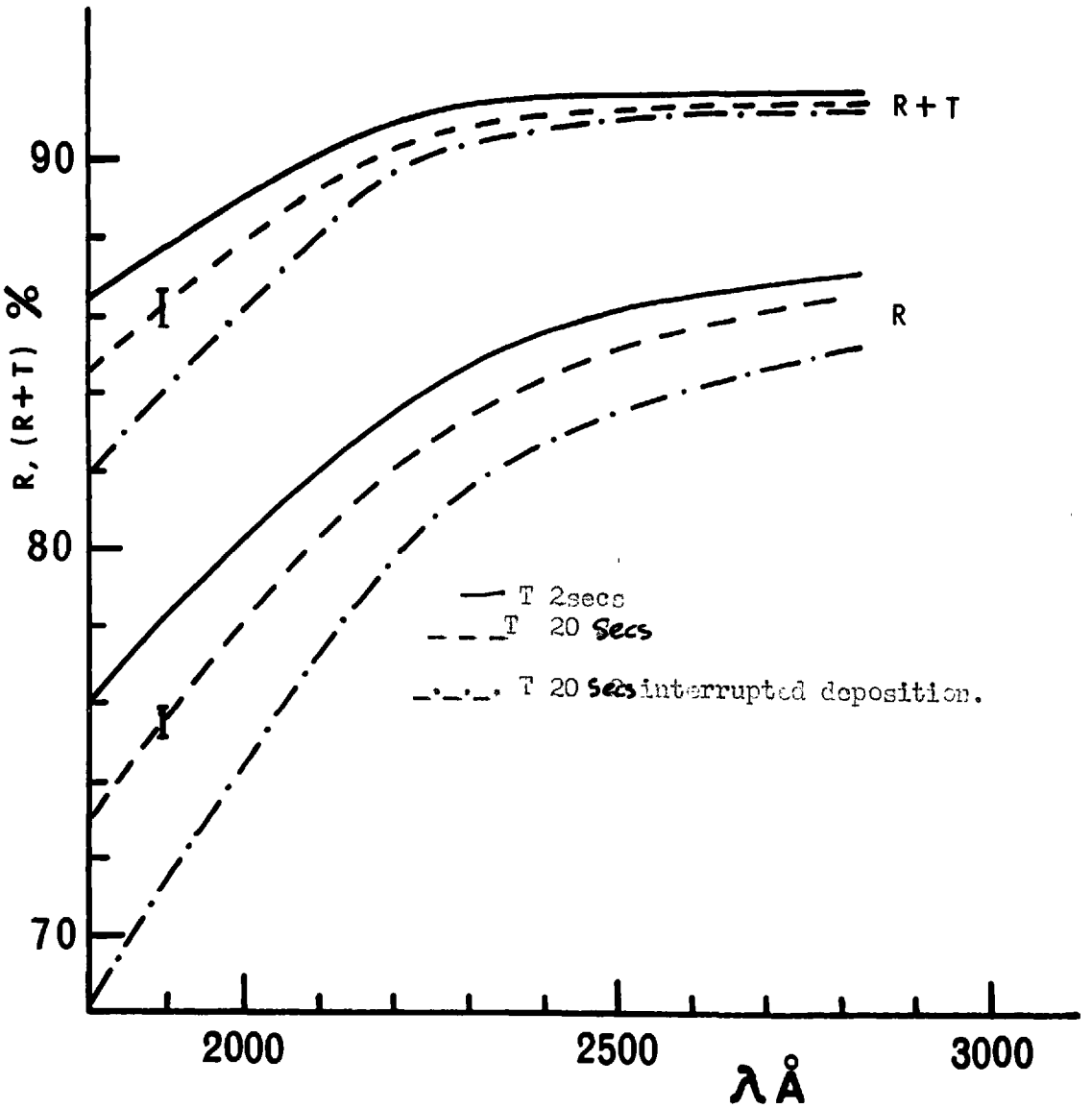
R+T
R
90
80
70
R, (R+T) %
2000
2500
3000
λ Å
T 2secs
T 20 Secs
T 20 Secs interrupted deposition.

Figure 6.5.

rate on film absorption is very marked for wavelengths shorter than 2200 Å and it is seen that the higher absorption is due to a decrease in reflectance.

Change in Optical Properties with Time.

Changes in values of R and T which occur upon exposure to the atmosphere for films prepared under the improved vacuum conditions are discussed in section 6.4.2.

Variation of Film Absorption with Film Thickness.

Figure 6.4. shows that the film absorption for the aluminium films prepared under the improved vacuum conditions increases as the film thickness is reduced. The dependence of absorption on film transmission is nearly a linear relationship for values of T up to approximately 20%. For thinner films, absorption increases more rapidly with increasing T.

This dependence of absorption on film thickness for the thicker films was not found previously for the poorer quality coatings. In addition, it is contary to the findings of Hass and Waylonis who observed that at 2200 Å the film absorption was independent of thickness for film thicknesses greater than 120 Å. However, in the present work slightly lower deposition rates have been employed than those used by Hass and Waylonis.

6.3.3. Optical Microscope Examination of Aluminium Films.

Several aluminium films prepared under the two different evaporation conditions have been examined in transmission using a Vickers optical microscope. Photographs 6.6.(a) and (b) were obtained for films prepared under the poorer and improved conditions respectively. The magnification in the prints shown is approximately a factor of 500.

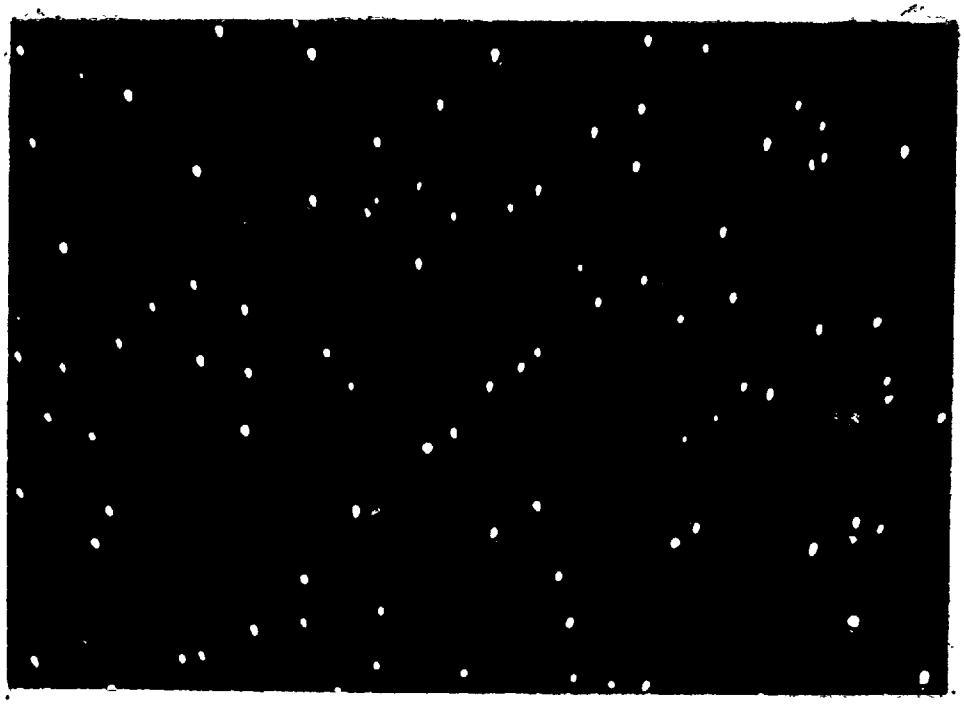

Fig.6.6a

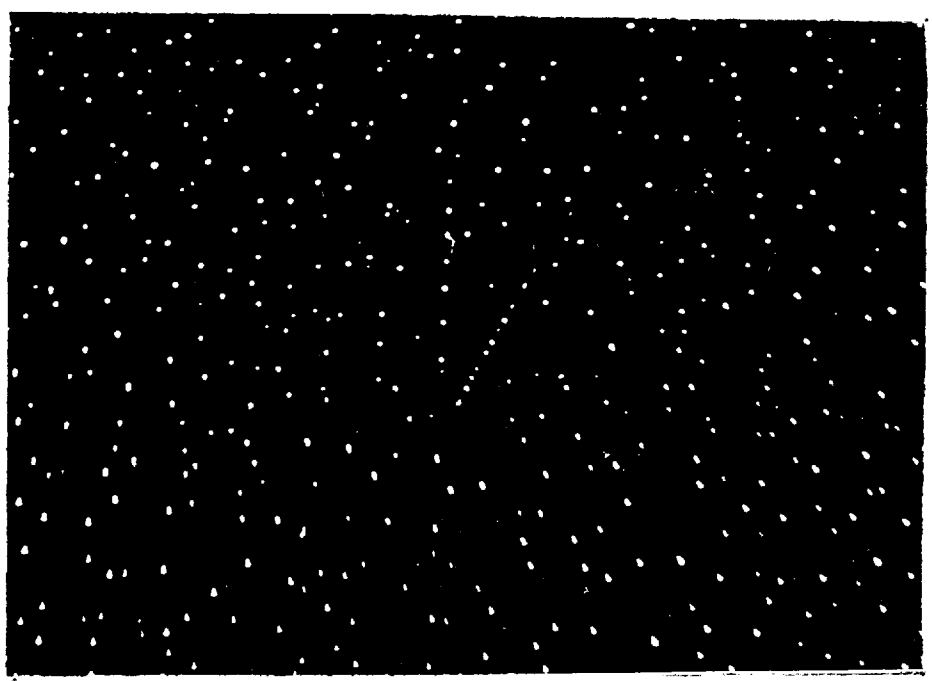

Fig.6.6b

These photographs show that 'microholes' have been formed in the aluminium films but there is both a difference in hole density and size for the two evaporation conditions. The mean size and surface density has been determined and is as follows.

	Poorer Conditions	Improved Conditions.
Mean diam(cm)	2.7×10^{-4}	1.6×10^{-4}
Mean Density cm^{-2} of sample	2×10^{5}	10^{6}
Surface Area of sample occupied by pinholes.	approx. 1%	approx. 2%

The formation of these holes has been examined for a film produced under the improved vacuum conditions. Upon removal from the coating plant the sample is completely free from defects. After 40 hours storage in a dessicator a few holes are present and many more appear to be developing, and after 90 hours most holes appear to have formed. A suggested mechanism for the formation of those holes is given in section 6.4.1.

For the aluminium - MgF2 double layers (section 6.5.) all samples examined showed no evidence of pinhole formation for storage periods of up to 3 years.

6.3.4. A Comparison between Measured and Computed Optical Properties For Single Aluminium Films.

In chapter 4 results were given for computed values of R and T for a single aluminium film deposited onto a non-absorbing substrate of

index 1.55. Figure 6.7. shows measured values of R and (R + T) compared with computed optical properties for an aluminium film 275 Å thick. Measured film properties are for a coating prepared under the improved conditions at a deposition rate of 100 -150 Å sec^{-1}.

It is seen from figure 6.7. that measured values of (R + T) after 15 hours exposure are considerably lower than those obtained from calculation, particularly at the shorter wavelengths. This difference between computed and measured properties is largely due to lower values of R. However, the optical properties of exposed aluminium films change with time (Chapter 3) and in figure 6.7. experimental values of R and (R + T) are given for measurements made after 15 minutes exposure to air. In this case the agreement between computed and measured values of (R + T) is well within limits of experimental error over the entire wavelength region 1800 to 2800 Å. The change in optical properties with time is further examined in section 6.4.2.

It must be remembered that the optical constants for aluminium films given by Hass and Waylonis were derived from measurements of films possessing a surface oxide thickness of about 15 Å (corresponding to 24 hours exposure) and therefore they do not represent an idealised, oxide free film. This therefore questions the validity of extrapolating these optical constants to wavelengths shorter than 2200 Å. However, according to Schroeder (1962) the extrapolation gives a reasonable agreement with the optical constants derived from opaque aluminium films at 1216 Å (Berning, Hass and Madden 1960).

From the present investigation it can be concluded that the extra-

FIGURE 6.7.

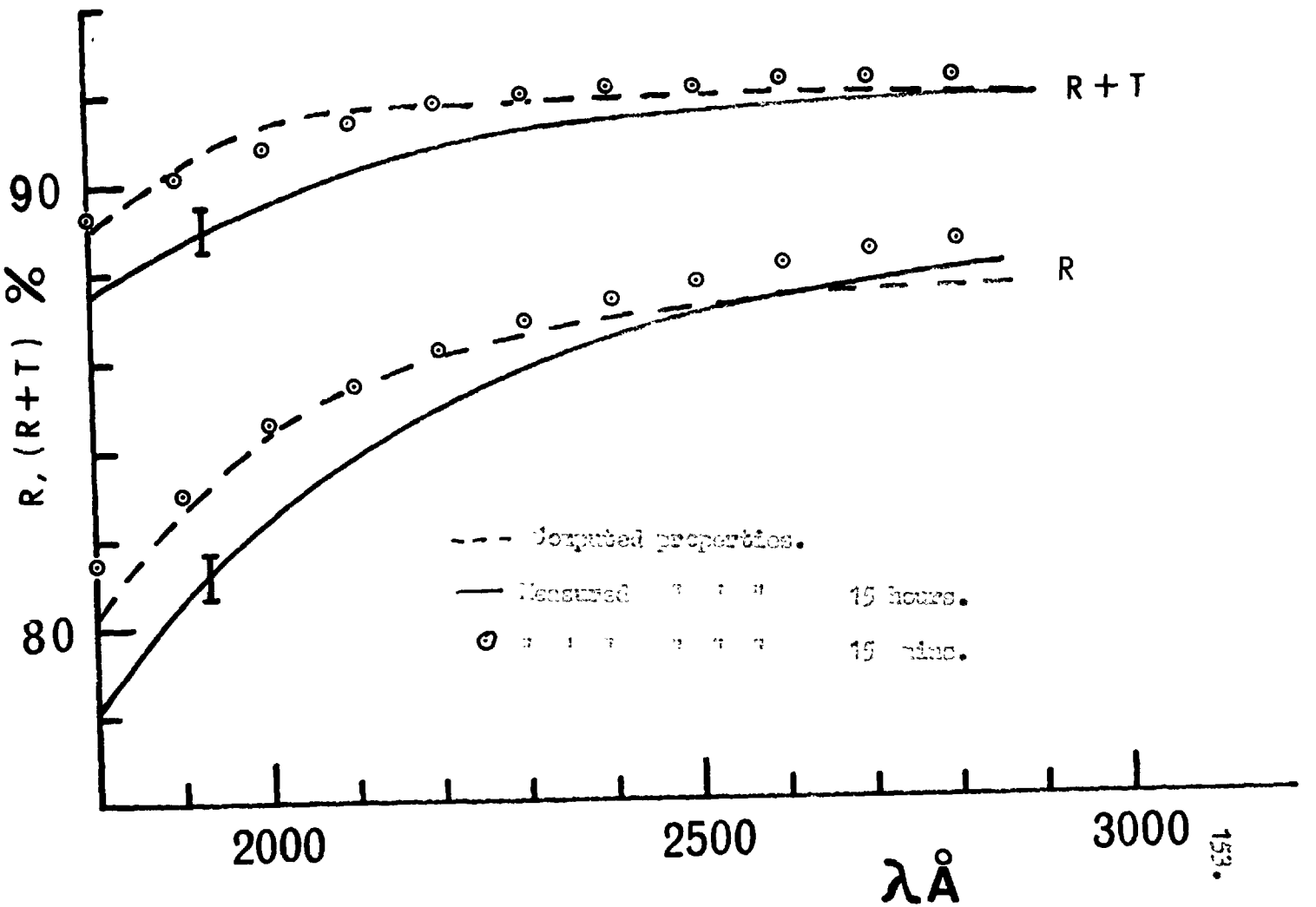
R + T
R
90
80
R, (R+T) %
2000
2500
3000
λÅ
--- Computed properties.
Measured 15 hours.
15 mins.

polated optical constants can be used for calculating the properties of (thick) aluminium films to 1800 Å and values so derived are in good agreement with experimental values (prepared under the above conditions) and also with measured values of reflectance for opaque, unexposed aluminium films (Chapter 3). This is of importance particularly for extending the work to include computation of the properties of protected types of films such as aluminium - MgF_2. A comparison between computed and measured properties for such films is made in a later section. However, for wavelengths less than about 1800 Å it must be realised that the experimental film properties will be dependent upon the delay time between completing the aluminium evaporation and applying the protective coating.

6.4. A Discussion of the Optical Properties of Single Aluminium Films.

6.4.1. Film Absorption - Dependence on the Preparation Conditions.

As already stated in section 6.3.1. the absorption values for the single aluminium films prepared under the poorer evaporation conditions were higher than had been expected. Whilst the properties of the aluminium - MgF_2 films (Section 6.5.) prepared under the same vacuum conditions are very much superior, it was because of the poor optical quality of these aluminium films that an improved coating plant was constructed during the course of the present investigation.

The remarkable difference in optical properties between the aluminium films produced under the two different evaporation conditions must be purely due to a difference in the content of the residual gas atmosphere

in the coating chambers since other pertinent parameters such as the rate of deposition, aluminium purity, source-target distance, substrate cleaning etc were the same in both cases. It is found that reducing the evaporation pressure from 10^{-5} Torr to 10^{-7} Torr causes a reduction in film absorption of some 2 to 3% over the wavelength region 1800 - 2800 Å. (Fig.6.8). This reduction in absorption is seen to be due to higher values of reflectance. Hass and Tousey (1959) found that changing the evaporation pressure from 10^{-5} to 10^{-4} Torr had little effect on the reflectance of opaque aluminium films deposited at rates of 400 Å sec^{-1}. For lower deposition rates however, the effect of increasing the evaporation pressure was to cause a significant decrease in reflectance (Chapter 3). Differences in reflectance were attributed to the fact that during deposition residual gas molecules in the coating chamber become trapped in the film. For high deposition rates at low pressures fewer impurity molecules are trapped and the resulting film is more compact and grows a thinner, tighter oxide layer upon exposure to the atmosphere. It is the oxide layer which causesa decrease in reflectance. The difference in optical properties of the present semi-transparent films is now considered on a similar basis.

According to Berning, Hass and Madden (1960) an aluminium film deposited under optimum conditions grows an oxide layer of about 15 Å after 24 hours exposure to air and will reach a limiting thickness of some 22 Å after about 1 month. If the film is deposited at a slow rate then the formation of a granular structure is promoted and the oxide layer can reach a limiting thickness of 90 Å (Holland 1956). At λ2200 Å

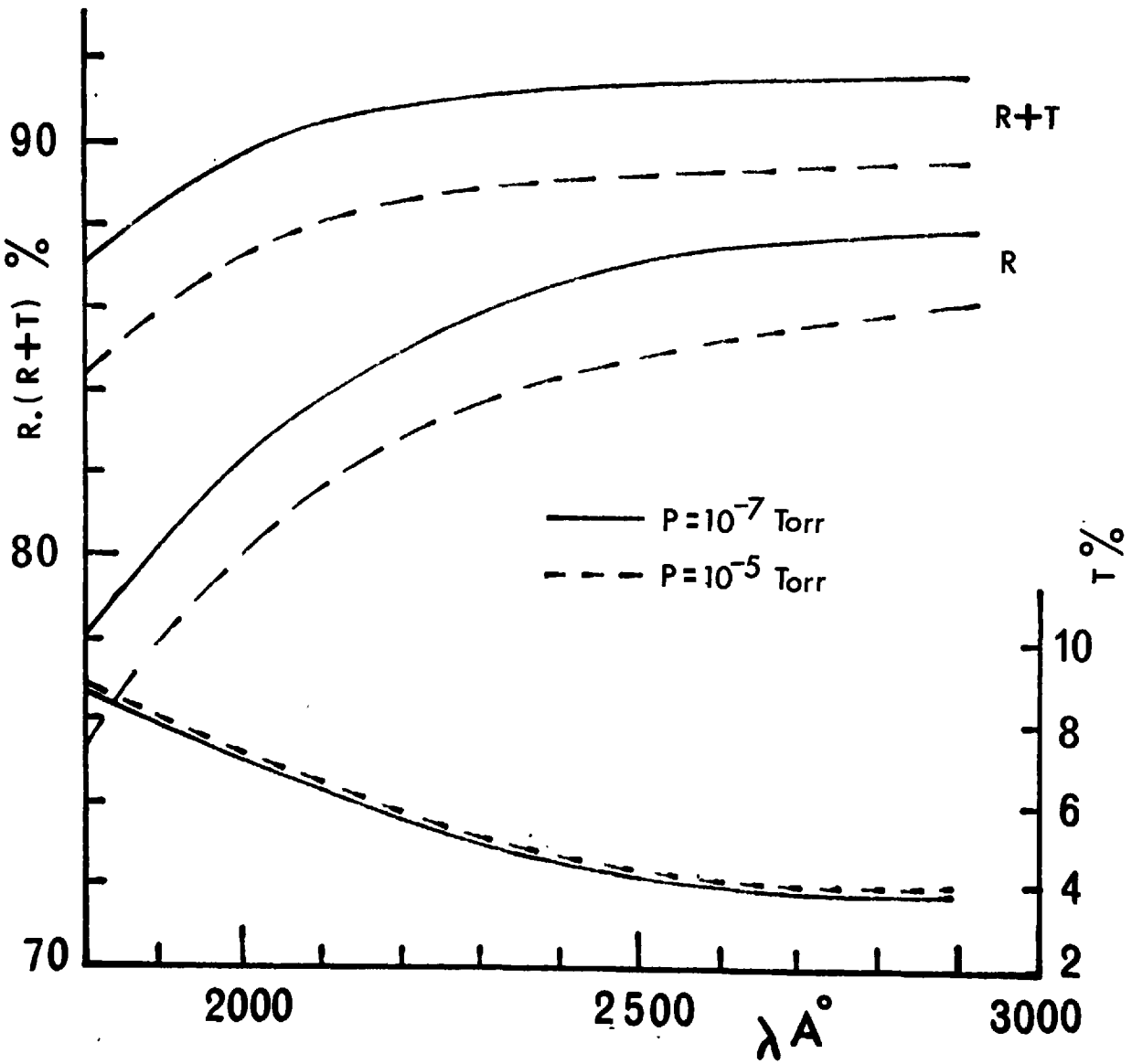

FIGURE 6.8.

values of (R + T) of 91% are obtained for the transmitting films deposited under the improved conditions (aged 24 hours). The corresponding (R + T) values for the poorer conditions is 88%. Computed results for aluminium films overcoated with a non-absorbing layer of index 1.85 (refractive index for Al_2O_3 is 1.85 at 2200 Å. Hass, Hunter and Tousey 1957), show that (R + T) is 91% for an oxide layer of thickness = 15 Å (See Chapter 4). For an (R + T) value of 88% the corresponding oxide thickness would be some 65 Å assuming the same n and k values for aluminium.

However, one must also consider the fact that not only has the evaporation pressure been reduced by two orders of magnitude but the composition of the residual gas atmosphere is also likely to have been altered. The residual gases present in the atmosphere of the coating chamber are emitted from the various components present in the system. Holland and Bateman (1962) have shown that the 'O' ring seals can become a dominant factor if made from silastic. A high content of water vapour, oxygen and nitrogen has been observed in the residual atmosphere by these authors when silastic seals have been employed and this has been largely attributed to the permeability of these gases through such seals. In the glass demountable system there was a considerable area of seals of this type partly exposed to the coating chamber and it is not unreasonable to assume that there was a high concentration of oxygen and water vapour present in the residual atmosphere.

In the improved metal coating plant all seals were either of indium or Viton A. With these types of seals the above authors found that there was a considerable reduction in the amount of water vapour present in

the residual gas atmosphere whilst the concentration of oxygen was reduced to an extremely low level. In addition, the inclusion of the liquid air Meissner trap inside the metal coating chamber condenses water vapour which then has a negligible vapour pressure at the trap temperature. Typically, the chamber pressure falls by about an order of magnitude when the liquid air is circulated through the trap. The effect of residual oxygen in the gas atmosphere on the optical properties of aluminium films has been discussed in Chapter 3. However, the presence of water vapour will also have a serious detrimental effect on film properties since aluminium will react with water vapour to form Al_2O_3 according to the reaction

$$2\,Al + 3\,H_2O \rightarrow Al_2O_3 + 3H_2.$$

Comparison of the back surface measurements made on thick and opaque films shows that lower absorption values are obtained for the improved conditions of preparation resulting from a higher reflectance at the aluminium-substrate boundary. This would suggest that under the poorer conditions the substrate surface might suffer greater contamination because of the higher water vapour content of the residual gas atmosphere in the coating chamber. Also, under the poorer conditions not only is the number of impurity molecules in the chamber atmosphere greater than for the improved conditions but the relative concentration of oxygen and water vapour is likely to be much higher. During deposition the growing film will trap more impurity molecules and the film will be less compact and grow a thicker oxide layer upon exposure to air. However, it is perhaps unlikely that the oxide film will grow to 65 Å as indicated by

computation since substrate contamination and other factors besides oxide layer formation must be considered which will contribute to film absorption.

After the discharge cleaning process (Chapter 5) the substrate surface will become contaminated by the residual atmosphere of the coating chamber. Water vapour will be condensed on the substrate surface which may become covered with an adsorbed film. The adsorbed film can be expected to lower the surface attraction forces of the substrate and also its surface tension (Holland 1964). If the substrate contamination is very great then water droplets are likely to spread over a larger surface area of the substrate (because of the lower surface tension forces) than if the water vapour concentration in the atmosphere is very small. When the aluminium is deposited residual gas molecules in the chamber atmosphere and vaporised substrate surface contaminants will become trapped in the growing film.

Films deposited under the poorer conditions are likely to posses a more porous structure and larger inclusions than those deposited under the better vacuum conditions. After deposition and upon exposure to the atmosphere the extent of the oxidation for the more porous film will be more pronounced. Also, within the films oxidation will occur because of the trapped oxygen and water vapour and again this will probably be of a greater extent for the more porous films. The attack of the aluminium by oxidation upon exposure to air and oxidation within the films, and the presence of irregularities and inclusions caused by trapped gases may lead to the breaking-up of the films observed in the

optical microscope examination (section 6.3.3.). If this is indeed the case, then it is to be expected that the size of the 'microholes' for the more porous films will be larger than those which develop in the films produced under the better vacuum conditions.

It was seen previously that the poorer optical properties were associated with the films having a smaller surface area of microholes but holes of a larger size. Whilst these films show a smaller density of holes it is likely that the deposited aluminium is of a poorer quality for the reasons outlined above. However, a more detailed explanation of the formation of the microholes and differences in optical properties brought about by the two vacuum conditions requires additional experimental evidence. In particular, a detailed structural examination of the films for the two preparation conditions would be required.

Nothing has yet been said of the aggregation or granularity of the deposited films. The optical microscope study of the aluminium films was not of a sufficiently high resolution to observe any indication of an aggregated structure. From a molecular view-point, a continuous layer will only be formed if the forces binding the aluminium atoms to the substrate are greater than the forces binding the metal atoms together (see e.g. Weaver 1962). It would therefore be expected that any factor which will reduce the binding forces of the aluminium to the substrate will contribute to an increased aggregation in the deposited film. Thus, substrate contamination and the presence of trapped impurity molecules are likely to result in an increased degree of aggregation which also depends on many other factors including the surface mobility

of the incident vapour atoms.(e.g. Heavens 1955). Again no definite conclusions can be made in the absence of a detailed structural examination of the films.

6.4.2. Changes in Optical Properties with Time.

Although the change in the optical properties of semi-transparent aluminium films exposed to air has not been previously studied in the far ultraviolet, extensive measurements have been made on the decrease in reflectance of opaque films. For coatings prepared under 'Optimum' conditions there is little change in R with time for wavelengths longer than 2200 Å. At shorter wavelengths however, the decrease in R becomes very substantial. This change in reflectance has been attributed to the growth of a surface oxide layer.(Chapter 3).

For transmitting films in the far ultraviolet it has been found in this investigation that there is an increase in T and a decrease in R and (R+T) with time during exposure to the atmosphere. The magnitude of these changes becomes greater at shorter wavelengths (fig.6.3. and fig.6.7.). For films deposited under the improved vacuum conditions there is little change in optical properties after 24 hours exposure to the atmosphere.

Again, the changes in optical properties for the transmitting films can be examined on the basis of surface oxide layer growth but in this case, any analysis is complicated by the uncertainty of the thickness of aluminium converted to oxide. For an opaque aluminium coating this problem is not so important. Because of this partial conversion of aluminium to aluminium oxide it would be expected that an oxide layer

would have a greater effect on the properties of transmitting films than for opaque layers and this indeed has been found to be the case.

Turbadar (1959) has calculated the thickness of aluminium converted to oxide purely from density and molecular weight considerations of the aluminium and aluminium oxide.

Thus, $$\frac{h_1}{h_2} = \frac{2M_1 d_2}{M_2 d_1}$$

where h_1 = the thickness of aluminium converted to oxide.

h_2 = the total thickness of the oxide layer

M_1 = the atomic weight of aluminium (27).

M_2 = the molecular weight of oxide (102)

d_1 = the density of aluminium (2.7 gm/c.c.).

d_2 = density of oxide (3.7 gm/c.c.)

On this basis, for an oxide layer of 20 Å thickness, the thickness of aluminium converted to oxide is 14.5 Å and the increase in total thickness of the deposited film is 5.5 Å. Previously Hass (1949) reporting on the properties of anodised aluminium films had found that the thickness of the oxide coatings is 1.38 times thicker than that of the aluminium layer replaced. This is in agreement with the above relationship of Turbadar although the agreement is somewhat false in that Turbqdar has taken a higher density than normally accepted for the Al_2O_3 layer 3.2 gm cm^{-3}. However, employing the relationship $h_2/h_1 = 1.38$ an indication of the expected change in R and T can be obtained by using computed optical properties for aluminium films coated with different thicknesses of non-absorbing surface layer of index 1.85 (Chapter 4).

As an example, the case of an oxide layer increasing from 5 to 15 Å

in thickness will be considered. This change in oxide thickness is approximately what might be expected for exposures to the atmosphere ranging from a few minutes to about 24 hours, for a film deposited under optimum conditions (Chapter 3). From the relationship given above this increase in oxide thickness by 10Å will reduce the aluminium thickness by some 7 Å. Suppose the original film (after a few minutes exposure) is 275 Å aluminium + 5 Å oxide then after 24 hours exposure the resulting film will be 268 Å aluminium + 15 Å oxide. Computed changes of optical properties under these conditions are given below. These computed changes are compared with values for a film prepared under the improved vacuum conditions measured after 15 mins and 15 hours exposure to air. (Optical properties change very little between 15 hours and 24 hours exposure).

Change in Optical Properties with Time.

Wavelength(A)	Calculated%			Measured%		
	R	T	(R+T)	R	T	(R+T)
2600	-0.8	+0.5	-0.3	-0.7	+0.2	-0.5
2200	-1.7	+1.0	-0.7	-1.6	+0.6	-1.0
1800	-2.5	+1.5	-1.0	-2.1	+0.9	-1.2

These measured and computed changes in optical properties are in reasonably close agreement considering the assumptions which have been made regarding thicknesses of oxide layer, conversion of aluminium to oxide, optical constants of aluminium and oxide etc. At least these computed results serve to illustrate that the changes in oxide layer thickness which might be expected during exposure to the atmosphere, may

to a considerable extent, account for the observed changes in optical properties with time.

In the case of the films deposited under the poorer vacuum conditions greater changes in optical properties with time were observed (fig.6.3. curves 3 and 3'). A similar calculation to the above could be made to compare with measured values. However, in this case, the thickness of oxide for different exposures is even more uncertain since for films produced under poorer vacuum conditions it is known that the oxide grows to a greater thickness and at a faster rate (Chapter 3). More important, it is seen from comparing figures 6.7. and 6.8. that the aluminium films prepared under the poorer conditions can in no way be represented by the optical constants for aluminium which have been used for computation in Chapter 4. For this reason, there is little information to be gained by a comparison between computed and experimental data as was done for the better optical quality films.

6.4.3. Film Absorption - Dependence on Film Thickness.

Hass and Waylonis (1961) state that the optical constants of aluminium films evaporated at high deposition rates, remain unchanged down to film thicknesses of 100 Å. Their experimental results show that at λ5461 Å a decrease in film thickness from 320 to 120 Å causes an increase in absorption by about 5% whilst at 2200 Å the corresponding change in absorption is insignificant. These results are strikingly different from previously reported data and it has already been stated (Chapter 3) that Burridge et.al. 1953 observed an almost linear increase

of absorption with decreasing film thickness (at λ2600 Å). However, the deposition rate used was very much lower than that employed by Hass and Waylonis.

The absorption of electromagnetic waves in a metal film arises from both free and bound electrons although, depending on the wavelength of the radiation, one of these sources of absorption may be dominant. The contribution to film qbsorption from bound electrons would not be expected to depend very greatly on the state of aggregation of the film but on the other hand, the contribution from free electrons will depend quite considerably on this factor due to scattering from the boundaries of the aggregates(see Heavens 1955). Absorption arising from free electrons is more important for longer wavelengths and the contribution to absorption from bound electrons predominates at shorter wavelengths.

Sennett and Scott (1950) found that for visible wavelengths aluminium films showed a maximum in absorption for film thicknesses of approximately 250 Å. These authors have studied the effect of evaporation rate on the structure of several types of metal films and suggest that the migration of a metal atom after reaching the substrate is probably the most important factor in determining the stable form of thin metallic films. This migration depends on the nature of the metal, the nature of the substrate and the substrate temperature. Also, the migration of an atom is altered by the arrival of other atoms in the same vicinity and this in turn is dependent on the rate of deposition. The principal factors influencing the mobility of adsorbed atoms have been discussed by Heavens (1955). Sennett and Scott found that aluminium films deposited

in 2 secs 'had an aggregated structure for all thicknesses less than 300 Å. The aggregates appeared to have poorly defined boundaries but to maintain their individuality even in quite thick films.'

Levenstein (1949) also studied the structure of evaporated metal films and found that the tendency to form agglomerates decreased as the evaporation rate was increased. It was suggested that at a high rate of deposition more nuclei are initially formed from which a fine grain deposit grows.

Lebedeva and Lebedev (1965) have considered the theoretical aspects of the propagation of electromagnetic waves in an homogeneous conducting layer and derived expressions for the dependence of R and T on film thickness (d). It was found that the absorption curve A = f(d) has a maximum value when R and T are equal and it was concluded by these authors that an experimentally observed absorption maximum of a film at the intersection of the R=f(d) and T=f(d) curves can be regarded as being a qualitative indication of the uniformity of the film. (It should be rembered that Sennett and Scott observed an absorption maximum at a thickness of 250 Å and in the visible region R $\simeq$ 89% and T $\simeq$ 2% for a film of such a thickness.)

Experimental evidence regarding the dependence of absorption of aluminium films on their thickness is far from conclusive. Walkenhurst (1941) finds that for aluminium films deposited at fast rates there is an absorption maximum (at λ 5500) for a film thickness of about 70 Å where R $\simeq$ T, a result which is strikingly in contrast to that of Sennett and Scott. Other notable investigations have already been mentioned.

In the present investigation again this dependance is not at all clear. For the films prepared under the poorer conditions there appears to be very little variation of absorption with film thickness except for very thin films ($T>15\%$) which are characterised by an increased absorption. On the other hand, for coatings prepared under the improved vacuum conditions there is a definite increase in absorption as the film thickness is reduced, even for thicker films (fig.6.4.). It should be pointed out however that in the former case film properties were determined after times of 2 to 24 hours exposure to air and of course optical properties are changing during this period (Section 6.4.2.). In the latter case, unless otherwise stated, optical properties were always determined after 24 hours exposure and this gives a more suitable comparison of films of different thickness. Yet even so, this cannot be the real explanation, since it will be seen for protected aluminium films (whose optical properties remain stable with time) that no systematic variation of absorption with thickness was observed for films prepared under the poorer conditions whilst for the improved conditions, again absorption was found to increase as the aluminium thickness was reduced.

Because of this dependence of absorption with thickness, agreement between computed and experimental optical properties of the films developed in this investigation can only be expected for the thicker films and not over the wide range of thickness as found by Hass and Waylonis.

6.5. The Optical Properties of the Semi-Transparent Aluminium -MgF2 Double Layers.

In this section results are given for the optical properties of transmitting aluminium - MgF2 films prepared under the two different vacuum conditions previously discussed.

6.5.1. Films Prepared under the Power Vacuum Conditions.

A number of samples have been prepared in which the thickness of the MgF2 layer (t) has been chosen to give optimum performance for the wavelength region 1850 - 1900 Å. From chapter 4 this requires a value of t given by

$$nt = \frac{\lambda_o}{4\pi} \left(\pi + \beta \right)$$

where n is the refractive index of MgF2 at the wavelength λo and β is the absolute phase change at the MgF2 - aluminium boundary. For λo = 1850 Å and 1900 Å values of t of 500 Å and 520 Å are required. As a check on the MgF2 thickness several of the films were converted into filters by the addition of a second aluminium layer after measurement of optical properties had been completed. The thickness of MgF2 can be determined from the wavelength of peak transmission (λ) using the relationship (chapter 4)

$$nt = \frac{\lambda}{2\pi} \beta$$

and the value of β appropriate to λ. For t = 500 Å the value of λ should be 2175 Å and it was found for all samples checked that the peak transmission occurred close to this wavelength.

Results of measurement of film properties after 24 hours exposure to air are shown in figure 6.9. The delay time between completing the aluminium evaporation and commencing the MgF2 deposition is about 30 secs. The difference between the properties of these double layer films and the single aluminium films prepared under identical conditions is quite evident. The increasing value of R with decreasing wavelength arises from interference of the waves reflected from the air-MgF2 and MgF2 - aluminium boundaries. At wavelengths between 1850 - 1900 Å the performance should be optimum. However, the actual maximum in R occurs at a wavelength of about 2100 Å and not 1850 Å simply because the reflectance of the aluminium is decreasing with wavelength.

In figure 6.9. the range of (R+T) values is shown for all but the sample with the thinnest aluminium film (No.5.). No systematic variation of film absorption with film thickness was found for all samples transmitting up to about 12%. At 1850 Å the range of the (R + T) values is between 89.6 and 91.7%. This is to be compared with the (R + T) values of some 85% obtained for aluminium films (aged 24 hours). The practical aspect of this reduced absorption from the point of view of application to F.P. spectroscopy is considered in section 6.7.

The optical properties of these double layer films were found to be extremely stable with time. No variation in optical properties, within the limits of error of the R and T values, were observed for samples stored for several months in a dessicator.

The pronounced effect on ultraviolet optical properties caused by overcoating an aluminium film with MgF2 is clearly illustrated in figure 6.10.

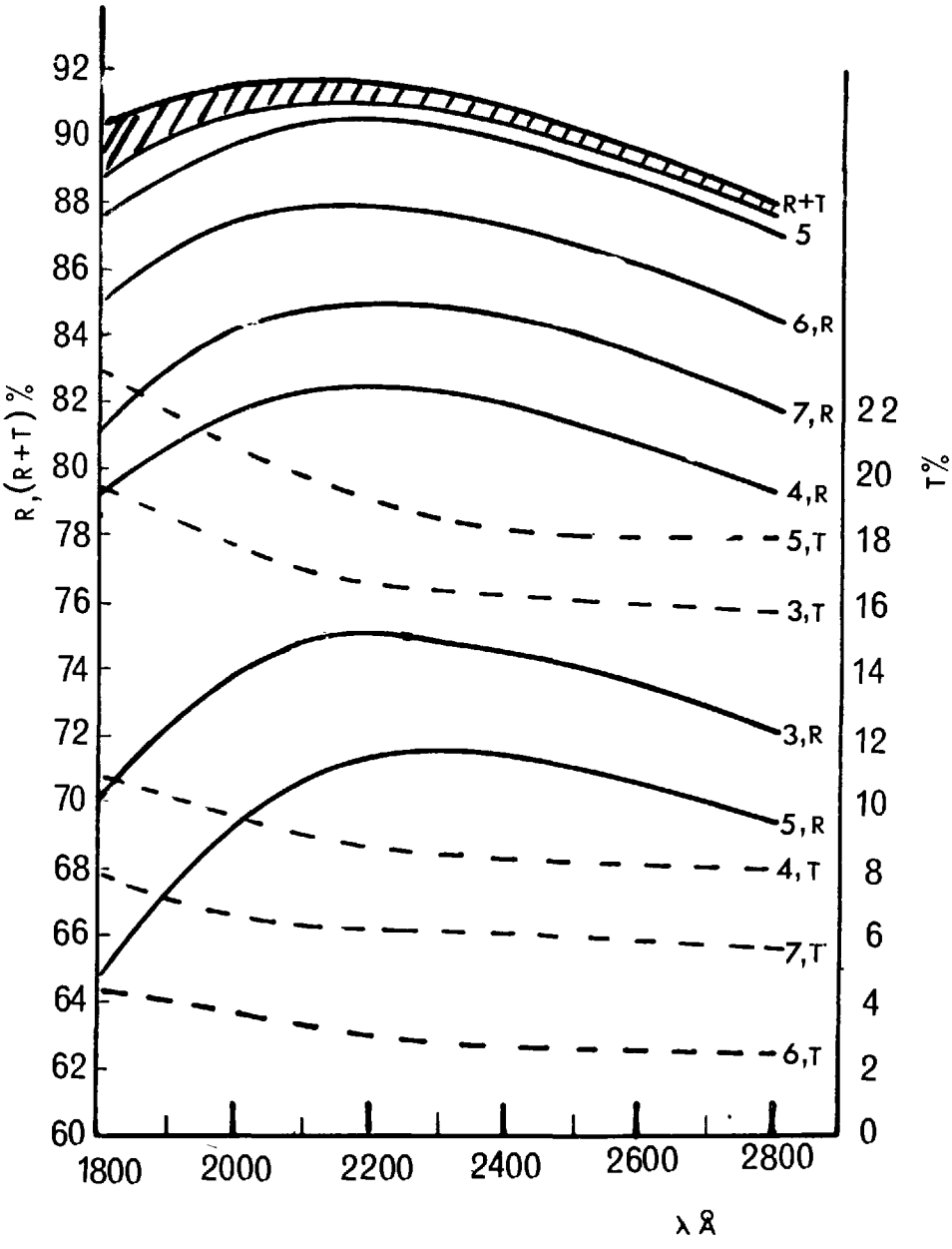
92
90
88
86
84
82
80
78
76
74
72
70
68
66
64
62
60
R,(R+T)%
R+T
5
6,R
7,R
4,R
5,T
3,T
3,R
5,R
4,T
7,T
6,T
22
20
18
16
14
12
10
8
6
4
2
0
T%
1800
2000
2200
2400
2600
2800
λ Å

FIGURE 6.9.

Two samples are shown. For sample 1 the MgF2 thickness was chosen to give optimum performance at a wavelength of 2000 Å. (MgF2 thickness = 570 Å). The MgF2 thickness of sample 2 was 230 Å to give a minimum reflectance at 2000 Å. The difference in the (R + T) values at this wavelength brought about by the different MgF2 thicknesses is over 7%.

6.5.2. Films Prepared under the Improved Vacuum Conditions.

In addition to the improvements made in the evaporation conditions experimental techniques were also developed such that the MgF2 deposition could be commenced within 20 secs after the completion of the aluminium deposition. Also, improvements were made to give a closer control of the MgF2 thickness during deposition. The variation of R, T and (R + T) with wavelength for a number of samples is shown in figure 6.11. The MgF2 thickness was chosen to give an optimum performance at 1850 Å (MgF2 thickness = 500 Å)

The effect of a 450 Å MgF2 layer on the optical properties is illustrated in curve d. The reduction in the (R + T) value caused by the different MgF2 thickness is quite small at λ1850 Å but at longer wavelengths the 50 Å difference in thickness has a much greater effect on optical properties. This is as expected from the computed curves given in Chapter 4.

It is seen from figure 6.11 that the (R + T) values are dependent on the thickness of the aluminium film as was found for the single layer films deposited under the same evaporation conditions.

Again optical properties have been found to be stable for coatings stored in a dessicator over periods of several months.

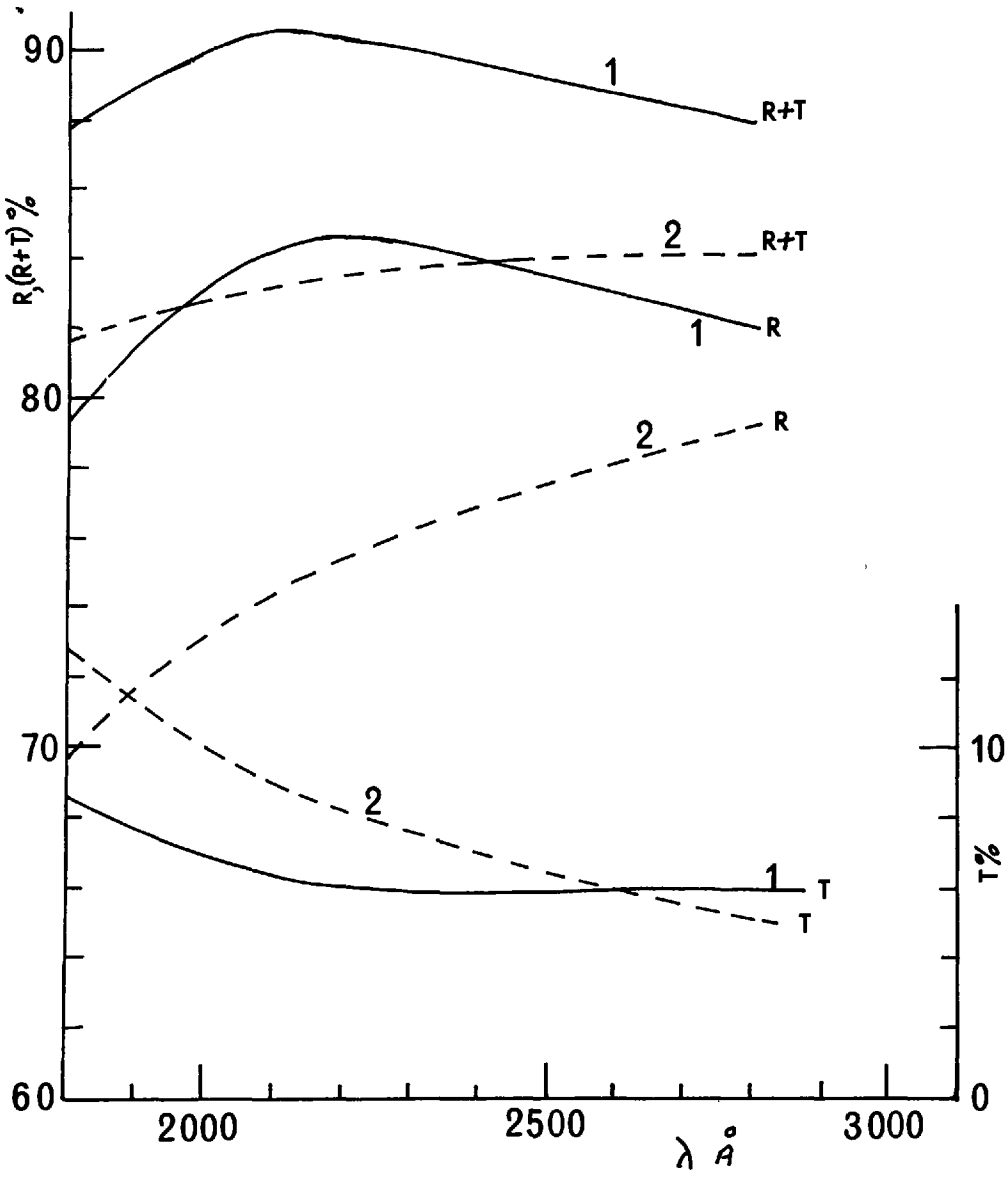

Figure 6.10,

FIGURE 6.11.

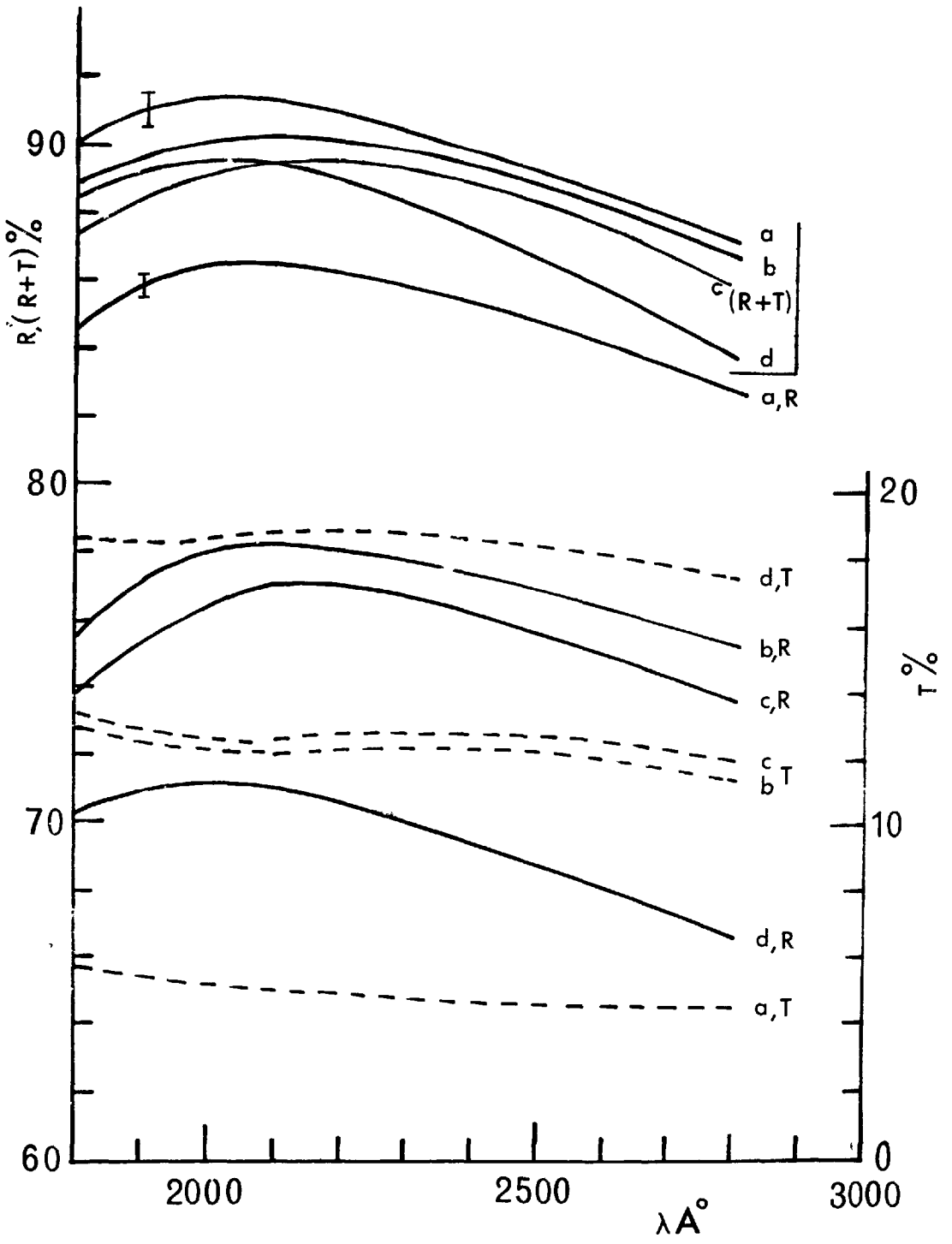
90
80
70
60
R,(R+T)%
a
b
c
(R+T)
d
a,R
d,T
b,R
c,R
c
b
T
d,R
a,T
20
10
0
T%
2000
2500
3000
λA°

6.5.3. A Comparison between Measured and Computed Optical Properties for the Double Layer Coatings.

Figure 6.12 compares measured optical properties for a double layer film prepared at 10^{-7} Torr with computed values for a 275 Å thick aluminium film overcoated with a 500 Å thick MgF2 layer. The reasons for the differences in the (R + T) values at shorter wavelengths is not very clear, particularly in view of the good agreement between computed and measured optical properties for the single aluminium films. It is difficult of course, to establish if the double layer films are at fault or, in fact, if the computed values are over optimistic. Measured optical properties have been found to be perfectly reproducible. However it is seen in figure 6.12. that after allowance for experimental errors, the difference between measured and computed values of (R + T) is only some 0.4%

Heavens and Smith (1957) have pointed out that the representation of thin evaporated dielectric films by parallel-sided, isotropic homogeneous layers of constant refractive index is likley to be an over simplification (see also Gonella and Robrieux 1962). Often films are not homogeneous but can contain voids and also may consist of large numbers of crystallites which may be randomly orientated or orientated in preferred directions. This tendency for crystal growth is dependent on the thickness of the deposited films. Schulz (1949) states that MgF2 films of thickness less than 1000 Å are amorphous whilst according to Heavens and Smith, electron diffraction studies indicate crystallites of

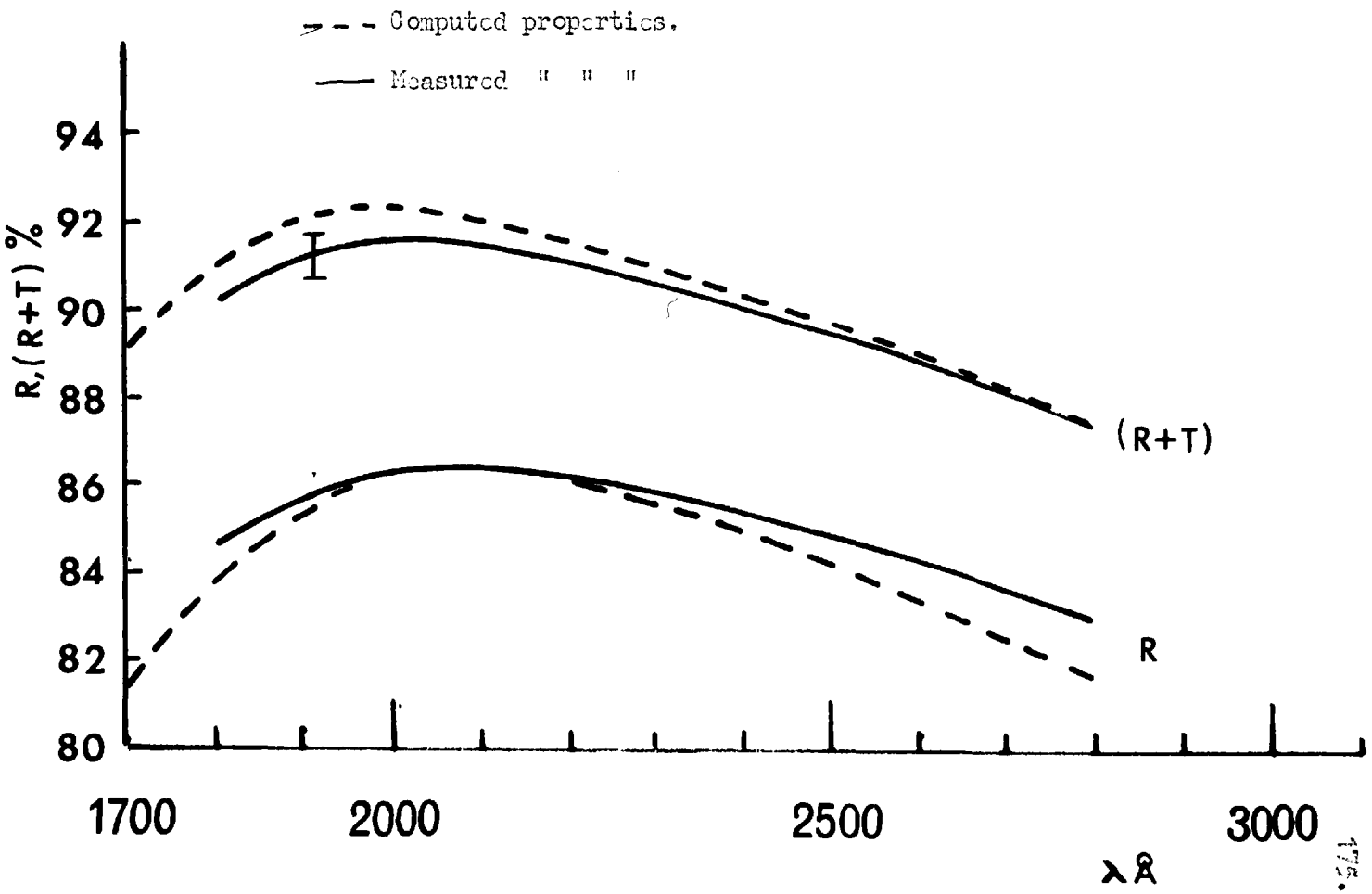
Computed properties.
Measured " " "
94
92
90
88
86
84
82
80
R,(R+T) %
(R+T)
R
1700
2000
2500
3000
λÅ

size 50 - 100 Å in films only a few hundred Angstroms thick. The presence of such crystallites in the deposited film may lead to the appearence of appreciable scattering, the magnitude of which will increase at shorter wavelengths. This could perhaps partly account for the above small difference in the (R + T) values as also could strain in the double layer films. (Schulz and Tangherlini, 1954).

6.6. A Discussion of the Optical Properties of the Double Layer Coatings.

At first sight a somewhat surprising feature of the results obtained for the double layer films was that the (R + T) values were not so critically dependent on the two vacuum conditions of preparation employed, unlike the case of the single aluminium films. It had been hoped that the improvement of the optical quality of the aluminium films, would lead also to an improved optical performance for the double layer coatings. The subsequent increase in the (R + T) values is not very great as can be seen by comparison of figures 6.9. and 6.11.

The different forms of the R and T curves as a function of wavelength are largely due to slight differences in MgF2 thickness. It will be remembered that for the poorer vacuum conditions optimum performance was aimed for the wavelength region 1850 - 1900 Å whilst for the improved conditions the MgF2 thickness was more strictly controlled for optimum at 1850 Å.

It is apparent from previous discussion that in reality the double layer films are not simply aluminium - MgF2 but are really of the form aluminium - Al_2O_3 - MgF2. It might be expected that the delay period

before applying the protective dielectric coating will have quite an influence on optical properties. Cranfield, Hass and Waylonis (1966) have studied the effect of this delay on MgF2 protected, opaque aluminium films. At a wavelength 1216 Å, the reflectance of the combination is lowered by approximately 1% if the delay time is increased from 15 secs. to 90 secs. (pressure during delay being 10^{-6} Torr). Cranfield et.al. have also shown that the effect of an interposed oxide layer on reflectance is not so severe as the effect of a surface oxide layer of the same thickness. For the different delay times used in the present investigation (20 and 30 secs.) it would be expected that this difference would have only a very small effect on optical properties, especially at wavelengths above 1800 Å where effects of oxidation on optical properties are not so severe as at 1216 Å.

It would appear from the evidence available in this investigation that it is oxidation which is the dominant factor likely to account for the different optical properties of the single aluminium films. For the poorer vacuum conditions, it can be expected that the more porous structure caused by inclusion of oxygen and water vapour will lead to more extensive oxidation upon exposure to air than for the films prepared under the improved vacuum conditions. However, when the aluminium films are protected from oxidation by the MgF2 layer then, if in fact oxidation is the dominant factor, smaller differences in optical properties would be expected for the double layer films prepared under the two different evaporation conditions. Small differences in (R + T) values which have been observed for these double layers may be due to substrate contamination,

structural differences in the aluminium films and oxidation before the protective layer is applied. Evidence from the optical microscope examination would also suggest that oxidation plays an important role in the breaking-up of the aluminium films (section 6.3.3.), since for the protected aluminium coatings no 'microholes' were formed in films stored over periods of three years.

It should be pointed out that the main emphasis of this investigation has been more concerned with the development of coatings suitable for ultraviolet interference spectroscopy rather than with a detailed study of mechanisms accounting for different optical properties. The models outlined above, in the absence of additional experimental evidence, can only partly explain the experimental results discussed in previous sections. In particular, a structural examination of the films is likely to give much useful evidence.

The performance of these coatings from the point of view of application to F.P. spectroscopy is considered in the following section.

6.7. Application to Multiple-Beam Interferometry.

The performance of coatings for F.P. spectroscopy are best presented in the form $\gamma A - N_R$ (Jacquinot 1960). Such curves are particularly sensitive to variations in coating absorption. (Chapter 2). For example, if N_R is 17 corresponding to a reflectivity of 83% the two values A = 10% and A = 12% give respectively values of γA = 17% and 9% i.e. a difference in absorption of 2% results in a factor of nearly two in peak transmission. The effect of absorption becomes more pronounced for high coating reflect-

ivities as was shown in figure 2.2.

Figure 6.13 compares the performance of aluminium films prepared under the two different vacuum conditions. The influence of the evaporation conditions on performance is clearly evident, particularly at the shorter wavelengths. In figure 6.14. results are summarised for both the single and double layer coatings at a wavelength of 1850 Å. The superiority of the double layer films over single aluminium films is clearly evident and the aluminium - MgF2 coatings at 1850 Å have a performance comparable with that of highest quality aluminium films at 4000 Å (Hass and Waylonis). Moreover, the optical properties of the MgF2 overcoated aluminium films remain stable over long periods. It should be remembered that much hyperfine structure and absolute wavelength determination work has been carried out in the past at longer wavelengths with coatings of poorer performance than the present aluminium - MgF2 coatings at 1850 Å.

Whilst it is necessary that the aluminium film in the double layer coatings must be thick in order to acheive a high reflectivity, the transmission in the visible (for most applications) is still sufficient to allow visual adjustment of a F.P. etalon employing these coatings. This is an additional practical advantage over the single aluminium films which must necessarily be more dense in order to obtain the same reflectivity. As a consequence, when single aluminium films are employed the fringe intensity in the visible is much reduced making visual adjustment of the etalon considerably more difficult.

As an example of what is now possible with the coatings developed in this work, F.P. interferograms have been obtained of λ1849 of HgI.

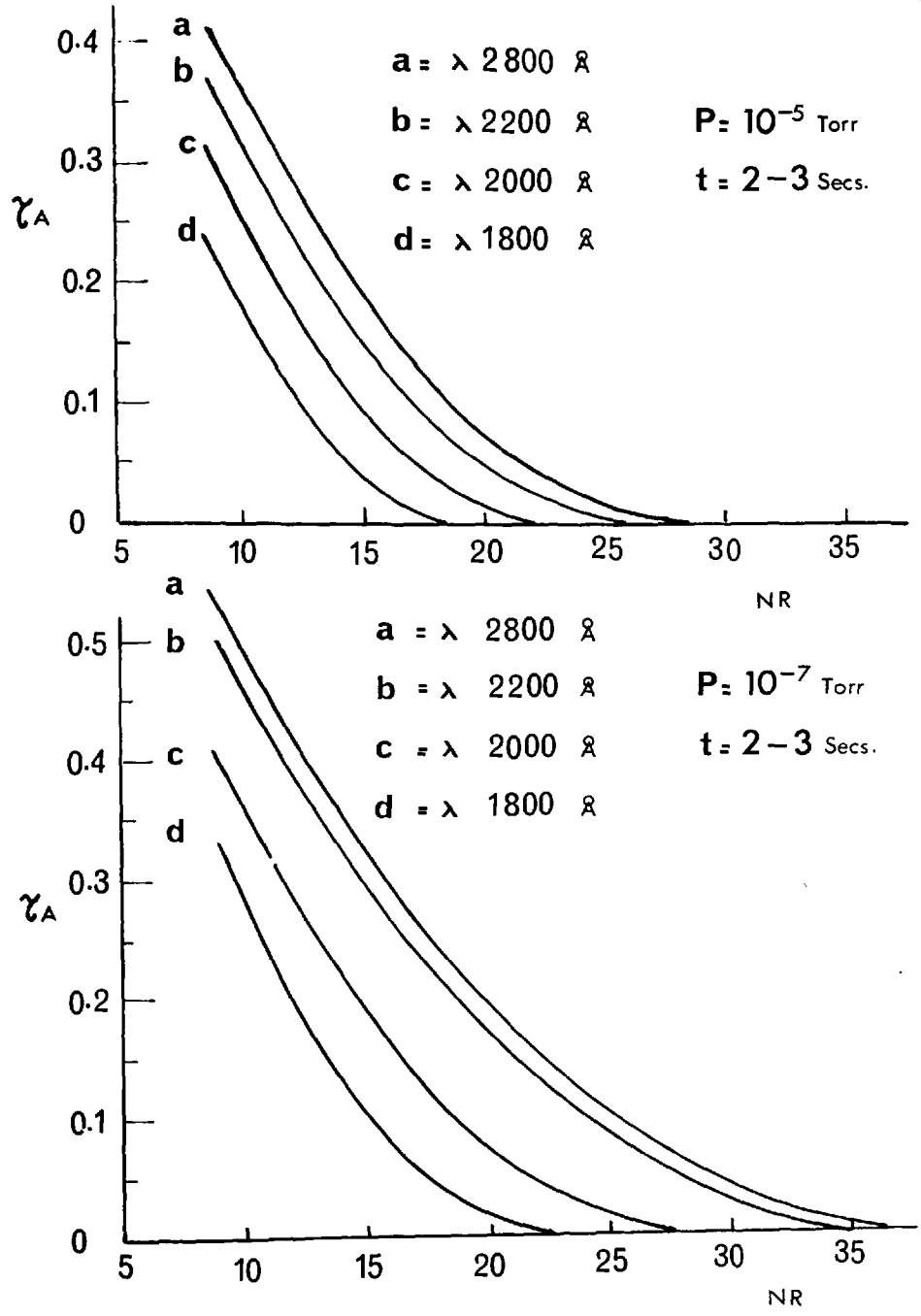
a
b
c
d
a = λ 2800 Å
b = λ 2200 Å
c = λ 2000 Å
d = λ 1800 Å
P = 10⁻⁵ Torr
t = 2–3 Secs.
γA
0.4
0.3
0.2
0.1
0
5
10
15
20
25
30
35
NR
a
b
c
d
a = λ 2800 Å
b = λ 2200 Å
c = λ 2000 Å
d = λ 1800 Å
P = 10⁻⁷ Torr
t = 2–3 Secs.
γA
0.5
0.4
0.3
0.2
0.1
0
5
10
15
20
25
30
35
NR

Figure 6.13.

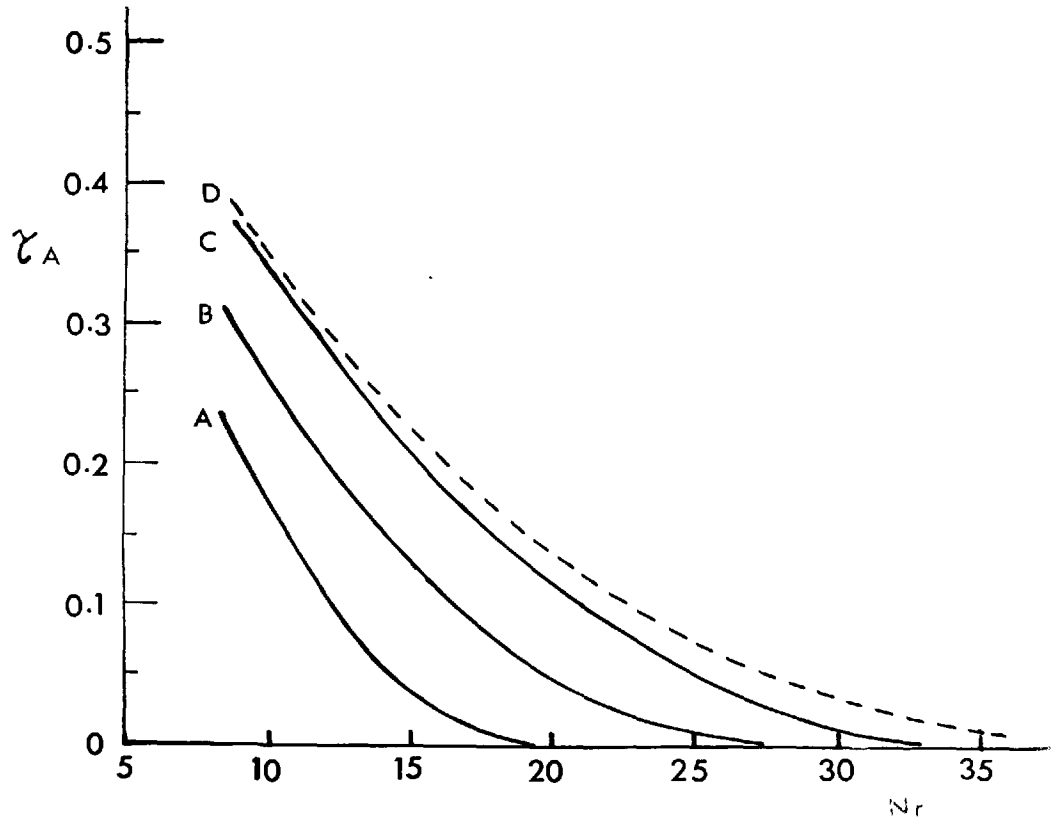

A — AL λ 1850 P = 10^{-5} Torr

B — AL λ 1850 P = 10^{-7} Torr

C — AL /MgF_2 λ 1850

D — AL λ 4000 (Hass and Waylonis)

Figure 6.14.

The 1849 line was isolated by two F.P. type interference filters (section 6.8.) which gave a transmission of 4% to 1849 Å with a reduction in transmission for the more intense 2537 Å radiation by a factor of 700. The fringe pattern was focussed onto the photographic plate (Ilford Type Q 2) using a 20 cm focal length 'Spectrosil ' lens. Focussing was achieved by a method of trial and error to obtain optimum. (In chapter 7 the advantage of an image converter camera for this purpose is illustrated). Because of oxygen absorption of 1849 radiation, the entire optical system between source and emulsion was purged with dry, oxygen free nitrogen.

Etalon flats worked to match better than $\lambda/150$ in the green (Optical Surfaces Ltd.) over a 6 cm diameter were coated over a 3 cm aperture with aluminium - MgF2 to give a reflectivity of 80%. The plates were assembled in a conventional mount (Tolansky 1947) and adjusted for parallelism by a small differential spring pressure. A plate separation of 1.m.m. was employed.

Figure 6.15 shows interferograms obtained using a Hg^{198} electrodeless source operated from a 2500 Mc/s oscillator. In figure 6.15.(a) the fringe pattern (etalon tilted) was obtained after the lamp had been switched only for a few seconds. The recorded pattern after 5 minutes is given in figure 6.15. (b) where there is now evidence of line broadening and self absorption in the hotter source. Exposure times were 10 seconds.

Self absorption is more clearly shown in figures 6.16 (a) and (b) in which an Eastern Blacklight 11-SC1 pencil lamp was used. Figure 6.16 (a) shows recorded fringes for a 'hot ' and 'cool' source. It is seen from these interferograms that there is some background in the fringes. This

FIGURE 6.15(a)

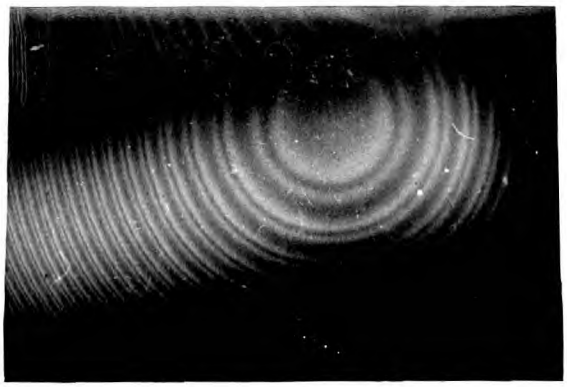

FIGURE 6.15(b)

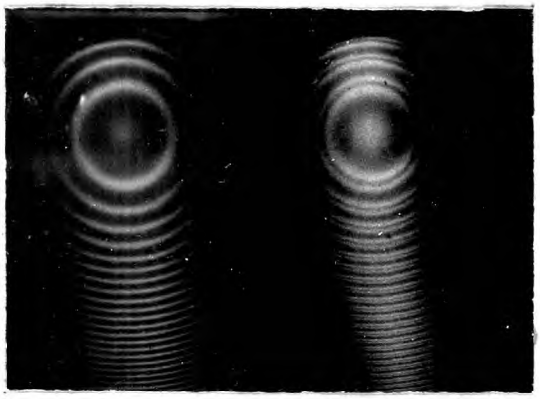

Fig.6.16(a)

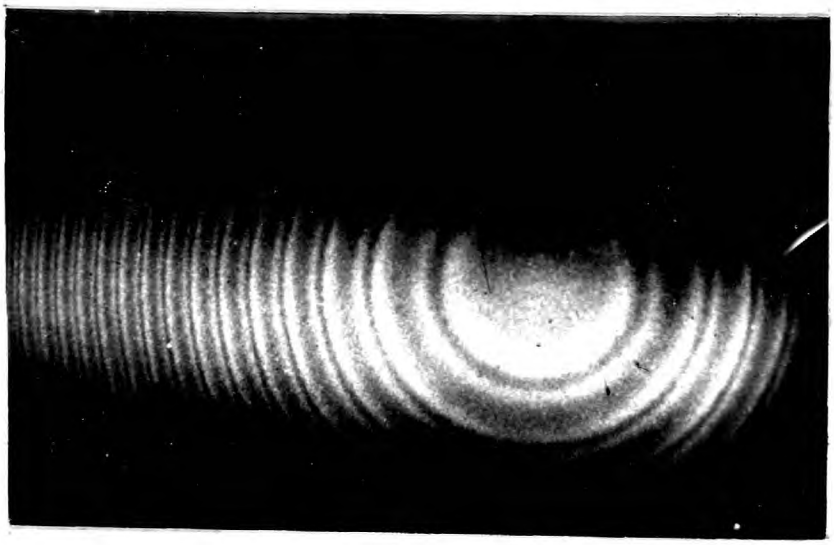

Fig.6.16(b)

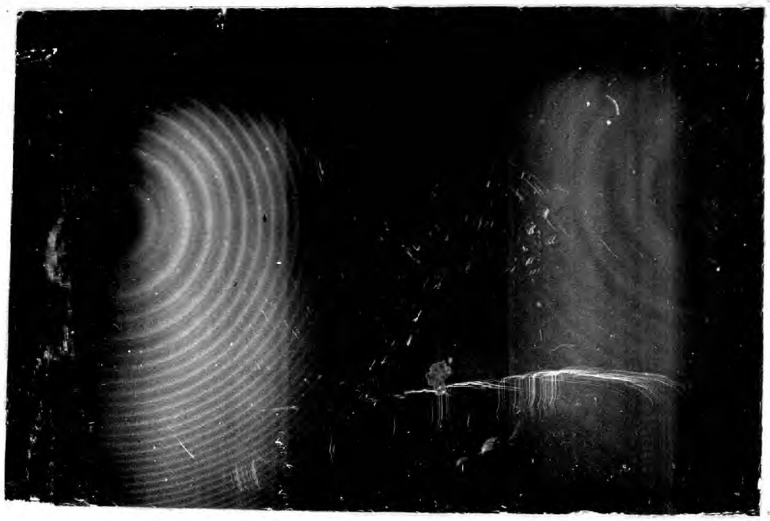

Fig.6.16(c)

partly arises from the non-foccussed 2537 Å fringe pattern because of transmission by the filters of this more intense radiation. Figure 6.16 (c) shows the contribution of this background. Recorded patters were obtained with the optical system purged and non-purged (same exposure). In the latter case much of the 1849 radiation is absorbed by atmospheric oxygen.

The results given previously for the double layer films show that coatings designed for optimum performance at a wavelength of 1850 Å still possess useful values of R and (R + T) at longer wavelengths. Thus, a satisfactory performance for application to multiple-beam interferometry should still be obtained over a fairly wide spectral range with such coatings. This performance at longer wavelengths is illustrated in figure 6.17 which shows recorded F.P. interferograms for λ 2537 Å of Hg I using the same coatings and etalon plate separation as above. In figure 6.17.(a) the source was a mercury 198 electrodeless discharge lamp and in figures 6.17(b) and (c) a natural mercury low pressure lamp (Philips) was employed. Again self absorption is clearly evident.

6.8. F.P. Type Interference Filters for the Far Ultraviolet.

The filters prepared in this investigation are of the type aluminium-MgF2 - aluminium as discussed in Chapter 2 and shown schematically in figure 2.7. A final MgF2 overcoating deposited onto the three layer filter serves two functions. It prevents oxidation of the second aluminium film and it also acts as an anti-reflecting layer at a wavelength corresponding to the transmission peak, thus increasing the filter peak transmission. This requires a MgF2 layer of optical thickness (nd) given by

Fig.6.17(a)

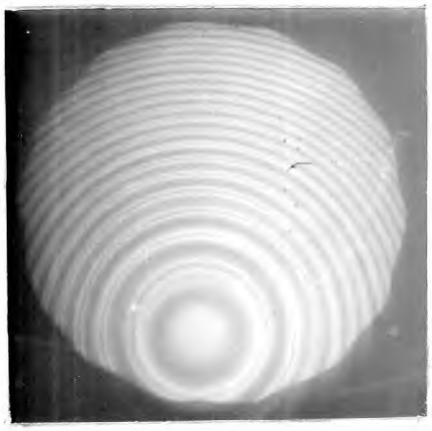

Fig.6.17(b)

Fig.6.17(c)

$$nd = \lambda_o \beta / 4\pi$$

where λ_o is the wavelength of peak transmission of the filter and β is the absolute phase change on reflection at the MgF2 - aluminium boundary (Chapter 4).

Methods of filter preparation and measurement of filter transmission characteristics have been described in Chapter 5 and section 6.2. respectively. (The contents of this section have been published. Bates and Bradley 1966 (a)).

6.8.1. First Order Filters.

Experimental transmission curves for a number of first order filters are shown in figure 6.18. These filters were deposited onto fused silica 'spectrosil B' substrates of either 1 or 2 m.m. thickness.

The spacer layer of filter A was chosen to give a peak transmission at a wavelength of about 1725 Å. However, the actual peak occurs at 1780 Å due to the effect of increasing absorption of the spectrosil substrate. If a thinner spacer layer had been employed, then a narrower bandwidth could have been obtained since the transmission characteristic of such a filter would be largely determined by the properties of the reflecting layers at wavelengths longer than the peak wavelength and by substrate absorption at shorter wavelengths.

The optical properties of the aluminium reflecting films can be derived from filter characteristics (after correction for substrate reflection and absorption losses) in the manner discussed in Chapter 2. These derived optical properties given below clearly show the deterioration

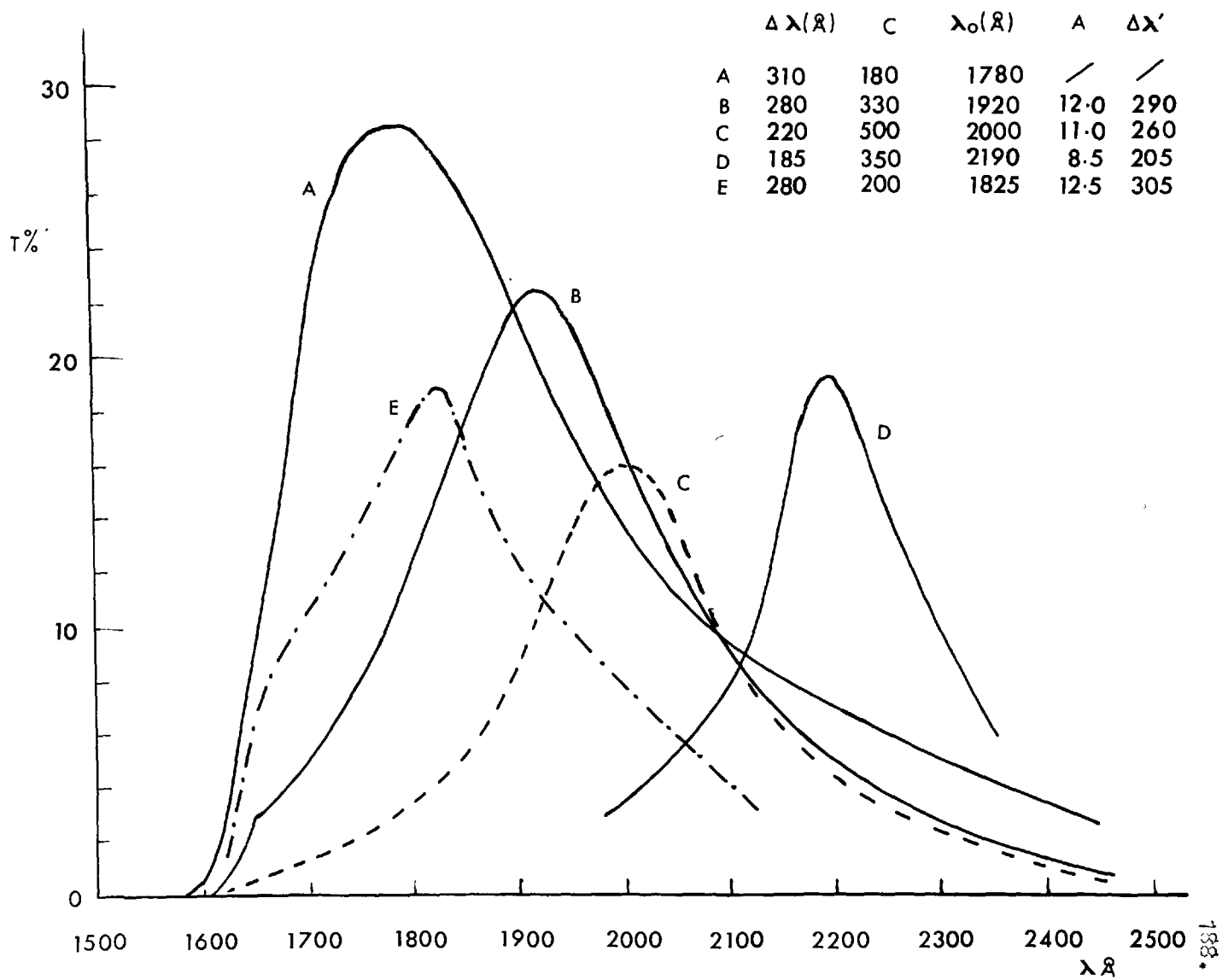
Δλ(Å) C λ₀(Å) A Δλ'
A 310 180 1780 / /
B 280 330 1920 12·0 290
C 220 500 2000 11·0 260
D 185 350 2190 8·5 205
E 280 200 1825 12·5 305
T%
30
20
10
0
A
B
C
D
E
1500 1600 1700 1800 1900 2000 2100 2200 2300 2400 2500
λÅ

FIGURE 6.18.

in filter performance of aluminium films with decreasing wavelength.

Optical Properties of Aluminium Films derived from Figure.6.18.

Curve	λ_o	$\Delta\lambda$ Å	R%	T%	A%	C	$\Delta\lambda'$ Å
A	1780	310	*	*	*	180	*
E	1825	280	79.5	8.0	12.5	200	305
B	1920	280	77.2	10.8	12.0	330	290
C	2000	220	81.7	7.3	11.0	500	260
D	2190	185	85.0	6.5	8.5	350	205

* it is not possible to determine optical properties from filter A because of distortion of the transmission profile by substrate absorption. ($\Delta\lambda'$ is the calculated filter bandwidth for a filter peak transmission of 25% (see below).).

A useful comparison of filter performance with the expected performance, calculated on the basis of extrapolated optical constants for aluminium by Schroeder (1962), can be obtained by normalising the filters to a peak transmission of 25%. The normalised filter characteristics can be calculated from the derived values of R, T and A given above assuming that aluminium absorption is independent of film thickness. (It has been seen from previous discussion that in fact the absorption of aluminium films does depend on the film thickness. However, over the range of aluminium thicknesses involved, the measured variation of absorption with film thickness has been found to have only a very small effect on this calculation.) The values of bandwidth so calculated for a filter transmission of 25% are given by $\Delta\lambda'$ above. These values of bandwidth are greater than those

computed by Schroeder who did not take into account the phase change on reflection at the aluminium - MgF2 boundaries.(Chapter 2.)

Figure 6.19. shows calculated values for filter bandwidth given by Schroeder and recalculated values in which this phase term has been taken into account (for filter peak transmissions of 25%). It is seen that there is good agreement, within $\pm$ 20 Å, between correctly calculated bandwidths and those derived from the experimental filter characteristics. ($\Delta\lambda'$ given above). The deterioration of the aluminium coatings at shorter wavelengths is shown by the variation of N_R with wavelength.

An important characteristic of a filter is its contrast or its ability to reject light at wavelengths distant from the pass band. An arbitary definition of contrast, which never the less permits useful comparisons to be made between filters, is the ratio of peak transmission to the transmission at 4000 Å (Schroeder). Contrast values C for the first order filters are given above. For a first order filter peaking at 1800 Å the contrast is of the order of 200. At wavelengths longer than 4000 Å the transmission of the filter is steadily decreasing due to the decreasing transmission of the aluminium films with increasing wavelength.

Peak transmissions at wavelengths shorter than those shown in figure 6.18 may be obtained by employing lithium fluoride, calcium fluoride or sapphire substrates. Figure 6.20. shows a first order filter deposited on a sapphire substrate of 1.m.m. thickness. A narrower bandwidth would be obtained with a thinner spacer layer by shifting the transmission peak to shorter wavelengths as discussed above. An improved performance over

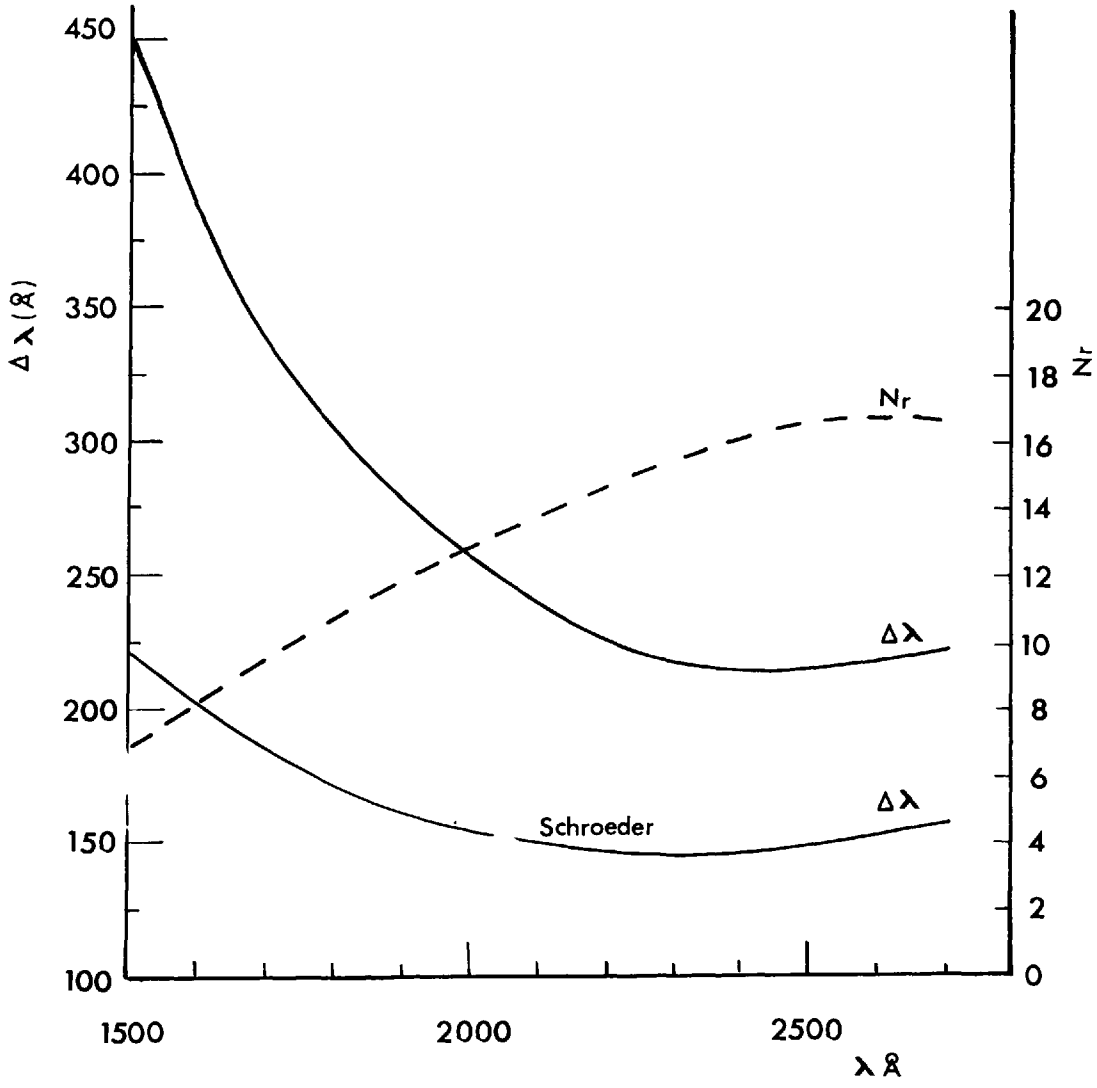
450
400
350
300
250
200
150
100
Δλ (Å)
20
18
16
14
12
10
8
6
4
2
0
Nr
Nr
Δλ
Δλ
Schroeder
1500
2000
2500
λ Å

FIGURE 6.19.

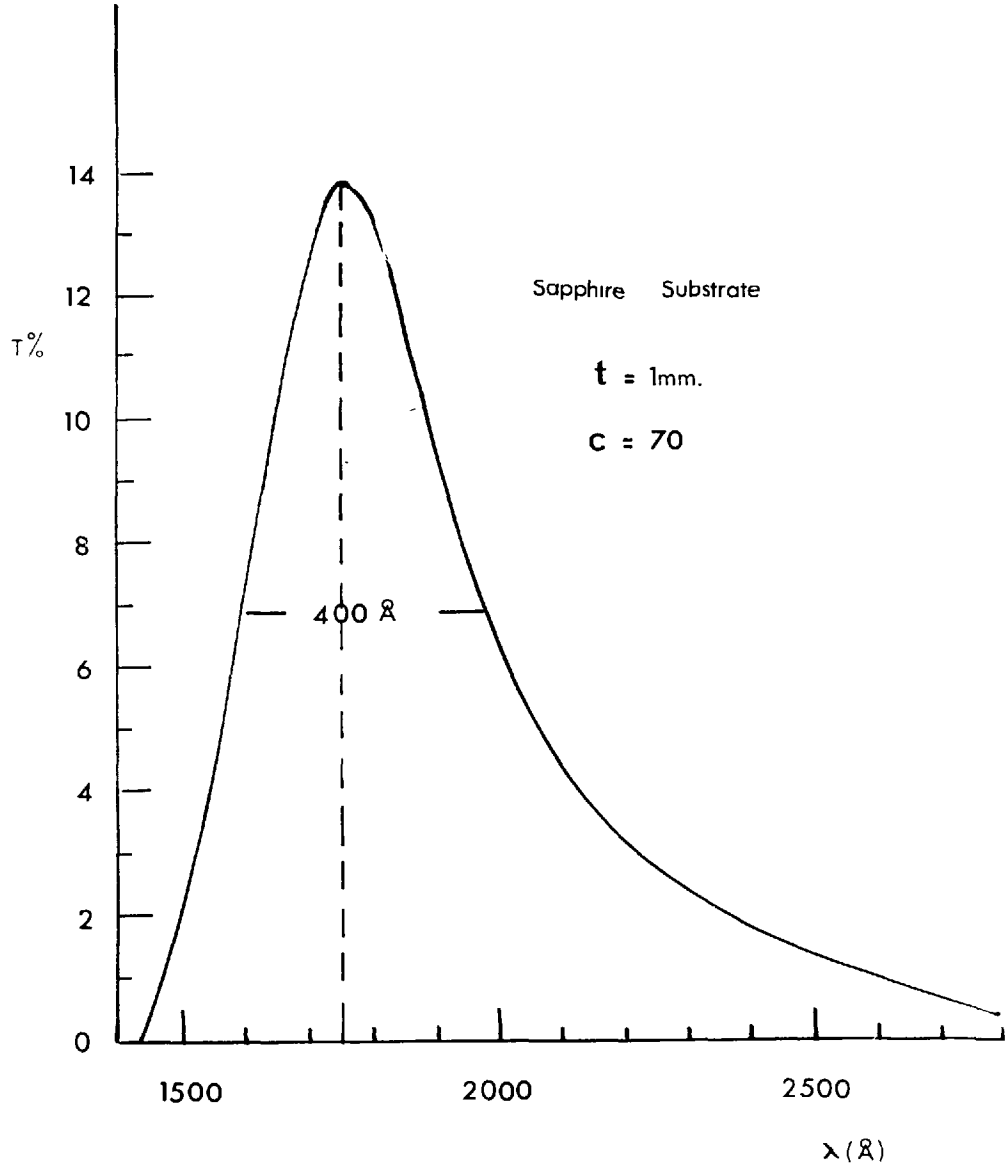
14
12
T%
10
8
6
4
2
0
Sapphire Substrate
t = 1mm.
c = 70
400 Å
1500
2000
2500
λ(Å)

FIGURE _6.20.

that shown in figure 6.20. would be expected from a filter deposited on a lithium fluoride substrate because of the higher transmission of this material compared to that of sapphire.

6.8.2. Second Order Filters.

It was shown in Chapter 2 that for a given reflectivity of the aluminium films, the filter bandwidth at a wavelength λo can be reduced by increasing the spacer layer thickness to employ higher interference orders. The properties of several second order filters having transmission peaks centred on wavelengths close to 2000 Å are shown in figure. 6.21.

The optical properties of the aluminium films have been derived as before from the filter transmission characteristics.

The Optical Properties of Aluminium Films derived from Figure 6. 21.

Curve	λo	$\Delta\lambda$	R%	T%	A%	$\Delta\lambda'$
B	1990	105	77.0	7.0	16.0	155
C	2130	80	82.5	6.2	11.3	110
A	2190	155	70.0	16.6	13.4	130

($\Delta\lambda'$ is again the calculated filter bandwidth for filter peak transmissions of 25%)

Comparison with the optical properties derived from first order filters shows that the aluminium films of these second order filters have an apparently inferior performance characterised by higher absorption values. This greater absorption may, infact, be due to increased scattering in the

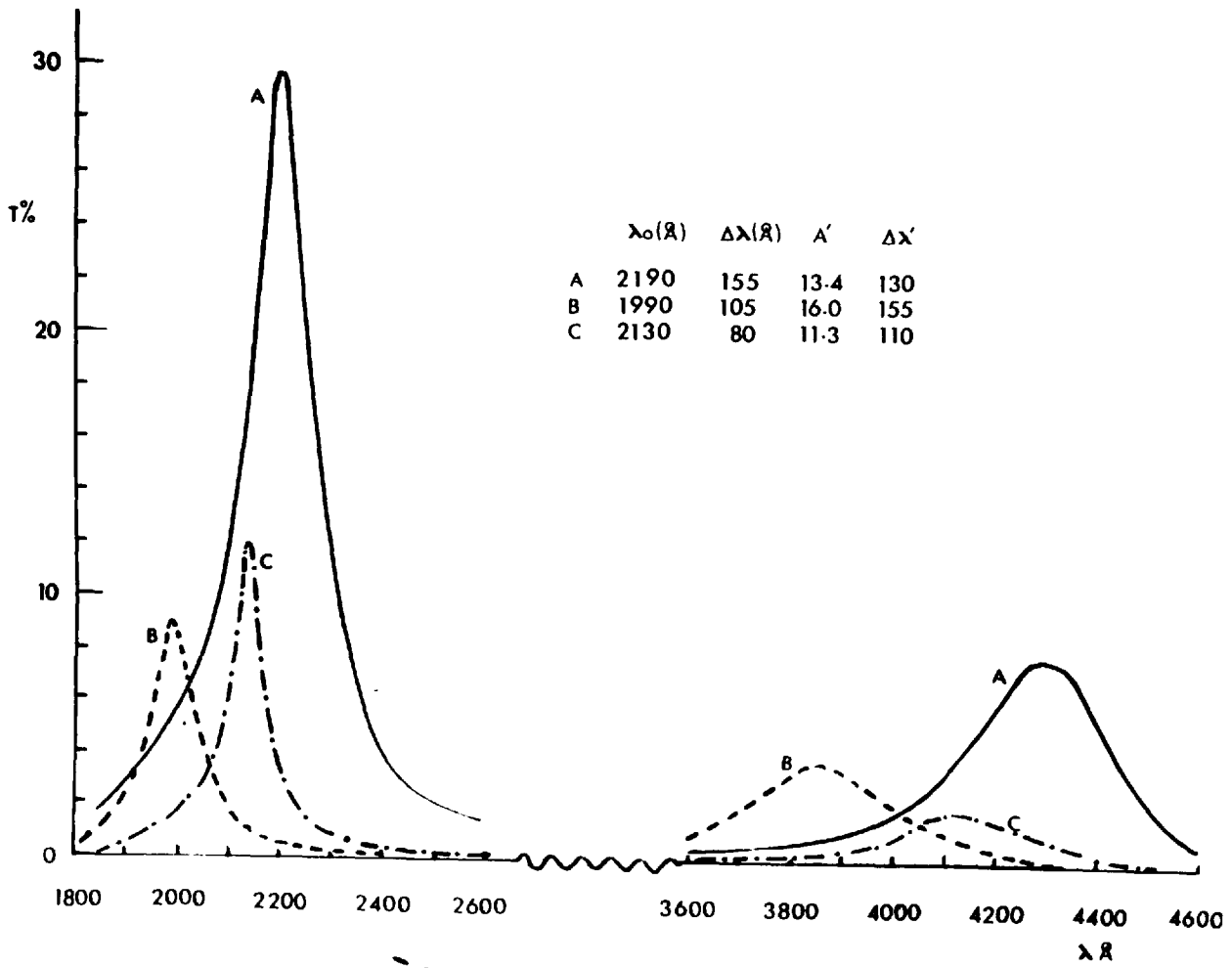
30
20
10
0
T%
A
B
C
λo(Å) Δλ(Å) A' Δλ'
A 2190 155 13·4 130
B 1990 105 16·0 155
C 2130 80 11·3 110
1800
2000
2200
2400
2600
3600
3800
4000
4200
4400
4600
λ Å

FIGURE 6.21.

spacer layer since MgF2 become more crystalline for thicknesses greater than 1000 Å. (Schulz 1949). For a first order filter peaked at a wavelength of 2000 Å, the spacer layer thickness required is approximately 420 Å. However, for a second order filter peaked at the same wavelength the corresponding spacer thickness required is about 1100 Å. Although in this investigation no attempts have been made to construct filters of higher than second order, the scattering within the spacer layer with increased thickness may well prove to be a serious limitation in the performance of such filters.

6.8.3. Change in Filter Characteristics with Time.

The stability or otherwise, of filter transmission characteristics over long periods of time is a matter of extreme importance for space research applications. Whilst no attempt has been made to make a detailed investigation of the change in properties with time the following observations have been made.

All filters show a change in properties within the first few days after preparation and exposure to the atmosphere. The changes are characterised by a shift in the transmission peak to a longer wavelength and by a reduction in the peak transmission. This is illustrated in Figure 6.22 which shows the transmission characteristics of a first order filter measured one day and fourteen days after preparation. During this period no special precautions were taken other than storing the filter in a dust-free atmosphere. No changes in properties have been observed after

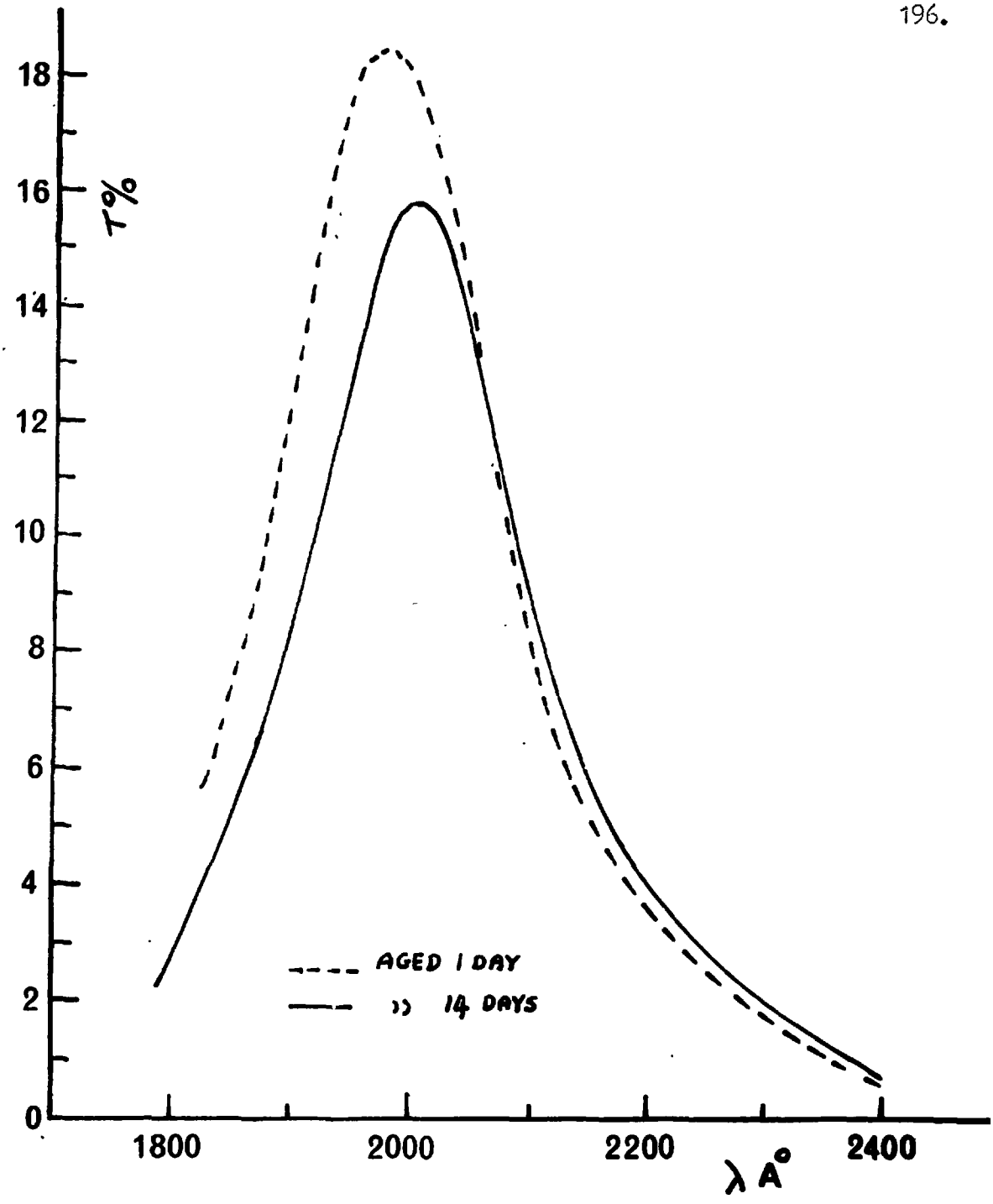

FIGURE 6.22.

the first week up to periods of eight months after preparation.

These changes in properties of filters during the first few days after preparation may be due to structural changes in the MgF_2 spacer layer, increasing absorption of the aluminium films because of continuing oxidation or strain relief at the aluminium - magnesium fluoride boundaries, (Schulz and Tangherlini 1954).

All the filter characteristics which have been shown were obtained from measurements made at least one week after manufacture, after which time the properties have become stable.

Conclusion.

First order interference filters with characteristics close to theoretical values at wavelengths above 1800 Å have been produced and filters with 25% peak transmission and bandwidths of 300 Å or less can be made for the wavelength region 1800 - 2400 Å not covered by multilayer dielectric filters. This is a satisfactory performance for broad-band photometry and three filters produced during this investigation will be flown in 1966 for the purpose of obtaining stellar spectral energy distributions at wavelengths near 2000 Å in an experiment designed by the Royal Observatory, Edinburgh. For laboratory applications such filters will permit additional filtering of longer wavelength stray light often present in ultraviolet spectrometers and spectrographs. For some sources these filters permit a simple and efficient means of isolating particular radiations without the necessity of other methods of predispersion (as discussed previously for the 1849 line of Hg I).

At wavelengths shorter than 1800 Å, because of the increasing absorption of aluminium films with decreasing wavelength, filter performance deteriorates. Also, the demands on preparation technique become more stringent if the expected performance shown in figure 6.19. is to be realised.

The effective contrast of first order filters can be increased by employing them in combination with wavelength selective detectors to eliminate response at longer wavelengths (Dunkleman, Fowler and Hennes 1962; see also section 7.6.). Similarly, it would be necessary to suppress the longer wavelength first order transmission of second order filters. Composite filters consisting of two or more filters in series on the same substrate would also substantially improve the contrast (Schroeder 1962; see also Chapter 3).

CHAPTER 7.

IMAGE INTENSIFIERS APPLIED TO INTERFERENCE SPECTROSCOPY.

7.1. Introduction.

An additional aspect of the present work has been an evaluation of the F.P. etalon - image intensifier combination. An apparatus to be used for spectroscopic investigations may be broadly characterised by the following parameters:-

1) Wavelength resolution.

2) Luminosity.

3) The number of spectral elements simultaneously recorded by the detector (a spectral element being the wavelength interval corresponding to the resolution limit of the entire apparatus.)

4) Time resolution.

5) Detector sensitivity.

6) Wavelength range.

7) Spatial resolution of the source.

The role of the photographic emulsion in spectroscopy is well known but it possesses a major disadvantage, amongst other shortcomings (Wilcock and Geake 1956), in its low sensitivity. Nowadays photoelectric methods of detection have gained ground largely because the development of multiplier photocells offers great advantages in sensitivity compared with the photographic emulsion. The fundamental advantages of the photoelectric detector lie in the high quantum efficiency of photo-

cathodes and their linear response to radiation intensity. Modern photocathodes can have an efficiency of conversion of photons to photoelctrons in the order of 10% whilst the corresponding figure for the activation of silver halide grains by photons incident onto a photographic emulsion may be only about 0.1% (McGee 1961). At very low levels of light flux the photographic reciprocity law breaks down and the emulsion becomes progressively less efficient. Thus, the information gathered in one spectral element in a given exposure time by the photographic emulsion may be compared with that obtained by applying a photoelectric detector to about 100 spectral elements in the same exposure time.

Against the inherent advantages of the photomultiplier as a detector must be offset the fact that it records the total light flux and hence only one spectral element at a time. On the other hand, the emulsion can record simultaneously data from a large number of spectral elements. Thus while one spectral element is being measured the light flux in remaining elements is wasted and it is apparent that for the study of extended spectra the photoelectric instrument will be relatively slow. However, the type of problems which will really benefit from the use of the photoelectric instrument are those in which only a few spectral elements are required and in which the radiant flux in each element is small. Such problems include high spectral resolution examination of weak sources and diagnostics of sources at a high time resolution. In such cases the accuracy of intensity measurement is limited by 'noise' arising from random disturbances inherent in the detector itself or in the sense of statistical fluctuations arising from the random arrival

of photons at the detector. These fluctuations can in principle be averaged out by integrating over long time periods since, if on the average n photons arrive per unit time at the detector then the R.M.S. fluctuation in the number arriving in a time of observation t is given statistically as $(nt)^{\frac{1}{2}}$. The signal-noise ratio associated with the photon stream is

$$s = \frac{nt}{(nt)^{\frac{1}{2}}} = (nt)^{\frac{1}{2}}$$

This ultimate limit could only be reached if each incident photon produced one detectable event which could be recorded. However, if q is the quantum efficiency of the detector defined as the average number of independent detectable events produced by each photon then the highest signal-noise ratio attainable is

$$s = (n\,q\,t)^{\frac{1}{2}}$$

The significance of the greater quantum efficiency of photocathodes over that of the emulsion where the integration time is to be limited is immediately obvious.

The high quantum efficiency and the linear response to light intensity of photoemissive surfaces combined with the information capacity of photographic plates makes the image intensifier a particularly attractive device for spectroscopic applications. For time-resolved spectroscopy the F.P. etalon - image intensifier permits continuous monitoring of a given source and more over enables spatial resolution to be simultaneously obtained. Nothing of this sort is obtainable with scanning interferometers. For ultraviolet spectroscopy an additional feature of the image intensifier

which can be used to great advantage is its property of image conversion. In this chapter some investigations of the etalon - intensifier combination with particular emphasis on time-resolved and ultraviolet spectroscopy are given. The first part of this chapter deals with the matching of the interferometer to the linear resolution limit of the detector employed.

7.2. The Optimum Conditions for matching the Interferometer to the Detector.

In the spectrographic method of employing the etalon it is necessary for optimum use to match the projected fringe halfwidth to the linear resolution limit of the detector. The radius of the $p^{TH.}$ ring from the centre of the fringe pattern has been given in equation 1.5. and is

$$r_p = f \left(\frac{2\,p}{m_o} \right)^{\frac{1}{2}}$$

$$= f \left(p/t\,\sigma \right)^{\frac{1}{2}} \qquad 7.1.$$

where f is the focal length of the camera lens employed. The linear halfwidth of the p^{TH} fringe (Δr_p) is given by a change in

p by an amount $\Delta p = 1/N$; N being the etalon finesse.

$$\therefore \Delta r_p = \frac{f}{2N} \left(\frac{1}{t\,\sigma\,p} \right)^{\frac{1}{2}} \qquad 7.2.$$

Thus to match the halfwidth of a particular fringe p_2 to the linear resolution limit (g) of the detector requires a lens of focal length

$$f = 2gN \left(t\,p_2\,\sigma \right)^{\frac{1}{2}} \qquad 7.3.$$

Since the spectral resolving power $R \simeq 2\,Nt\sigma$ (see Chapter 2) then

$$f \sim g \left(2N\,p_2\,R \right)^{\frac{1}{2}}$$

Maximum use is made of the detector area if the etalon is tilted and half the ring pattern employed. This is important in the case of image tube detection where it is necessary to make full use of the limited size of the photocathode. For a photocathode of linear dimension L then the maximum number of fringes which can be employed is obtained from equation 7.1, assuming throughout that the linear halfwidth of fringe p_2 is matched to g.

$$L = r_{p2} - r_{p1}$$
$$= 2gN\, p_2^{\frac{1}{2}} \left(p_2^{\frac{1}{2}} - p_1^{\frac{1}{2}} \right)$$

and the maximum number of fringes is

$$(p_2 - p_1) = \frac{L}{gN} \left(1 - \frac{L}{4gNp_2} \right) \qquad 7.4.$$

Thus, for a detector of given size and resolution limit then the maximum number of fringes is dependent only on the etalon finesse and p_2. Since the angular dispersion decreases with increasing p it is best to make p_1 the first ring from the centre of the fringe pattern.

When the F.P. ring pattern is superposed on a slit image then the linear width (a) is determined by the finite range of angles of incidence admitted by the slit. When light of wavelength λ is passed normally by the etalon and wavelength $\lambda - d\lambda$ is transmitted in the same order at an angle θ then

$$2t = m\lambda$$
$$2t \cos\theta = m(\lambda - d\lambda)$$

and

$$\frac{1}{R} = \frac{d\lambda}{\lambda} = (1 - \cos\theta) \simeq \frac{\theta^2}{2} = \frac{1}{8} \frac{a^2}{f^2}$$

which gives a linear slit width of

$$a = 4g\sqrt{Np_2}. \qquad 7.5.$$

In an evaluation of the F.P. etalon-image intensifier combination for time-resolved spectroscopy (section 7.5.) the fringe pattern superposed on a slit image is swept across the photocathode of the intensifier. Spectral resolving power of the swept image is little affected by ring curvature for a slit of width given by equation 7.5. For the p^{TH} ring the maximum height of the fringe chord can be obtained from equations 7.1., 7.3 and 7.5. and is $g\,(p_2/p)^{\frac{1}{2}}$. This is also the same value as the halfwidth of fringe p calculated from equations 7.2 and 7.3. and therefore the effect of fringe curvature does not alter from fringe to fringe.

7.3. Image Intensifiers.

In this section only a brief account is given of the image intensifiers which have been employed in the present investigation. Further details of construction and performance may be obtained from reviews made by McGee (1961) and Morton (1964).

7.3.1. The Single Stage Intensifier.

The simplest form of image intensifier is that in which an optical image is focussed onto a photocathode producing free electrons. These electrons are then accelerated and focussed to form an electron image on a phosphor screen.where the electron energy produces a fluorescent light image. Electron focussing may be acheived by electrostatic lenses or by employing both an accelerating electric field together with a parallel,

uniform magnetic field. If the photocathode and phosphor effeciences can be made high enough and if a sufficiently high accelerating voltage can be applied to the image tube, then a greater number of photons may be produced by each photoelectron striking the phosphor than was required to produce each photoelectron.

An analysis of this process has been given by Mandel (1955). For example, for a ZnS; Ag activated phosphor screen the wavelength of the emitted light is $\simeq$ 4500 Å (corresponding photon energy $\simeq$ 2.75 eV). Assuming a 20% efficiency of conversion of photoelectrons to photons for electrons accelerated up to 15 K V (Bril and Klasens 1952), there will be approximately 1100 photons liberated for each photoelectron striking the screen. However, approximately $\frac{1}{3}$ of these photons are absorbed by the phosphor screen and the glass window upon which the screen is deposited. An opaque aluminium backing screen deposited onto the phosphor layer serves to reflect photons into the forward 2π direction and to prevent light from being radiated back towards the photocathode. Approximately 66% of the photons produced in the screen emerge in the forward 2π solid angle.

For a photocathode of 10% efficiency this would represent a light gain of about 70. If the phosphor output is to be photographed by conventional optics this overall gain is necessarily reduced. For an F1 camera system the efficiency of transfer for unit magnification is about 4% and the overall photon gain is roughly a factor of 3. An order of magnitude gain over this figure has been reported for contact print recording (McGee and Wheeler 1961).

7.3.2. Cascade Image Intensifiers.

An increased photon gain can be acheived by effectively cascading a series of single stage intensifiers. Considerable effort has been devoted to the development of cascaded phosphor-photocathode intensifying screen tubes following the patent of the method by Philips Gloeilampen-fabrieken in 1928 (see e.g. McGee 1961). In this method the phosphor of one stage is deposited on one side of a thin glass or mica membrane and the photocathode is deposited on the opposite side of the membrane. Overall tube voltages of 30 - 40 KV have been employed.

The following values indicate the type of tube performances which have been reported.

Number of Stages	Light Gain	Resolution (Line pairs mm^{-1})	Reference
4	$\sim 10^5$	15-18	Davis 1963
3	$\sim 10^{3}$	23	Catchpole 1963
3	5×10^4	50	Aslam 1965
2	900	65	" "

The light gain referred to here is for input radiation of approximately the same wavelength as that emitted by the phosphor output screen.

7.3.3. Transmission Secondary Emission Intensifiers.(T.S.E.)

Image intensification may also be realised by accelerating the primary electrons and focussing them onto a thin screen which has the property of ejecting secondary electrons when bombarded with high energy primaries (Wilcock, Emberson and Weekley 1960 a, b.). The screen or dynode consists of an aluminium oxide supporting film coated on one side with an aluminium backing layer and on the opposite side

with the secondary emitting material. Both KCl and BaF_2 have been employed for this purpose. Electron gain is acheived by accelerating and focussing these secondary electrons onto a further dynode, a process which is repeated until adequate electron multiplication is obtained. The electrons from the final dynode are then accelerated and focussed onto the output phosphor screen.

For an efficient dynode consisting of a 500 Å thick Al_2O_3 film and an equal thickness of KCl, a secondary emission ratio of 4-5 and 6-7 is obtained for primary electron voltages of 4 KV and 5 KV respectively. A serious disadvantage arises from the penetration of primary electrons through the dynodes. For the above primary electron voltages this can amount to about 10% and 25% of the primary electrons (Morton 1964). These higher velocity electrons are not focussed on the output screen. (see Section 7.5.). Also, the signal-noise ratio for this type of intensifier is poorer than for the cascade tube due to greater fluctuations in the multiplication process.

Light gains of about 10^5 and a resolution of 30 line pairs mm^{-1} have been acheived. Further developments in progress include that of making the secondary emitting films of a porous structure and then applying an electric field across the film. Secondary emission ratios of 50 or more have been acheived in this process (see Morton 1964).

7.3.4. Electronographic Image Intensifier.

Much progress has been made at Imperial College by McGee and co-workers on the development of an image intensifier in which the photo-

electrons are accelerated upto a sufficiently high energy to penetrate a thin mica window (approximately 4μ thick). Recording of the electron image is made with a nuclear emulsion which is pressed against the mica window (Wheeler 1962, Khogali 1964). A remarkable image resolution of 90 line pairs mm^{-1} has been reported with a gain factor of some 10-20 over direct photography.

7.3.5. Channelled Secondary Emission Image Intensifiers.

In this method of intensification proposed by McGee 1953 the image is divided into a two dimensional array of picture points. The photo-electrons produced from each picture point are then multiplied innumber in separate channels by the process of reflected secondary emission. The multiplied output electron currents from the multipliers are then combined to produce a fluorescent image on a phosphor screen or may be used to generate a picture signal. Provided electrons can be prevented from straying from their correct channels, then the definition of the final image will be determined by the number of channels employed. The main limitation of this device has been the difficulty in making the channels sufficiently small and correctly aligning the dynodes in order to give a reasonable image definition.(McGee, Flinn and Evans 1960; Flinn 1962; Theodorou 1963; Wiley and Hendee 1962). Electron gains of 2×10^4 with a resolution of 2 line pairs mm^{-1} have been reported for experimental tubes developed at Imperial College.

For this type of tube a high working voltage is not essential and moreover this voltage need not be very precisely stabilised from the point

of view of resolution, since the voltage does not affect the focus. No magnetic focussing is required. Because of the small size and weight of this device, the low working voltage (<10 KV) and its simplicity of use then its main application may lie in the field of space research. For in this type of application these advantages may outweigh the major disadvantage of this device, namely its low resolution. The use of the channelled intensifier with the F.P. interferometer is considered in the following section.

7.4. The F.P. Interferometer - Image Intensifier Combination.

The results described in this section are for the F.P. interferometer used with both a channelled and a single stage intensifier. The latter tube was used to record first reported F.P. interferograms at a wavelength <2000 Å. (Bradley, Bates, Juulman and Majumdar 1964 a).

7.4.1. The Channelled Intensifier.

For a given resolving power, the superior angular dispersion of the interferometer compared with grating dispersers reduces the demands made on the linear resolution limit of the detector. For example, the angular dispersion for an echelle grating of blaze angle θ employed in a Littrow mounting is $2 \tan\theta / \lambda$. If the detector resolution limit is g_1 then the focal length of camera lens required is

$$f = g_1 \quad R/2 \tan\theta$$

where R is the resolving power.

In the case of the F.P. spectrograph, then for the same values of f and R the detector resolution limit required is g_2 (section 7.2.) where

$$f = g_2 \ (2 N p_2 R)^{\frac{1}{2}}$$

$$\therefore \ \frac{g_1}{g_2} = \frac{2 \tan\theta (2 N p_2)^{\frac{1}{2}}}{R^{\frac{1}{2}}}$$

For a blaze angle of 63° then comparing the grating instrument with an etalon of a finesse = 10, then for $p_2 = 4$ we obtain

$$\frac{g_1}{g_2} \simeq \frac{40}{R^{\frac{1}{2}}}$$

Thus, for a resolving power of 10^4 the resolution limit of the detector may be 2.5. times greater for the F.P. spectrograph than that required in the case of the grating instrument.

In effect, for a given detector the focal length of the camera lens employed in the grating instrument must be greater than that of the F.P. spectrograph in the ratio $R^{\frac{1}{2}}/2 \tan\theta (2 N p_2)^{\frac{1}{2}}$. Since the illumination of a spectral element $\propto 1/f^2$ then this increase in f leads to a reduction in illumination directly proportional to the resolving power.

The gain in illumination of a F.P. spectrograph over that of a blazed grating spectrograph employed in the Littrow mounting is approximately

$$G = \frac{A}{A^1} \quad \frac{R}{8 \tan\theta^2 p_2 N.}$$

where A and A^1 are respectively the utilised areas of etalon and grating and equal transmissions of flux by each system is assumed. Taking the

values of θ , p_2 and N given above then G $\sim$ 0.8 for R = 10^4 and 80 for R = 10^6 assuming an etalon area of $^1/_{10}{}^{TH}$ that of the grating area. Use of the grating off blaze angle leads to a reduction in angular dispersion and an increase in the value of G. The gain in illumination is entirely due to the reduction in the focal length of the camera lens made possible by the greater dispersion of the interferometer.

In the channelled intensifiers developed at Imperial College the diameter of the separate multiplying channels is 0.5 mm giving an effective resolving limit of 1-2 line pairs mm^{-1}. A tube with such a limited resolution still permits a spectral resolving power of about 10^4 for a camera focal length of 30 cm, an etalon finesse of 10 and employing the second fringe (p_2 = 2), of the Haidinger pattern (eqn.7.3.) Figure 7.1. shows λ5461 Å interferograms of HgI recorded with a developmental channelled intensifier made at Imperial College. The source was an 'Osram' low pressure lamp and the 5461 line was isolated with a Kodak filter. The camera lens focal length was 30 cm and the etalon finesse for the 2 cm aperture employed was approximately 10, giving a spectral resolving power of about 10^4 .

The etalon plate separation was 0.04 mm. and this was achieved by using 3 ball bearings as spacers. The steel balls were mounted 120° apart in a stainless steel annulus and were polished to equal thickness. Plates and spacer were placed in a conventional mount with spring adjustments (Tolansky 1947) and parallelism achieved by a small differential spring pressure. It should be mentioned here that whilst plate

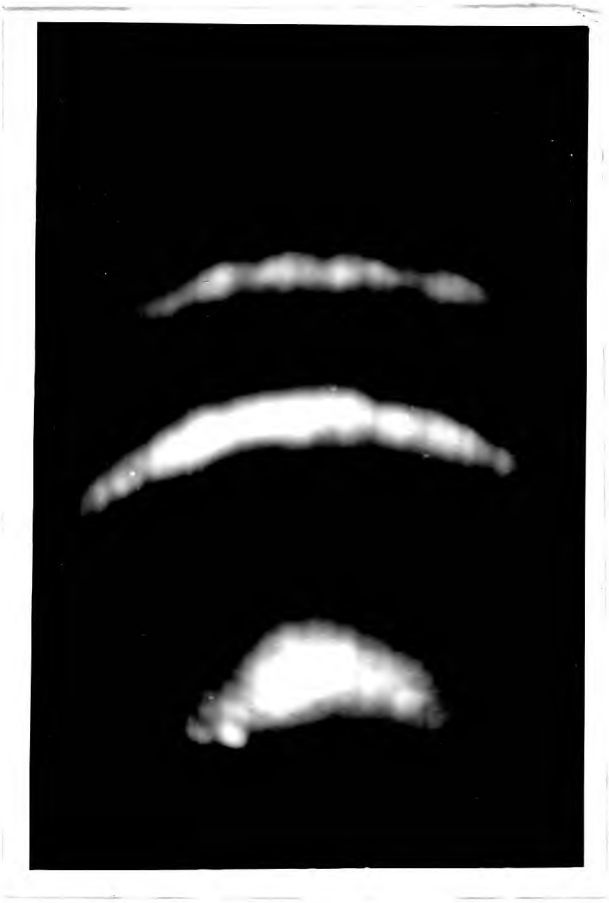

FIGURE 7.1.

parallelism could be easily achieved the use of ball bearings of this size ($\frac{1"}{64}$) is not to be recommended, since for only small spring pressures the steel balls caused indentations on the etalon plates. For steel balls of greater than 3 times this diameter no troubles of this type were experienced.

The gain of this experimental tube was not very uniform(fig.7.1) but the results indicate the potential of the interferometer, simple image tube combination in particular for space research applications.(section. 7.3.5.).

7.4.2. The Single Stage Intensifier.

It has already been seen in section 7.3. that the photographic gain of the simple, single stage image intensifier is not particularly high. However, one attractive feature of such an image tube is its property of image conversion. Concurrent with the development work on ultraviolet coatings for F.P. spectroscoy, a single stage image tube was constructed by S. Majumdar (1966) and F. Barlow (Imperial College) having a fused silica 'Spectrosil' end window and cathode plate. This image converter camera and the newly developed coatings were both employed to obtain the first reported F.P. interferograms of λ1849 HgI.

The photocathode was $SbCs_3$ of sensitivity 20μA lumen $^{-1}$ equivalent to a quantum effeciency of about 5%. Focussing of the electron image onto the output phosphor screen (ZnS: Ag) was achieved with a uniform axial magnetic field. The 1849 Å line was isolated using a prism mono - chromator and the entire optical system from entrance slit to converter

camera was purged with dry, oxygen free nitrogen in order to reduce the air absorption of this radiation.

An Eastern Blacklight 11SC - 1 low pressure Hg lamp was mounted within 1 mm of the monochromator entrance slit. This source was operated with a choke and ballast resistance directly from the mains supply and the operating current of 10 - 15 mA was not stabilised. The 60° 'spectrosil' prism was set for minimum deviation at λ1850 Å and the image converter greatly aided this adjustment. A standard Hilger and Watts interferometer type B297 with 1" diameter plates of flatness quoted as $\lambda/70$ (in the green) was employed. The plates were coated with Al - MgF_2 over a 2 cm aperture.

Because of the large source width of the 1849 Å resonance line of this lamp (which was not cooled) it was necessary to use a large free spectral range for the etalon. For this purpose 3 aluminium spacers were made from foil of 0.075 mm. thickness and the foil folded to give a spacer thickness of 0.15 mm. The spacers were mounted between the etalon plates at 120° intervals and the plates adjusted for parallelism by differential spring pressure. Using this method it was found to be somewhat difficult to adjust for parallelism since if one spacer was compressed too greatly it was then necessary to dismantle the etalon and remake the spacers. However, once adjustment had been made for parallelism the adjustment was found to be very stable and it would appear that the thin foil had made a reasonable optical contact with the etalon plates. This method was found very suitable for setting up interferometers of small plate separation in spite of the frustrating procedure for adjustment. In chapter 8 a more sophisticated approach

to the problem of a permanently adjusted etalon is considered.

The plate separation of 0.15 mm corresponds to a free spectral range of the interferometer of 1.1Å and 2.1Å at 1849 and 2537 Å respectively. Figure 7.2. shows F.P. interferograms obtained for λ 1849 Å using the single stage tube operated at a potential of 12 KV. The phosphor output was recorded using an F-1 optical system at unity magnification in an exposure time of 10 secs. (the imperfection in one of the fringes is caused by a defect in the phosphor screen). The recorded finesse of only approximately 5 was largely limited by the quality of the etalon plates. To confirm this, fringes of λ2537 Å were recorded (figure 7.3.) and a finesse of 7 directly proportional to the increase in wavelengths was obtained showing that the defects finesse dominates. The exposure in this case for the considerably more intense 2537 Å radiation was $\frac{1}{60}^{TH}$ sec. The quality of these interferograms should be compared with those shown in Chapter 6 where improved coatings were employed but more important, where the etalon flats were figured to be better than $\lambda/180$.

The spatial resolution limit of the overall recording system was determined by imaging a test pattern onto the tube photocathode using white light.(Baum. 1961). An overall linear resolution of about 20 line pairs mm^{-1} was acheived (N.B. this value is lower than might be expected. The linear resolution of the tube itself was about 30 line pairs mm^{-1}. The lower figure for the overall resolution was subsequently found to be due to a very small displacement of the focussing screen of the 'Exacta' camera used to photograph the phosphor output). From equation 7.3. this would indicate that the minimum focal length of lens (for imaging the

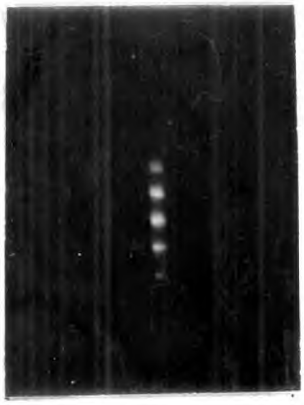

FIGURE 7.2

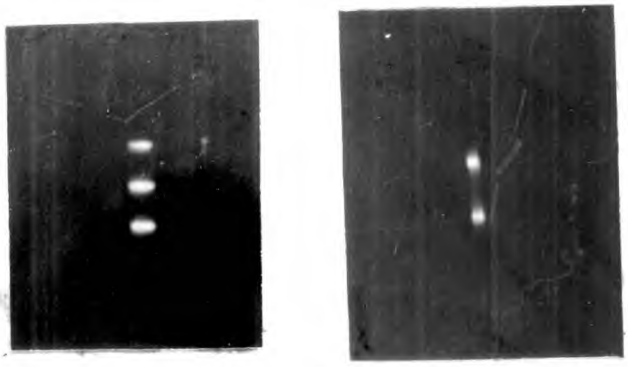

FIGURE 7.3.

fringe pattern) required to match this detector resolution limit need be only about 4 cm. In fact, the focal length of camera lens used was 20 cm giving adequate resolution and the quality of the recorded fringes should in no way be affected by the resolution limit of the detector for this focal length lens.

A real advantage of the image converter camera over direct photography for ultraviolet F.P. spectroscopy is that it enables the fringe pattern to be focussed visually and a final photographic record to be obtained using convential optics. For direct photography at wavelengths shorter than 2200 Å it is necessary to use the rather fragile ultraviolet sensitive emulsions. (e.g. Ilford Q emulsion - Chapter 6) whilst the image converter system permits the use of the standard photographic films currently employed in the visible region. There is a further advantage arising from the property of image conversion when it is required to make relative intensity measurements in the ultraviolet over a range of wavelengths. For example, intensity measurements from F.P. interferograms requires a knowledge of the film sensitivity to the incident radiation i.e. density as a function of relative exposure. This film sensitivity is dependent upon the wavelength of the incident radiation. Using the converter camera, the wavelength of the output radiation is dependent only on the type of phosphor screen employed and is not dependent on the incident radiation. This means that the film ~~sensity~~ sensitivity can be directly obtained by projecting onto the converter camera a calibrated density wedge and for this purpose visible radiation can be used. The value of the film gamma so derived (for given development conditions) may then

be used for relative intensity measurements for any other radiation of different wavelength incident on the converter camera. This method was used to determine the fringe intensity halfwidths for the interferograms shown in figures 7.2. and 7.3. for the wavelenths 1849 and 2537 Å, by recording a white light image of a calibrated density wedge with the converter camera. Without the image converter it would have been necessary to determine the film sensitivity at both these wavelengths. The full benefit would of course be derived when a wide range of wavelengths is to be recorded.

7.5. Time-Resolved Photoelectric Recording of F.P. Interferograms.

In this section results are given of preliminary investigations made to evaluate the performance of the F.P. etalon with electron-optical image detection for time-resolved spectroscopy. It has already been stated in chapter 1 that the oscillating F.P. spectrometer, which has been powerfully applied to plasma diagnosis, suffers from a serious disadvantage in that the time and wavelength dispersions are superposed. The use of the etalon with image tube detection overcomes many limitations of the oscillating instrument and a brief comparison of the two methods is given in section 7.5.6.

The principle of the method which was used to examine the performance of the etalon-intensifier combination for time-resolved spectroscopy is illustrated in figure 7.4.(a). The F.P. ring pattern superposed on a slit image, as in the spectrographic method of use, is swept across the photocathode of the image intensifier and the recorded output from the

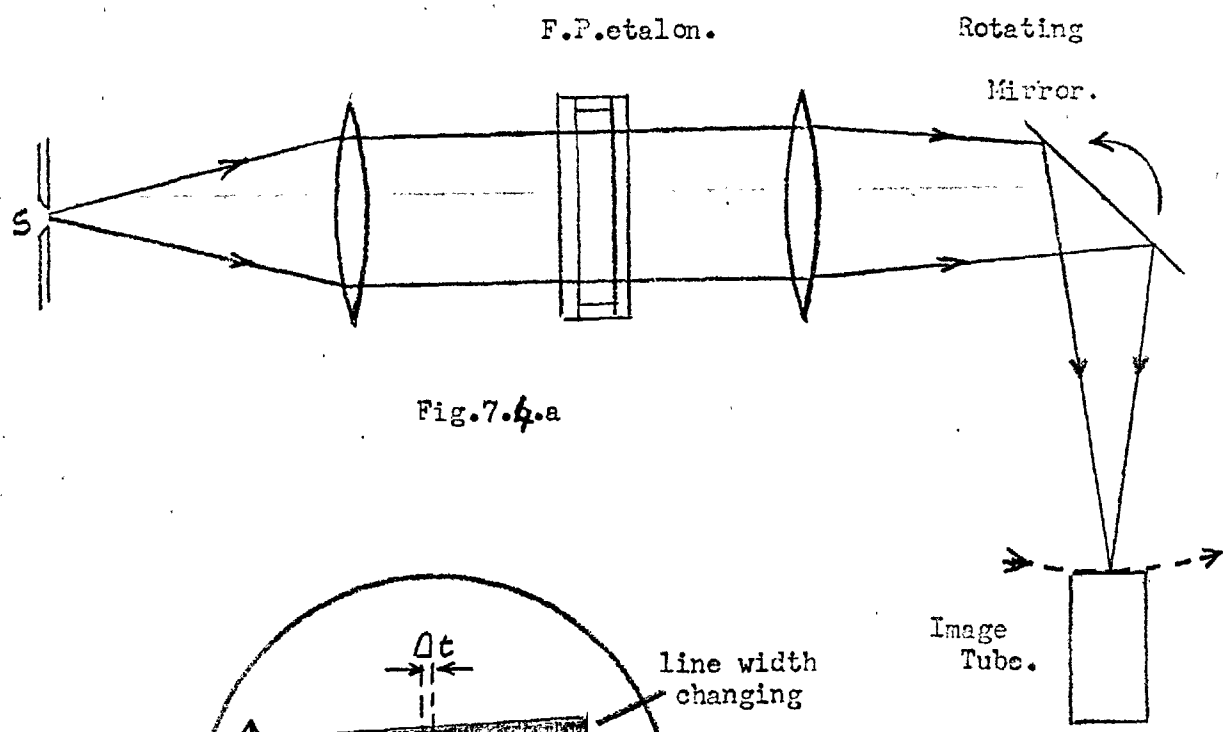

Fig.7.4.a

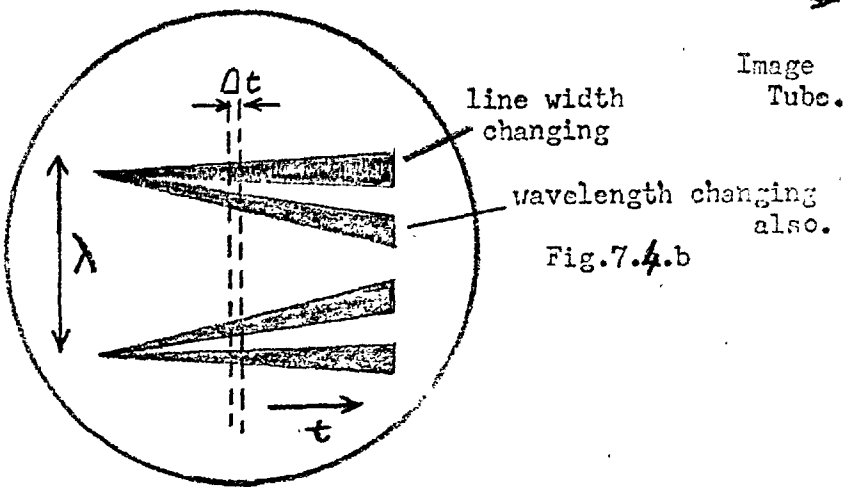

Fig.7.4.b

Figure 7.4 Principle of method for time-resolved recording of F.P interferograms.

phosphor screen will appear as shown in figure 7.4.(b). It is now seen that with such a system the time and wavelength dispersions are in mutually perpendicular directions. For simple testing of the performance the time scan was obtaining by using a rotating mirror. The phosphor output of the image intensifier was recorded using an F-1 camera system at unity magnification.

7.5.1. Single Stage Intensifier.

Initial tests were carried out by the author using a single stage magnetically focussed image tube. The light source was a high pressure Hg lamp and the 5461 Å line was isolated using a Kodak filter. For the etalon plate separation of 4 mm and silver coatings of $\simeq$ 89% reflectivity a spectral resolving power of about $3.2. \times 10^5$ was obtained.

Figure 7.5. shows a swept scan of the 5461 Å fringes at a time resolution of 6×10^{-4} secs. There are 60 time elements on each fringe. A microdensitometer trace of the central fringes is shown in figure 7.6. Variations in intensity and halfwidth arise from instabilities in the high pressure Hg lamp.

Further tests using essentially the same technique were carried out on cascade, T.S.E. and Lenard window tubes. This work was undertaken by C.O.L. Juulman. (Bradley, Bates, Juulman and Majumdar 1964 b) and these results will be merely summarised.

7.5.2. T.S.E.Tube.

The system was tested with a 5- stage T.S.E. intensifier (20th

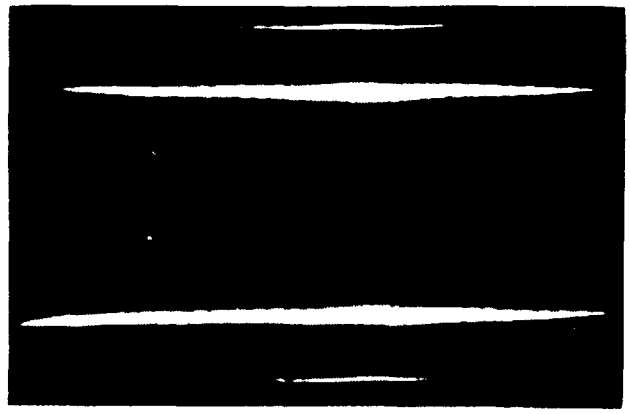

Fig 7.5 λ5461 high-pressure mercury lamp. Single-stage image tube. Time resolution 6×10^{-4} sec; spectral resolution 3.3×10^5

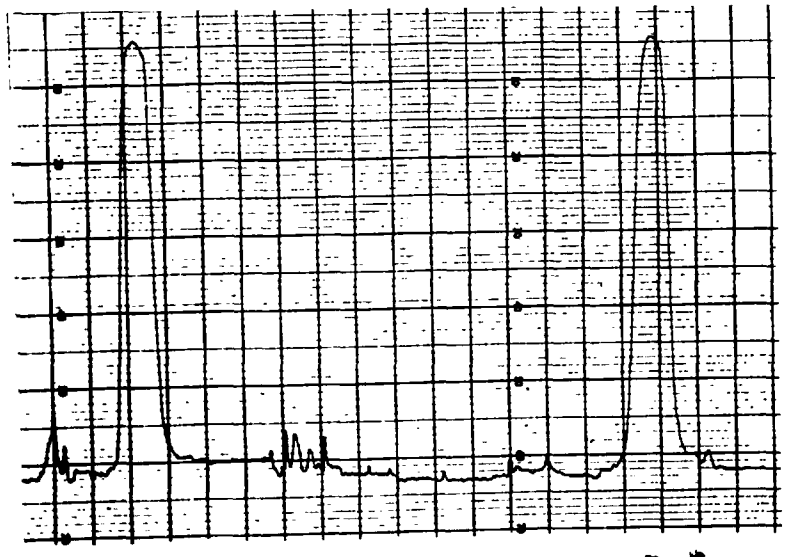

Fig. 7.6 Microphotometer trace of Fig. 7.5

Century electronics Type I P M 29/25) which was magnetically focussed. This tube had a linear resolution of 30 line pairs mm^{-1} and a blue light gain of 10^5 at 33 KV. The background scintillations at this voltage amount to 10^3 sec^{-1} cm^{-2}. Figure 7.7. shows a swept scan for the λ5461 line of a high pressure Hg lamp using a tube operating voltage of 26 KV. The time resolution limit corresponds to 2×10^{-6} secs and 80 time elements per fringe are shown. Spectral resolution in this case is about 3×10^4.

Figures 7.8.(a) and (b) show respectively static fringes obtained by direct photography and recorded with the T.S.E. tube. The presence of a signal induced background is clearly evident.(section.7.5.5.).

7.5.3. Cascade Tube.

Figure 7.9. shows scanned fringes obtained using a 3 stage magnetically focussed cascade tube developed at Imperial College (McGee and Catchpole 1962). Time resolution in this case is 10^{-5} secs with 50 time elements on each fringe. The spectral resolution is again approximately 3×10^4. Unfortunately the light gain of this tube had fallen at the time of these experiments and a greater time resolution could not then be attained.

7.5.4. Lenard Window Tube.

A Lenard window tube also developed at Imperial College was employed (McGee and Wheeler 1962) but due to a low cathode photosensitivity only a moderate time resolution was achieved. The tube was operated

Figure 7.7 λ5461 high pressure mercury lamp. I.S.2. Image intensifier. Time resolution 2×10^{-8} secs. Spectral resolution 3.2×10^{4}.

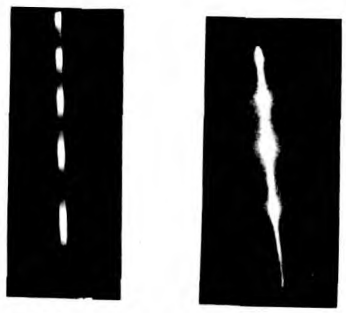

Figure 7.8 Interference fringes on slit (a) Direct photography. (b) I.S.2. Image intensifier.

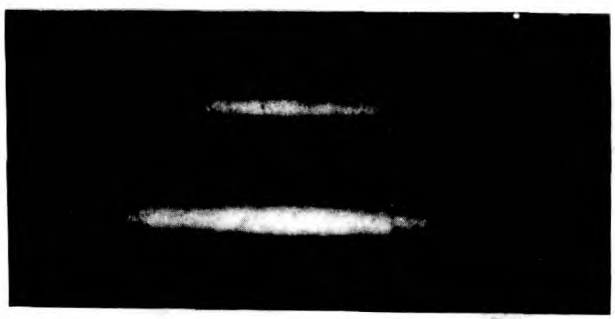

Figure 7.9 λ5461 Hg. Cascaded image intensifier time resolution 10^{-9} secs. Spectral resolution 3.2×10^{4}.

Fig. 7.10 λ5461 low-pressure mercury lamp fringes. Lenard window electronographic image tube. Exposures 1/50 and 1/25 sec.

at 40 KV and the electron image was recorded on Ilford G 5 nuclear emulsion using the technique described by McGee and Wheeler (1962).

Figure 7.10 shows λ 5461 Å fringes obtained using a low-pressure Hg lamp in exposure times of $^1/_{50}$ and $^1/_{25}$ sec. The spectral resolving power is 3×10^4. Because of the low photocathodes sensitivity it was not possible to obtain a time resolution $< 10^{-3}$ secs with the lamp employed.

7.5.5. A Comparison of the Different Intensifiers for Time- Resolved Spectroscopy

From these preliminary experiments on the performance of the etalon - intensifier combination it is possible to draw some conclusions regarding the suitability of the different types of intensifier for time-resolved recording of F.P. interferograms. For the T.S.E, tube, which was operated only at a potential of 26KV, the signal induced background and noise and the wide spread in multiplication factor in producing secondary electrons causes a decrease in the effective signal-noise ratio in the recorded image. This presents a severe limitation in the application of this device to the problem under consideration.

The fact that the noise is signal induced and not due to dark background was confirmed by operating the tube with no incident signal of the photocathode. For the period of exposure equivalent to that shown in figure 7.7, no background was discernible. The signal induced noise is mainly due to the effect of unfocussed penetrating primary electrons, whilst the signal induced background is probably largely

the result of focussed electrons. This latter effect arises from the incident radiation transmitted by the photocathode being reflected back to the cathode from the first dynode.

For the single stage intensifier the signal induced background is much smaller since there are no penetrating primary electrons and in addition, the incident radiation transmitted by the photocathode is reflected from the aluminium backing layer of the phosphor screen situated some 20 cm from the cathode. In the case of the T.S.E. tube the first dynode is situated about 7 cm from the cathode. Because of the much smaller solid angle subtended at the cathode by the phosphor output screen compared with the solid angle subtended by the first dynode of the T.S.E. tube, the effect of back reflected light is considerably reduced. In the case of the cascade intensifier there are again no penetrating primary electrons and the signal-noise ratio is much superior to that of the T.S.E. tube.

For the Lenard window intensifier the signal-noise performance is outstanding and the excellent recording of the fringe pattern is indicated by the absorption line in the fringes shown in figure 7.10. Additional gain for this device could be achieved by the inclusion of a phosphor-photocathode gain stage. The gain stage would increase the photographic speed by a factor of 50 - 100 although this would be at the expense of some loss in linear resolution. The Lenard window tube certainly appears to have a high potential for spectroscopy in view of the superb signal-noise performance. In addition, this tube has an advantage of a linear density -exposure relationship.(McGee and Wheeler

1962).

7.5.6. A Comparison between the Oscillating F.P. Spectrometer and the Etalon-Intensifier Combination.

A real disadvantage of the oscillating spectrometer arises from the fact that time and wavelength dispersions are superposed. Thus, if the etalon finesse is N, it is necessary to scan at a rate N times faster than the rate of change of the phenomena under investigation. This leads to a waste of photons and consequently a reduction in the signal-noise ratio attainable with a given source. Continuous monitoring of the phenomena is evidently not possible. In addition, since a point source must be employed simultaneous time and spatial resolution cannot be obtained.

A further disadvantage arises from the dynamical bowing of the moving etalon plate at high scan rates (Greig 1965) which consequently places a restriction on the finesse attainable. However, although in the current oscillating F.P. spectrometers the minimum resolvable time is set by practical limitations, there is a theoretical minimum resolution time whenever the F.P. interferometer is employed. This limitation is set by the time taken for a wavefront to pass through the etalon forming a large number of transmitted wavefronts which interfere to form the Haidinger fringe pattern. Ideally the number of interfering beams is infinite and the intensity distribution is given by the Airy formula (Born and Wolf 1964). However, when the number of interfering beams is other than infinite but is some finite value p , the resulting in-

tensity distribution is the same as for the Lummer - Gehrcke interferometer.

$$\frac{I(p)}{Io} = \frac{1 + G \ \mathrm{Sin}^2 \delta/2}{1 + F \ \mathrm{Sin}^2 \delta/2} \quad (1 - R^p)^2$$

where $G = 4 R^p/(1-R^p)^2$ (Born and Wolf.)

$F = 4 R/(1-R)^2$

and δ = phase difference between successive beams $(4\pi nt \cos\theta/\lambda)$

When p is finite then it is found that the etalon finesse N has the same value as obtained for an infinite value of p (chapter 2) provided the reflectivity of the coatings is not too large. For a coating reflectivity of 94% an etalon finesse of 50 is obtained for p infinite (perfect plates are assumed). However if the number of interfering beams is 30 then the resultant finesse for this reflectivity is only 30 (see Born and Wolf 2^{nd} revised edition p 346). For an etalon plate separation of 0.25 cm (corresponding to a free spectral range of 1Å at λ5000 Å) the time taken to build up the fringe pattern for the 30 interfering beams is 5×10^{-10} secs, which is the fundamental time resolution limit for this given spectral resolving power (1.5×10^5). Thus, with the oscillating F.P. spectrometer such a time resolution can only be achieved at the expense of spectral resolution. Or alternatively, if the spectral resolving power is to be maintained, then a sacrifice must be made in time resolution by a factor N (in this example = 30). In addition, since a photomultiplier is employed in the F.P. spectrometer, variations in time of electron flight for light incident on different

positions of the photocathode lead to an ultimate time resolution, Recent developments in photomultiplier design have greatly reduced these variations and photomultipliers capable of a time resolution of about 10^{-10} secs for employment of a cathode area of a few m.m. have been reported.(Rees and Parker Givens 1966). According to Butslov et.al. (1962) an image intensifier exceeds the best photomultipliers by at least 3 orders of magnitude with respect to time resolution.

The luminosities of the F.P. spectrometer and the etalon - intensifier combination are not very different. There is a gain in luminosity over the spectrometer arising from the fact that the fringes are continuously and simultaneously recorded and not for just $1/N^{th}$ of an order at a time. (Malyshev, Razdobarim and Sokolova 1963). If m fringes are utilised the total gain is m N. However, there is also a loss in luminosity since for a slit width (a) then only a fraction of the complete ring is recorded given by (section 7.2.).

$$a/2\pi r_p = 1 / \pi (Np)^{\frac{1}{2}}$$

Best use is made of the photocathode area if the etalon is tilted and only half the ring pattern employed. Thus, for each fringe the gain in luminosity is

$$G \sim \frac{1}{\pi} \left(\frac{N}{P} \right)^{\frac{1}{2}}$$

which for normal values of N and P employed differs little from unity.

However, it must be remembered that because of the parabolic dispersion of the interferometer then, whilst the density of each fringe remains constant, the elementary resolution area decreases with increasing p. Thus, by increasing p to gain spatial resolution a small sacrifice has to be made in the luminosity. This follows from equation 7.3. since

the focal length of the camera lens must be appropriately chosen to match the halfwidth of fringe p to the detector resolution limit.

A comparison of the two methods of using the interferometer is based on the assumption that the signal-noise ratio of the intensifier is not lower than that of the photomultiplier. In the intensifier the device noises do not add up since each point on the input cathode is represented by a point on the output phosphor screen. However, it has been seen that in the case of the T.S.E. tube the signal-induced background and noise is at present a serious drawback in the use of this device for time-resolved spectroscopy. This drawback was not encountered for the other intensifiers which have been tested.

7.5.7. Electron-Optical Sweeping.

The preliminary investigations discussed above indicated that the etalon-intensifier combination is a powerful method for time-resolved spectroscopy, particularly since it overcomes many of the drawbacks of the oscillating instrument. This work has since been continued and further developed by Bradley and Majumdar (1966) using the intensifier as an active element employing techniques for image storage (McGee, Beesley and Berg 1966) and electronic shuttering (Mandel 1961). A multiple-beam tube has been developed which is designed to produce consecutive discrete time-resolved interferograms. For diagnostic spectroscopy only a small picture area is required and it is possible to store time-dispersed photoelectron images inside an equipotential drift section which are separated out into time sequential frames by multiple reflection and

deflection in mutually perpendicular electric and magnetic fields. The application of a low voltage gating pulse at the end of the event being investigated then extracts these frames which are imaged onto the intensifier output phosphor screen. (Majumdar 1966).

7.6. The Wavelength Selective Photocathode.

In recent years there has been considerable development of wavelength selective photoemissive surfaces which respond to radiation in the far and vacuum ultraviolet but which are insensitive to light of longer wavelengths. Such surfaces have been described as being 'solar blind' indicating that they are relatively unresponsive to radiation of wavelengths longer than 3000 Å corresponding to the approximate ultraviolet cut off of solar radiation by the earth's atmosphere (Dunkelman 1955). A review of the properties of solar blind photodetectors has been given by Dunkleman, Fowler and Hennes (1962).

Spectrally selective photocathodes are particularly attractive for astrophysical applications and also for laboratory applications wherever long wavelength stray light is undesirably large. The spectral response curves for representative ultraviolet photocathodes are shown in figure 7.11. (Dunkeleman and Hennes 1964). It is seen that the CsI cathode is relatively unresponsive to wavelengths greater than 2100 Å and at 1850 Å the quantum efficiency is about 0.7%, which increases at shorter wavelengths, The use of a photomultiplier with CsI cathode together with experimental interference filters developed in the present work for broad band stellar photometry below 2000 Å has

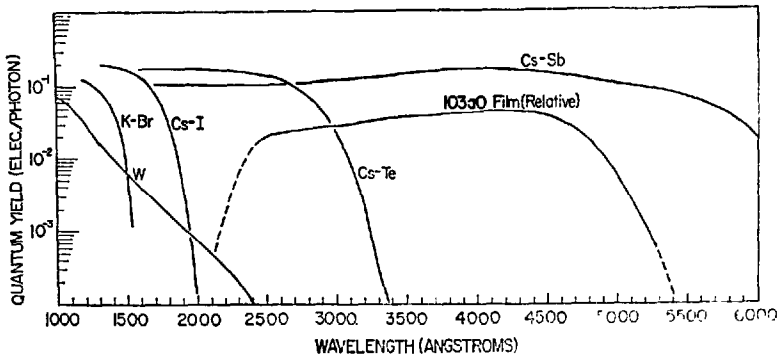

Spectral response of typical UV photocathodes.

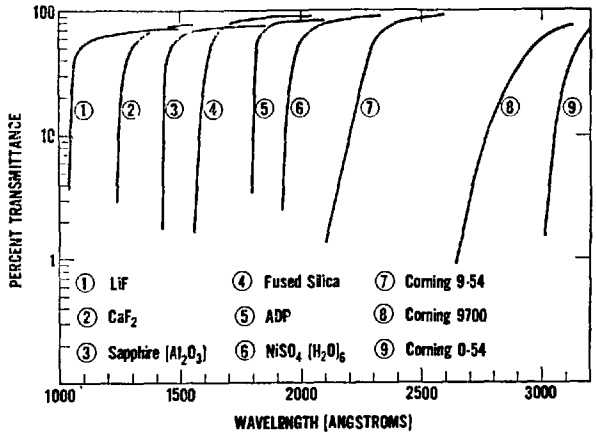

UV optical materials.
Transmittance curves, uncorrected for surface reflections, are shown for materials of thickness: 1-1.2 mm; 2-1 mm; 3-1 mm; 4-1 mm; 5-2.5 mm; 6-3 mm; 7, 8, and 9 are each about 2 mm.

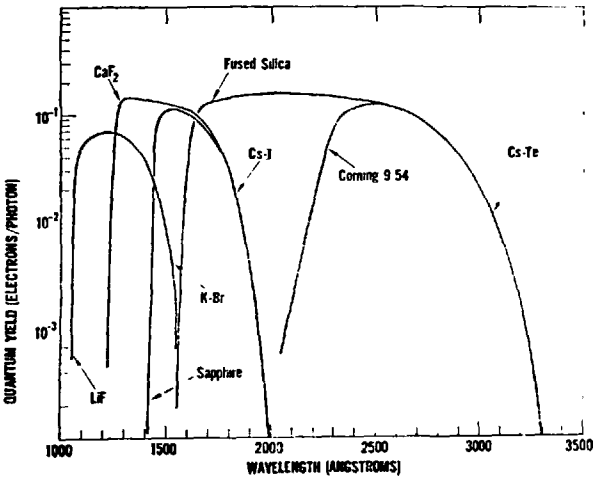

Spectrally selective UV photodetectors.
These curves are produced by combining some of the cathodes and filters

already been mentioned in Chapter 6. It is quite apparent that an image intensifier with a selective cathode would also have many advantages for far ultraviolet spectroscopy. Dunkelman and Hennes (1964) have described an image converter camera employing a CsI photocathode.

Such an intensifier would have been of great benefit in recording the λ1849 HgI interferograms shown in Chapter 6. These fringes were recorded by direct photography employing interference filters to isolate the 1849 Å radiation. Because of the long wavelength tail of these filters it is seen that the considerably more intense 2537 Å radiation contributes a background to the 1849 Å fringe pattern. Recording of the fringes with an intensifier employing a CsI cathode would eliminate response to the 2537 A° radiation giving a much improved constrast. On the more practical side, the property of image conversion from ultraviolet to visible would greatly facilitate focussing of the fringe pattern. More generally, for application to vacuum ultraviolet spectroscopy the effects of stray light of wavelengths longer than 2100 Å would be eliminated.

In the present programme on developing techniques for ultraviolet interference spectroscopy, the construction of an image intensifier for the far ultraviolet was begun but for a variety of technical reasons has not yet been completed. Constructional details of the tube, cathode preparation and expected performance have been discussed by Majumdar (1966). Essentially the proposed device consists of a CsI photocathode and a convential output phosphor screen but with the inclusion of a phosphor-photocathode gain stage (section 7.3.). The operating voltage of the tube would be 30 - 35 KV and a uniform axial magnetic field used for focussing

the electron image.

For a good quality phosphor-photocathode sandwich an incident photo-electron of energy $\gtrsim$ 20 KeV should realise a yield of 70 to 100 photo-electrons. These electrons are then accelerated through a potential of $\simeq$ 15 KV and focussed onto the output screen. For a CsI cathode of 0.7% efficiency then a photon gain of about 400 could be realised. Two stage intensifiers developed at Imperial College have been reported in which the linear resolution in 65 line pairs mm^{-1} (Aslam 1965).

It is apparent that an intensifier of this type would have a high potential for vacuum ultraviolet spectroscopy. The first stage of development was for a tube using a 'Spectrosil' end window and cathode plate. Extension to shorter wavelengths could be acheived by employing LiF in place of the Spectrosil. At shorter wavelengths additional photon gain would be realised because of the increasing quantum efficiency of the CsI cathode (fig.7.11.). Whilst no such tube has been completed, although near completion was reached on more than one occasion, valuable experience has been gained in the techniques required, in particular for the preparation of the CsI photoemissive surfaces (Majumdar 1966). In view of the promise of such a device it is hoped that this work will be continued.

Further useful developments might include the extension of the spectral range of the Lenard window tube into the vacuum ultraviolet with also the inclusion of a phosphor-photocathode gain stage.

CHAPTER 8.

SOME RECENT DEVELOPMENTS IN THE APPLICATION OF THE F.P. INTERFEROMETER TO SPACE RESEARCH.

8.1 Introduction.

Advances in the detection, identification and measurement of wavelengths in the solar spectrum have usually followed new developments in optical instrumentation. Spectrographic equipment is required which possesses a sufficiently high spectral resolution and dispersion such that closely spaced lines can be separated. Additionally, the spectrograms must be calibrated with sufficient accuracy so that meaningful wavelength assignments can be made.

During the 19^{TH} century advances were made in spectroscopic techniques which provided the basis for the mapping of the visible solar spectrum. Fraunhofer ruled a plane transmission grating and visually observed 571 dark lines in the solar spectrum. Angstrom measured the wavelengths of over 1000 Fraunhofer lines whilst during the period 1895 to 1897 some 20,000 solar absorption lines in the wavelength region 2975 to 7330 Å were measured by Rowland with his new concave grating as the dispersing element. In 1902 Fabry and Perot applied their interferometer to the accurate determination of wavelengths in the solar Fraunhofer spectrum.

The current method for improving the resolution and dispersion of spectrographic instruments designed for the visible spectrum is to rule larger gratings and to construct larger spectrographs. The standard

solar atlas currently used for this wavelength region was obtained with a plane grating spectrograph 23 metres long having a reciprocal plate factor of 0.3. Å m.m.$^{-1}$ and a theoretical resolution of 1.5 x 10^5 (Minnaert, Mulders and Houtgast, 1940).

From ground based observatories, ultraviolet solar emissions can be detected only down to wavelengths of about 2900 Å. This abrupt termination in the spectrum was shown by Fabry and Buisson in 1913 to be due to absorption by ozone in the earth's atmosphere. Later high altitude balloon flights were still unsuccessful in penetrating this ozone layer. In 1946 captured German V2 rockets enabled spectrographic equipment to be carried above the ozone layers and for the first time photographs of the solar spectrum were recorded at wavelengths shorter than 2900 Å by the U.S. Naval Research Laboratory (Baum et.al,1946 see also Tousey 1961). The spectrogram extended the range of the solar spectrum to λ 2200 Å and of considerable interest was the intense absorption doublet of ionised Mg at λ 2803 and 2795 Å corresponding to the well known near ultraviolet H. (3968 Å) and K (3934 Å) lines of singly ionised Ca.

It is obvious that rocket-bourne experiments present many special difficulties which are not encountered from ground based observatories. Firstly there is the limited time for observation above the ozone layer; secondly, the roll pitch and yaw of the rocket have to be encountered imposing limitations on the pointing accuracy of the optical payload and thirdly, the rocket vehicle imposes restrictions as to the size and weight of equipment flown. These are but a few of the difficulties.

Of course, satellites offer a means of overcoming the observation time limitation and many advances in solar and stellar spectroscopy are to be expected with the development of orbiting observatories.

For a few years after the first N.R.L. flight only moderate advances were made in solar ultraviolet spectroscopy until a biaxial pointing control, designed to keep the spectrograph pointed at the sun regardless of the attitude of the rocket, was developed by the University of Colorado. (Stacey et.al. 1954). With this control it became possible to point the spectrograph at the sun within an accuracy of 1 arc minute (N.B. the angular diameter of the sun from the earth is approximately 30 arc mins). Following this development there came an improvement and many advances in rocket ultraviolet spectroscopy (see e.g. Friedman 1962).

The first thirteen years of rocket spectroscopy provided an excellent survey of the solar spectrum from the ozone cut off into the extreme ultraviolet. It next remained to improve on instrumention in an endevour to re-examine the ultraviolet region in greater detail. An example of improved instrumentation and technique is demonstrated by the discovery of the reversal of the solar hydrogen Lyman-alpha line at λ 1216 Å (Purcell and Tousey 1961). The determination of the true profile of a spectral line in the solar spectrum requires a resolving power of 10^5 to 10^6. The development of the echelle grating by Harrison (1949) and subsequent improvements in the technique for ruling echelles have made it possible to build spectrographs of a high resolving power but of small enough dimensions for rocket work. Purcell, Boggess and Tousey (1958) designed a spectrograph to photograph the solar spectrum between 2200 and 3000 Å

with sufficiently high spectral resolution to separate Fraunhofer blends and to obtain contours of the Mg II doublets. The dispersing element was an echelle grating of 80 grooves mm^{-1}. in the Littrow mounting crossed with a CaF_2 prism. Difficulties were encountered in flight such that the spectral resolution achieved was 0.1 Å although the pre-flight laboratory performance was found to be 0.04 Å. Never the less, line profiles of the Mg II doublet were obtained in new detail showing the half-widths of the emission lines to be approximately 0.4 A.

An improved performance using the essentially the same technique was obtained in a very sucessful later flight described by Purcell, Garrett and Tousey (1963). A section of their echelle spectrogram is shown in figure 8.1. in which the intense Mg II doublet is clearly seen. A comparison was made between the instrument profiles of this spectrograph and that of the 21 foot Gottingen spectrograph. The width of both profiles is 0.03 Å at half maximum intensity and they are essentially the same down to about 10% maximum. Below this intensity level the rocket spectrograph profile broadens out into ghost like wings which are produced by the echelle itself. (Fig.8.2.).

The contours of the Mg II lines are also given in figure 8.1. (linear density scale). The strong broad absorption is the first component of each line of the doublet which causes the continuum to be depressed over many Angstroms. The emission lines form the second component and an absorption in each line forms the third component. These lines are very similar to their Ca II H and K counterparts but the emission components are much more intense than H_2 and K_2. The reasons

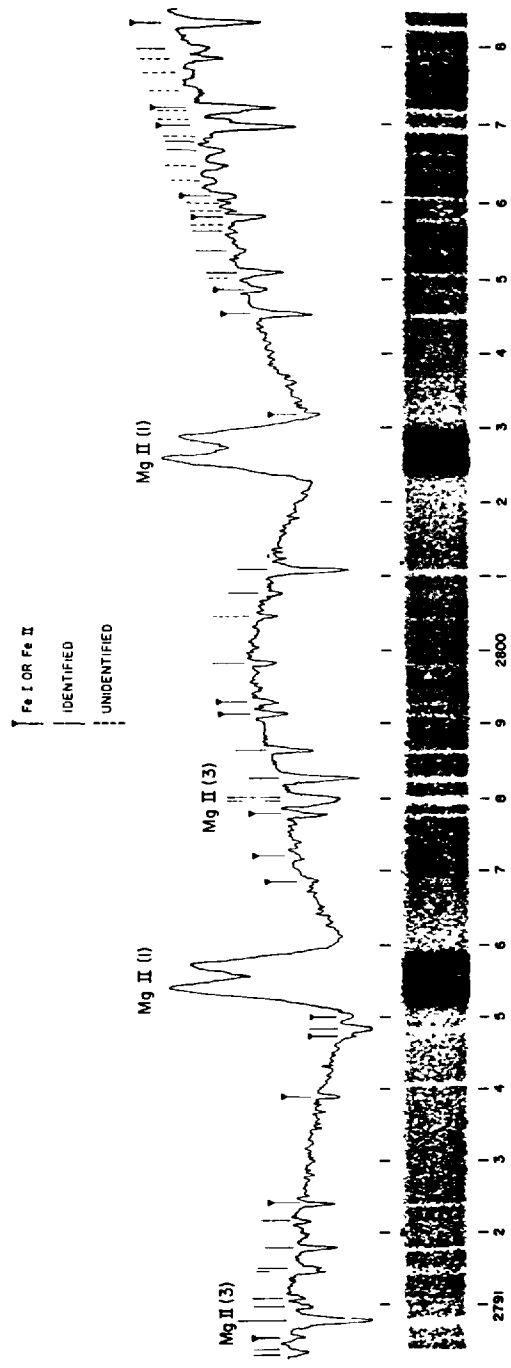
Fe I OR Fe II
IDENTIFIED
UNIDENTIFIED
Mg II (1)
Mg II (3)
Mg II (1)
Mg II (3)
2791
2800

Figure 5.1.

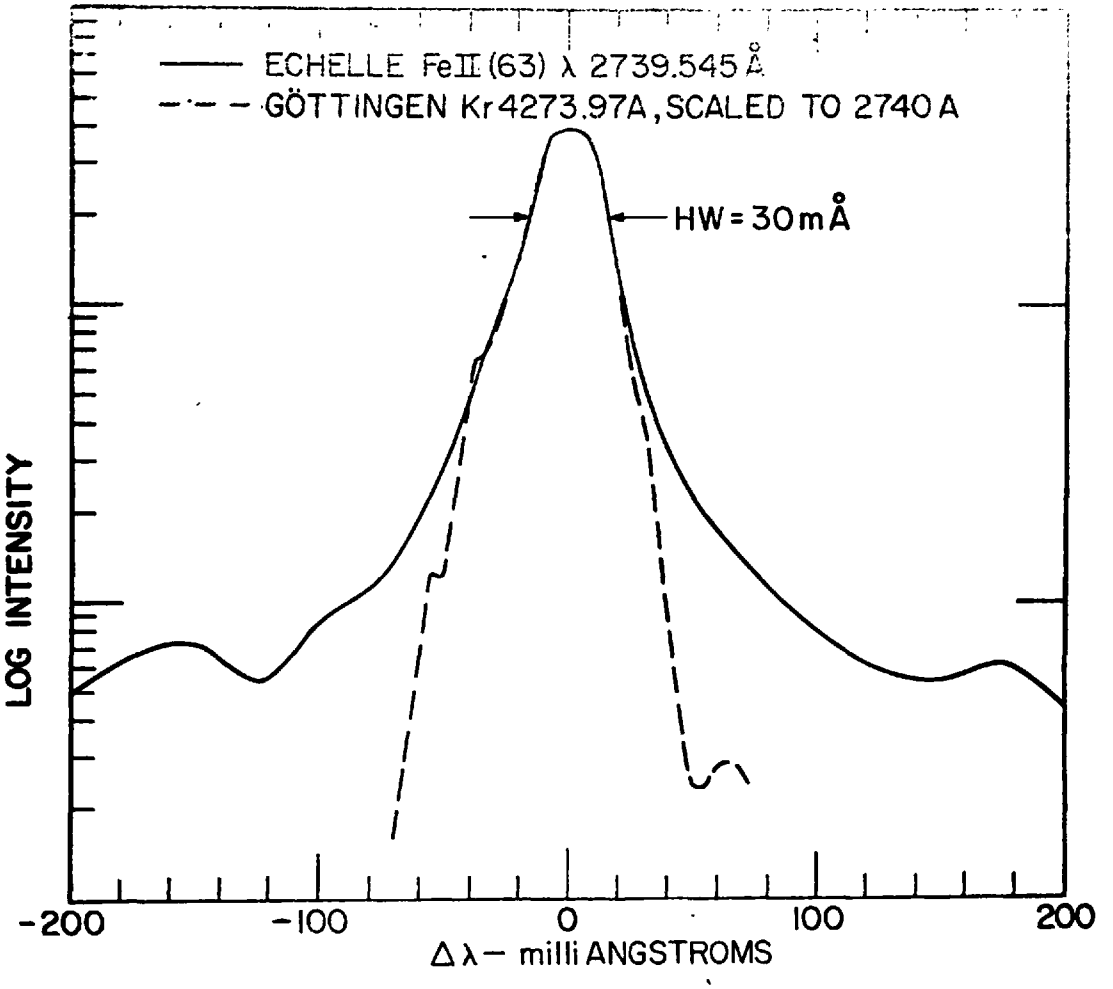
ECHELLE FeII(63) λ 2739.545 Å
GÖTTINGEN Kr 4273.97A, SCALED TO 2740 A
HW = 30 mÅ
LOG INTENSITY
-200
-100
0
100
200
Δλ — milli ANGSTROMS

FIGURE 8.2.

for this are that there is more ionised Mg than Ca at high levels in the solar atmosphere and also the continuum is far less intense at 2800 Å than at 3950 Å. When one considers the considerable information which has been gained from studies of the Ca II H and K lines it is quite apparent that the Mg II doublet is likely to be of tremendous importance in solar spectroscopy.

In 1961 the need for a British stabilised rocket was examined by the National Committee for Space Research and it was decided to develop an attitude control unit (A.C.U.) to operate on payloads carried by the well proven 'Skylark' rockets. The initial specification was for the unit to be sun pointing stabilised in 3 axes with the lateral control to be better than one degree and the roll control to be of the order of a few degrees. Further developments include Stage II - improved sun pointing accuracy and Stage III - a moon pointing system for night sky observations.

For a series of experiments to study the ultraviolet emission of the chromosphere and corona the U.K.A.E.A. (Culham Lab.) required a sun pointing accuracy better than 1 arc min. which considerably exceeds the stage I specification for the A.C.U.

This laboratory has developed an optical servo alignment system which operates on a collector mirror to maintain the position of the solar image on the spectrograph slit. Results from earlier flights show a remarkable degree of stabilisation in that the maximum lateral error of the fine alignment system is approximately 13 arc secs (r.m.s. $\pm$ 2 - 3 arc secs). The corresponding roll figures are $\sim 10^{\circ}$ peak to peak (Black et.al. 1965). An improved performance was achieved on later

flights which is such that a lateral displacement of $\pm$ 5 arc secs and a roll of 2 degrees might now be expected (Shenton 1966).

Two joint experiments with the Culham Laboratory are now in progress in which the aim is to exploit both the fine optical alignment system developed by Culham and the high luminosity and great angular dispersion of the F.P. interferometer. The purpose of these experiments is to obtain high spectral resolution profiles of the Mg II doublet with a spatial resolution of the solar disc of the order of 6 arc secs. In the following section some advantages of the interferometer for space spectroscopy are discussed and in the later sections a brief description is given of the method of approach to the first of these experiments.

8.2. Some Advantages of the F.P. Interferometer in Space Spectroscopy.

Dunham (1956) has discussed how the F.P. spectrometer can be exploited for high spectral resolution, stellar spectroscopy from large ground based telescopes. In the method considered, the stellar image is focussed onto the slit of a grating monochromater which is used to provide the necessary pre-dispersion for the etalon. The etalon may be placed in the parallel beam either preceding or following the grating. For a resolving power R , the angular diameter required for the analysing diaphragm centred on the optic axis and in the focal plane of the fringes, is $2\ (2/R)^{\frac{1}{2}}$.(Jacquinot 1954). For maximum efficiency, the optical system must be designed so that the total flux in the stellar image passes through the diaphragm.

Dunham considers the case of an etalon of 4" aperture used in con-

junction with a 100" telescope. For a resolving power R of 5×10^5 then the angular diameter of the analysing diaphragm cannot exceed 4×10^{-3} radians. For an optimum optical system, then if the angular diameter of the stellar image is α at the focus of the telescope it will be magnified to an angular diameter β in the focal plane of the etalon-monochromator system. The values of α and β are related according to

$$\beta = D_1 \alpha / D_2$$

where D_1 is the aperture of the telescope and D_2 the aperture of the etalon. The importance of a large etalon aperture is apparent since the stellar image must not be magnified to such an extent that flux fails to pass through the analysing diaphragm.

If the angular diameter α of the stellar image is 10^{-5} radians (approx 2 arc sec) then this will be magnified to a value of $\beta = 2.5 \times 10^{-4}$ radians. These parameters are for comparatively poor seeing conditions but nevertheless, even with a 100" telescope the magnified stellar image only occupies $\frac{1}{16}^{TH}$ of the diameter of the analysing diaphragm. In fact, the etalon aperture could be reduced to a value of $\frac{1}{4}$" before flux would be held back by the diaphragm. The advantages of a smaller etalon aperture from the point of view of realising the necessary plate defects finesse has been considered in Chapter 2.

In the application of the F.P. spectrometer to stellar spectroscopy from space vehicles the 'seeing' limitations introduced by the earth's atmosphere are now replaced by guidance limitations. Again for a resolving power of 5×10^5 the angular diameter of the analysing diaphragm is 4×10^{-3} radians or about 13 arc min. Thus the demands on the guidance

tolerance is only some $\pm$ $6\frac{1}{2}$ arc min. If a telescope aperture of 6 cm diam. is employed with a 3 cm F.P. aperture then the magnified stellar image will become 10^{-5} radians (an angular stellar diameter of 1 arc sec is assumed). Thus, the magnified stellar image occupies only $1/400$ TH of the diameter of the analysing diaphragm. This means that for the same telescope aperture and resolving power the etalon aperture could be reduced to only 75μ before any flux in the stellar image is held back by the diaphragm. However, whilst the use of such a small etalon aperture would be extremely desirable from the point of view of realising the necessary etalon finesse, in practise such a small aperture could not be employed except in the case of a very narrow gap etalon. The reason for this arises from the lateral displacement of succesive beams transmitted by the interferometer. For example, in the above case if an etalon gap of 0.05 cm is employed (Comparable with the plate separation required for the experiment described in the following section) then for a coating reflection finesse of 50 the number of interfering beams required to give an intensity halfwidth within 1% of the ideal Airy halfwidth is approximately 1.4 N_R (Born and Wolf 1964; Greig 1965). In such a case, the minium etalon aperture required is approximately 300μ .

A comparison of this performance of the F.P. spectrometer may be made with an echelle grating used under the most favourable conditions in the Littrow mounting. For a resolving power R a beam width W is required given by

$$R = 2W \sin \theta / \lambda .$$

Using a grating of blaze angle $\theta = 63^{\circ}$ then for $\lambda =$ 2800 Å the value of $W \simeq 8$ cm. for $R = 5 \times 10^5$. The aperture of the echelle appears very fore shortened from the collimator and a ruled operating length of $W/\cos\theta \sim 18$ cm is required.

If all the flux collected by the telescope fills the collimator then the angular diameter of the stellar image subtended at the collimator (β) is given by the usual relation

$$\beta / \alpha = f1/ f_2 = D1/D2$$

where f_1 is the focal length of the telescope of aperture D_1

f_2 is the focal length of the collimator of aperture D_2

and α is the angular diameter of the star at the focus of the telescope. Accordingly, for a 6 cm aperture telescope the value of β is 3.75×10^{-6} radians for a value of $\alpha =$ 1 arc sec. The angular dispersion of the echelle employed in the Littrow mounting is $4/\lambda$ for a blaze angle of 63° and an angular slit width of 8×10^{-6} radians is required. Under these condtions the stellar image occupies approximately one half the slit width and the guidance tolerance would become a severe value of $\pm \frac{1}{2}$ arc sec.

Besides this important advantage in the relaxation of the demands on guidance tolerance the interferometer possesses several other advantages over grating instruments for application to space research. For the same resolving power the F.P. spectrometer is considerably more luminous than grating dispersers of equal area.(Jacquinot 1954). This superior luminosity permits a higher speed of recording and more rapid scanning of

line profiles. Thus, a greater number of spatial resolution elements could be covered during the limited observation time of a single rocket flight. Also, the F.P. spectrograph has a much greater illumination than gating spectrographs for a resolving power greater than about 2×10^4 (see section 7.4.1.). It has already been shown in Chapter 7 that in addition the superior angular dispersion of the interferometer permits a relaxation on the demands of the linear resolution of the detector. This has been illustrated by using a channelled image intensifier of only 2 line pairs mm^{-1} resolution for recording F.P. interferograms.

Because of the superior angular dispersion of the interferometer the F.P. spectrograph can be made considerably more compact than is possible with grating instruments. This is of vital importance in space spectroscopy where full use must be made of the limited space available in the vehicle.

For many astrophysical problems where resolving powers of 10^5 to 10^6 are required the echelle and the F.P. interferometer are the only dispersers capable of providing this high resolving power. However in the ultraviolet < 2500 Å the resolving power of the echelle falls of rapidly because satellite intensities near line centres are increasing and scattered light begins to intrude (Learner 1965).(see also figure 8.2 .)

Finally, mention should be made of another important property of the interferometer, for which it is well known, namely that of its unique use for accurate, absolute wavelength determinations. The interferometer will therefore permit absolute wavelength measurements to be made of solar Fraunhofer lines at wavelengths shorter than 2900 Å.

It is apparent that the interferometer possesses several advantages over the echelle grating for space research applications. In the following two sections brief consideration is given to the approach of an experiment exploiting some of these advantages and also to some of the difficulties to be overcome.

8.3. A Rocket Spectrograph Employing the F.P. Interferometer.

The resonance lines of Mg II at 2795 and 2802 Å are particularly important for studies in solar physics. A first experiment, which is already in progress, will employ the F.P. etalon for a detailed study of the profiles of these lines and their spatial distribution over part of the solar disc. For this experiment a sun pointing stabilised Skylark rocket will be used which will include a fine optical alignment system operating on a collector mirror to maintain the solar image to a pointing accuracy within ± 5 arc secs.

This first experiment is purely photographic and the dispersion of the interferometer is crossed with an echelle spectrograph. The system will be optimised for the Mg II lines to give a spectral resolution in the fringes of about 0.03 Å. For a free spectral range of 1Å required at 2800 Å the etalon plate separation is 0.04 cm and for the required spectral resolution an etalon finesse of 30 is necessary. The approach to this problem is discussed in section 8.4. The echelle slit will be set to give a resolution limit of 0.25 Å.

A schematic outline of the optical system for the rocket spectrograph is shown in figure 8.3. The echelle has 300 grooves mm^{-1} blazed

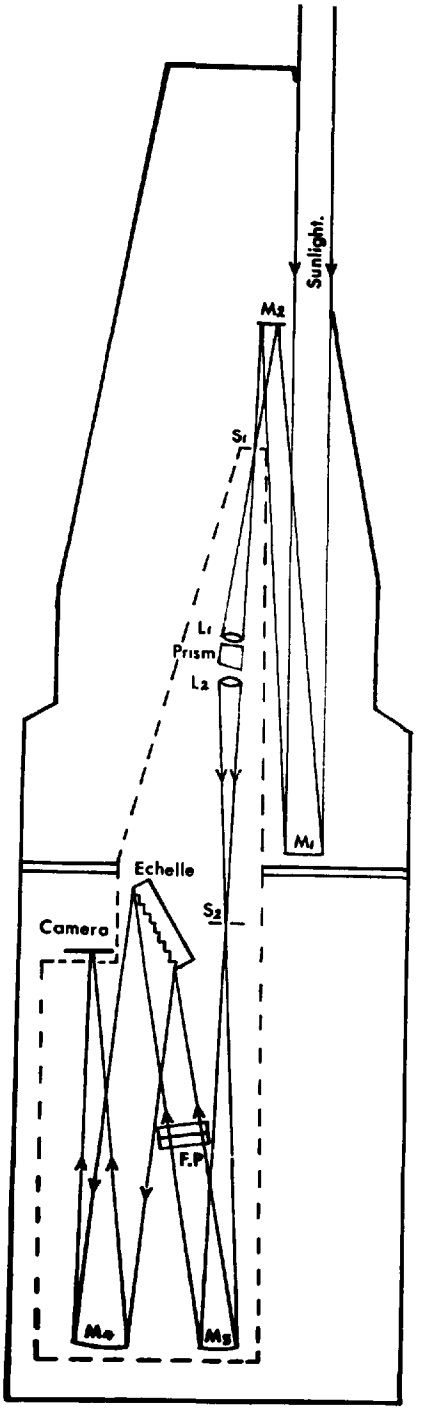

Figure 8.3.

at an angle $\tan^{-1}\theta = 2$. At λ 2800 Å the free spectral range of the echelle is 120 Å and a thin prism pre-disperser is used to isolate 100 Å centered on 2800 Å at the entrance slit of the echelle spectrograph.

The etalon is placed in the parallel beam preceding the echelle since the width of the parallel beam is smallest in this region. A maximum etalon aperture of 2.5 cm will be employed. A major problem in the design of the spectrograph in view of the limited space available was the difficulty in preventing obstruction of the diffracted beam by the interferometer and mount. If the angles of incidence and diffraction are $(\theta + x)$ and $(\theta - x)$, θ being the blaze angle, then the ratio of the widths of the diffracted and incident beams w'/w increases with x in accordance with the relationship

$$w'/w = \cos(\theta - x)/\cos(\theta + x)$$

Also, an increase in x causes a reduction in the angular dispersion of the echelle since

$$d\beta / d\lambda = 2/\lambda (\cot\theta + \tan x).$$

The value of x should therefore be kept as small as possible. In the present design the smallest value of x which could be acheived was 6°.

For a 50 cm focal length collimating mirror an echelle slit width of 147μ is required to isolate 0.25 Å. Using a camera mirror of 40 cm focal length this slit width is reduced to 118μ on the photographic film. For the purposes of microdensitometry of F.P. interferograms such a slit width has been found to be adequate. The effective solar diameter on the film (equivalent to slit height) is about 1 cm. Across this solar diameter there will be 9 fringes which requires that the etalon is tilted

through an angle of $\theta = (p\lambda/t)^{\frac{1}{2}}$ ($\sim 7.5^{\circ}$) where the value of $p \simeq 25$ is obtained from equation 7.4.

The angular halfwidth of fringe p (see eqn.7.2.).

$$\text{is } d\theta = \frac{1}{2N}\left(\frac{\lambda}{tp}\right)^{\frac{1}{2}}$$

$$= \frac{1}{(2NRp)^{\frac{1}{2}}}$$

For N = 30, R = 10^5 and p $\simeq$ 25 the value of $d\theta \sim 8 \times 10^{-5}$ radians. For the 40 cm focal length camera the corresponding F.P. resolution width of approximately 30 μ represents a spatial resolution of the solar disc of about 6 arc secs.

The echelle slit ($\equiv$ 0.25 Å) crossed with F.P. fringes will occupy a strip $\sim$ 21 arc secs wide of the solar disc across a solar diameter. Spatial resolution along a solar arc will depend on the rocket roll which is the most difficult axis for stabilisation but it is hoped to acheive a resolution along a solar arc of 2 degrees. The optical alignment system will be programmed so that between exposures the solar disc will be moved relative to the fringes to give a wider spatial coverage. Different exposures will perhaps be obtained by reducing the width of the etalon aperture using an iris diaphragm. This method has the advantage that an improved finesse is likely to be obtained for the reduced etalon aperture. In addition to the data on the Mg II doublet a spectral region of about 80 Å close to 2800 Å will be photographed with the same spectral and spatial resolutions. The final photographic record will be contained in a film area of approximately 4 x 1 cm.

A second planned experiment will employ a scanning F.P. crossed with an echelle spectrometer. In this case the high luminosity of the centre fringe will be exploited by scanning through many line profiles and recording photoelectrically with two solar blind e.g. CsTe photomultipliers at a spectral resolution of $\simeq$ 0.03 Å. An estimated scan time of 10^{-1} secs is required to record the emission lines with this resolution. For an observation time in one flight of 300 secs above 100 Km, 3×10^3 spatial resolution elements of 10 x 10 arc secs could be recorded. This corresponds to roughly 10% of the solar disc. Full details of methods of scanning and maintainence of parallelism during scan have yet to be decided upon but plans for an experimental piezo-electric system are already in progress.

8.4. An Optically Contacted Permanently Adjusted F.P. Etalon.

For the rocket spectrograph a permanently adjusted etalon with a finesse of approximately 30 is required. It is therefore apparent that the final performance in the experiment will be critically dependent on the adjustment and the stability of the interferometer.

All dielectric multilayer coatings (Perkin Elmer Inc) will be employed to give a reflectivity of 94% (N_R= 50) with an absorption of less than 2%, enabling a value of τA in excess of 45% to be obtained. With these coatings, then for an overall finesse of 30 to be achieved, the defects finesse cannot be much less than 37 at λ 2800 Å over the aperture of 2.5. cm. to be employed. These demands are of course very great particularly when it is realised that the etalon has to withstand the

rigourous conditions to be expected in launch and flight. There are three main approaches to the problem of obtaining a permanently adjusted etalon; solid interferometers, automatic servo-control for parallelism and optically contacted air gap interferometers.(

Solid interferometers (Lau 1931) have been reported in the past but it is extremely difficult to work both faces of the material over a reasonably large area for flatness and smoothness and particularly for the parallelism required. Any inhomogeneity in the refractive index of the material would also result in a lower defects finesse. In addition, the reflectivity at the plate-reflecting surface boundary would be less than that for an air gap instrument. Consequently, higher coating reflectivities would have to be employed and this would lead to a decrease in the interferometer transmission. (Chapter 2). For the free spectral range of 1 Å at 2800 Å the thickness of the solid etalon if made from fused silica would be approximately 0.27 m.m. This would be an extremely fragile plate even assuming that the required optical polishing could be achieved for a plate of this thickness.

Barium titante ceramics whose length can be varied in response to an electrical signal have been used to obtain the correcting movements necessary to maintain precise control for parallelism of two etalon flats (Ramsey 1962). A similar approach is being considered for the second experiment where a F.P. spectrometer will be used for scanning profiles of the Mg II doublet. However, the degree of complexity of such a system is necessarily high and requires considerable development. Since the first planned experiment is purely photographic it was decided to use an

approach which kept the design and complexity of the spectrograph as simple as possible, particularly in view of the fact that the first experiment is an exploratory one in which experience gained will be used for more detailed subsequent experiments.

The most logical choice appeared to be an optically contacted air gap interferometer. Such an interferometer with 10 cm spacers has been previously employed in the near infrared but the fringe finesse obtained was not recorded (Jackson and Kuhn 1935). For a 10 cm gap it would not have been possible to measure the instrument profile with the light sources then available. For the present work, the etalon plates of 'Spectrosil A' (Thermal Syndicate Ltd.) of 6 cm diameter and 1 cm thickness are polished to a flatness of better than $\lambda/180$ (in the green) over their full physical apertures. Three spacers also of spectrosil were cut out from selected portions of a large plate of 0.4 mm thickness worked flat and parallel to better than $\lambda/40$ over a 4 cm length. The spacers of 6 mm diameter are optically contacted onto both plates on a pitch circle diameter of 5.4. cm at angular intervals of 120°. The polishing of the plates and spacers and the assembly of the etalon was carried out by Mr. H.W. Yates (Optical Surfaces Ltd.)

Before optically contacting the assembly, the interferometer plate surfaces were coated with silver films over a 3 cm. central aperture. The silver was overcoated with a thin layer of MgF_2 to prevent deterioration of the coating during testing. Optical properties of the coatings were determined by the method of Giacomo (1952) and the mean reflectivity

for the two surfaces was approximately 94%.

Figure 8.4. shows fringes obtained for the λ 5461 line of a Hg^{198} source employing a 2 cm etalon aperture. The fringes were recorded on Kodak Tri-X film with an exposure of 15 secs. To determine the finesse of the etalon from microdensitometer traces it is necessary to obtain the film 'Gamma'. This was achejved by photographing a calibrated density wedge also in λ 5461 and a value of $\gamma = 0.9 \pm 0.1$. was determined for the development time of 11 mins. The corresponding microdensitometer trace for the above fringes is shown in fig.8.5. in which the density scale is linear. The position corresponding to the intensity halfwidth is indicated and a recorded fringe finesse of 30 ± 3 was derived.

The recorded finesse was found to depend on the etalon aperture. If the aperture is increased to 3 cm the fringe finesse falls to 22 whilst for an aperture of 1 cm a finesse of 43 is obtained. Over a period of two months the adjustment was found to be perfectly stable and pressure could be applied and then removed from the plates without affecting the finesse. The decrease in the recorded finesse with increasing aperture is due to a slight wedge effect. It could be observed visually that one of the spacers was not completely contacted over its full area and this may have been due to incomplete cleanliness during the contacting process.

The fact that the variation in finesse with etalon aperture was due to a wedge was verified by placing the etalon in an invar mount with 3 phosphor bronze spring adjustments. It was found that the wedge could be eliminated with a very small differential pressure and a recorded

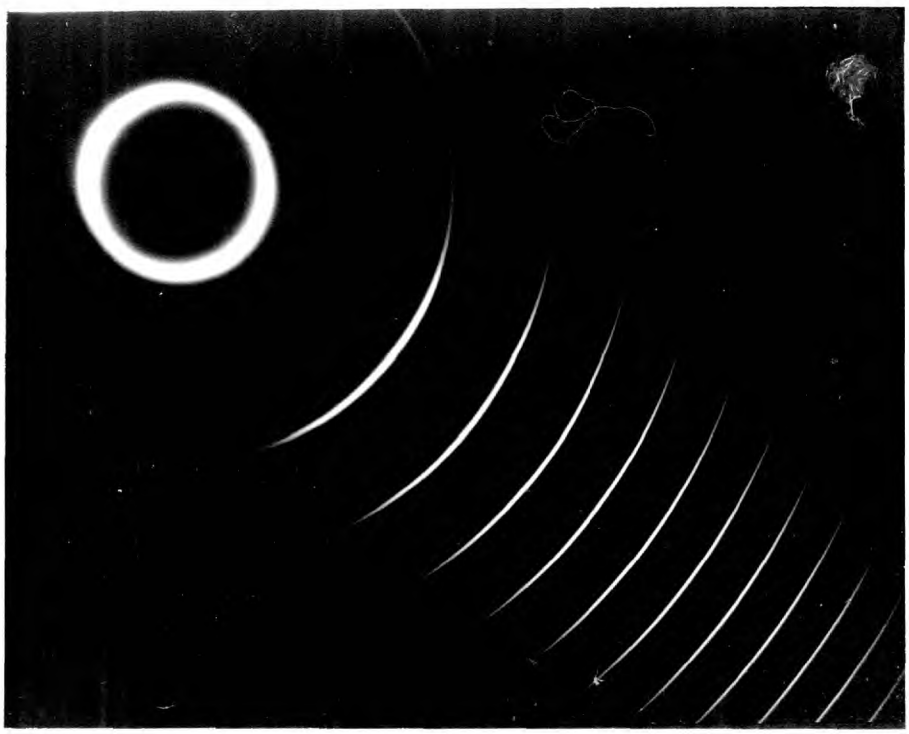

FIGURE 8.4.

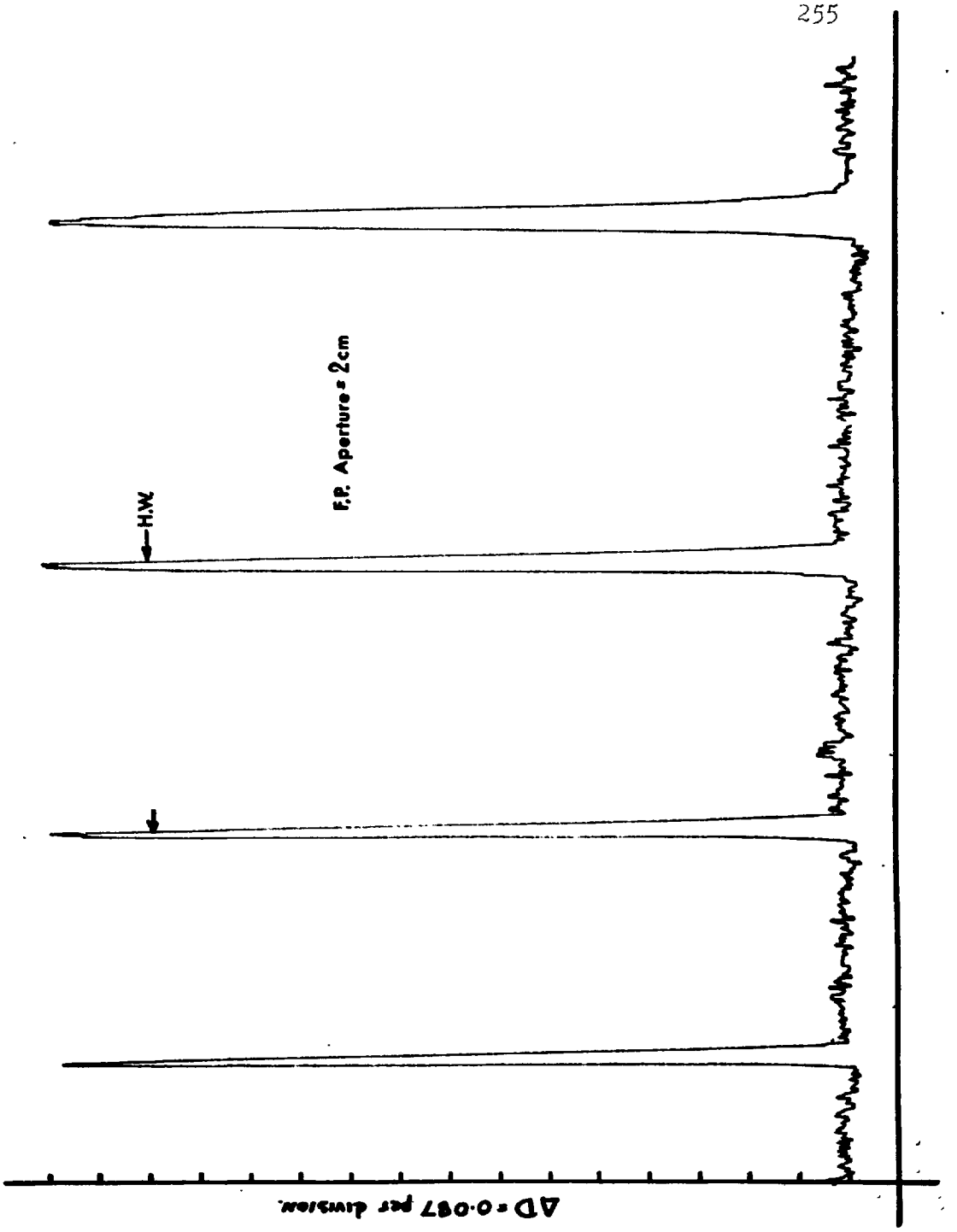

Figure 8.5.

finesse of approximately 50 was then obtained. Fringes obtained for λ5461 of Hg^{198} for a 3 cm aperture with the etalon mounted and free are shown in figure 8,6,a.b. respectively. The adjustment also remains stable for the etalon in the mount with spring adjustments and the etalon finesse was found to be very little dependent on the etalon aperture as expected if the wedge is eliminated. The recorded finesse of 50 is now mainly limited by the coating reflectivity employed. Some initial experiments show that placing the etalon into a vacuum chamber appears to have no effect on the optical contacting of the spacers and the performance.

The above experiments are only first steps in the investigation but they indicate the great promise of the optically contacted etalon for the particular application considered. Further experiments will be carried out using high reflectance coatings at 2800 Å. Additional experiments will also include the effect of rigorous vibration testing of the etalon. However, in view of its permanent adjustment, such an optically contacted etalon has a high potential for F.P. spectroscopy for applications besides those of space research. This is particularly true for experiments in which long time exposures are required for in these cases stability in adjustment is of prime importance.

With care the optical contacts can be broken and new spacers of different thickness contacted onto the same etalon plates. This is an advantage over the solid interferometer in that the optically contacted etalon retains the property of stability in adjustment yet possesses an advantage of choice of plate separation and therefore, free spectral range. In addition, for a large free spectral range the optical contacted interferometer has the important advantage of a considerably greater robustness.

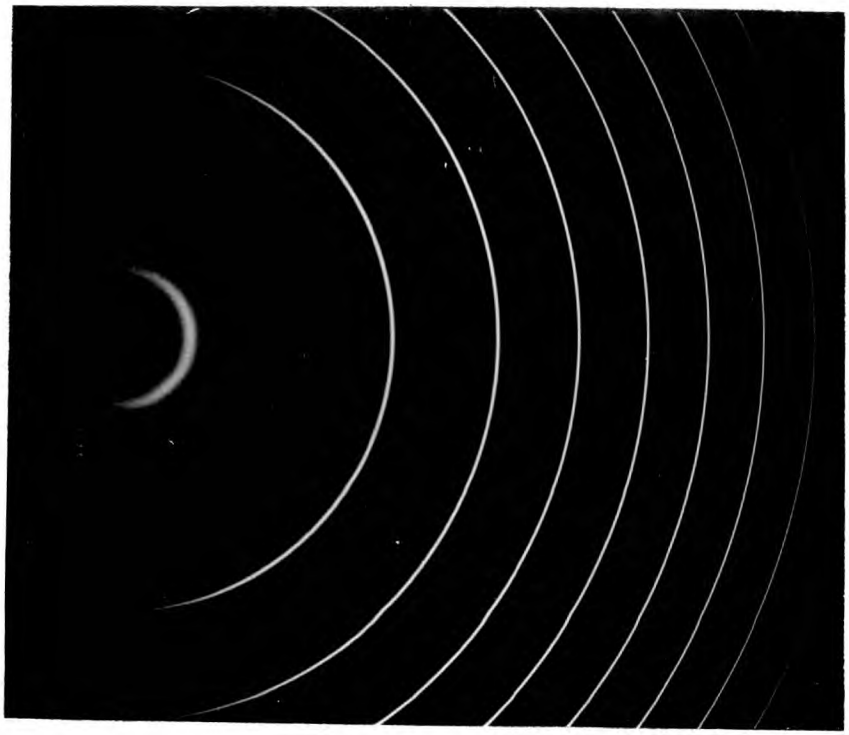

FIG.3.6(a)

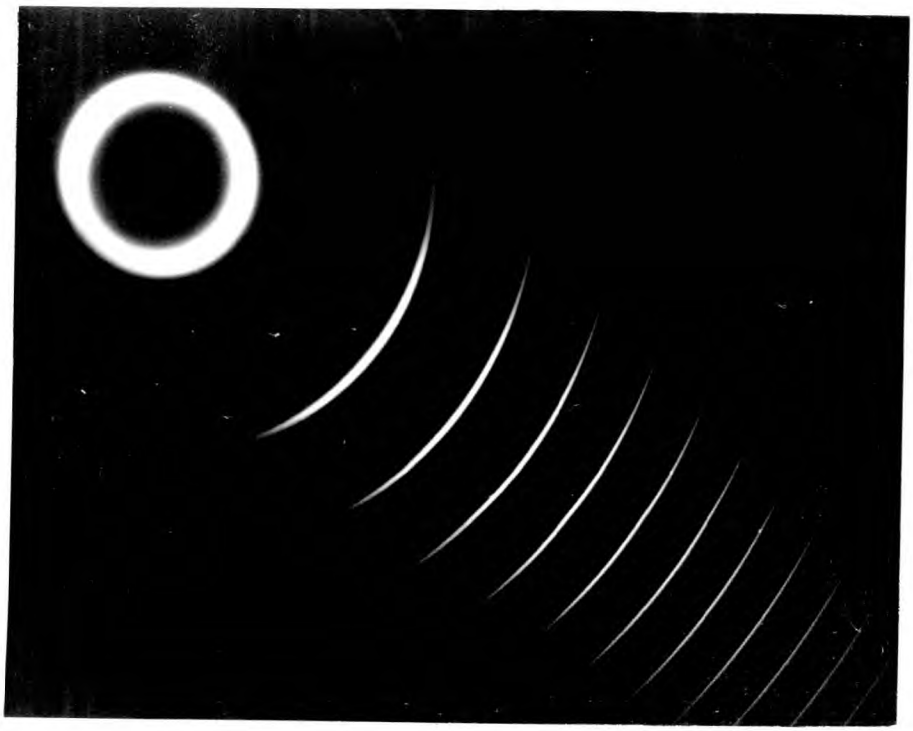

FIG.3.6(b)

CHAPTER 9.

SUMMARY.

It is seen that much of the emphasis in this investigation has been more on the development of techniques for far ultraviolet interference spectroscopy rather than one of the application of such techniques. The feasability of extending the spectral range of the F.P. interferometer into the far and vacuum ultraviolet using the newly developed semi-transparent aluminium - MgF2 coatings has been clearly demonstrated. It would appear that the optical properties of the double layer films do not fall far short of optimum performance. Yet, the author feels this in only a first step and there is little doubt that an improved performance can be obtained over that of the present double layer films. The next likely stage of development is to consider the deposition of several dielectric layers deposited onto a high quality aluminium film. Evaporated fused silica or barium fluoride films might provide a basis for extension of techniques.

The optical performance of the present coatings is suitable for many problems to a wavelength of 1800 Å. Measurement of optical properties should next be carried out on films optimised for wavelengths shorter than 1800 Å. It has already been stated that much hyperfine structure and absolute wavelength determination work has been carried out in the past at longer wavelengths employing coatings of ~~power~~ POORER performance than the double layer films at 1850 Å. Whilst the author's own interest is

more on the employment of the F.P. interferometer for space research applications (as discussed in Chapter 8), there are immediate laboratory applications of some of the techniques developed in this work. For example, these could include the determination of absolute wavelength standards (e.g. GeI lines 1800 to 2200 Å) with subsequent extension to shorter wavelengths by the Combination Principle (Edlen 1963). In addition, high resolution studies of the hyperfine structure and isotope shifts of lines such as the 1849 Å line of HgI (Popescu and Novikov 1964) could be made perhaps in the detailed manner as discussed by Schweitzer (1963) for the very much studied 2537 Å line.

The F.P. type interference filters developed in this investigation have already seen application. For space research applications broad band photometry has been carried out by employing the combination of wavelength selective detectors with different absorbing materials. The spectral profile of such a combination is of course governed by the absorption and sensitivity characteristics of a limited choice of materials. However, the techniques developed in this programme offer a means of constructing a set of band-pass filters for the far ultraviolet in which the spectral transmission characteristics can be controlled (within certain limits) to suit particular experimental requirements.

Again, as in the case of the coatings, one can envisage improvements in filter performance from that given in Chapter 6. If two independently worked flats coated with the aluminium - MgF_2 layers could be separated by a very small vacuum gap and adjusted for the parallelism required, then the bandwidth of such a filter would be approximately half of that

obtained with the present filters for the same value of peak transmission. Of course, this means a sacrifice must be made in the simplicity and convenience of use since nothing much simpler than the present filters can be obtained for isolating a wavelength interval of a few hundred Å with the same high transmission. From previous considerations it will be realised that any improvements which can be made to the optical properties of far ultraviolet coatings can be applied to give an improvement to filter performance. Again this emphasises the need for further development and for extension of measurements of optical properties to shorter wavelengths.

Progress in this direction can be greatly aided by computational techniques but these of course require the ability to ascribe meaningful optical constants to give a representation of the coating layers employed. Such progress is often hindered by the fact that optical properties are so much dependent on the conditions of preparation as illustrated in the case of aluminium films. The author feels that the main application of the present coatings (and of subsequent improved coatings) to filter work might lie in extending into the far ultraviolet tunable, narrow band filters of the type described for visible wavelengths by Ramsey and Tanaka (1965). Such filters used alone or in conjunction with the F.P. interferometer would have a considerable potential for both space and laboratory applications.

On the image tube side, the construction of an intensifier with wavelength selective photocathode is to be encouraged. For application to interference spectroscopy from space vehicles the channelled intensifier

with a spectrally selective cathode might also be a particularly useful device for it has been seen that the main drawback of this type of intensifier, namely its low resolution, need not be too serious for this application (chapter 7.).

In chapter 8, some advantages of the F.P. interferometer over grating instruments for space research applications were considered. It now remains to overcome several technical difficulties to see if these advantages can be fully realised. If this is indeed the case, then techniques can be extended to satellites for solar work and for investigation of weak nebular sources and interstellar lines.

In conclusion, the main objectives of this programme which were set out in Chapter 1 have been fulfilled. It was stated in Chapter 1 that little development of the interferometer had taken place for many years until 1948 when the F.P. spectrometer was first described. Since then, advances in development have been considerable and new applications are increasing. It is to be hoped that this investigation has contributed to a further phase in development by extending its spectral range into the far ultraviolet. The new application of the interferometer to the field of space research should offer the opportunity of much exciting and rewarding research in future years.

Acknowledgements.

The author is indebted to Professor J.D.McGee F.R.S. for the facilities of his laboratory and for the loan of several image intensifiers used during this investigation.

An experimental programme of the type which has been described requires considerable technical backing. The author wishes to thank members of the Applied Physics technical staff for their considerable help during this investigation, in particular to G.E. Busby for his enthusiastic participation in the design and development of the automatic film thickness control unit.

In addition, thanks are also due to S.Majumdar, F. Barlow, C.O.L. Juulman, T. Kohno and to the technical staff of the Physics Department, Royal Holloway College.

Finally, the author wishes to express his gratitude to Dr.D.J.Bradley not only for his interest and supervision of this programme but also for his considerable contribution of ideas during the course of this investigation.

References.

Angel D.W., Hunter W.R. and Tousey R. - (1961) J.Opt.Soc.Am. 51. 913

Apfel J.H. (1966) Paper presented to Opt.Soc.Am. March. 1966.

Aslam M. (1965) Ph.D. thesis Univ.London.

Bass A.M. (1948) J.Opt.Soc. Am. 38 977.

Bates B. and Bradley D.J. 1966(a) Applied Optics 5 971

1966(b) ~~to be~~ submitted to J.Opt.Soc.Am.

Bates B.,Bradley D.J., Kohno T. and Yates H.W. (1961) J.Sci.Instrum. 43 476.

Baum W.A. (1961) Proc.2nd.Symp.on Photoelectric Imaging Devices p.391(Academic Press

Baum, W.A. et.al. (1946) Phys.Rev. 70 781.

Baumeister P.W. (1965) Private Communication.

Baumeister P.W. and Costich V.R.(1965) Applied Optics 4 364.

Bauple R. et.al. (1950) J.Opt.Soc.Am. 40 788.

Bennett J.M. (1964) J.Opt.Soc.Am. 54 612.

Bennett H.E. and Porteus J.O.(1961) J.Opt.Soc.Am. 51 123.

Berning P.H. Hass G, and Madden R.P. (1960) J.Opt.Soc.Am. 50 586.

Bifford I.H. (1966) Applied Optics 5 105

Black W.S. et.al. (1965) Nature 206 654.

Born M. and Wolf E.(1964) Principles of Optics (Pergamon Press

Bradley D.J. (1961) Ph.D. Thesis Univ. of London.

Bradley D.J. (1962)	J.Sci.Instr. 39 41
(1963)	Applied Optics 2 539
(1966)	S.A.D.E.S.I. (in Press)
Bradley D.J., Bates B. and Juulman C.O.L. (1963)	Proc.VI Conf.Phenomenes d'Ionization dans le Gaz 4 791
Bradley D.J. et.al. (1964)	Nature 199 1281
Bradley D.J., Bates B. Juulman C.O.L. and Kohno T. (1966)	Proc.Symp.Orsay 1966. (to be published in J.de Physique).
Bradley D.J., Bates B. Juulman C.O.L. and Majumdar S.	
1964 (a)	Nature 202 579
1964 (b)	Japanese J.Appl.Phys. 4 Suuplement 1. 467.
1964 (c)	Applied Optics 3 1461
Bradley D.J. and Majumdar S. (1966)	to be published J.Photo.Science.
Braga C.L. and Lumb M.D. (1966)	J.Sci.Instr. 43 341
Bril A. and Klasens H.A. (1952)	Philips Res.Repts. 7 401
Burridge J.C., Kuhn, H. and Pery A.(1953)	Proc.Phys. Soc. B. LXVI 963
Butslov M.M. et.al. (1963)	Optics and Spectroscopy 12 229.
Catchpole C.E. (1963)	Ph.D. Thesis Univ. of London
Chabbal R. 1953	J.Rech C.N.R.S. (Paris)24 138
1958	Rev. d'Optique 37 49,336,501,608.
Cooper J. and Greig J.R.(1963)	J.Sci.Instrum. 40 433.
Cranfield L.R., Hass G. and Waylonis J.E. (1966)	Applied Optics 5 45

Crawford M.F.,Gray W.M.	J.Opt.Soc.Am. 39 888.
Schawlow A.L. and Kelly F.M. (1949)	
Davis G.P. (1962)	Adv.Elect.and Elect.Phys. 16 113.
Dunham T. (1956)	Vistas in Astronomy 2 1223
Dunkelman L. (1955)	J.Opt.Soc.Am. 45 134.
Dunkelman L. and Hennes J.P. (1964)	Jap.J.Appl.Phys. 4 Supl. 1 p.511
Dunkelman L., Fowler W.B. and Hennes J.P. (1962)	Applied Optics 1 645.
Dushman S. (1949)	Vacuum Technique p.19. (Wiley.)
Edlen B. (1963)	Repts.Prog.Physics XXVI 181
Eley D.D. and Wilkinson P.R.(1959)	Structure and Properties of Thin Films (Wiley). p.508
Fabre D. (1964)	Rev. d'Optique 43 504.
Fabre D., Romand J. and Vodar B.(1964)	J.de Physique 25 55.
Flecken F. and Noller H.G.(1962)	Vacuum Symp.Trans. p.58 Pergamon Press (Oxford.)
Flinn E.A. (1962)	Ph.D. Thesis Univ. London.
Friedman H. (1962)	Repts.Prog.Physics XXV 163.
Gerrard H.G. and Turpin J.(1965)	J.Opt.Soc.Am. 55 453.
Giacomo P. (1952)	C.R.Acad.Sci.(Paris.) 235 1627
Gonella J.R. and Robrieux B.(1962)	Optica Acta. 9 101
Greig J.R. (1965)	Ph.D. Thesis Univ.London.
Hadley L.N. and Dennison D.M. (1947)	J.Opt.Soc.Am. 37 451
Hall J.F. (1957)	J.Opt.Soc.Am. 47 662
Harrison G.R. (1949)	J.Opt.Soc.Am. 39 522

Hass G. (1949)	J.Opt.Soc.Am. 39 352
Hass G. and Tousey R. (1954)	J.Opt.Soc.Am. 49 593
Hass G. and Waylonis J.E. (1961)	J.Opt.Soc.Am. 51 719
Hass G. Hunter W.R. and Tousey R.	J.Opt.Soc.Am. 47 1070
Heavens O.S. (1955)	Optical Properties of Thin Solid Films - Butterworths (London)
Heavens O.S. and Smith S.D.(1957)	J.Opt.Soc.Am. 47 469.
Holland L. (1956)	Vacuum Deposition of Thin Films Chapman and Hall.
(1960)	Vac.Symp.Trans. p.168. Pergamon Press (Oxford.)
(1964)	The Properties of Glass Surfaces Chapman and Hall.
Holland L. and Bateman S.K. (1962)	Vac.Symp.Trans. p.1201. Pergamon Press (London)
Jackson D.A, (1961)	Proc.Roy.Soc. A.263 289
Jackson D.A. and Kuhn H. (1935)	Proc.Roy.Soc. A.148 335.
Jacquinot P. (1954)	J.Opt.Soc.Am. 44 761
(1960)	Repts.Prog.Phys. 23 267
Jacquinot P. and Dufour C.	J.Rech.C.N.R.S.(Paris) 6 1.
Kasha M. (1948)	J.Opt.Soc.Am. 38 929
Khogali A. (1964)	Ph.D. Thesis Univ.London.
Knapp R.A. (1963)	Applied Optics 2 1334.
Kuhn H. (1951)	Repts.Prog.Phys. XIV 64
Lau E. (1931)	Ann.der Physik 10 71

Learner R.C.M. (1965)	Private Communication
Lebedeva V.V. and Lebedev.I.V.(1965)	Optics and Spectroscopy XVII 58
Lés,F. and Lés Z. (1962)	Acta Physica Polonica XXI 523
Lés.F. Lés Z. and Gabla L. (1963).	Acta Physica Polonica XXIII 211
Levenstein S. (1949)	J.Appl.Phys. 20 306
Lissberger P.H. and Ring J. (1955)	Optica Acta. 2 42
Madden R.P. (1963)	Physics of Thin Films p. 123 Academic Press London.
Madden R.P. and Cranfield L.R.(1961)	J.Opt.Soc.Am. 51 838
Madden R.P. Cranfield L.R. and Hass G. (1963)	J.Opt.Soc.Am. 53 620
Majumdar S. (1966)	Ph.D. Thesis Univ.London.
Malitson I.H., Murphy F.U. and Rodney W.S. (1958)	J.Opt.Soc.Am. 48 72
Malyshev G.M. Razdobarim G. T. and Sokolova L.U. (1963)	Sov.Phys.Doklady 7 701
Mandel L. (1955)	J.Sci.Instrum. 32 405
(1961)	Proc.5th.High Speed Photography Conf.Washington.
McBride W.M. (1963)	J.Opt.Soc.Am. paper F.C.II.
McClung F.J. and Hellwarth R.W.(1963)	Proc.I.E.E.E. 51 46.
McGee J.D. (1953)	Brit.Patent No. 790416
(1961)	Repts.Prog.Phys. XXIV 167
McGee J.D. Beesley J. and Berg A.D. (1966)	J.Sci.Instrum. 43 153

McGee J.D. and Catchpole C.E.(1962) Brit.I.E.E.Conf.Rept.Series 5.p182

McGee J.D., Flinn E.A. and Evans H.D. Adv.Elect.& Elect.Phys. 12 87

McGee J.D. and Wheeler B.E. (1961) J.Photograph.Sci. 9 106

(1962) Adv.Elect.and Elect.Phys. 16 47

Meissner C. (1960) Vac.Symp.Trans. p.196

Pergamon Press (Oxford .)

Minnaert M., Mulders G.F.W. and Houtgast J. (1940) Photographic Atlas of the Solar Spectrum p.5. Schnabel (Amsterdam.)

Mohler N.H. and Loofbourow J.R.(1952) Amer.J.Phys. 20 499, 579.

Morton G.A. (1964) Applied Optics 3 651

Peacock N.J. Cooper J. and Greig J.R. Proc.Phys.Soc. 83 803

(1964)

Perkin-Elmer Inc.(1966) Manufacturers Information

Popescu I.M. and Novikov L.N.(1964) C.R.Acad.Sci.(Paris.) 259. 1321

Purcell J.D. and Tousey R.(1961) Proc.1st.Int.Space.Sci.Symp.1960 p.590 (North Holland Publishing Co.)

Prucell J.D., Boggess III A. and Tousey R.(1958) I.G.Y. Rocket Rep.Ser.No.1.p.198

Prucell J.D. Garrett D.L. and Tousey R.(1963) Proc.3rd.Int.Space Sci.Symp.1962 p.781 (North Holland Publishing Co.

Putner T. (1959) Brit.J.Appl.Phys. 10 332

Ramsey J.V.(1962) Applied Optics 1 411

Ramsey J.V. and Mugridge E.G.V.(1962) J.Sci.Instrum. 39 636

Ramsey J.V. and Tanaka K. (1965) J.Sci.Instrum. 42 334

Rees J.D. and Parker Givens M.(1966) J.Opt.Soc.Am. 56 93.

Ring J. (1956)	Astronomical Optics and Related Subjects p.381 (North Holland Pub.Co.
Ring J. and Wilcock W.L.(1953)	Nature 171 648
Sabine G.B. (1939)	Phys.Rev. 55 1064
Schroeder D.J. (1962)	J.Opt.Soc.Am. 52 1380.
Schulz L.G. (1949)	J.Chem.Phys. 17 1153.
Schulz L.G. and Tangherlini F.R.(1954)	J.Opt.Soc.Am. 44 357
Schweitzer W.G. (1963)	J.Opt.Soc.Am. 53 1055.
Sennett R.S. and Scott G.D. (1950)	J.Opt.Soc.Am. 40 203
Seya M. and Masuda.F. (1963)	Science of Light 12 9.
Shaw C.H. and Foreman W.T.(1959)	J.Opt.Soc.Am. 49 724
Shenton B. (1966)	Private Communication.
Stacey D.S. et.al.(1954)	Electronics 27 149.
Theodorou D. (1963)	Ph.D. Thesis Univ.London.
Tolansky S. (1947)	High Resolution Spectroscopy Metheun (London.)
(1948)	Multiple-Beam Interferometry of Surfaces & Films (Clarendon Press Oxford.)
(1960)	Surface Microtopography, Longmans.
Tolansky S. and Bradley D.J. (1959)	N.P.L. Symp.on Interferometry p.375 (H.M.S.O. London.)
Turbadar T. (1959)	Vacuum 9 139.
Tousey R. (1961)	Science 134 441
Vasicek A. (1960)	Optics of Thin Films. (North Holland Publishing Co.)

Weaver C. (1962)	Adv.in Phys. XI 83
Wheeler B.E. (1962)	Ph.D. Thesis Univ. London.
Wilcock W.L. and Geake J.E. (1956)	Estratto dai Supplementi alle Memorie della Societa Astronomica Italiana.
Wilcook W.L., Emberson D.L. and Weekley B. (1960) (a)	Nature 185 370.
(1960) (b)	Trans. I.R.E. NS-7 p.126
Wiley W.C. and Hendee C.F. (1962)	Trans I.R.E. NS -9 p.103
Wolf C.M. and Pertel R. (1964)	J.Opt.Soc.Am. 54 1168.
Walkenhurst W. (1941)	Z. Tech.Phys. 22 14.
Yates H.W. (1966)	Private Communication.

(*Reprinted from Nature, Vol. 202, No. 4932, pp. 579–580, May 9, 1964*)

Multiple-beam Interferometry in the Vacuum Ultra-violet

For orbiting astronomical telescopes and photometers, interference filters and the Fabry–Perot interferometer have considerable advantages in luminosity, speed of recording and compactness over prism and grating instruments[1–3]. Thus it is important to extend the range of multiple-beam interferometry into the vacuum ultra-violet.

The limitation so far has been in obtaining suitable reflecting coatings. Below 2400 Å there is no high-index material for dielectric multilayer films[4]. However, reported measurements[5] on the optical properties of semi-transparent aluminium films down to 2200 Å, when analysed, showed that aluminium improves in performance for multiple-beam interferometry with decreasing wave-length, provided a reflecting finesse of 20 is sufficient. It must be remembered that the defects finesse also decreases with decreasing wave-length and, even with the best-quality flats, will not greatly exceed 18 at 1800 Å, so that a higher reflecting finesse is neither required nor desirable[6]. For interference filters, the band-width decreases with decreasing wave-length and, for a given band-width, the finesse required is proportionally smaller, provided the resulting decrease in contrast can be tolerated.

This analysis and recent improvements[7] in the technique of depositing opaque aluminium films, overcoated with thin layers of magnesium fluoride to prevent oxidation and to enhance reflectivity in the vacuum ultra-violet, led us to believe that a similar improvement could be obtained in the performance of semi-transparent coatings for this spectral region. Our first results[8] indicated that thinner aluminium films, similarly overcoated, were suitable for multiple-beam interferometry down to 1900 Å. We now wish to report our results on filters with peak transmittances at ~ 1800 Å and Fabry–Perot interferograms of λ1849 of HgI.

Fig. 1 shows the transmission characteristics of two Fabry–Perot type first-order interference filters deposited on fused quartz substrates, each consisting of two aluminium reflecting layers separated by a half-wave layer of magnesium fluoride. The outer aluminium layer is protected from oxidation by a magnesium fluoride coating, approximately 400 Å thick. Curve *A* represents a filter peaking at 1825 Å. Below 1800 Å the finesse decreases because of the falling reflectivity of the aluminium layers, but at approximately 1660 Å the rapidly increased absorption of the 'Spectrosil' substrate leads to a sharp cut-off.

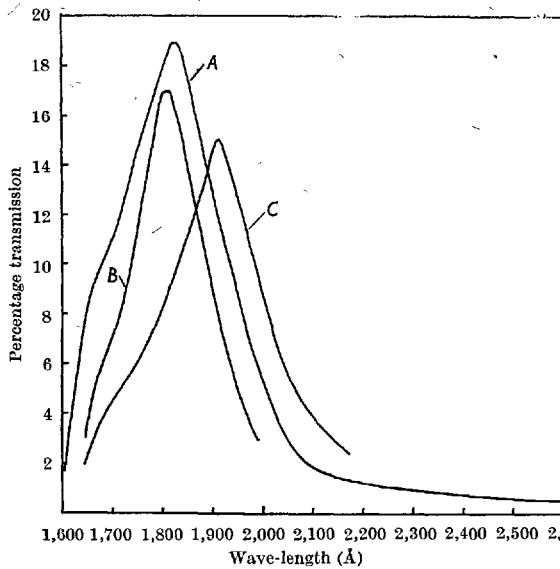

Fig. 1. Transmission curves of first-order Fabry–Perot type filters

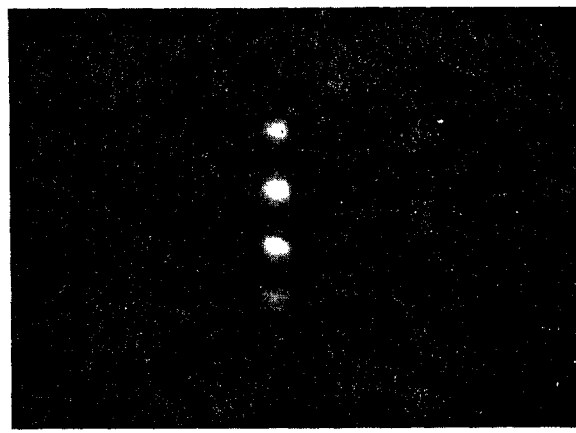

Fig. 2. Fabry–Perot interferogram of λ1849 HgI. Interferometer spacing, 0·15 mm

The transmission profile above 1800 Å corresponds to a half-width of 225 Å and a finesse (N) of 8. The recorded peak transmission of 0·19 when corrected for absorption in the substrate becomes 0·21, giving for the aluminium films a mean reflectivity $R = 0{\cdot}68$, transmissivity $T = 0{\cdot}15$, and an absorption $A = 0{\cdot}17$.

Table 1. Optical Properties of Aluminium Films derived from Fig. 1

Curve	N	R	T	A	$(R + T)$
A	8	0·68	0·15	0·17	0·83
B	8·5	0·69	0·135	0·175	0·825
C	8·5	0·70	0·12	0·18	0·82

Curve B is the same filter tilted through 8° to displace the peak wave-length to 1805 Å, and curve C represents another filter with a peak transmission of 0·15 (corrected 0·165) at 1910 Å. Because of an error in monitoring the second aluminium layer the performance of this filter is not optimum. The optical properties of the aluminium films derived from the longer wave-length half-profiles of these curves are summarized in Table 1.

The transmission curves below 2000 Å were measured on a vacuum Seya monochromator. Curves A and B were obtained when the filter was six weeks old and had been frequently exposed to ultra-violet light. Curve C was determined on the day following the manufacture of this filter. The longer wave-length tail of curve A was measured on a Perkin–Elmer 350 spectrophotometer. For this filter the transmission falls to 0·4 per cent at 2600 Å and to 0·3 per cent at 2800 Å. Greater contrast and a narrower band-width could be obtained with a second-order filter provided a selective detector[9] is used to suppress the longer wave-length peak. Alternatively, two filters could be used in series or deposited as a double filter[10] on the same substrate.

So far as we know these are the only results reported for interference filters < 2000 Å apart from Schroeder[10], who reports a double filter with a half-width of 200 Å but a peak transmission of only 0·7 per cent at 1900 Å.

Finally, 'Spectrosil' Fabry–Perot plates were coated. Fig. 2 shows fringes of λ1849 of HgI obtained with a 'Spectroline' 11*SC*–1 lamp. The line was isolated by a 'Spectrosil' prism spectrograph purged with nitrogen. A single-stage magnetically focused image converter, with a 'Spectrosil' window and cathode substrate, constructed for this work greatly facilitated detection and recording of the fringes (the imperfection in one of the fringes is caused by a defect in the image converter phosphor). The fringe finesse of about 5 is mainly limited by the quality and adjustment of the interferometer plates, which are, of course, very critical at these short wave-lengths. To confirm this, fringes of λ2537 were recorded and a finesse of 7 directly proportional to the increase in wave-length was obtained, showing that the defects finesse dominates. These are the first reported Fabry–Perot interferograms below 2000 Å. A high-quality interferometer is being constructed and we hope to extend the spectral range to 1600 Å or less so as to permit the utilization of the instrument, either in its oscillating form[11] or in its spectrographic method of use[8], for plasma diagnostic spectroscopy in this spectral region, in addition to space research applications.

We thank Prof. J. D. McGee for his advice, Prof. W. R. S. Garton for lending us equipment, and Mr. D. S. Widner for making the filter measurements on the Seya monochromator. Assistance from the British National Committee for Space Research for the purchase of equipment and the support of one of us (C. O. L. J.) is gratefully acknowledged. One of us (S. M.) is supported by a Colombo Plan fellowship.

D. J. Bradley
B. Bates
C. O. L. Juulman
S. Majumdar

Department of Physics,
Imperial College of Science and Technology,
London, S.W.7.

[1] Jacquinot, P., *J. Opt. Soc. Amer.*, **44**, 761 (1954).
[2] Dunham, T., *Vistas in Astronomy*, **2**, 1223 (Pergamon Press, London, 1956).
[3] Bradley, D. J., *Proc. Roy. Soc.*, A, 262, 529 (1961).
[4] Honica, G., and Krebs, K., *Z. Physik*, **156**, 117 (1959).
[5] Hass, G., and Wayonlis, J. E., *J. Opt. Soc. Amer.*, **51**, 719 (1961).
[6] Chabbal, R., *J. Rech. C.N.R.S.*, **24**, 138 (1953).
[7] Hunter, W. R., *Optica Acta*, **9**, 255 (1962).
[8] Bradley, D. J., Bates, B., and Juulman, C. O. L., *Proc. Sixth Conf. Phénomènes d'Ionization dans le Gaz*, **4**, 79 (Paris, 1963).
[9] Dunkelman, L., Fowler, W. B., and Hennes, J., *App. Optics.*, **1**, 695 (1962).
[10] Schroeder, D. J., *J. Opt. Soc. Amer.*, **52**, 1380 (1962).
[11] Bradley, D. J., *Proc. Conf. Optical Instruments and Techniques*, 31 (Chapman and Hall, London, 1961).

Printed in Great Britain by Fisher, Knight & Co., Ltd., St. Albans.

APPLICATION OF PHOTOELECTRIC INTERFERENCE SPECTROSCOPY AND IMAGE INTENSIFIERS TO PLASMA DIAGNOSIS

by

D.J. BRADLEY*, B. BATES and C.O.L. JUULMAN

Instrument Technology Section
Physics Department, Imperial College, London S.W.7.

Abstract

A method of employing a Fabry-Perot interferometer - image intensifier combination to obtain simultaneously time, spatial and spectral resolution is described. Comparison is made with an oscillating Fabry-Perot interferometer. Three types of image tube were tested and time resolution of 2×10^{-6} sec obtained. Causes of signal-induced background are discussed as is also the combination of an oscillating interferometer with the system. First results are given of aluminium films making possible the extension of the interferometer spectral range into the vacuum U.V.

Introduction.

The advantages and optical principles of an oscillating Fabry-Perot spectrometer for time-resolved spectroscopy have been previously discussed[1,2] and instruments employing electro-mechanical[3] and piezo-electric drives[4] have since been fully developed. In addition to the superior luminosity of the interferometer the high quantum efficiency of a photo-multiplier is utilized and a linear intensity display is immediately obtained. However, this method of use of the interferometer suffers from the serious disadvantage that time and wavenumber dispersion are superposed. It is thus necessary to scan at a speed sufficiently greater than the rate of change of the phenomenon studied so that photons are wasted and continuous monitoring is not possible. Moreover a point source is utilized and simultaneous spatial and time resolutions are not then attainable. Other minor disadvantages are the limited number of scanned fringes which can be recorded on the oscilloscope screen if accuracy is to be maintained and, with piezo-electric drives, the change in finesse from fringe to fringe. Also since a photomultiplier is employed variations in electron path length and time-of-flight lead to a time resolution limit of 10^{-6} to 10^{-10} secs.

The development of image intensifiers[5] combining the high quantum efficiencies of photocathodes with the information content of photographic plates, led us to investigate the possibility of employing the Fabry-Perot interferometer in its classical photographic method of use for time-resolution spectroscopy. The principle of the method is illustrated in figure 1. The image of the slit crossed with interference fringes is swept by a rotating mirror across the photocathode of the image-tube. Alternatively, electron-optical sweeping may be employed[6] but at a cost of linear resolution in the image-tube. The advantages of the method are immediately obvious.

Firstly a continuous time record is obtained since wave-number and time dispersions are now crossed. Secondly, since there is a one-to-one correspondence between source and ring pattern, simultaneous spatial resolution is achieved, also crossed with the time dispersion. Finally there is a gain in luminosity depending upon the order of the fringe employed.

The Interferometer.

As usual it is necessary to match the linear resolution g of the image tube to that of the projected fringe halfwidth. This requires, for the pth ring from the centre, a focal length of $f = 2gN\sqrt{ps\nu}$, N is the finesse, ν the wavenumber and s the interferometer separation. Maximum use is made of the image-tube photocathode area if the interferometer is tilted and only half of the ring pattern employed. For a cathode of linear dimension l, the maximum number of rings is then $(p_2 - p_1) = l/2gN$, independent of p_1, p_2 if the halfwidth of the p_2^{th} ring from the centre is matched to g. Angular dispersion decreases from the centre so it is best to start with the first ring out. Then $p_1 \leq 1$. Also for a given image-tube the maximum number of rings depends only on the finesse.

The angular width α of the slit is determined by the usual relation $\alpha = 2\sqrt{Ns\nu}$ giving a linear width $a = 4g\sqrt{Np}$. Spectral resolving power of the swept image is little affected by ring curvature for a slit of this width. A typical value of g is 100 - 200 μ so that for a 2 cm photocathode 100 - 200 time resolution elements are obtained on each of the 5 or 10 fringes.

The gain in luminosity over the oscillating Fabry-Perot spectrometer arises from the fact that the fringes are continuously and simultaneously recorded not just $(1/N)$ of an order at a time. If m fringes are utilized the total gain is mN. However there is a loss in luminosity since only a fraction of a fringe $(\simeq 1/\pi\sqrt{Np})$ of a complete ring is recorded for a slit of width a. So for each fringe the gain G in luminosity is $\simeq \frac{1}{\pi}\sqrt{N/p}$. This gain decreases with increasing p and has its maximum value at $p = \frac{1}{2N}$ (the central fringe). For $p = 1$, $N = 10$ the gain is about unity.

It is not very useful to consider the total gain in luminosity[6] for while the density of each fringe remains constant, because of the parabolic dispersion of the interferometer the elementary resolution area decreases from the central fringe outwards so the information rate decreases. This also follows from the decrease in luminosity for increasing p. Thus spatial resolution has to be paid for to a small extent by decreasing the rate of scan. Putting

$p = 5$, $N = 10$ gives $G \cong 0.5$. The information in the central rings is of course correspondingly greater.

The Image Detector.

The above comparison of the two methods of use of the interferometer is based on the assumption that the signal-to-noise ratio of a photomultiplier and an image-tube with photographic recording of the output can be made equal. Unfortunately this is not always true of all image-tubes presently available. Though tube background is negligible for rapid time-resolved spectroscopy, with some tubes signal induced background can be serious.

The system was first tested with a five-stage magnetically focused transmission secondary-emission image intensifier (20th Century Electronics Type IPM 29/25) of the type developed at Imperial College[5]. This tube has a linear resolution of 30 lp/mm, a 20 mm photocathode of 20 μ A/lumen sensitivity and a blue light gain of 10^5 at 33 kV with a tube background of 10^3 scintillations sec^{-1} cm^{-2}. An interferometer separation of 0.4 mm and coatings of 65% reflectivity gave a spectral resolving power of 32,000 for λ 5461 HgI. Fig. 2 shows the swept fringes of λ 5461 of a high preseure mercury lamp with a tube voltage of 26 kV. The slit width of 125 μ was magnified to 250 μ on the tube photocathode giving 80 time resolution elements per fringe which, with a mirror speed of 100 c/s, corresponds to a 2×10^{-6} sec time resolution limit. The effect of signal-induced background is immediately apparent as is also the wide spread in the multiplication factor for individual photoelectrons, both effects leading to a decrease in the effective signal/noise ratio in the recorded image.

The signal-induced background is mainly due to unfocused penetrating primary electrons combined with focused photoelectrons from light reflected back from the first dynode. The photocathode transmits some of the incident light and this is of course common to most types of image intensifier. Thicker photocathodes should help to reduce the effect which would be expected to be wavelength dependent also. The magnitude of the penetrating primaries effect is dependent on such factors as the thickness and structure of the dynodes. It is to be hoped that both these effects can be greatly reduced but meanwhile signal-induced background limits the use of transmitted secondary-emission image intensifiers for swept time-resolved spectroscopy. This type of background is clearly seen from figure 3. A 125 μ slit crossed with interference fringes was focused on the tube photocathode, of which all but a narrow slit was covered over so that any possible scattered light effect was eliminated. The output was recorded in 10^{-3} secs with a F 1 camera system. On the left is a direct photograph of the fringes on a 300 μ slit.

A single stage magnetically focused tube was employed to test the relative importance of signal-induced background arising from back reflected light. The aluminium backed phosphor screen of this tube is 20 cm from the photocathode compared with 7 cm between photocathode and first dynode of the transmitted secondary-emission tube. The gain of such a tube with F 1 optical coupling to a photographic recorder is about 5 or with contact print recording about 50.[5] Figure 4 shows a swept scan of λ 5461 of the high pressure mercury lamp. Spectral resolving power is now 3.2×10^5; the time resolution limit is 6×10^{-4} seconds with 60 time elements on each fringe. Variations in intensity and halfwidth arise from source instability. A microphotometer trace through the two central fringes is shown in figure 5. The greatly improved signal-to-noise ratio is immediately evident and can be accounted for by the absence of penetrating primary electrons and the smaller solid angle subtended at the photocathode by the phosphor output screen.

Finally a three-stage magnetically focussed cascaded phosphor-photocathode image intensifier of the type developed at Imperial College by McGee and Catchpole was employed as detector. This tube originally had a blue light gain of 80,000 at 45KV but the gain has since dropped somewhat. Optical coupling to the phosphor output was again a F1 system. Figure 6 shows a swept scan of λ5461. A slit width of 0.5 mm on the phosphor screen corresponds to a time resolution limit of 10 μ sec with 50 resolution elements per fringe. A faster scan giving 3 μ sec resolution was also obtained but the density is not so high. Figure 7 shows a microphotometer trace of Figure 6. Spectral resolving power is again 3.2×10^4. The signal-to-noise ratio of the cascaded phosphor-photocathode tube(run at 33 KV) is much superior to that of the T.S.E. tube.

Combination of Oscillating Fabry-Perot and Swept Slit Image.

Figure 8 shows the expected result if an oscillating Fabry-Perot, instead of a fixed gap interferometer, is employed in the above arrangement. Such a system is ideally suited for a source of cylindrical symmetry. A continuous record of a line profile is obtained as a function of radial distance. Along the axis of the recorded pattern the usual oscillating interferometer record is obtained.

Conclusion

The combination of a Fabry-Perot interferometer and an image intensifier provides a powerful diagnostic tool for plasma physics, providing as it does simultaneous spectral spatial and time resolution. Image intensifiers are of course still being developed and perfected and the above results will undoubtedly be greatly improved upon. For very rapid time spectroscopy electron-optical sweeping permits shorter time resolution and it is hoped to test such a system.

Recent developments in coating techniques (7) make possible extension of the spectral range of the interferometer into the extreme ultra-violet region. An automatic evaporation plant has been built for this purpose. Aluminium films are evaporated in about 3 seconds and immediately, without breaking the vacuum, overcoated with magnesium fluoride to both prevent oxidation of the metal and enhance reflectivity. The optical properties of interferometer type coatings have not been previously measured below λ2200 (8). Early results from our new plant indicate that a reflecting power of 93 % with about 3% transmission is obtainable at λ1900 with magnesium fluoride coated aluminium. Below λ2200 the absorptio

Of semi-transparent aluminium alOne increases rapidly from 0.1 to 0.24 at λ1900.

Finally we would like to point out that when only an isolated line without any neighbouring satellites is being examined, as is frequently the case in plasma diagnosis, high reflecting powers, as normally employed for hyperfine structurs work, of > 85 %, are not always necessary. Luminosity can often be greatly decreased by reducing the reflectivity of the interferometer coating (tO as low as 75%) and at the same time maintaining the spectral resolving power by increasing plate separation.

Acknowledgement.

We wish to thank Professor J.D.McGee and Mr. C. Catchpole for useful discussions and for the loan of one of their cascaded image intensifiers.

A preliminary report on some of this work was given at the annual meeting of the Spectroscopy Group of the Institute of Physics and the Physical Society in London 1962.

References.

1. Tolansky, S. and Bradley, D.J., Symposium on Interferometry, London, H.M.S.O. 375 (1959).
2. Bradley, D.J., Proc.Roy.Soc.A 262, 529 (1961).
3. Bradley, D.J., Proceedings of Conference on Optical Instruments and Techniques, p.31. London, Chapman & Hall (1961).
4. Cooper, J., Greig, J.R. and Peacock, N.J. This Conference (1963).
5. McGee, J.D., Reports on Progress in Physics 24, 167 (1961).
6. Malyshev, G.M., Razdobarim, G.T. and Sokolova, L.V., Soviet Physics - Doklady 7, 701 (1963).
7. Hunter, W.R., Optica Acta 9, 255 (1962).
8. Hass, G. and Waylonis, J.E., J.Opt.Soc.Am. 51, 719 (1961).

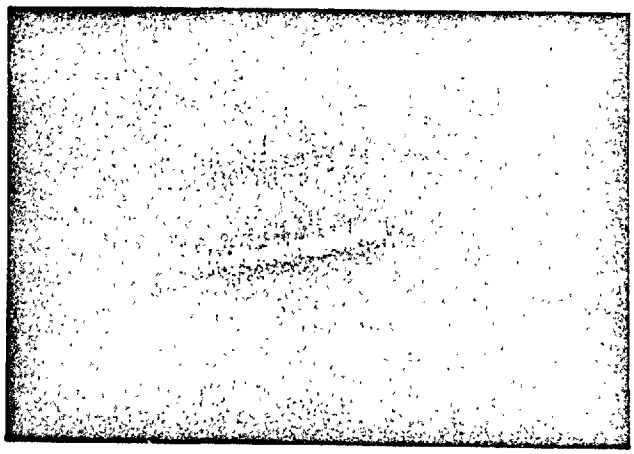

Figure 7.7 λ5461 high pressure mercury lamp. T.S.E. image intensifier. Time resolution 2×10^{-8} secs. Spectral resolution 3.2×10^{4}.

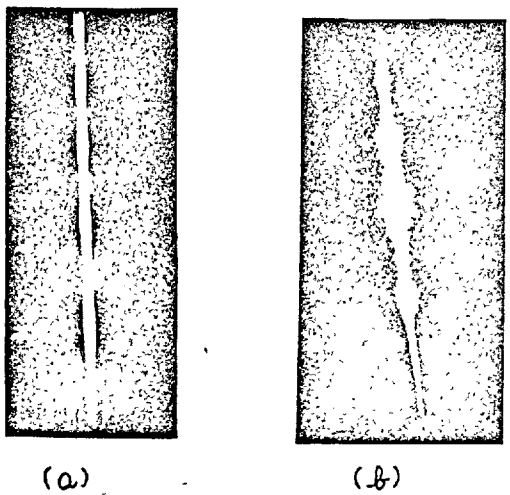

Figure 7.8 Interference fringes on slit (a) Direct photography, (b) T.S.E. image intensifier.

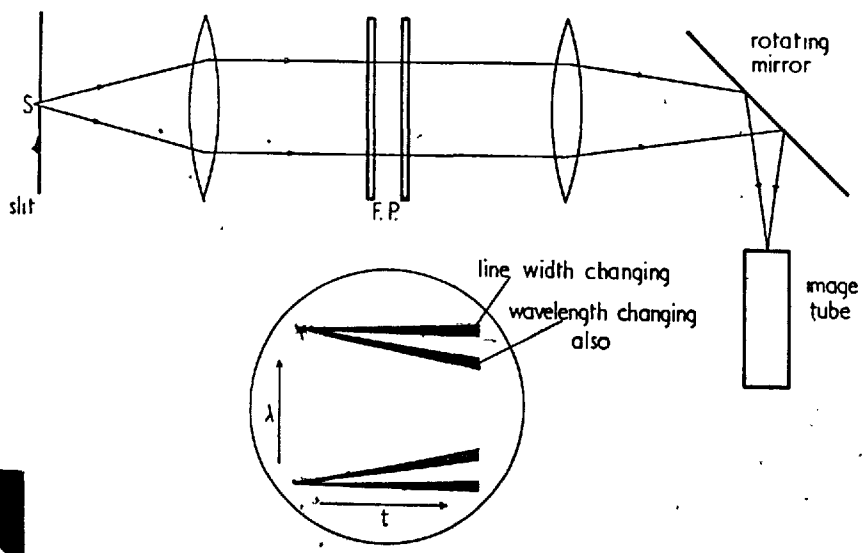

Figure 1: Principle of the Method.

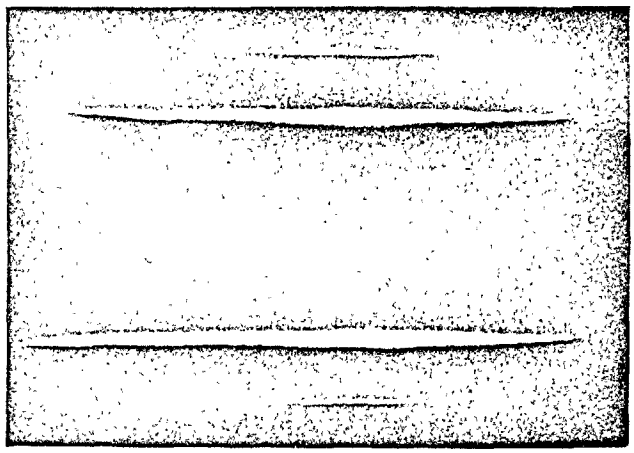

Figure 4: λ 5461 high pressure mercury lamp. Single stage image intensifier. Time resolution 6×10^{-4} seconds. Spectral resolution 3.2×10^{5}.

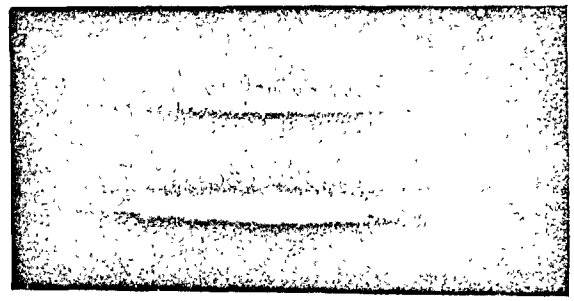

Figure 7.9 λ 5461 Hg. Cascaded image intensifier time resolution 10^{-5} secs. Spectral resolution 3.2×10^{4}.

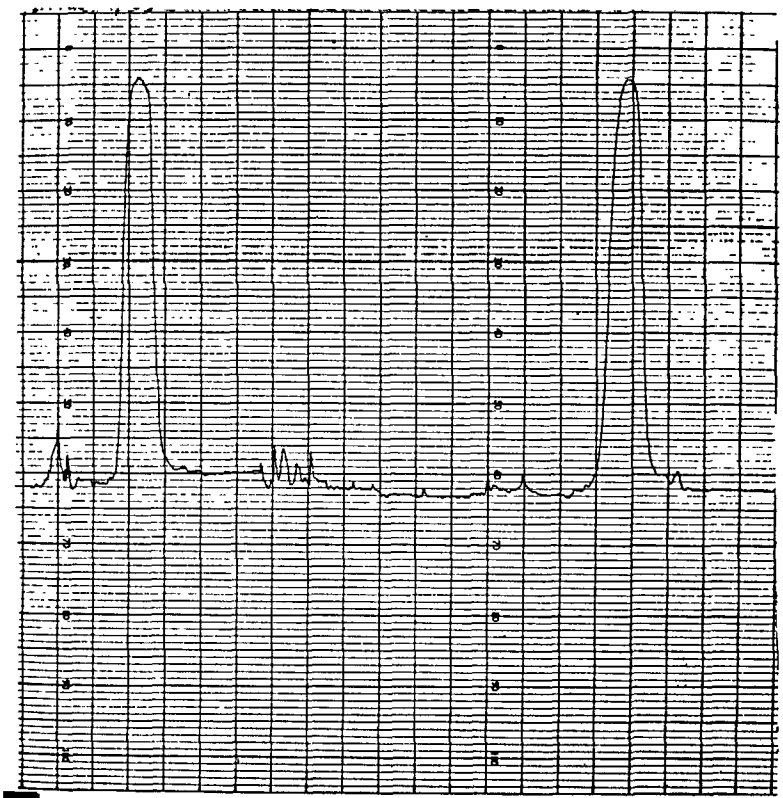

Figure 5: Microphotometer trace of figure 4.

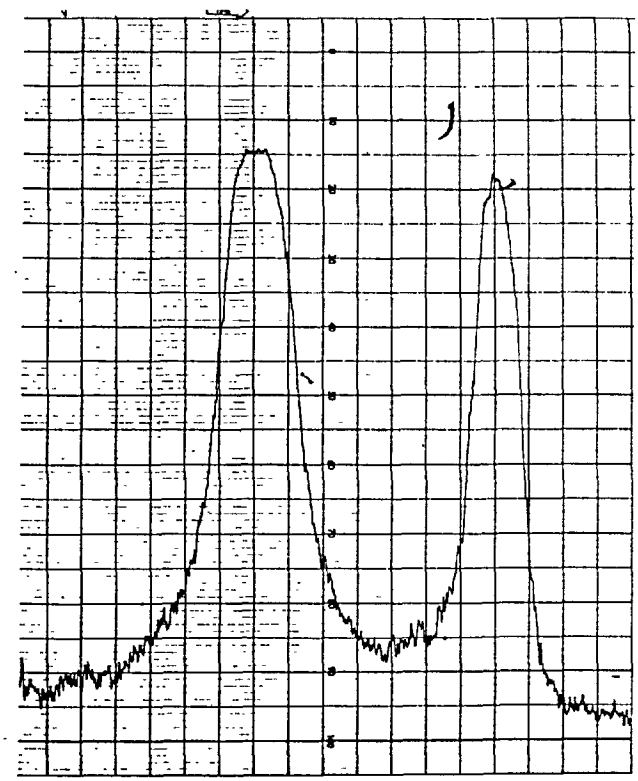

Figure 7: Microphotometer trace of figure 7.

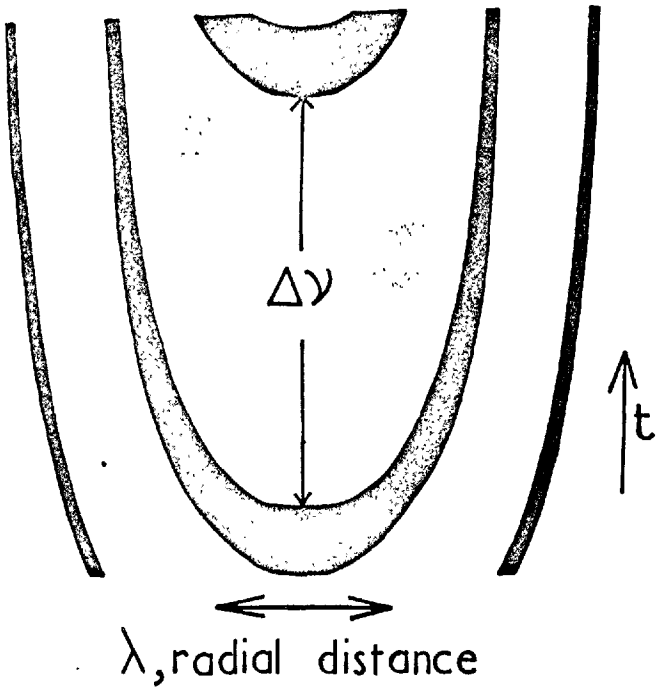

Figure 8: Combination of oscillating Fabry-Perot and and swept slit image.

DISCUSSION

Question by J. KATZENSTEIN (ITALY) :

Was the TSE image converter gated and if not how do you know that the noise was signal induced rather than due to dark emission.

Answer by D. J. BRADLEY (U.K.) :

The image intensifier was not pulsed but without a signal on the cathode no background was discernible in the exposure time. The exposure time had to be increased greatly to bring up the dark emission.

JAPANESE JOURNAL OF APPLIED PHYSICS VOL. 4, SUPPLEMENT I, 1965
PROCEEDINGS OF THE CONFERENCE ON PHOTOGRAPHIC AND SPECTROSCOPIC OPTICS, 1964

The Fabry-Perot Interferometer in the Middle and Vacuum Ultraviolet

D. J. BRADLEY, B. BATES, C. O. L. JUULMAN, and S. MAJUMDAR
Department of Physics, Imperial College, London S. W. 7, England

The factors affecting the performance of Fabry-Perot interferometers in the middle and vacuum ultraviolet are considered. Improvement of performance in the middle ultraviolet to 2000 Å and extension of the useful spectral domain of the instrument into the vacuum ultraviolet are reported.

The preparation and optical properties for ultraviolet multiple beam interferometry of double layer aluminium-magnesium fluoride semi-transparent reflecting coatings are discussed. Fabry-Perot type Al-MgF_2 interference filters for these spectral regions are also described and an interferogram of λ 1849 of HgI obtained with an ultraviolet sensitive image converter is illustrated. Applications of these techniques to space research and to laser and plasma spectroscopy are mentioned.

Introduction

The Fabry-Perot interferometer is being increasingly employed for diagnostic spectroscopy of plasma discharges and laser sources both in its oscillating form[1)-3)] and in the classical etalon method of operation with image tube and photographic detection.[4)-7)] For orbiting astronomical telescopes and photometers the considerable advantages of the interferometer[8)] in luminosity, speed of recording and compactness over prism and grating instruments are also of importance.[9),10)] For all these applications it is important to extend the range of multiple beam interferometry, including interference filters, as far into the vacuum ultraviolet as possible. This will be particularly needed for spectroscopic examination of laser light higher harmonics (the ruby laser light fourth harmonics occurs at about λ 1735), where the high resolving power of the interferometer is essential, and for space research applications. The two factors affecting the extension of the spectral range are the transmission and optical quality of the interferometer flats and the availability of suitable reflecting coatings.

The Optical Flats

It is desirable for maximum luminosity that the defects finesse N_D of the flats should not exceed the reflecting finesse N_R of the coatings.[11)] Fuzed quartz seems to be the most suitable material for attaining the high optical surface finish required at short wavelengths both for a high microdefects finesse (which for a given surface decreases with decreasing wavelength) and low scattering. This material, if completely pure, should be transparent down to about 1490 Å but in practice, for the best quality commercially available, a transmittance of $> 50\%$ is obtained down to 1670 Å for a 5 mm path required for a Fabry-Perot flat. If polished with care a surface finish of r.m.s. roughness of approximately 3 Å can be achieved.[12)] Etalon plates can be easily worked to match better than $\lambda/150$ in the green over 6 cm diameter. Cultured quartz can be obtained with a transmittance of 50 to 60% at 1600 Å for a 10 mm path but this material is more difficult to optically polish.

For fuzed quartz the surface roughness can be neglected in calculating the final defects finesse N_D. If the flats are adjusted parallel to $\lambda/150$ also, then N_D is about 18 at 1800 Å. For a smaller diameter aperture a correspondingly higher defects finesse should be obtained. If spherical mirrors are employed then the aperture required is greatly reduced.[13)]

Thus a defects finesse in the range 16–24 is attainable with flats transmitting a useful fraction of the light in the spectral region 1600–2400 Å.

The Reflecting Coatings

The limitation to date in extending the spectral range of the interferometer has been in obtaining suitable reflecting coatings. No high index material, transmitting below 2400 Å for multilayer dielectric coatings, has been

discovered so far.[14] However, reported measurements[15] on the optical properties of semi-transparent aluminium films down to 2200 Å, when analysed by us, showed that aluminium improves in performance for multiple-beam interferometry with decreasing wavelength, provided a reflecting finesse of 30 is adequate. This is illustrated in figure 1,

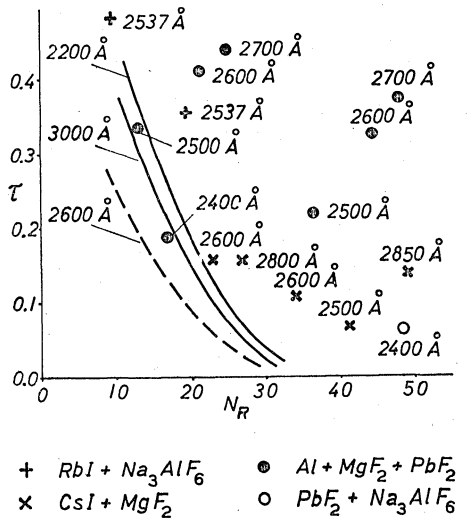

Fig. 1. Al, Al–dielectric multilayers and dielectric multi-layers in the ultraviolet spectral region. Al 2200 Å and 3000 Å;[15] Al 2600 Å;[16] Al–MgF_2–PbF_2 multilayers;[26] CsI–MgF_2 multilayers;[27] RbI–Na_3AlF_6 multilayers;[28] PbF_2–Na_3AlF_6 multilayers.[14]

which includes plots of the interferometer transmission τ as a function of the reflecting finesse N_R for aluminium films based upon the results of Hass and Waylonis.[15] It can be seen that for a given value of N_R the peak fringe transmission τ is greater at 2200 Å than for 3000 Å for all values of N_R. The points corresponding to various dielectric and dielectric-aluminium multilayer combinations for wavelengths > 2400 Å, also given in the figure, indicate their superiority over aluminium films for the longer wavelengths. The curve for 2600 Å derived from earlier results on aluminium films[16] shows the advance obtained with improved evaporation techniques.

Since, as we have seen, the defects finesse decreases with decreasing wavelength so that the reflecting finesse required decreases also, N_R=20 will be adequate at 2200 Å.

Previous to this analysis improvements[17] in the evaporation technique of depositing opaque aluminium films, overcoated with thin layers of magnesium fluoride to prevent oxidation and to enhance reflectivity in the vacuum ultraviolet, led us to believe[9] that a similar improvement could be obtained in the performance of semi-transparent aluminium films so as to permit extension to this spectral region for interference spectroscopy from an earth satellite. Our first results[4] indicated that thinner aluminium films similarly overcoated are suitable for multiple-beam interferometry down to 1900 Å. Since then we have further studied the optical properties of such films down to 1800 Å and employed them in Fabry-Perot type interference filters and for interference spectroscopy.

Method of Film Preparation and Optical Measurements

Aluminium of 99.99% purity is rapidly evaporated from heated tungsten wire filaments in an automatically controlled evaporation plant evacuated by a mercury diffusion pump. The reflectivity of a metal film is controlled by a shutter actuated by a reflectance monitoring unit, while the thickness of the magnesium fluoride overcoating is similarly controlled by monitoring the front surface reflection from a glass plate during the evaporation. In both cases the monitoring light is of wavelengths 4300–4500 Å. The aluminium is evaporated in about 3 seconds at a deposition rate of the order of 100 Å per second. The MgF_2 evaporation begins within about 20 seconds after the completion of the aluminium evaporation and takes about 50 seconds to complete. The initial pressure is about 5×10^{-6} mm of Hg though there is a slight increase during the aluminium evaporation. The results obtained are quite reproducible provided care is taken in cleaning both the aluminium and substrate.

The "Spectrosil" B substrates, usually 30 mm diameter discs 2 mm thick and polished to plate glass finish (2 fringes) are ultrasonically cleaned in detergent, then immersed in isopropyl alcohol with a final isopropyl alcohol vapour wash. The aluminium wire is cleaned in 50–50 hydrochloric acid, washed in water and then in acetone. Before evaparation, glow discharge cleaning is

carried out.

The reflectance and transmission of samples are measured at 10° incidence on a reflectometer attached to a nitrogen purged "Optica" CF4 grating spectrophotometer. An area 2 mm×6 mm of a coating is measured but the variation in reflectance over a disc does not usually exceed ~0.5%. As a check, reflectances and transmittances were also measured at normal incidence by the method of Giacomo[18] and the results were in fair agreement with the reflectometer values within the error in R and T of ±0.5%.

Optical Properties of Coatings

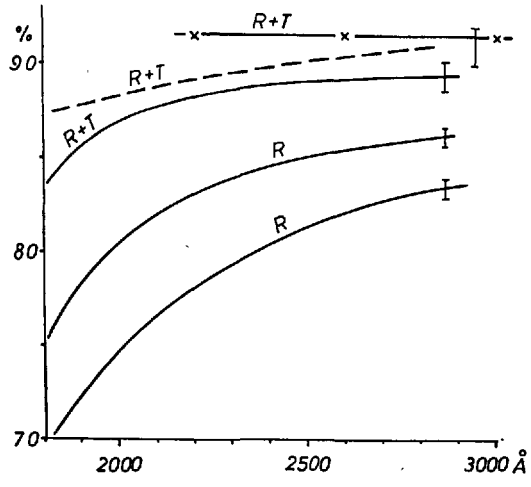

Fig. 2. Aluminium films. $(R+T)$ curve for back surface — — — — —. × Points at 2200 Å, 2600 Å, 3000 Å Hass and Waylonis.[15]

Figure 2 shows the reflectance R and the sum of the reflectance and transmittance $(R+T)$ for two thicknesses of aluminium film as measured within 24 hours of their preparation. The corresponding $(R+T)$ values obtained by Hass and Waylonis[15] for films measured within one hour after evaporation and with about the same R values at 2200 Å are indicated at λ2200, λ2600 and λ3000. There should be little change in the reflectance at wavelengths longer than 1900 Å within 24 hours.[19] The back surface reflectance for the thicker of our films was also measured and the $(R+T)$ curve obtained after correction for the substrate refractive index and absorption is given. At 2200 Å the $(R+T)$ values obtained for both back and front surfaces of our films are 2–3% less than the Hass and Waylonis value.

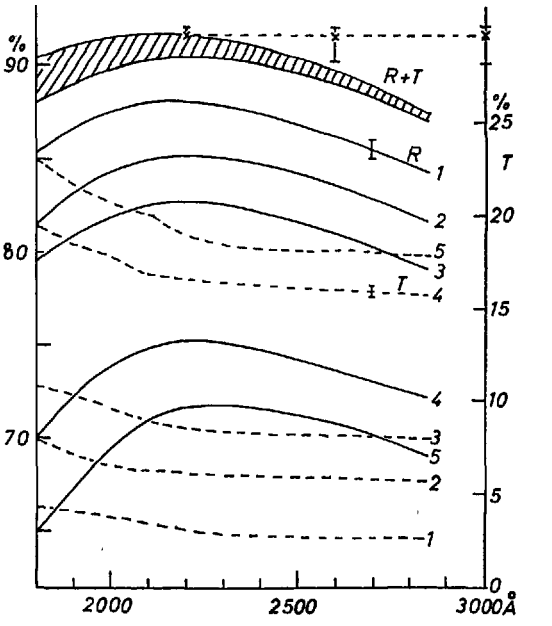

Fig. 3. Al–MgF_2 double layers. × Points at 2200 Å, 2600 Å, 3000 Å. Aluminium films Hass and Waylonis.[15]

Figure 3 gives R, T and $(R+T)$ curves for five samples of aluminium overcoated for optimum performance at 1850–1900 Å. As for figure 2, the reflectances and transmissions, measured within 24 hours, have been corrected for substrate absorption and reflection at the uncoated substrate face. The thickness of the MgF_2 overcoating is determined from the usual relation:

$$\lambda/2 = 2n.d - (\lambda/2\pi)\beta \qquad (1)$$

where β is the phase change on reflection at the MgF_2–Al interface. The value of β was calculated by substituting the values for the optical constants n_1, k_1 of aluminium, derived by extrapolation from the results of Hass and Waylonis,[20] in the formula[21]

$$\tan\beta = -2nk_1/(n_1^2+k_1^2-n^2) \qquad (2)$$

n is the refractive index of MgF_2.

The shaded area in figure 3 shows the spread in the $(R+T)$ values for the five samples, similar to that in the Hass and Waylonis values for 3000 Å for aluminium alone.

The performances of the various types of reflecting coatings for Fabry-Perot interferometry are compared in figure 4. The superiority of the double layers at 1900 Å

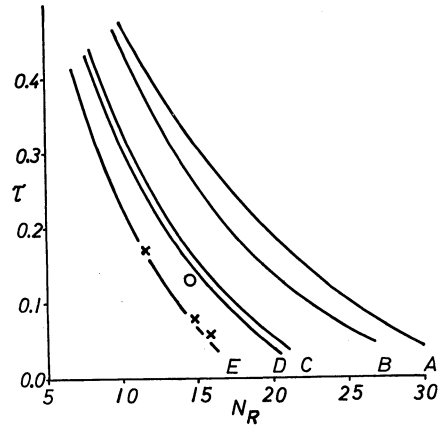

Fig. 4. Al and Al-MgF_2 reflecting coatings.
Curves A: Al at 2200 Å, Hass and Waylonis.[15]
B: Al-MgF_2 double layers at 1900 Å.
C: Calculated curve for Al at 1900 Å.
D: Al at 2200 Å.
E: Al at 1900 Å.
× Points back surface of Al-MgF_2 at 1900 Å.
○ Point back surface of Al at 1900 Å.

is clear but it should be noted that the curve corresponding to the back surfaces of these coatings reveals a performance inferior to the back surface of a single aluminium film. Why this is so is not clear, but it may be due to strain in the double coating.[22] It is interesting to compare these curves with the curve for pure aluminium calculated from the optical constants, derived as for formula (2). This suggests that the double layers are not optimum and from figure 2 it is likely that the aluminium layer is mainly at fault.

$N_R-\tau$ curves are very sensitive to variations in absorption in a coating. Using the relation[11]

$$\tau=[1-A/(1-R)]^2 \qquad (3)$$

it can be seen, for example, that for $N_R=17$, corresponding to $R=0.83$, the two values $T=0.07$ and $T=0.05$ give respectively $\tau=0.17$ and $\tau=0.09$, i.e. a difference in absorption of 2% results in a factor of nearly two in peak transmission.

It is hoped to increase the optical performance of the double layers for multiple beam interferometry by improved evaporation technique including a higher vacuum, with special attention to water vapour, and control of the substrate temperature.[15] This we feel will be specially important for coatings to be employed down to 1600 Å.

However, the performance of our present double layers at 1850 Å is as good as or better than that obtained previously with aluminium coatings, even in the near ultraviolet and visible. We have obtained Fabry-Perot interferograms of λ 1849 of HgI. Such coatings, might also prove suitable for a laser cavity working at these short wavelengths.

Fabry-Perot Interferogram at λ 1849

"Spectrosil" plates matched to λ/70 in the green were coated with Al-MgF_2 double layers designed to give optimum performance

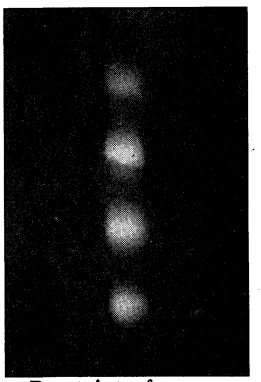

Fig. 5. Fabry-Perot interferogram of λ 1849 HgI. Interferometer spacing 0.15 mm.

at λ 1849. Figure 5 shows fringes of λ 1849 of HgI obtained with a "Spectroline" 11 SC-1 lamp. The line was isolated by a "Spectrosil" prism spectrograph purged with nitrogen and the interferogram was recorded by a single-stage magnetically focused image converter[23] with a "Spectrosil" window, S-9 photocathode, and a phosphor screen output. The image converter, specially constructed by us for this work, greatly facilitated detection and recording of the fringes (the imperfection in one of the fringes is due to a defect in the phosphor screen). The linear resolution of the image tube of 30 line pairs/mm was more than adequate for the fringes. An etalon separation of 0.15 mm was easily achieved with aluminium foil spacers and this arrangement proved to be stable.

The recorded fringe finesse of about 5 is mainly limited by the quality and adjustment of the interferometer plates. To confirm this, fringes of λ 2537 were also recorded and a finesse of 7, directly proportional to the increase in wavelength, was obtained, showing that the defects finesse dominates.

A high quality 6 cm diameter Fabry-Perot interferometer with plates of "Spectrosil A" matched to better than $\lambda/150$ in the green has now been constructed and we hope to extend the spectral range below 1700 Å for diagnostic spectroscopy and space research applications, employing the instrument both in its oscillating form and in its spectrographic method of use. Image intensifiers incorporating time resolution devices and solar blind photocathodes are being developed for this work.[6]

Fabry-Perot Type Interference Filters

For satellite and rocket photometry it is important to obtain interference filters capable of operation at wavelengths below 2000 Å. Such filters could also be used to isolate line structures for higher resolution study by the interferometer (e.g. λ 1640 of HeII). We have already reported[24] on the transmission characteristics of first order interference filters deposited on "Spectrosil" substrates. These filters consist of two aluminium reflecting layers separated by a magnesium fluoride spacing layer of thickness d given by

$$(m-1)\lambda = 2nd-(\lambda/2\pi)2\beta \qquad (4)$$

where n and β are the same as in equations (1) and (2) above, and m is an integer. The outer aluminium layer is protected from oxidation by a magnesium fluoride overcoating.

In figure 6, curve A is the transmission characteristic of a filter peaking at 1825 Å. Below 1800 Å the finesse decreases because of the falling reflectivity at the Al-MgF_2 interfaces, but at about 1660 Å the rapidly increasing absorption of the substrate leads to a sharp cut-off. Above 1800 Å the transmission profile corresponds to a halfwidth of 225 Å and a finesse of 8.

Curve B is the transmission characteristic of the same filter tilted through 8° to displace the peak wavelength to 1805 Å. Also indicated on the figure is the halfwidth of 115 Å for a filter with peak transmission of 19% at 1825 Å, composed of two double-layer Al-MgF_2 reflectors separated by a vacuum gap. The halfwidth and peak transmission are calculated from the results shown in figure 3.

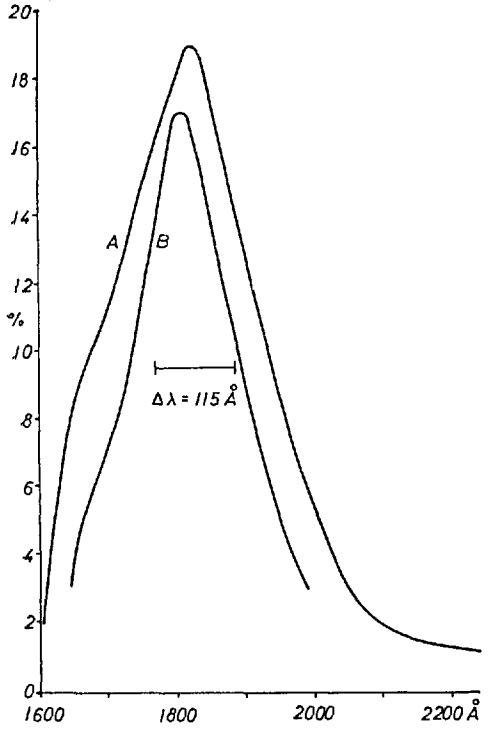

Fig. 6. Transmission curves of first-order Fabry-Perot type filter.

Conclusion

The feasibility of multiple beam interferometry down to 1800 Å has been demonstrated and we hope to extend the spectral range to 1600 Å for diagnostic spectroscopy and space applications. Employing lithium fluoride or sapphire substrates interference filters should be feasible to about 1500 Å. Interferometric determination of wavelength standards in this spectral region is now possible with extension to shorter wavelengths by the Combination Principle.[25]

Acknowledgements

We thank Professor J. D. McGee for his advice and encouragement, Professor W. R. S. Garton for helpful discussion and the generous lending of equipment, and Mr. D. S. Widner for making the filter measurements in the Seya monochromator. Assistance from the British National Committee for Space Research for the purchase of equipment and the support of one of us (C. O. L. J.) is gratefully acknowledged. One of us (S. M.) is supported by a Colombo Plan Fellowship.

References

1) S. Tolansky and D. J. Bradley: N. P. L. Symposium on Interferometry (H. M. S. O., London, 1959).
2) N. J. Peacock and E. T. Hill: U. K. A. E. A. Culham Laboratory Report on Time-Resolved Interferometric Measurements of Emission Line Profiles (U. K. A. E. A. Culham Laboratory, Culham, 1964).
3) D. R. Herriot: Applied Optics **2** (1963) 865.
4) D. J. Bradley, B. Bates, and C. O. L. Juulman: Proc. Sixth Conf. Phénomènes d'Ionization dans le Gaz **4** (C. I. P. I. G., Paris, 1963), p. 79.
5) G. M. Malyshev, G. T. Razdobarim, and L. V. Sokolova: Soviet Physics – Doklady **7** (1963) 701.
6) D. J. Bradley, B. Bates, C. O. L. Juulman, and S. Majumdar: Applied Optics **3** (1964) 1461.
7) D. J. Bradley, A. W. De Silva, D. E. Evans, and M. J. Forrest: Nature **199** (1963) 1281.
8) P. Jacquinot: Reports on Progress in Physics **23** (1960) 267.
9) D. J. Bradley: *Proceedings of the Conference on Optical Instruments and Techniques* (Chapman and Hall, London, 1961), p. 31.
10) T. Dunham: *Vistas in Astronomy*, Vol. 2 (Pergamon Press, London, 1956), p. 1223.
11) R. Chabbal: J. Rech. C. N. R. S. **24** (1953) 138.
12) H. E. Bennett and J. O. Porteus: J. Opt. Soc. Am. **51** (1961) 123.
13) D. A. Jackson: Proc. Roy. Soc. **A 263** (1961) 289.
14) G. Honica and K. Krebs: Z. Physik **156** (1959) 117.
15) G. Hass and J. E. Waylonis: J. Opt. Soc. Am. **51** (1961) 719.
16) J. C. Burridge, H. Kuhn, and A. Pery: Proc. Phys. Soc. **B 46** (1953) 963.
17) G. Hass and R. Tousey: J. Opt. Soc. Am. **49** (1959) 593.
18) P. Giacomo: Compt. Rend. **235** (1952) 1627.
19) P. H. Berning, G. Hass, and R. P. Madden: J. Opt. Soc. Am. **50** (1960) 586.
20) D. J. Schroeder: J. Opt. Soc. Am. **52** (1962) 1380.
21) J. M. Bennett: J. Opt. Soc. Am. **54** (1964) 612.
22) L. G. Schulz and F. R. Tangherlini: J. Opt. Soc. Am. **44** (1954) 357.
23) J. D. McGee: Reports on Progress in Physics **24** (1961) 167.
24) D. J. Bradley, B. Bates, C. O. L. Juulman, and S. Majumdar: Nature **202** (1964) 579.
25) B. Edlén: Reports on Progress in Physics **26** (1963) 181.
26) Z. Lés, F. Lés, and L. Gabla: Acta Physica Polonica **23** (1963) 211.
27) A. Stendel: J. Phys. Radium **19** (1958) 312.
28) R. Lennuier: J. Phys. Radium **19** (1958) 319.

DISCUSSION

Mangus, J. What size, diameter, plates are you using?

Bradley, D. J. We have now 6 cm plates flat to $\lambda/150$ in the green.

Hartman, P. L. What material are you hoping to use for 4th harmonic generation of ruby light?

Bradley, D. J. Crystal quartz.

Reprinted from APPLIED OPTICS, Vol. 3, page 1461, December 1964

Time Resolved Photoelectric Spectrography by Electron-Optical Image Detection of Etalon Interferograms

D. J. Bradley, B. Bates, C. O. L. Juulman, and S. Majumdar

The application of a Fabry–Perot etalon combined with an electron-optical image detector to obtain simultaneously time, spatial, and spectral resolution of plasma and laser sources is discussed, and comparison is made with oscillating Fabry–Perot interferometers. Matching of the interferometer to the image tube is considered, and optimum conditions are determined. Four types of image tubes were tested and the effects of signal-induced background and noise are described. Finally, the interpretation of time-resolved interferograms of wavetrains of very short duration, such as obtained from laser giant pulses, is dealt with, and extension of the interferometer spectral range in the vacuum uv reported.

Introduction

The superior angular dispersion and large light gathering power of photoelectric interferometric spectrometers are being increasingly exploited for plasma diagnostic spectroscopy. In particular, the oscillating Fabry–Perot interferometer has proved to be a powerful tool for time-resolved spectroscopy, and the technique has been extended to laser spectroscopy where the high spectral resolving powers required can be obtained by interferometric means only. The advantages and optical principles of the oscillating interferometer for time-resolved spectroscopy have been previously discussed,[1,2] and instruments employing electromechanical[1,3–5] and piezoelectric drives[6–8] have since been fully developed. However, this method of use of the interferometer suffers from the serious disadvantage that time and wavenumber dispersion are superposed. It is thus necessary to scan at a speed N times greater than the rate of change of the phenomena studied (where N is the interferometer finesse) which leads to a decrease in the signal-to-noise ratio attainable with a given source. Also, continuous monitoring is not possible, and, since a point source is utilized, simultaneous spatial and time resolutions are not obtained.

With the development of Q-spoiled laser systems[9] with outputs lasting <20 nsec and spectral widths[10] <0.01 cm^{-1}, time-resolved interferometric spectroscopy in the nanosecond region is now required. At these speeds, time-sequential spectral scanning results in a distorted recorded profile because of Doppler shifts at the moving mirror. However, the increase in the time resolution limit by the factor N (usually about 20) is the most serious limitation, since the time resolution limit set by the source itself cannot be achieved, as will be shown, and time resolution is obtained only at the expense of spectral resolving power, and the study of phenomena such as multimoding would not be possible.[10]

The development of image intensifiers[11] combining the high quantum efficiencies of photocathodes with the information capacity of the photographic plate led us to explore the possibility of employing the Fabry–Perot interferometer in combination with an image-tube detector for time-resolved spectroscopy to overcome the limitations of the oscillating instrument, and reports of our preliminary investigations have been made.[12,13] We now wish to summarize these, and more recent results employing electronography, to comment further on the optimum conditions of matching the interferometer and the image tube, and to discuss the application of the method to laser spectroscopy.

The Photoelectric Spectrographic Method

The Fabry–Perot ring pattern superposed on a slit image, as in the classical photographic method of use, is swept across the output phosphor of an image tube to give a continuous time record, since wavenumber and time dispersions are now crossed. We have initially tested the system with a rotating mirror system (Fig. 1). The slit-ring pattern was swept across the photocathodes of four different types of image tube. The time resolution limit of 2 μsec was set entirely by the intensity of the mercury arc source. For laser and plasma source, electron-optical sweeping[14,15] or a multiple-beam image tube[15] may be employed.

The advantages of the method are immediately obvious. The only limit to time resolution is now the

The authors are with the Physics Department, Imperial College, London, England.

Received 25 March 1964.

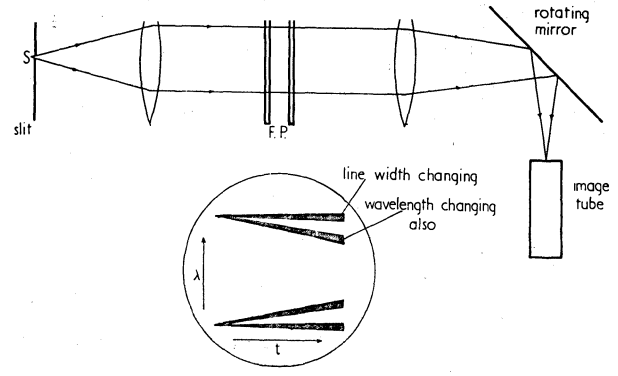

Fig. 1. Principle of the method.

intensity of the source, and maximum spectral resolution of laser modes is then possible. Secondly, a continuous time record is obtained with wavenumber and time dispersions crossed, and, since there is normally a one-to-one correspondence between source and ring pattern, simultaneous spatial resolution is achieved, also crossed with the time dispersion. Finally, there is a gain in luminosity depending upon the order of the fringe employed, and, just as for the scanning interferometer, because of its superior angular dispersion, the Fabry–Perot spectrograph has a gain in illumination over grating spectrographs, and this gain increases with resolving power.[16]

The Interferometer

As usual, it is necessary to match the linear resolution g of the image tube to that of the projected fringe half-width. This requires, for the pth ring from the center, a focal length of $f = 2gN\sqrt{ps\nu}$; N is the finesse, ν the wavenumber, and s the interferometer separation. Maximum use is made of the image-tube photocathode area if the interferometer is tilted and only half of the ring pattern employed. For a cathode of linear dimension l, the maximum number of rings is then $(p_2 - p_1) = (l/gN)[1 - (l/4gNp_2)]$ if the half-width of the p_2th ring from the center is matched to g. Angular dispersion decreases from the center, so it is best to start with the first ring out. Then $p_1 \leqslant 1$. Also, for a given image tube, the maximum number of rings depends only on the finesse.

The angular width α of the slit is determined by the usual relation $\alpha = 2/\sqrt{Ns\nu}$, giving a linear width $a = 4g\sqrt{Np_2}$. Spectral resolving power of the swept image is little affected by ring curvature for a slit of this width. Since the linear diameter D_p, of ring p, is equal to $4gN\sqrt{pp_2}$, then the maximum height of the fringe chord is $(a/2)^2/D_p = g\sqrt{p_2/p}$, the half-width of fringe p, so that the effect of ring curvature does not vary from fringe to fringe. A typical value of g is 100 μ, so that for a 2-cm photocathode two hundred time-resolution elements are obtained on each of the fringes.

The gain in luminosity over the oscillating Fabry–Perot spectrometer arises from the fact that the fringes are continuously and simultaneously recorded, not just $(1/N)$ of an order at a time. If m fringes are utilized, the total gain is mN. However, there is a loss in luminosity, since only a fraction of a fringe $(= 1/\pi\sqrt{Np})$ of a complete ring is recorded for a slit of width a. So for each fringe the gain G in luminosity is $= (1/\pi)\sqrt{N/p}$. This gain decreases with increasing p and has its maximum value at $p = 1/2N$ (the central fringe). For $p = 1$, $N = 10$, the gain is about unity.

It is not very useful to consider the total gain in luminosity,[14] for, while the density of each fringe remains constant, because of the parabolic dispersion of the interferometer, the elementary resolution area decreases from the central fringe outward, so the information rate decreases. This also follows from the decrease in luminosity for increasing p. Since the width of the fringe p is $g\sqrt{p_2/p}$, the information decreases as $1/\sqrt{p}$. The angle subtended by a slit of width a situated at position of fringe p_2 is $\alpha = a/R_{p_2} = 2/\sqrt{Np_2}$ (Fig. 2), so a sector slit of angular width α will have a linear width $\alpha R_p = 4gN\sqrt{p}$ at fringe p. Such a sector slit then provides the same amount of information from each fringe, and, more importantly, gives an increased number of time-resolution elements per linear length of each higher order fringe, the interferometer being tilted to use only one-half of the fringe pattern. A similar argument also applies when the interferometer is employed as a polychromator with photomultiplier detection.

The Image Detector

This comparison of the two methods of use of the interferometer is based on the assumption that the signal-to-noise ratio of a photomultiplier and an image tube with photographic recording of the output can be made equal. Unfortunately, this is not always true of all image tubes presently available. Though tube background is usually negligible for rapid time-resolved spectroscopy, with some tubes signal-induced background and noise can be serious.

The system was first tested with a five-stage magnetically focused transmission secondary-emission image intensifier (20th Century Electronics Type IPM 29/25) of the type developed at Imperial College.[11,17] This tube had a linear resolution of 30 lp/mm, a 20-mm photocathode of 20-μA/lm sensitivity and a blue light

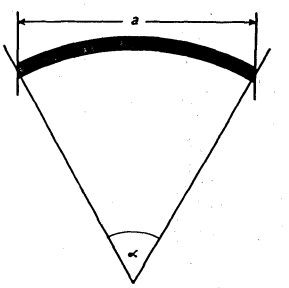

Fig. 2. Slit angle.

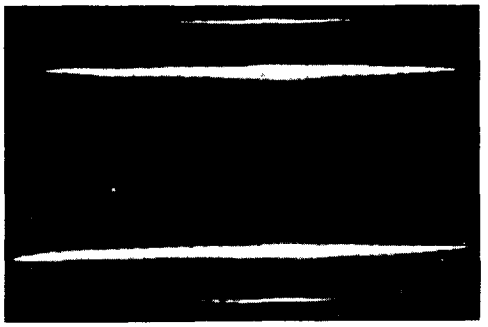

Fig. 3. λ5461 high-pressure mercury lamp. Single-stage image tube. Time resolution 6×10^{-4} sec; spectral resolution 3.3×10^5 sec.

gain of 10^5 at 33 kV with a tube background of 10^3 scintillations sec^{-1} cm^{-2}. An interferometer separation of 0.4 mm and coatings of 85% reflectivity gave a spectral resolving power of 32,000 for λ5461 HgI of a high-pressure mercury lamp. The slit-width of 125 μ was magnified to 250 μ on the tube photocathode, giving eighty time-resolution elements per fringe which, with a mirror speed of 100 cps, corresponds to a 2×10^{-6} sec time resolution limit. Even with a tube voltage of only 26 kV, the signal-induced background and noise and the wide spread in the multiplication factor for individual photoelectrons resulted in such a decrease in the effective signal-to-noise ratio in the recorded image as to make it unsuitable for diagnostic spectroscopy.

The signal-induced noise is mainly due to unfocused penetrating primary electrons, whereas the signal-induced background arises from focused photoelectrons from light reflected back from the first dynode. The photocathode transmits some of the incident light, and this is, of course, common to most types of image intensifier. Thicker photocathodes should help to reduce the effect which would be expected to be wavelength-dependent also. The magnitude of the penetrating primaries' effect is dependent on such factors as the thickness and structure of the dynodes. It is to be hoped that both these effects can be greatly reduced, but meanwhile signal-induced noise limits the use of transmitted secondary-emission image intensifiers for swept time-resolved spectroscopy.

A single-stage magnetically focused tube was employed to test the relative importance of signal-induced background arising from back reflected light. The aluminum-backed phosphor screen of this tube is 20 cm from the photocathode compared with 7 cm between photocathode and first dynode of the transmitted secondary-emission tube. The gain of such a tube with F 1 optical coupling to a photographic recorder is about 5 or with contact print recording about 50.[11] Figure 3 shows a swept scan of λ5461 of the high-pressure mercury lamp. Spectral resolving power is now 3.2×10^5, and the time-resolution limit is 6×10^{-4} sec with sixty time elements on each fringe. Variations in intensity and half-width arise from source instability. A microphotometer trace of the two central fringes is shown in Fig. 4. Penetrating primary electrons are absent, of course, and the smaller solid angle subtended at the photocathode by the phosphor output screen reduces the effect of back reflected light.

Next a three-stage magnetically focused cascaded phosphor-photocathode image intensifier of the type developed at Imperial College by McGee and Catchpole[18] was employed as detector. This tube originally had a blue light gain of 80,000 at 45 kV, but the gain had dropped somewhat. Optical coupling to the phosphor output was again an F 1 system. Figure 5 shows a microphotometer tracing of a swept scan of λ5461. A slit-width of 0.5 mm on the phosphor screen corresponds to a time-resolution limit of 10 μsec with fifty resolution elements per fringe. A faster scan giving 3-μsec resolution was also obtained, but the density was not so high. Spectral resolving power is again 3.2×10^4. The signal-to-noise ratio of the cascaded phosphor-photocathode tube is much superior to that of the transmitted secondary-emission multiplier tube.

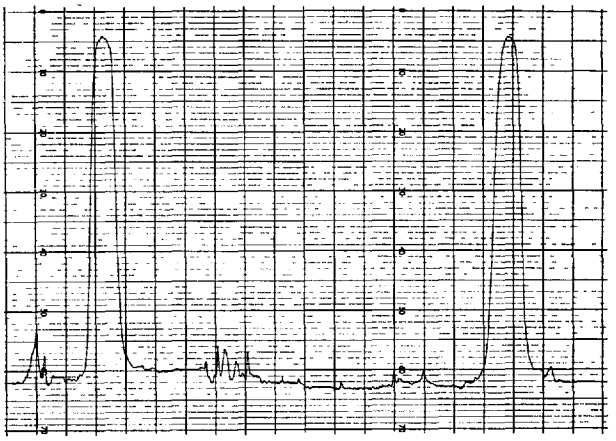

Fig. 4. Microphotometer trace of Fig. 3.

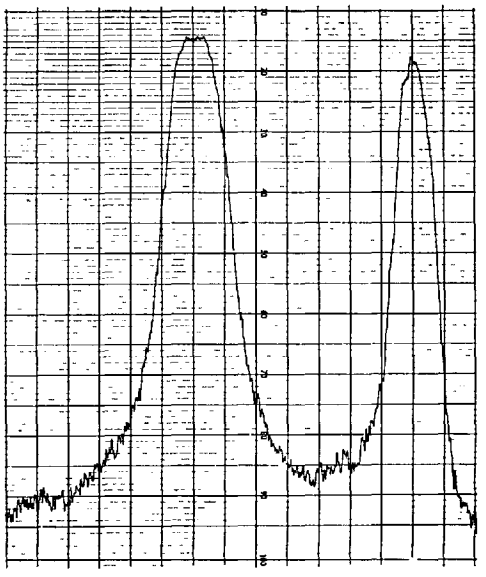

Fig. 5. Microphotometer trace of λ5461 fringes. Cascaded image intensifier. Time resolution 10^{-5} sec, spectral resolution 3.2×10^4 sec.

ectronography

Finally a Lenard window image tube, also developed by McGee[19] at Imperial College, was employed. This particular tube had a low cathode sensitivity of ~16 μA/lm but was otherwise satisfactory. The mica window was 5 mm × 30 mm and about 4 μ thick, and the tube was operated at an over-all voltage of 40 kV. The Ilford G5 nuclear emulsion was mounted on a Melinex strip, and the method of operation of the tube was as described by McGee.[19]

The slit-width of 300 μ was magnified 3× on the photocathode, and the interferometer was tilted to obtain five fringes across the 5-mm width of the mica window. A Philips low-pressure mercury lamp (Type 93109) was employed as light source, and the λ5461 line was isolated by a filter. Figure 6 shows the fringes recorded for exposures of 0.02 sec and 0.04 sec. Signal-induced background is completely absent across the whole of the 30 mm of the window, and the excellent recording of the pattern is indicated by the absorption line in the middle of the fringes.

Because of the low sensitivity of this particular tube, it was not possible to obtain a time resolution of <1 msec with the Philips lamp, without resorting to track counting. A tri-alkali cathode and the employment of Ilford Ilfex emulsion should reduce this limit to ~20 μsec. A tube with a phosphorphotocathode sandwich gain stage would increase the speed by a further factor of 50× to 100×, but with some loss of linear resolution. For spectroscopy in general, the Lenard window has outstanding signal-to-noise performance with, in addition, the great advantage of a linear density-exposure relationship.[11]

Time-Resolved Interferograms from Pulsed Wavetrains

By employing electron-optical sweeping and multiple beam image tubes, it should prove possible to obtain nanosecond time resolution of laser sources, and it is interesting to consider the type of interferogram recording expected. Consider a constant-amplitude wavetrain of length Δl and spectral width $\Delta\nu \cong c/\Delta l$. Even for a perfect interferometer, the finesse is no longer determined by the reflectivity of the coatings, since the number of interfering beams is limited by the length of the wavetrain, and the intensity distribution in the transmitted pattern is now the same as that of the Lummer–Gehrcke interferometer,[20]

$$I(p) = \frac{1 + G_p \sin^2 p\delta/2}{1 + F \sin^2 \delta/2} (1 - R^p)^2 I_0,$$

Fig. 6. λ5461 low-pressure mercury lamp fringes. Lenard window electronographic image tube. Exposures 1/50 and 1/25 sec.

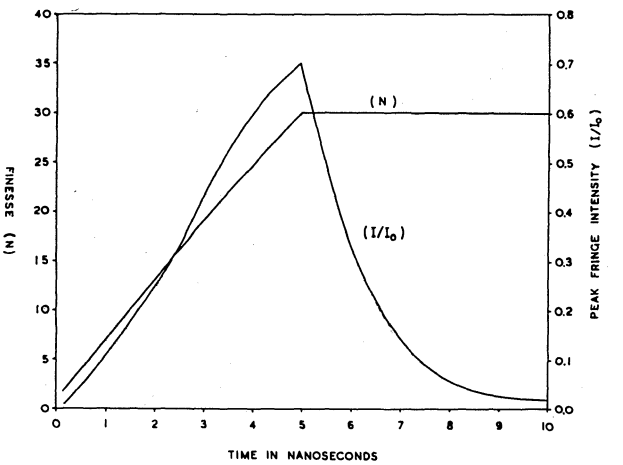

Fig. 7. Time variation of finesse and peak fringe intensity of interferogram of 150-cm wavetrain.

where $G_p = 4R^p/(1 - R^p)^2$; $F = 4R/(1 - R)^2$; and p is the number of interfering beams.

To obtain a recorded spectral width equal to that of the source width (assuming a perfect etalon), it is necessary that the interferometer finesse equal the number of interfering beams. The condition is easily obtained from Fig. 7.70 of ref. 20. Taking, for example, a typical laser giant pulse wavetrain[10] lasting 5 nsec so that Δl = 150 cm, then an interferometer reflectivity of 0.94 gives a finesse N = 30. A plate separation of 2.5 cm then produces thirty interfering beams and a fringe width of 200 Mc/sec as required.

However, it takes 5 nsec for the interference pattern to build up to its maximum intensity and finesse. Although the finesse remains constant after this, the intensity of the fringe maxima will decrease rapidly and continuously as the earlier transmitted beams cease to contribute to the interferogram. For our particular example, the rate of decrease will be by R^2 every 1.7×10^{-10} sec (5/30 nsec) and after a further 5 nsec the fringe peak is only $0.02\,I_0$ [$I_0 = (T/1-R)^2$]. The time variation of both finesse and peak fringe intensity to be expected in this elementary case is shown in Fig. 7.

Discussion

The combination of a Fabry–Perot interferometer and an image intensifier provides a powerful diagnostic tool for laser and plasma sources, providing as it does simultaneous spectral, spatial, and time resolution. No other system seems capable of the high temporal and spectral resolving powers required.

Recent developments in coating techniques[21] make possible the extension of the spectral range of the interferometer into the vacuum ultraviolet region. An automatic evaporation plant has been constructed for this purpose. Aluminum films are evaporated in about 3 sec and immediately, without breaking the vacuum, overcoated with magnesium fluoride to both prevent oxidation of the metal and enhance reflectivity. We have now succeeded in obtaining Fabry–Perot fringes

at λ1849 and an interference filter with a bandwidth of 200 Å and 19% peak transmission at this wavelength.[22]

Finally, we would like to point out that when only an isolated line without any neighboring satellites is being examined, as is frequently the case in plasma diagnosis, high reflecting powers, as normally employed for hyperfine structure work, of >85%, are not always necessary. Luminosity can often be greatly increased by reducing the reflectivity of the interferometer coating (to as low as 75%) and at the same time maintaining the spectral resolving power by increasing plate separation.

We wish to thank J. D. McGee for his interest, encouragement, and helpful discussion during the course of this work and, in particular, for the loan of both cascade and Lenard window image tubes. S. Majumdar is supported by a Colombo Plan Fellowship and C.O.L Juulman by the British National Committee for Space Research.

References

1. S. Tolansky and D. J. Bradley, *N.P.L. Symposium on Interferometry* (Her Majesty's Stationery Office, London, 1959), p. 375.
2. D. J. Bradley, Proc. Roy. Soc. (London) **A262,** 529 (1961).
3. D. J. Bradley, *Proceedings of Conference on Optical Instruments and Techniques* (Chapman and Hall, London, 1961), p. 31.
4. D. J. Bradley, J. Opt. Soc. Am. **52,** 222 (1962).
5. D. R. Herriot, Appl. Opt. **2,** 865 (1963).
6. J. Cooper and J. R. Greig, Nature **195,** 371 (1962).
7. J. V. Ramsay, Appl. Opt. **1,** 411 (1962).
8. N. J. Peacock and E. T. Hill, "Culham Laboratory Report", U.K.A.E.A. Culham, England (1962).
9. F. J. McClung and R. W. Hellwarth, Proc. IEEE **51,** 46 (1963).
10. D. J. Bradley, A. W. Desilva, D. E. Evans, and M. J. Forrest, Nature **199,** 1281 (1964).
11. J. D. McGee, *Reports on Progress in Physics* (The Physical Society, London, 1961), Vol. 24, p. 167.
12. D. J. Bradley, Institute of Physics and The Physical Society Spectroscopy Group, London meeting abstracts (1962).
13. D. J. Bradley, B. Bates, and C. O. L. Juulman, *Proc. of VI Conf. Phenomenes d'Ionization dans les Gaz, Paris (1963),* (Centre d'Etudes Nucleaires, Saclay, France, 1963), Vol. 4, p. 791.
14. G. M. Malyshev, G. T. Razdobarim, and L. V. Sokolova, Soviet Physics-Doklady **7,** 701 (1963).
15. D. J. Bradley and S. Majumdar, to be published.
16. P. Jacquinot, *Reports on Progress in Physics* (The Physical Society, London, 1960), Vol. 23, p. 267.
17. W. L. Wilcock, D. L. Emberson, and B. Weekley, Nature **185,** 370 (1960).
18. J. D. McGee and C. E. Catchpole, British I.E.E. Conf. Rept., Series 5, p. 182 (1962).
19. J. D. McGee and B. E. Wheeler, *Advances in Electronics and Electron Physics* (Academic, London, 1962), Vol. 16, p. 47.
20. M. Born and E. Wolf, *Principles of Optics* (Pergamon, London, 1959), pp. 340–346.
21. W. R. Hunter, Optica Acta **9,** 255 (1962).
22. D. J. Bradley, B. Bates, C. O. L. Juulman, and S. Majumdar, Nature **202,** 579 (1964).

The measurements given in the table were made starting with the highest voltage and then reducing it. The first exposure of an etched platinum foil to 8 or 9 kv usually resulted in a decrease of ion current with time to a steady value. When an etched foil was not first exposed to 8 or 9 kv it was effective in ionizing nitrogen with only 4 kv applied. An etched foil which had never been exposed to more than 4 kv gave at this voltage a current of 4×10^{-8} A when nitrogen was present at 0·35 mtorr pressure. 8 kv was then applied to the foil for a few minutes: on lowering the potential to 4 kv again, the total current was less than 4×10^{-10} A. Possibly protrusions which intensify the electric field were torn off, or smoothed by field evaporation, at the higher voltage.

Attempts were made to improve the efficiency of razor blades by various etching procedures, grinding and stropping, heating in vacuum and reduction in hydrogen, but no significant increase of ion current resulted.

The etched platinum foil was used in a mass spectrometer with the simpler of the two ion sources described by Robertson and Viney (1966). With oxygen present O_2^+ was observed, and with nitrogen N_2^+. The resolved ion beam of O_2^+ was 2×10^{-13} A with an oxygen pressure in the ion source of 0·1 mtorr and a voltage of 6 kv between the foil and the adjacent plate containing a slit. A resolved N_2^+ beam of 1×10^{-14} A was obtained with a nitrogen pressure of 0·2 mtorr and 9·5 kv. Only about one in 10^5 of the ions formed was transmitted through the mass spectrometer, so there is much scope for improvement by the use of focusing systems in the ion source.

Since the chief requirement for field ionization is a high electric field, it seems likely that the etched foils owe their efficiency to a very sharp edge; however, the problem of the importance of the nature of the metal used in field ionization needs further investigation. The reason for the failure of etching procedures to improve razor blades is not clear: perhaps the blades owe their efficiency to surface roughness which is removed by etching. For a linear variation of field ion current with gas pressure (Robertson *et al.* 1963) the best results for nitrogen shown in the table correspond to an ion current of 10^{-14} A at a pressure of 0·1 ntorr. It seems that the development of a focusing system for ions in a field ionization mass spectrometer ion source would make possible gas analysis by this method in the ultra-high vacuum region.

Acknowledgments

We thank the Gas Council, the Institute of Petroleum and the Science Research Council for financial support.

References

BECKEY, H. D., 1963, *Z. InstrumKde*, **71**, 51–4.

ROBERTSON, A. J. B., and VINEY, B. W., 1966, *Advances in Mass Spectrometry*, Vol. 3, Ed. W. L. Mead (London: Institute of Petroleum), pp. 23–33.

ROBERTSON, A. J. B., VINEY, B. W., and WARRINGTON, M., 1963, *Brit. J. Appl. Phys.*, **14**, 278–83.

J. SCI. INSTRUM., 1966, VOL. 43

An optically contacted permanently adjusted high finesse Fabry–Pérot interferometer

B. BATES,† D. J. BRADLEY,† T. KOHNO† and H. W. YATES‡

† Royal Holloway College, Department of Physics, Englefield Green, Surrey

‡ Optical Surfaces Ltd., Stoats Nest Road, Coulsdon, Surrey

MS. received 31*st March* 1966

Abstract. A Fabry–Pérot interferometer constructed with three fused silica optically contacted spacers for a solar rocket spectrograph is described. A recorded fringe finesse of 30 was obtained with a 2 cm etalon aperture using a ^{198}Hg source.

For space research applications (Bradley 1966 to be published) and for laser and plasma diagnostic interference spectroscopy (Bradley *et al.* 1964), a permanently adjusted Fabry–Pérot interferometer would have many advantages in ease of use and the reproducibility of results. Solid interferometers (Lau 1931) have been employed in the past but it is exceedingly difficult optically to work the faces of a block of sufficient aperture to be both flat and parallel to the required accuracy. This is particularly true if the interferometer is to be used in the far ultra-violet (<3000 Å) since the surface finish requirements increase linearly with the decreasing wavelength and it would be necessary for many experiments to have the faces parallel and flat to better than $\lambda/150$ in the green; also any inhomogeneity of the material would result in a lower defects finesse (Jacquinot 1960). In addition the reflectivity at the quartz-reflecting coatings interfaces would be less than for an air-gap instrument. Thus if aluminium–magnesium fluoride overcoatings were employed (Bradley *et al.* 1965) at, say, λ 1850 the effective reflectivity would be reduced by about 2%. This would result in a reduction of the reflecting finesse (Jacquinot 1960) from 16 to 14 and of the interferometer transmission from 20 to 16%.

An optically contacted 10 cm air-gap etalon has been previously employed in the near infra-red (Jackson and Kuhn 1935) but the fringe finesse obtained was not recorded. For a 10 cm gap it would not have been possible to measure the instrumental profile with the light sources then available.

An interferometer spacing of 0·4 mm and a clear aperture

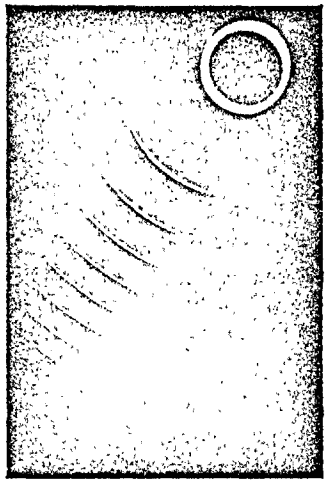

Figure 1. λ 5461 fringes of ^{198}Hg. Optically contacted etalon aperture 2 cm. Interferometer spacing 0·4 mm.

mately 94% reflectivity over a central aperture of 3 cm. The silver was overcoated with a thin layer of magnesium fluoride to prevent oxidation.

Figure 1 shows the fringes obtained with the λ 5461 line of a ^{198}Hg source employing a 2 cm etalon aperture. The fringes were recorded on Tri-X Pan film (Kodak Ltd.) with an exposure of 15 sec and a gamma of 0·9. The corresponding microdensitometer trace (linear in density 0·087 cm^{-1}) is shown in figure 2; the half-width is indicated by the arrow. From this a recorded fringe finesse of 30 was derived. If the aperture is increased to 3 cm the fringe finesse decreases to 22 while an aperture of 1 cm gives a finesse of 43. The adjustment has remained stable for a period of two months to date. This decrease in recorded fringe finesse with increasing aperture is due to a slight wedge effect. This probably arises from incomplete optical contact over the full area of one of the spacers as can be observed visually.

If the fixed gap etalon is placed in a conventional mount with spring adjustments (Tolansky 1947) the wedge can be eliminated with very small differential spring pressure, and a

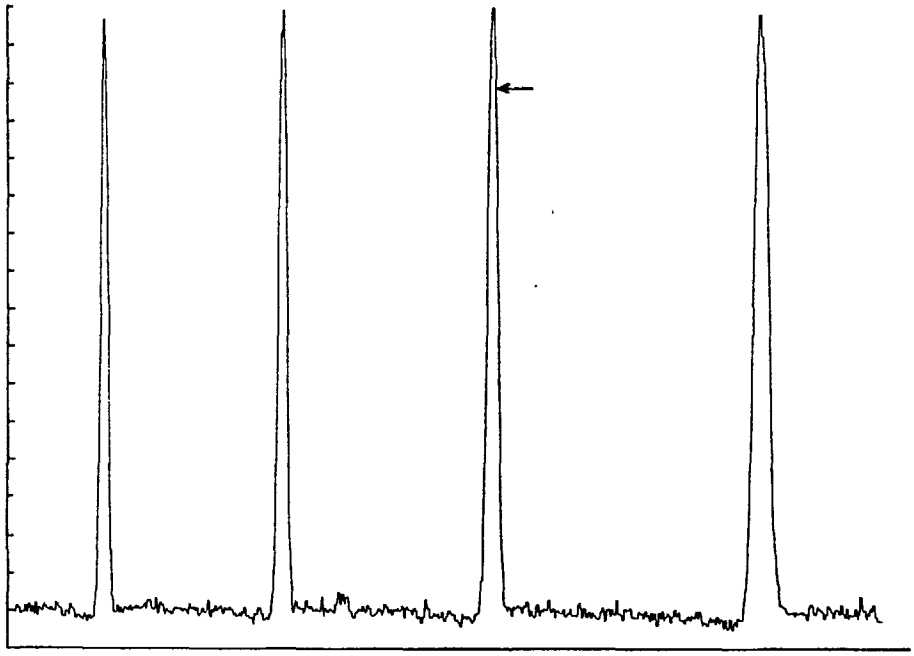

Figure 2. Microdensitometer trace of fringes of Figure 1. Linear density scale 0·087 cm^{-1}.

of 3 cm is required for an etalon for a solar spectrograph which is to be flown in a stabilized Skylark rocket. (If a solid etalon were to be employed the resulting 0·28 mm thick plate would be very fragile indeed.) The plates, of Spectrosil A (Thermal Syndicate Ltd.) of 6 cm diameter and 1 cm thick, were polished flat and smooth to better than λ/180 over their full physical apertures. The 0·4 mm thick, 6 mm diameter cylindrical Spectrosil spacers were cut out from selected portions of a large plate worked flat and parallel to better than λ/40 over a distance of 4 cm. The spacers are optically contacted to both plates on a pitch circle of 5·4 cm diameter at angular intervals of 120°.

Before optically contacting the assembly, the interferometer plate surfaces were coated with silver films of approxi-

recorded finesse of the order of 50 is then obtainable. Under these conditions the adjustment also remains stable.

References

BRADLEY, D. J., BATES, B., JUULMAN, C. O. L., and MAJUMDAR, S., 1964, *Appl. Opt.*, **3**, 1461–5.

—— 1965, *Jap. J. Appl. Phys.*, **4**, Suppl. 1, 467–72.

JACKSON, D. A., and KUHN, H., 1935, *Proc. Roy. Soc.* A, **148**, 335–52.

JACQUINOT, P., 1960, *Rep. Progr. Phys.* (London: The Physical Society), **23**, 267–312.

LAU, E., 1931, *Ann. Phys., Lpz.*, **10**, 71–80.

TOLANSKY, S., 1947, *High Resolution Spectroscopy* (London: Methuen), p. 139.

Interference Filters for the Far Ultraviolet (1700 Å to 2400 Å)

B. Bates and D. J. Bradley

The transmission characteristics of Fabry–Perot type aluminum–magnesium fluoride–aluminum interference filters for the wavelength region 1700 Å to 2400 Å are described. Typical peak transmissions of 0.25 with bandpasses <300 Å are obtained with first-order filters on fused silica substrates. Second-order filters give narrower bandpasses. Methods of filter preparation are described briefly, and the effects of the optical properties of the aluminum reflecting layers on filter performance are discussed.

ntroduction

For broadband stellar photometry and for auxiliary pectral filtering of spectrometers, spectrographs, and pectroheliographs flown in rockets and satellites, the solation of bandwidths of a few hundreds of angstroms s required in the spectral region <3000 Å. With heir high luminosity[1], compactness, and simplicity of ounting, Fabry–Perot type interference filters are articularly suitable for space spectroscopy. Also, he transmission characteristics of this type of filter an, within limits, be optimized during manufacture suit the particular experimental requirements.

For wavelengths <2400 Å[2], no high-index transitting material suitable for multilayer dielectric atings has been discovered so far. However, the cent extension of the effective spectral range of mulple-beam interferometry into the vacuum uv[3] by ıploying semitransparent aluminum films overcoated ith magnesium fluoride indicated the possibility of anufacturing interference filters for this difficult ectral region <2400 Å. This aluminum–dielectric–uminum type of filter is, of course, particularly atactive for space research since it becomes *self-blocking* longer wavelengths because the aluminum attenuan increases with increasing wavelength. We have eady reported preliminary results[4] on the transssion characteristics of a first-order interference er with a peak transmission of 19% at 1825 Å, and w we wish to describe the characteristics of first- d second-order filters with useful bandwidths and adequate peak transmissions* at wavelengths down to 1725 Å.

Interference Relations and Definitions

Figure 1 shows a schematic diagram of the four-layer type of interference filter described in the present work. The optical thickness (nd) of the magnesium fluoride spacer layer required for maximum transmission at wavelength λ_0 is given by

$$nd = (\lambda_0/2\pi)[(m - 1)\pi + \beta], \; m = 1, 2, \ldots , \qquad (1)$$

where m is the order of interference ($m = 1$ representing a filter of minimum spacer thickness, a so-called first-order filter), β is the absolute phase change[7] on reflection at the magnesium fluoride–aluminum boundaries, and n is the refractive index of the dielectric spacer layer. For an opaque aluminum layer coated with a dielectric, this phase shift is given by

$$\tan\beta = + 2nk_1/(n^2 - n_1^2 - k_1^2), \qquad (2)$$

where n_1 and k_1 are the optical constants of the aluminum, of complex refractive index $n_1 - ik_1$. The value of β varies with the thickness of the aluminum layer, but for the film thickness employed in our interference filters (200 Å to 300 Å) the variation of phase change with thickness is small[5] and the value of β given by Eq. (2) is satisfactory for determining the spacer layer thickness. Then the transmission properties of aluminum–magnesium fluoride–aluminum bandpass filters are given by the following relations:

oth authors were in the Physics Department, Imperial Col-, London, when this work was done; they are now at the ysics Department, Royal Holloway College (University of ıdon), Englefield Green, Surrey, England.

eceived 7 November 1965.

his paper was read at the Optics in Space Conference of the itute of Physics and the Physical Society, Southampton, gland, September 1965.

* Schroeder[5] first discussed the feasibility of producing these aluminum–dielectric–aluminum filters for wavelengths down to 1500 Å on the basis of an extrapolation of the optical constants of aluminum measured by Hass and Waylonis[6] for wavelengths >2200 Å. However, the values of expected filter bandwidths computed by Schroeder were incorrect, because he did not take into account phase changes on reflection at the dielectric–metal interfaces [see Eq. (4) below].

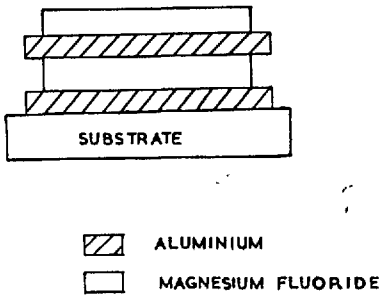

Fig. 1. Schematic diagram of the aluminium–magnesium fluoride–aluminum interference filter.

$$\text{peak transmission } \tau = 1/[1 + (A/T)]^2; \quad (3)$$

$$\text{bandwidth } \Delta\lambda = (\lambda_0/N_R)[(m - 1) + (\beta/\pi)]^{-1}, \quad (4)$$

where A is the absorption and T the transmission of a single semitransparent aluminum layer. N_R is the reflection finesse[1] which depends on the reflecting power R of the dielectric–metal interface according to the relation:

$$N_R = \pi R^{\frac{1}{2}}/(1 - R). \quad (5)$$

It is the absorption of the semitransparent aluminum layers which has previously been the major obstacle in extending the spectral range of interference filters into the far uv since, as can be seen from Eq. (3), the peak transmission of a filter is dependent on film absorption.

The final magnesium fluoride overcoating layer serves two functions. In addition to preventing oxidation of the second aluminum film, it also acts as an antireflecting layer and thus increases the filter peak transmission. This requires a final dielectric layer of optical thickness:

$$nd = \lambda_0\beta/4\pi. \quad (6)$$

Method of Filter Manufacture

High-optical-quality aluminum films for the far uv require evaporation at high deposition rates and low pressures.[8] In the construction of the coating plant currently being employed for the production of interferometer coatings and interference filters, special attention has been paid to the reduction of water vapor in the residual gas atmosphere of the coating chamber. Thus, the chamber and baseplate that are constructed of stainless steel and indium vacuum seals have been used for sealing throughout except for two *Viton A* demountable seals. A liquid-nitrogen-cooled Meissner coil acts as a fast trap, particularly for water vapor, inside the coating chamber, which is bakeable to 120°C and evacuated by a mercury diffusion pump. Typically, a vacuum pressure in the range 5×10^{-8} torr to 10^{-7} torr is obtained prior to evaporation. There is an increase in pressure to 10^{-5} torr during the aluminum evaporation even though the aluminum has been thoroughly cleaned and previously outgassed. However, the pressure quickly recovers to 10^{-7} torr when the aluminum evaporation is completed. The aluminum is deposited at a rate of 100 Å sec^{-1} to 150 Å sec^{-1} and the film thickness is controlled by an automatic monitoring system. (This will be described in a later publication dealing with the reflectance and transmittance of aluminum in the far uv.) Deposition of the magnesium fluoride spacer layer begins within 20 sec of the completion of the aluminum evaporation to prevent oxidation of the aluminum film.[9] The rate of deposition of the magnesium fluoride layer is 20 Å sec^{-1}; and, since this is a slow evaporation, manual control is adequate. A separate monitor plate is used for each of the four layers and a monitoring light source of wavelength ~4400 Å is employed.

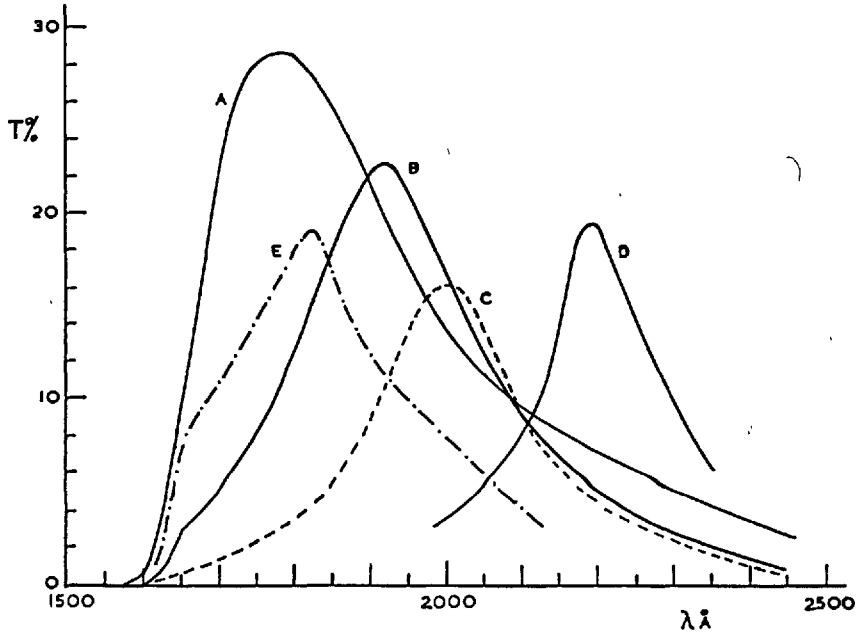

Fig. 2. Experimental transmission curves of first-order filters deposited on Spectrosil B substrates.

Results

Filter transmission characteristics have been determined at wavelengths >1850 Å with a nitrogen-purged Optica-CF_4 grating monochromator. A vacuum Seya monochromator has been used to check measurements in the wavelength region 1850 Å to 2400 Å and to extend the measurements to approximately 1500 Å. The properties of a number of filters have also been checked in the region 1500 Å to 1900 Å using a normal-incidence vacuum monochromator.

Filter transmission characteristics were measured at normal incidence over a sample area of 2 mm × 6 mm. The accuracy of measurement in transmission is ±0.2% at wavelengths >1900 Å and ±0.4% at shorter wavelengths.

First-Order Filters

Transmission curves for a number of first-order filters are shown in Fig. 2. These filters were deposited on to fused silica Spectrosil B substrates of either 1 mm or 2 mm thickness.

The spacer layer of filter A was chosen to give a peak transmission at a wavelength of about 1725 Å. However, the actual peak occurs at λ 1780 Å owing to the effect of increasing absorption in the Spectrosil substrate.

The optical properties of the aluminum films can be derived from the filter characteristics using Eqs. (3), (4), and (5) after correction for substrate reflection and absorption losses. These derived optical properties given in Table I clearly show the deterioration in filter performance of aluminum films with decreasing wavelength.

A useful comparison of filter performance with the expected performance, calculated on the basis of extrapolated optical constants,[5] can be obtained by normalizing the filters to a peak transmission of 25%. The normalized filter characteristics can be calculated from the derived optical properties of Table I, assuming that aluminum absorption is independent of film thickness. (Over the range of aluminum thicknesses involved the measured variation of absorption with film thickness has been found to have a negligible effect on this calculation.) The values of bandwidth (Δλ) so calculated are given in the last column of Table I.

Table I. Optical Properties of Aluminum Films Derived from Fig. 2[a]

Curve	λ_0 (Å)	Δλ (Å)	R (%)	T (%)	A (%)	C	Δλ (Å) for τ = 25%
A	1780	310	—	—	—	180	—
E	1825	280	79.5	8.0	12.5	200	305
B	1920	280	77.2	10.8	12.0	330	290
C	2000	220	81.7	7.3	11.0	500	260
D	2190	185	85.0	6.5	8.5	350	205

[a] It was not possible to derive optical properties from Filter A because the filter transmission profile is distorted by substrate absorption.

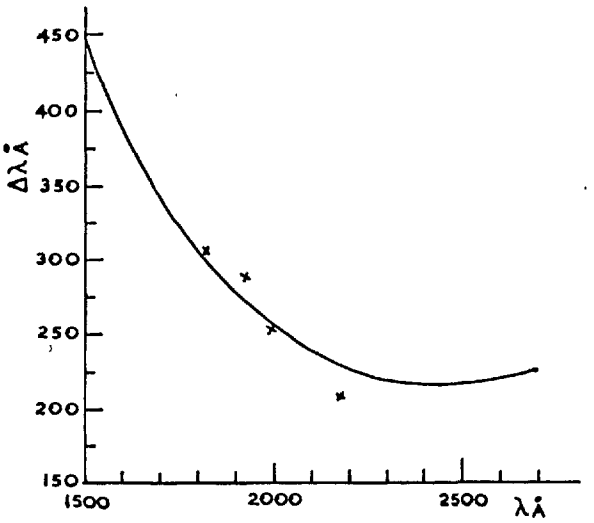

Fig. 3. Calculated bandwidth of first-order filters as a function of wavelength for peak filter transmissions of 25%. Bandwidths derived from experimental filter characteristics (Table I) are shown as X.

These values of bandwidth are greater than those previously computed[5] without taking into account the phase term β of Eq. (4). The good agreement, within ±20 Å, between the correctly calculated bandwidths and those derived from the experimental filter characteristics of Table I is shown in Fig. 3.

An important characteristics of a filter is its contrast or its ability to reject light at wavelengths distant from the passband. An arbitrary definition of contrast, which nevertheless permits useful comparisons to be made between filters, is the ratio of peak transmission to the transmission at 4000 Å.[5] Contrast values C for the first-order filters of Fig. 2 are also given in Table I. For a first-order filter peaking at 1800 Å the contrast is of the order of 200. At wavelengths >4000 Å the transmission of the filter is, of course, steadily decreasing owing to the decreasing transmission of aluminum with increasing wavelength.

Peak transmissions at shorter wavelengths may be obtained by employing lithium fluoride, calcium fluoride, or sapphire substrates. Figure 4 shows a first-order filter deposited on a sapphire substrate of 1 mm thickness. A narrower bandwidth would be obtained with a thinner spacer layer. The consequent shift of the transmission peak to a shorter wavelength would lead to the properties of the filter being largely determined by the properties of the reflecting layers at wavelengths greater than the peak wavelength and by the substrate absorption at shorter wavelengths. An improved performance over that shown in Fig. 4 could also be expected from a filter on a lithium fluoride substrate because of its higher transmission.

Second-Order Filters

Equation (4) shows that for a given reflectivity of the aluminum films, the filter bandwidth at a wavelength

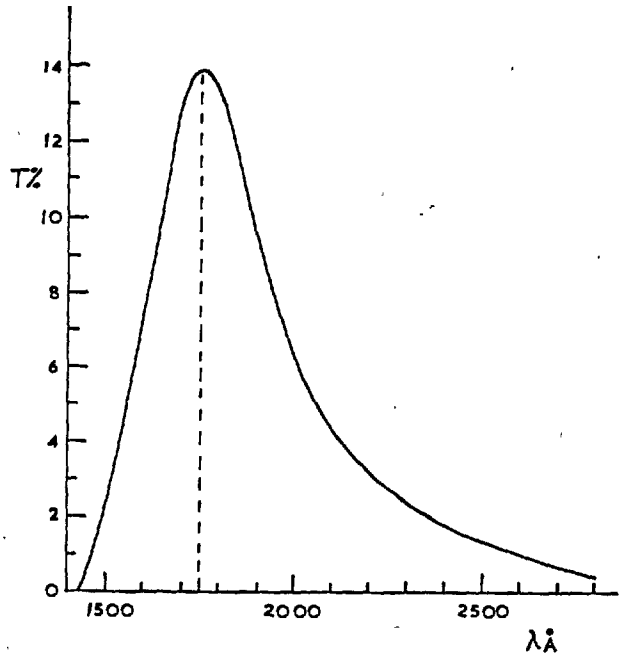

Fig. 4. Experimental transmission characteristic of a first-order filter deposited on a sapphire substrate.

Table II. The Optical Properties of Aluminum Films Derived from Fig. 4

Curve	λ_0 (Å)	$\Delta\lambda$ (Å)	R (%)	T (%)	A (%)	$\Delta\lambda$ (Å) for τ = 25%
B	1990	105	77.0	7.0	16.0	155
C	2130	80	82.5	6.2	11.3	110
A	2190	155	70.0	16.6	13.4	130

λ_0 can be reduced by increasing the spacer-layer thickness to give higher orders of interference. The properties of several second-order filters having transmission peaks centered on wavelengths close to λ 2000 Å are shown in Fig. 5.

The optical properties of the aluminum films have been derived as before from the filter transmission characteristics, and values are listed in Table II. Comparison with properties derived from first-order filters shows that the aluminum films of the second-order filters have an apparently inferior performance characterized by higher absorption values. This greater absorption may, in fact, be owing to increased scattering in the spacer layer since magnesium fluoride films become crystalline for thicknesses greater than approximately 1000 Å.[10] For a first-order filter peaked at λ 2000 Å, the spacer-layer thickness (d) is approximately 420 Å; but for a second-order filter peaked at the same wavelength, the corresponding thickness is 1100 Å. Although we have not attempted to make filters of higher than second order for wavelengths near 2000 Å, the scattering within the space layer with increased thickness may well prove to be a serious limitation in the performance of such filters.

Change in Filter Characteristics with Time

The stability of filter transmission characteristics over long periods of time is a matter of extreme importance for space research applications. While no attempt has been made to make a detailed investigation of the change in properties with time, the following observations have been made.

All filters show a change in properties within the first few days after preparation and exposure to the atmosphere. The changes are characterized by a shift in the transmission peak to a longer wavelength and

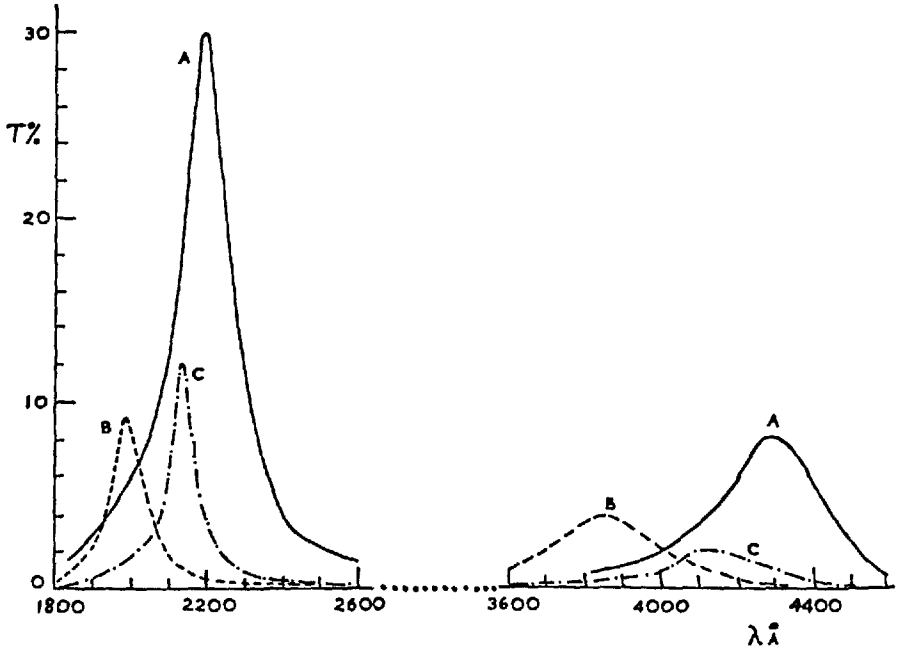

Fig. 5. Experimental transmission curves of second-order filters deposited on Spectrosil B substrate.

by a reduction in the peak transmission. This is illustrated in Fig. 6 which shows the transmission characteristics of a first-order filter measured one day and fourteen days, respectively, after preparation. During this period no special precautions were taken other than storing the filter in a dustfree atmosphere. No changes in properties have been observed after the first week up to periods of three months after preparation.

These changes in properties of filters during the first few days after preparation may be the result of structural changes in the magnesium fluoride spacer layer, increasing absorption of the aluminum films because of continuing oxidation or strain relief at the aluminum-magnesium fluoride boundaries.[11]

All the filter characteristics shown were obtained from measurements made at least one week after manufacture, after which the properties became stable.

onclusion and Discussion

First- and second-order interference filters with characteristics close to theoretical values at wavelengths 1800 Å have been produced, and filters with 25% eak transmissions and bandwidths of 300 Å or less an be made for the wavelength region 1800 Å to 2400 not covered by multilayer dielectric filters. This is a atisfactory performance for broadband photometry. t wavelengths <1800 Å performance deteriorates cause of the increasing absorption of aluminum oxide ith decreasing wavelength filter. Also, the demands n preparation technique become more stringent if the pected performance shown in Fig. 3 is to be achieved. ne effective contrast of first-order filters could be increased by employing them in combination with wavelength-selective detectors[12] to eliminate response at ger wavelengths. Similarly, it would be necessary suppress the first-order peak transmission of second- er filters. Composite filters consisting of two or re first-order filters in series on the same substrate[5] uld also substantially improve contrast. Interfer- e fringes of λ 1849 of Hg I have been recorded emying two first-order filters to isolate the line and so press the strong λ 2537 line.

Ve are indebted to J. D. McGee for general laboratory support and encouragement, to W. R. S. Garton the use of a Seya monochromator, and to C. B. as of UKAEA, Culham Laboratory, who checked, normal-incidence monochromator the transmission everal of our filters.

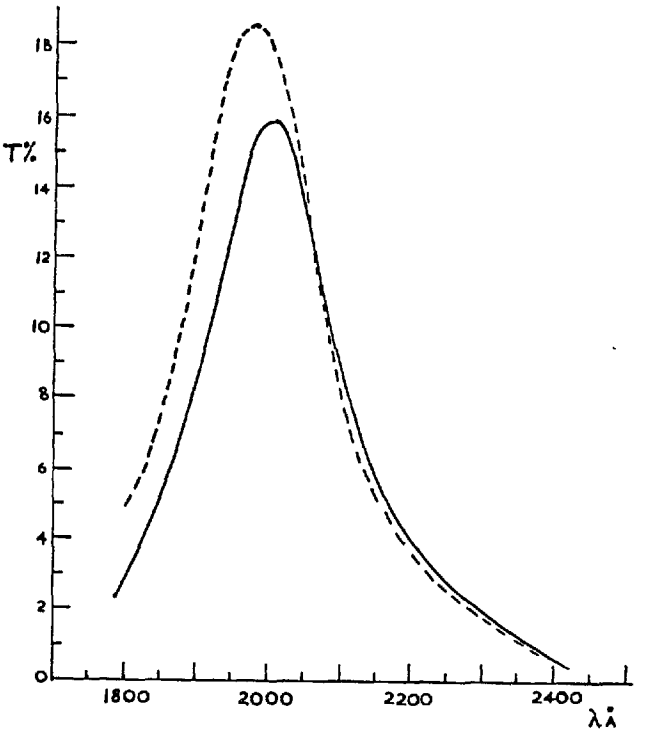

Fig. 6. The change in properties of a first-order filter with time. Transmission characteristics were measured one day (broken curve) and fourteen days (full curve) after preparation.

References

1. P. Jacquinot, Rept. Progr. Phys. **23**, 267 (1960).
2. G. Honica and K. Krebs, Z. Physik **156**, 117 (1959).
3. D. J. Bradley, B. Bates, C. O. L. Juulman, and S. Majumdar, Nature **202**, 579 (1964).
4. D. J. Bradley, B. Bates, C. O. L. Juulman, and S. Majumdar in *Proceedings of the Conference on Photographic and Spectroscopic Optics*, Suppl. #1, Japan. J. Appl. Phys. **4**, 6 (1965).
5. D. J. Schroeder, J. Opt. Soc. Am. **52**, 1380 (1962).
6. G. Hass and J. E. Waylonis, J. Opt. Soc. Am. **51**, 719 (1961).
7. J. M. Bennett, J. Opt. Soc. Am. **54**, 612 (1964).
8. G. Hass and R. Tousey, J. Opt. Soc. Am. **49**, 593 (1959).
9. R. P. Madden, L. R. Canfield and G. Hass, J. Opt. Soc. Am. **53**, 620 (1963).
10. L. G. Schulz, J. Chem. Phys. **17**, 1153 (1949).
11. L. G. Schulz and F. R. Tangherlini, J. Opt. Soc. Am. **44**, 357 (1954).
12. L. Dunkleman, W. B. Fowler, and J. Hennes, Appl. Opt. **1**, 695 (1962).